

Direct Programming of Neural Progenitors into Medium Spiny Neurons by Transcription Factor Transfection



Charlene Geater
September 2014
PhD Thesis

DECLARATION

This work has not been submitted in substance for any other degree or award at this or any other university or place of learning, nor is being submitted concurrently in candidature for any degree or other award.

Signed (candidate)
Date

STATEMENT 1

This thesis is being submitted in partial fulfillment of the requirements for the degree of PhD

Signed (candidate)
Date

STATEMENT 2

This thesis is the result of my own independent work/investigation, except where otherwise stated.
Other sources are acknowledged by explicit references. The views expressed are my own.

Signed (candidate)
Date

STATEMENT 3

I hereby give consent for my thesis, if accepted, to be available for photocopying and for inter-library loan, and for the title and summary to be made available to outside organisations.

Signed (candidate)
Date

STATEMENT 4: PREVIOUSLY APPROVED BAR ON ACCESS

I hereby give consent for my thesis, if accepted, to be available for photocopying and for inter-library loans **after expiry of a bar on access previously approved by the Academic Standards & Quality Committee.**

Signed (candidate)
Date

Summary

Huntington's disease is an autosomal dominant neurological disease caused by an elongated CAG repeat in exon 1 of the *huntingtin* gene. There is currently no cure and treatments are limited. The genetic mutation causes selective cell death of the medium spiny neurons which reside in the striatum of the basal ganglia. Current disease models don't necessarily recapitulate all aspects of the human disease and so alternatives are needed. The advent of induced pluripotent stem cells (iPSC), has allowed for HD patient specific pluripotent stem cells to be derived, hence differentiation of these cells *in vitro* could provide a disease model for drug testing and investigation of disease pathology. Current protocols for differentiation of pluripotent stem cells into medium spiny neurons (MSNs) are often inconsistent and lead to low yields of MSNs. Directing differentiation through forced expression of transcription factors has been used to differentiate neurons from fibroblasts and pluripotent stem cells, often with increased efficiency. Utilising transcription factors vital in post-mitotic MSN development, this study has aimed to produce MSNs *in vitro*, by transfection of transcription factors or combinations thereof in a multicistronic plasmid into ventral forebrain neural progenitors.

This study has involved the cloning and expression of 5 different transcription factors important in MSN development in iPSC-derived neural progenitors. Two of these transcription factors; NOLZ1 (ZNF503) and ISL1 were further investigated for their ability to differentiate neural progenitors into MSNs. This study showed that transfection of ISL1 enabled differentiation of neurons to produce a higher proportion of cells resembling MSNs, characterised by co-expression of the MSN markers DARPP32 and CTIP2 and expressing FOXP1. The combination of NOLZ1 and ISL1 in transfection improved functional maturation of neurons, becoming

increasingly spontaneously active and increased excitability, as well as responding to GABA and NMDA, with dopamine D1 agonist enhancement of NMDA currents.

Acknowledgements

Firstly, I'd like to thank the MRC for funding my PhD studentship and also the CHDI for funding the consumables, which enabled me to carry out my PhD.

Secondly I'd like to thank both my supervisors Paul & Nick, providing me with guidance and support, throughout the PhD.

I'd also like to acknowledge the work that Dr Vsevelod Telezhkin and Dr Christian Schnell carried out to generate the electrophysiology data in this thesis, and also the work Emma Cope did in order to make the original plasmid backbone.

I'd also like to thank the many colleagues whom I have worked with over the past 4 years, for the advice and friendship. Special mention to Rachel, Emma, Shona, Sali, Brenno, Irene, Stu, Becky, Martin, Tom, Jules, Lydia, B, Al and Dave for keeping me sane, for our social events and late night lab sessions. I no longer think of you as colleagues but friends, who I will endeavour to stay in contact with in future. A special mention to B, Al and Dave who have provided me with feedback for my thesis writing.

I would also like to thank my husband Geat, for being so supportive over these last 4 years, having the patience when I'm inevitably late after an experiment has overrun and for all the extra dog walking he had to provide for Barkley and Howley, who never failed to put a smile on my face. I'd like to thank my parents for supporting me emotionally and financially through university, allowing me to pursue my undergraduate degree and PhD, and for allowing us to move home in the final few months.

Abbreviations

ANR	Anterior Neural Ridge
BDNF	Brain-derived neurotrophic factor
bHLH	Basic Helix-Loop-Helix
BSA	Bovine serum albumin
CNS	Central nervous system
DIV	Days <i>in vitro</i>
EB	Embryoid body
EDTA	Ethylenediaminetetraacetic acid
EGTA	Ethylene-glycol-tetra-acetic acid
EPSCs	excitatory post-synaptic currents
GABA	γ -amino butyric acid
GSK3	Glycogen synthase Kinase
HD	Huntington's Disease
HDACi	Histone deacetylase inhibitor
HEPES	N-2-hydroxyethylpiperazine-N'-2-ethanesulfonic acid
hESCs	Human Embryonic Stem Cells
HH	Hamburger-Hamilton (stages of chick embryonic development)
ICM	Inner Cell Mass
iPS	Induced Pluripotent stem cells
IPTG	Isopropyl thiogalactoside
KSR	Knockout serum replacement
LB	Luria-Bertani
LGE	Lateral Ganglionic Eminence
LIF	Leukemia inhibitory factor
MAPK	Mitogen activated protein kinase
MEFis	Inactivated mouse embryonic fibroblasts
mESCs	Mouse Embryonic stem cells
MGE	Medial Ganglionic Eminence
MSN	Medium Spiny Neuron
MZ	Mantle Zone
NMDA	N-Methyl-D ₂ aspartic acid
NMDG	N-Methyl-D-Glucamine
PBS	Phosphate buffered saline
QA	Quinolinic acid
RA	Retinoic acid
RAR	Retinoic Acid Receptor
RIPA	Radio-immunoprecipitation assay
SDS	sodium dodecyl sulphate
SOC medium	Super optimal broth with catabolite repression
SVZ	Subventricular Zone
TAE	Tris-acetate- Ethylenediaminetetraacetic acid
TGFβ	Transforming growth factor β
TSAP	Thermo-sensitive alkaline phosphatase
V_m	Resting membrane potential
VPA	Valproic acid
VZ	Ventricular Zone
XGAL	5-bromo-4-chloro-3-indolyl-beta-D-galacto-pyranoside

Table of contents

Summary	2
Acknowledgements	4
Abbreviations	5
Table of contents.....	6
1. Introduction.....	2
1.1 Stem cells.....	2
1.2 Huntington's Disease.....	7
1.2.1 Huntington's Disease.....	7
1.2.2 Huntington's Disease Modelling	8
1.3 The Striatum.....	14
1.3.1 Types of Medium Spiny Neuron	16
1.3.2 Compartmentalisation of the Striatum.....	19
1.4 Development of the Striatum.	21
1.4.1 The Telencephalon.....	21
1.4.2 FGF8 signalling	24
1.4.3 Sonic hedgehog signalling.....	25
1.4.4 Retinoic acid signalling	29
1.4.5 WNT and BMP signalling.....	31
1.4.6 The role of FoxG1.....	32
1.4.7 The roles of Dlx1/2, Gsx1/2 and Ascl1.....	34
1.5 The Relevance of Transcription Factors in Striatal Development	38
1.5.1 EBF1.....	38
1.5.2 FOXP1.....	40
1.5.3 Islet1	45
1.5.4 NOLZ1	47
1.5.5 OCT6.....	48
1.6 Striatal neuronal differentiation <i>in vitro</i>	52
1.6.1 Neural induction.....	53
1.6.2 Terminal differentiation into MSN	55
1.7 Directed differentiation by transcription factor expression	59
1.8 Aims & Objectives	61
2. Methods	64
2.1 Materials.....	64
2.2 Sourcing transcription factors	64
2.2.1 RNA extraction	64
2.2.2 cDNA synthesis	64
2.3 Cloning of transcription factors and subcloning into multicistronic vectors	65
2.3.1 Cloning of transcription factors	65
2.3.2 Subcloning.....	70
2.4 Cell culture	71
2.4.1 Transfection of HEK293 cells	72
2.4.2 iPS cell culture.....	72
2.4.3 Early differentiation.....	73
2.4.4 Terminal differentiation	74
2.4.5 Transfection of plasmids for differentiation	75
2.4.6 G418 Kill curve	76
2.5 Protein analysis	76
2.5.1 Western blotting.....	76

2.5.2	Immunofluorescence	79
2.6	Sholl analysis	82
2.7	Electrophysiology	83
2.7.1	Electrodes.....	83
2.7.2	Patch pipettes.....	83
2.7.3	Whole cell patch clamp.....	83
2.7.4	Current clamp	86
2.7.5	Voltage Clamp (VT)	88
2.8	Statistical analysis	88
3.	Transcription factor cloning and plasmid validation	90
3.1	Introduction.....	90
3.2	Cloning, Subcloning & Plasmid Verification.....	94
3.3	EBF1.....	95
3.4	ISLET1.....	100
3.5	NOLZ1	107
3.6	FOXP1.....	118
3.7	OCT6.....	124
3.8	Conclusions.....	132
3.8.1	The transcription factors	132
3.8.2	Plasmid design features	133
3.8.3	Limitations of the methods.....	135
4.	Protein characterisation of differentiation protocol.....	137
4.1	Introduction.....	138
4.2	Immunofluorescence of differentiation.....	139
4.2.1	Doublecortin expression	139
4.2.2	MAP2/S100 β expression	140
4.2.3	MAP2/synaptophysin expression.....	141
4.2.4	PSD95/Synaptophysin expression	142
4.3	Initial transfection of the 9 plasmids for driven differentiation of neural stem cells 144	
4.4	Further investigation into the use of NOLZ1 and ISL1 transfection for differentiation 150	
4.4.1	G418 kill curves	150
4.4.2	Characterisation of transfections by immunofluorescence.....	154
4.5	Conclusions.....	163
4.5.1	Protein characterisation of the SCM1/2 protocol	163
4.5.2	ISL1 is a likely candidate for specifying a MSN phenotype.....	165
4.5.3	NOLZ1-ISL1 co-expression in the differentiation	167
4.5.4	Limitations of the methods in this chapter.....	168
5.	Morphological and electrophysiological characterisation of transfected neurons	170
5.1	Introduction.....	171
5.2	Morphological analysis of differentiated neurons.....	172
5.2.1	Week 1	172
5.2.2	Week 2	175
5.2.3	Week 3	178
5.3	Basic electrophysiological characterisation.	180
5.3.1	Passive properties of transfected neurons.....	180
5.3.2	Induced action potentials and trains	183
5.3.3	Spontaneous activity of transfected cells.....	191
5.3.4	Na ⁺ and K ⁺ currents.....	194
5.3.5	Voltage gated Na ⁺ channel activation and inactivation	197

5.4	GABA currents and NMDA currents with enhancement by dopamine D1 agonist	202
5.4.1	GABA miniature post synaptic currents	202
5.4.2	GABA currents.....	204
5.4.3	NMDA currents with D1 enhancement.....	205
5.5	Conclusions.....	207
5.5.1	Cells become less complex during <i>in vitro</i> culture	208
5.5.2	NOLZ1/ISL1 combined transfections improved the neuronal phenotype at week 3	209
5.5.3	ISL1 and NOLZ1-ISL1 were the best at inducing a MSN-like phenotype ...	210
5.5.4	Limitations of the methods in this chapter.....	212
6.	Discussion & Future work.....	214
6.1	Summary of data in this thesis	214
6.2	ISL1 transfections improve MSN phenotype	215
6.3	Driving differentiation with forced expression of NOLZ1 and ISL1	218
6.4	Limitations of the thesis	218
6.4	Future work:	219
6.4.1	Improving the transcription factor delivery	219
6.4.2	A Huntington's disease model	220
7.	Thesis conclusion.....	222
8.	References.....	224
9.	Appendix	240
9.1	Sequencing alignments	240
9.1.1.1	Homo sapiens ISL LIM homeobox 1 (ISL1), mRNA	240
9.1.1.2	Re-cloned Homo sapiens ISL LIM homeobox 1 (ISL1), mRNA	241
9.1.2	Homo sapiens zinc finger protein 503 (ZNF503), mRNA	242
9.1.3	Homo sapiens zinc finger protein 503, mRNA (cDNA clone IMAGE:2967616), complete cds	245
9.1.4	Homo sapiens early B-cell factor 1 (EBF1), mRNA	246
9.1.5	Homo sapiens POU class 3 homeobox 1 (POU3F1), mRNA	248
9.1.6	Homo sapiens forkhead box P1 (FOXP1), transcript variant 1, mRNA	250
9.2	Recipes	256
9.3	Materials.....	257

CHAPTER 1:
INTRODUCTION

1. Introduction

1.1 Stem cells

Stem cells are undifferentiated cells which can divide indefinitely giving rise to daughter cells. These daughter cells can remain as stem cells or differentiate into any number of cell types as a result of signalling cues. Stem cells are found in most areas of the human body and help to maintain the population of cells in that area. These are termed adult stem cells and are multipotent, meaning they can differentiate, on cue, into several cell types which would reside in that area. For example, bone marrow mesenchymal stem cells can form cells of different connective tissues and bone. Pluripotent stem cells can differentiate into any cell of the developing embryo, excluding the extra-embryonic tissue, such as the placenta. The pluripotent stem cells are isolated from the inner cell mass of the developing embryo (Figure 1.1) and are termed embryonic stem cells (ESCs).

ESCs were first isolated from the mouse embryo (mESCs) by Evans & Kaufman (1981). They delayed embryonic development by performing an ovariectomy on mice which were 2.5 days post fertilisation and injected the mice with progesterone (Evans & Kaufman 1981). This caused the embryos to hatch from the zona pellucida, but not implant into the endometrium (Evans & Kaufman 1981). The embryos were then harvested 4-6 days later and cultured *in vitro* in droplets of media (Evans & Kaufman 1981). The blastocyst attached to the tissue culture plastic and the trophectoderm (which would form the extraembryonic tissue) grew out from the blastocyst attachment and differentiated (Evans & Kaufman 1981). The inner cell mass (ICM), remained as an egg-like structure as part of the blastocyst, this was removed and trypsinized (Evans & Kaufman 1981). The individual cells were grown on mitomycin-inactivated STO mouse embryonic fibroblasts, and then stem cell colonies formed. It took 17 years for human embryonic stem cells to be

successfully isolated and cultured, most likely due to the problems with obtaining human embryos, the ICM was isolated, following a previously utilised protocol to isolate rhesus monkey ESCs (Thomson et al., 1998b), by immunosurgery with rabbit antiserum to BeWO cells (a cell line isolated from a malignant gestational choriocarcinoma of the fetal placenta), grown on inactivated mouse embryonic fibroblasts (MEFis) (Thomson et al., 1998a). The human ESCs were found to express pluripotent cell surface markers and could still differentiate into cells of all 3 germ layers of the embryo after being cultured in a pluripotent state for several months (Thomson et al., 1998a).

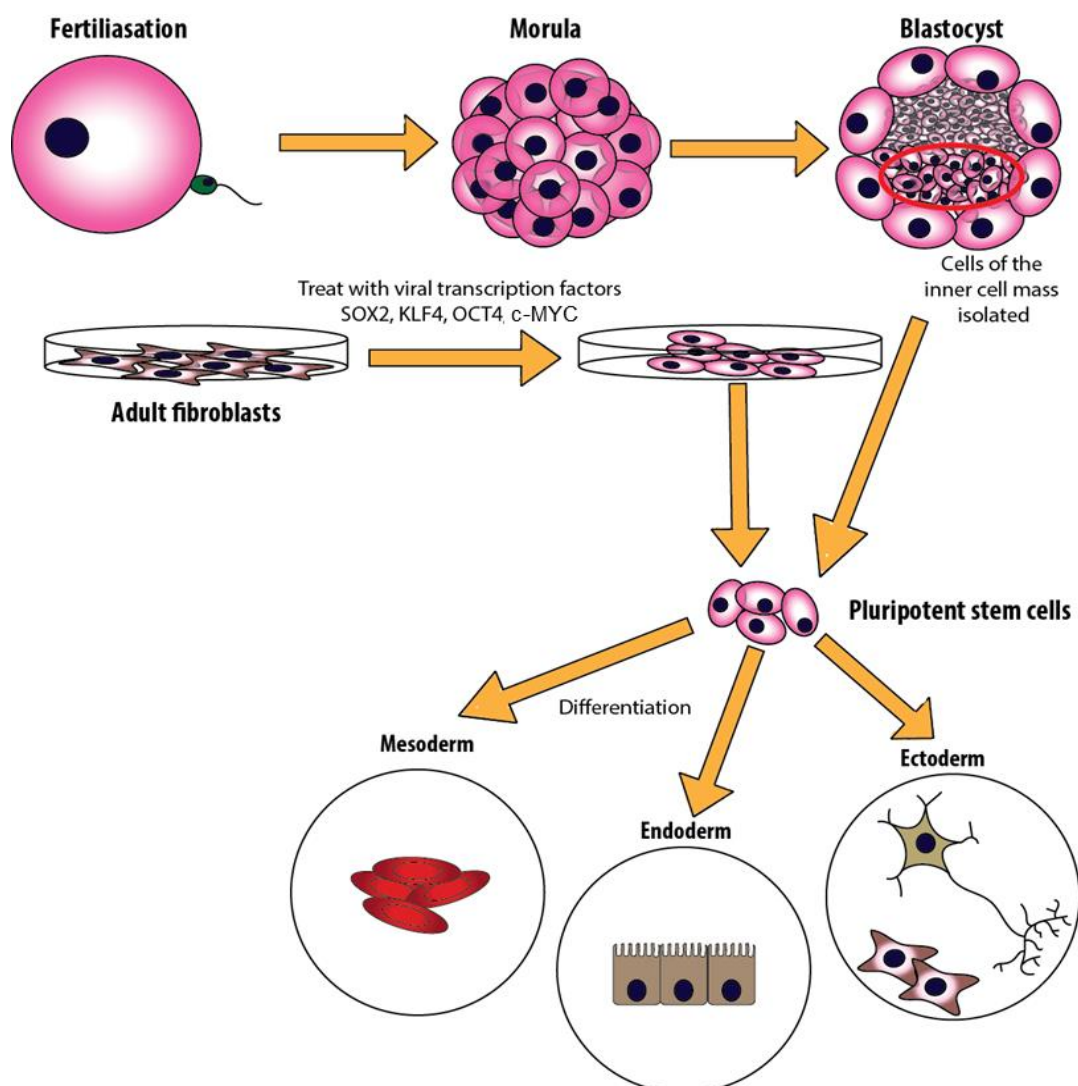


Figure 1.1: Derivation of embryonic stem cells and induced pluripotent stem cells. Embryonic stem cells are harvested from the inner cell mass of the fertilised embryo when the embryo has progressed through development to the blastocyst. Induced pluripotent stem

cells are derived from adult or embryonic fibroblasts and transduced with viruses containing the 4 pluripotent transcription factors OCT4, KLF4 SOX2 and c-MYC. Both sets of pluripotent stem cells can be cultured to form cells of all 3 germ layers of the developing embryo.

Induced pluripotent stem cells (iPSCs) have been derived from human and mouse fibroblasts. They were first derived from mouse embryonic and adult fibroblasts by retroviral transduction of 4 pluripotent transcription factors, *Oct3/4*, *Sox2*, *Klf4* and *c-Myc* (Takahashi & Yamanaka 2006). Mouse iPSCs were found to behave as pluripotent stem cells by forming colonies, expressing mouse ESC markers, enabled the formation of chimaeras when injected into a blastocyst and formed teratomas containing cells of all 3 germ layers when subcutaneously injected into the mouse (Takahashi & Yamanaka 2006). The derivation of human iPSCs occurred not long after, using the same transcription factors in 4 retroviruses, colonies were observed 25 days post induction with efficiency of induction of 0.02% and 3-6 integration sites of each of the viruses into the genome (Takahashi et al., 2007). The integration of the viruses into the genome was shown to cause tumorigenic properties, mostly through the action of *c-Myc*, with 20% of offspring from chimeras forming tumours (Okita et al., 2007). One study showed that the random integration of viruses into the genome can cause pluripotent reprogramming without the use of transcription factors (Kane et al., 2010). However, this was at a much lower efficiency of 0.000004% (Kane et al., 2010) in comparison to the 0.02% by Takahashi et al., (2007).

As a result of viral integration into the genome causing problems of tumorigenicity and random integration of viral DNA causing the dedifferentiation of cells, other methods have been sought to induce pluripotency. *LoxP* enzyme sites were introduced to the 5' and 3' ends of the coding region of the pluripotent transcription factors used for reprogramming, the cells were co-transduced with a doxycycline inducible Cre recombinase in order to excise the pluripotent transcription factors

that integrated into the genome on completion of pluripotent induction (Soldner et al., 2009). This was also done by Kaji et al., (2009), but instead of having 4 vectors one for each of the transcription factors, they utilised the 2A peptide linkers between the 4 genes in a non-viral vector which limited the number of integration sites. They also combined this vector with the use of *piggyBac* transposon integration to produce iPSCs, which allowed the removal of the integrated DNA and left no foreign DNA in the chromosome, (Kaji et al., 2009, Woltjen et al., 2009). Adenoviruses have also been used to induce pluripotency. However, there was still integration into the chromosomes (Okita et al., 2008). The recombinant proteins of the 4 pluripotent transcription factors that possessed a poly-arginine tag in order to enhance cell uptake have proved successful in inducing pluripotency when supplemented in the culture media at 8 µg/ml (Zhou et al., 2009). This was carried out in combination with valproic acid (VPA) treatment, a histone deacetylase inhibitor (HDACi), which has been shown to improve rate of pluripotency induction (Zhou et al., 2009).

In order to reduce the number of transcription factors involved in inducing pluripotency, several studies have been performed to reduce the number or totally eliminate the use of transcription factors. When brain derived neural stem cells were treated with the 4 transcription factors (Oct4, Sox2, c-Myc and Klf4) to induce pluripotency, dual inhibition of glycogen synthase kinase 3 (GSK3), and mitogen activated protein kinase (MAPK) alongside treatment with the cytokine leukemia inhibitory factor (LIF), improved aspects of pluripotency (Silva et al., 2008). These included Oct4 and Nanog stabilisation, X chromosome reactivation, transgene silencing and somatic and germline chimerism (Silva et al., 2008). It was found that c-Myc and Sox2 were not needed to induce pluripotency of these cells (Silva et al., 2008). The requirement for Oct3/4 in induction was superfluous when replaced with the transcription factor *GATA3* along with *KLF4*, *c-MYC* and *SOX2* (Montserrat et al., 2013). iPSCs were produced albeit at a lower efficiency at 0.001%, possibly due

to the decreased up-regulation of endogenous *OCT4* and *NANOG* expression as compared to using the original 4 transcription factors (Montserrat et al., 2013). The use of small molecules to induce pluripotency has also been explored. CHIR99021 (a GSK3 inhibitor) and tranilcypromine (an inhibitor of lysine-specific demethylase 1) have been used to induce human primary keratinocytes into iPSCs with the use of only *OCT4* and *KLF4* transcription factors (Li et al., 2009). TGF- β inhibition was found to replace the need for *Sox2* and *c-Myc* expression, by inducing *Nanog* expression (Maherali et al., 2009, Ichida et al., 2009). Building on the protocols by Li et al (2009), Maherali et al., (2009) and Ichida et al., (2009), only *OCT4* forced expression was required with the addition of VPA and 616452 (a TGF- β inhibitor), to induce pluripotency, with an efficiency of 0.002-0.03% (Li et al., 2011). To remove the need for any transcription factor for pluripotency induction, the removal of *OCT4* expression was investigated by using an *Oct4* promoter driven GFP expressing MEF cell line with *Sox2/c-Myc/Klf4* transduction and subsequent screening of thousands of small molecules, which induced GFP expression (Hou et al., 2013). Forskolin (an adenylate cyclase activator) was found to be sufficient and therefore was used in combination with the 4 molecules from Li et al., (2011), to induce pluripotency (Hou et al., 2013). Further enhancement of induction of pluripotency was carried out by addition of DZNep (a global histone demethylation inhibitor (Miranda et al., 2009)) at 16 days post treatment (Hou et al., 2013). DZNep reduced methylation of DNA and H3K9 at the *Oct4* promoter (Hou et al., 2013). The addition of the retinoic acid receptor ligand, TTNPB further enhanced efficiency of induction to pluripotency of MEFs to be comparable with transcription factor induced pluripotency at up to 0.2% (Hou et al., 2013).

Human ESC and human iPSC have been derived, which carry the *HTT* mutation, these can be utilised in disease modelling (Section 1.2.2.3)

1.2 Huntington's Disease

1.2.1 Huntington's Disease

Huntington's disease (HD) is a neurodegenerative disorder which arises from a genetic mutation, mapped to chromosome 4 in humans (Gusella et al., 1983). The gene affected is the *huntingtin* gene; the mutation consists of an elongated CAG repeat (over 36 repeats) in exon 1, encoding a polyglutamine stretch of amino acids at the N-terminus of the protein (The Huntington's Disease Collaborative Research Group 1993). This expanded CAG repeat leads initially to extensive but selective cell death of medium spiny neurones (MSN) in the striatum of the ventral forebrain, more specifically the enkephalin⁺ MSNs which synapse with the external globus pallidus (Albin et al., 1992, Richfield et al., 1995). There is a significant decrease in volume of the caudate nucleus (57%) and putamen (64%) as seen in post mortem (de la Monte 1988). Further to striatal degeneration, the volume of the substantia nigra decreases by about 40% (Oyanagi et al. 1989), the cerebral cortex by 21-29% volume (de la Monte et al., 1988) and a 35% neuronal loss in the CA1 region of the hippocampus (Spargo et al., 1993).

Patients with HD experience a decline in cognitive function, incoordination and uncontrolled movement of limbs, deterioration of speech, and depression being another common symptom (Walker 2007) with ~7-10% of the HD population resorting to suicide (Baliko et al., 2004, Di Maio et al., 1993). Finally, death occurs around 20 years from diagnosis (Folstein 1989) usually resulting from complications of falls, dysphagia or aspiration (Walker 2007). There is presently no cure, and current treatments are limited to medications and therapies to reduce symptoms, such as antidepressants, muscle relaxants and anticonvulsants (Ross & Tabrizi 2011). Clinical trials of neural transplantation into the striatum of HD patients to

replace those cells lost in the disease have met with varied levels of success (reviewed by Dunnett & Rosser 2007).

1.2.2 Huntington's Disease Modelling

1.2.2.1 Animal models of HD – excitotoxic models

A wide variety of Huntington's disease models have been generated (reviewed by Pouladi et al., 2013), from different species to different methods of generation. Before the genetic causation of HD was discovered, the use of excitotoxic lesion of the striatum was utilised to try and recapitulate motor phenotypes of the disease, which involved injection of glutamate receptor agonists such as ibotenic or kainic acid, causing selective loss of the GABAergic MSNs (McGeer & McGeer 1976, Schwarcz et al., 1984, Coyle & Schwarcz., 1976). However, this method of lesion creation also caused loss of the striatal interneurons and as a result the NMDA receptor agonist, quinolinic acid, was used due to its more specific effects (Beal et al., 1986, Schwarcz et al., 1983, Beal et al., 1991, Ferrante et al., 1993). These models result in rapid degeneration of the neurons in the striatum and therefore do not recapitulate the disease process.

1.2.2.2 Animal models of HD – genetic models

Once the genetic mutation was discovered, genetic models were made in mice, rats, sheep, mini-pigs and monkeys, as well as disease models of *Caenorhabditis elegans* and *Drosophila melanogaster* have also been created. These models either used full length *Htt* gene or truncated N-terminal fragment models, with expanded CAG repeats. Expression of the N-terminal fragment of the human *HTT* gene, with 150 CAG repeats, in sensory neurons of *C. elegans* caused aggregation of HTT protein, neuronal dysfunction and neurodegeneration of the sensory neurons (Faber et al., 1999), in contrast to expression of a 128 CAG repeat in mechanosensory neurons of *C. elegans*, there was no neuronal degeneration, but they were

insensitive to touch and there was nuclear accumulation of HTT aggregates (Parker et al., 2001). Studies in *D. melanogaster* have focussed on expression of the N-terminal fragment of mutant *HTT* in the compound eye of the *Drosophila*, all show neuronal degeneration of the rhabdomeres of the eye (Jackson et al., 1998, Steffan et al., 2001, Steffan et al., 2004, Lee et al., 2004, Kaltenbach et al., 2007), pan-neuronal expression of human mutant *HTT* also led to deficits in climbing behaviour and reduced survival of adults (Steffan et al., 2001, Steffan et al., 2004, Lee et al., 2004, Kaltenbach et al., 2007). Interacting proteins of mutant HTT have been identified, which have enhanced or reduced the phenotype of degeneration of rhabdomeres when overexpressed or knocked down (Kaltenbach et al., 2007). A full-length mutant *HTT Drosophila* model has also been created and shows similar deterioration of climbing behaviour when expressed pan-neuronally, there was also a Ca^{2+} -dependent increase in neurotransmitter release efficiency, loss of synaptic transmission, but an absence of nuclear accumulation of HTT protein aggregates (Romero et al., 2008).

Many mouse disease models have been created (reviewed by Pouladi et al., 2013), which recapitulate many aspects of the disease phenotype. One of the first models was the R6/1 and R6/2 mouse models, an N-terminal fragment human *HTT* with 116 and 144 CAG repeats respectively, although in the R6/2 mouse, the length of the CAG repeats showed instability, with an increase in the number of repeats (Mangiarini et al., 1996). This mouse model recapitulated the chorea observed in HD patients, and in the R6/2 mouse, the brains are smaller compared to wild-type littermate controls, with a decreased striatal size, but no neuronal loss (Mangiarini et al., 1996). HTT protein aggregates are also observed in the R6/2 mouse (Safren et al., 2014). Full length human HTT knock-in models have also been generated, with 140 CAG repeats which replicated increased locomotor activity during early disease progression, before progressing to a hypoactivity phenotype at later stages of the

disease, HTT nuclear aggregates are formed in the striatum, and layers II, III and deep layer V of the cerebral cortex and changes in gait are also observed (Menalled et al., 2003).

Transgenic mouse models of HD have also been created; one example is the YAC128 mouse, which was created by homologous recombination with yeast artificial chromosome to express the full length human HTT containing 128 CAG repeats, using human regulatory elements (Slow et al., 2003). The mice showed hyperactivity phenotypes originally, then progressing to motor deficits and hypokinesia with a decrease in performance on the rotarod test (Slow et al., 2003). HTT protein inclusions were observed at 18 months, as well as cortical and striatal atrophy, with an 8% decrease in number of MSNs, judged by DARPP32 expression (Slow et al., 2003). Rat models of HD have also been created by BAC transgenesis, expressing the full-length human protein, with 97 CAG/CAA repeats to increase stability of the CAG expansion (Yu-Taegar et al., 2012). These rats showed motor deficits (measured by rotarod, hindlimb clasp on tail-suspension, and shorter steps with increased stride width) and increased HTT aggregates (Yu-Taegar et al., 2012). Rhesus macaque monkey models have also been created, with 84 CAG repeats, which showed evidence of HTT nuclear inclusions, dystonia, chorea and difficulty swallowing (Yang et al., 2008).

1.2.2.3 Cellular models of HD

The use of animal models has been extremely helpful in discovering certain aspects of HD, however, many disease correcting effects of drugs from animal studies do not necessarily cross over in to human clinical trials with the same level of success (Kaye & Finkbeiner 2013), with the human brain size and organisation being fairly different in comparison to rodent models, the studies of which, form the bulk of the information and rationale for disease modifying drugs. Human tissue is hard to obtain to evaluate effects of disease and test out possible drug treatments.

Recently, human cell models have been created, either derived from embryos (ESCs), or through the formation of iPSC. iPSC and ESC models have been derived from monkey (Chan et al., 2010, Laowtammathron et al., 2010) and the R6/2 mouse (Castiglioni et al., 2012) as well as a rat neuroprogenitor cell model (Dong et al., 2011). Here, I focus on the human cell models of HD. Derivation of hESC from preimplantation genetic diagnosis *in vitro* fertilisation embryos has provided cell models with 37 and 51 CAG repeats, which showed partial and full penetrance of the phenotype, but there has also been evidence of instability of the CAG repeat length, neurons and astrocytes have been created from this cell source (Niclis et al., 2009). Further characterisation of these cell lines showed that dysregulated genes in HD remained comparable to the controls in these HD cells when differentiated into β III-tubulin (a neuronal marker)/GABAergic neurons, but there were elevated glutamate-evoked responses observed by a larger $[Ca^{2+}]_i$ (Niclis et al., 2013). MAP2⁺ (a mature neuronal marker) neurons have also been made from hESCs with various CAG repeat lengths in the *HTT* gene (Bradley et al., 2011). Other HD hESC, with 40-51 CAG repeats, have been differentiated to MAP2⁺ neurons for the purpose of analysing gene expression changes, with 3 genes being either up-regulated (coiled-coil helix coiled-coil helix domain containing 2, *CHCHD2*, tripartite motif containing 4, *TRIM4*) or down-regulated (protein kinase inhibitor β , *PKIB*) in the HD hESC in comparison to the control cells (Feyeux et al., 2012). These genes have a role in mitochondrial function (*CHCHD2*), and protein kinase A (PKA) dependent regulation (Feyeux et al., 2012). Transfection of hESC has also been used to deliver *HTT* exon 1 fragments with expanded CAG repeats (Lu & Palacino 2013). These have been differentiated into Tuj1⁺/MAP2⁺ neurons, (Tuj1, another neuronal marker), which showed insoluble mutant HTT protein aggregates and neurodegeneration, which was proportional to the levels of soluble monomeric mutant HTT (Lu & Palacino 2013). Basal culture of these neurons without growth

factors also led to neurodegeneration (Lu & Palacino 2013). Rhes, a HTT toxicity modifier, rescued the neurodegeneration observed; siRNA knock-down also decreased the amount of soluble monomeric HTT (Lu & Palacino 2013).

Park and colleagues (2008) were the first to report the derivation of a human HD iPSC line, which possessed the HTT gene with 72 CAG repeats and was subsequently differentiated into nestin⁺/PAX6⁺/SOX1⁺/OCT4⁻ neural stem cells and further differentiated into DARPP32⁺ neurons (~10%, Zhang et al., 2010). The derived neural stem cells showed increased caspase 3/7 activity on growth factor withdrawal, an important feature of HD pathology (Zhang et al., 2010). Further work on this cell line has highlighted the appearance of EM48⁺ HTT aggregates in neurons which were 27% DARPP32⁺ and 38% GABA⁺, however they only appeared after proteasome inhibitor treatment of the iPSC or after engraftment into a P2 mouse brain, and observed at 33 and 40 week post-transplant (Jeon et al., 2012). These neural precursors have provided behavioural recovery when implanted into the 12 month YAC128 mouse and GABAergic neurons are formed, and no HTT aggregates are observed at 12 weeks post transplantation (Jeon et al., 2014). The HD72 iPSC cell line has also showed disparity in protein expression compared to H9 control hESC line in the pluripotent state (Chae et al., 2012). Proteins involved in oxidative stress and programmed cell death, as well as cytoskeletal associated proteins (Chae et al., 2012). They also observed that cell death was increased in the HD iPSCs; neurite outgrowth was stunted in the HD iPSCs when differentiated into MAP2⁺ neurons, as well as a decreased efficiency of differentiation in the HD iPSCs compared to control (Chae et al., 2012). MicroRNAs (miRNAs) have been used to improve the phenotype of HD iPSC and also a HD transgenic mouse model, miR-196a decreased the number of mutant HTT aggregates in iPSC and in the transgenic mouse model (Cheng et al., 2013). TNF α (tumour necrosis factor α) dominant negative inhibitor (XPro1595) has suppressed the inflammatory response

of an astrocyte enriched culture derived from HD iPSC, and it also protects against cytokine induced toxicity of neurons derived from the same iPSC (Hsiao et al., 2014). The HD iPSC consortium recently published data using iPSC derived from HD patients, which showed gene expression changes between several HD iPS cell lines with varying lengths of CAG repeats and also showed decreased levels of cell adhesion in HD neuroprogenitor cells (HD iPSC consortium 2012). There was also a decrease in spontaneous and induced action potentials in HD neurons, an increased cell death in response to BDNF withdrawal in HD neurons and a change in Ca^{2+} dyshomeostasis in HD cells (HD iPSC consortium 2012). Another protocol, which formed neurons from HD iPSCs, one with 50 CAG repeats, the other with 109 CAG repeats, differentiated to neurons and were engrafted into the normal adult mouse brain and were characterised as phenotypically normal (Juopperi et al., 2012). However, when astrocytes were derived from these cells, cytoplasmic vacuoles were observed that appeared empty, which were more pronounced in the cell line with 109 CAG repeats (Juopperi et al., 2012). An increased number of lysosomes has also been observed in HD iPS cells (Camnasio et al., 2012).

A disease modifying approach has been attempted in the HD72 iPS cells derived by Park and colleagues, utilising homologous recombination of full length *HTT* with 21 CAG repeats, the cells were able to be differentiated into striatal neurons, and the cell death phenotype, increased caspase activity and BDNF levels were able to be rescued by the homologous recombination (An et al., 2012).

These data show that cell models of HD, reproduce aspects of the disease phenotype, can be differentiated into striatal neurons and can have the disease phenotype corrected by genetic manipulation. The range of cell lines available is increasing and therefore will allow for more models to be produced, with varying disease severity dependent on CAG repeat length. The protocols currently in use tend to make non-specified neurons, which do not allow characterisation of the

disease phenotype, as not all cells are affected to such an extent as the MSNs by HD. Provided a more reproducible differentiation protocol can be established to create the MSNs of the striatum, then dysfunction of the disease at the cellular level could be further investigated.

1.3 The Striatum

The striatum is one of the nuclei of the basal ganglia (Figure 1.2). The striatum is a collection of the caudate nucleus, putamen and nucleus accumbens. The striatum is made up of several populations of neurons, the majority being the MSNs constituting around 90% of the total population, the rest consisting of various populations of: interneurons, large acetylcholine⁺ neurons possessing long dendrites lacking branches (Bolam et al., 1984); several types of somatostatin⁺ medium aspiny neurons with cell bodies <20 µm in diameter, invaginated oval nuclei and long branched dendrites of up to 120 µm in length, receiving few inputs (Difiglia & Aronin 1982, Vincent & Johansson 1983), and; parvalbumin⁺ neurons (Gerfen et al., 1985). MSNs possess a cell body with a diameter of around 20-25 µm, have many branched dendrites that are densely populated with spines. The spines start to appear on dendrites ~20 µm from the soma and populate the dendrites all the way to the dendritic tip (Kemp and Powell 1971, Wilson and Groves 1980). The dendritic arbours spread between 150-250 µm in diameter and can synapse with many neighbouring neurons (Gerfen 1992). The axons form from a large dendritic trunk or through the cell soma tapering, the axon travels up to 1 mm to reach the globus pallidus (Wilson & Groves 1980).

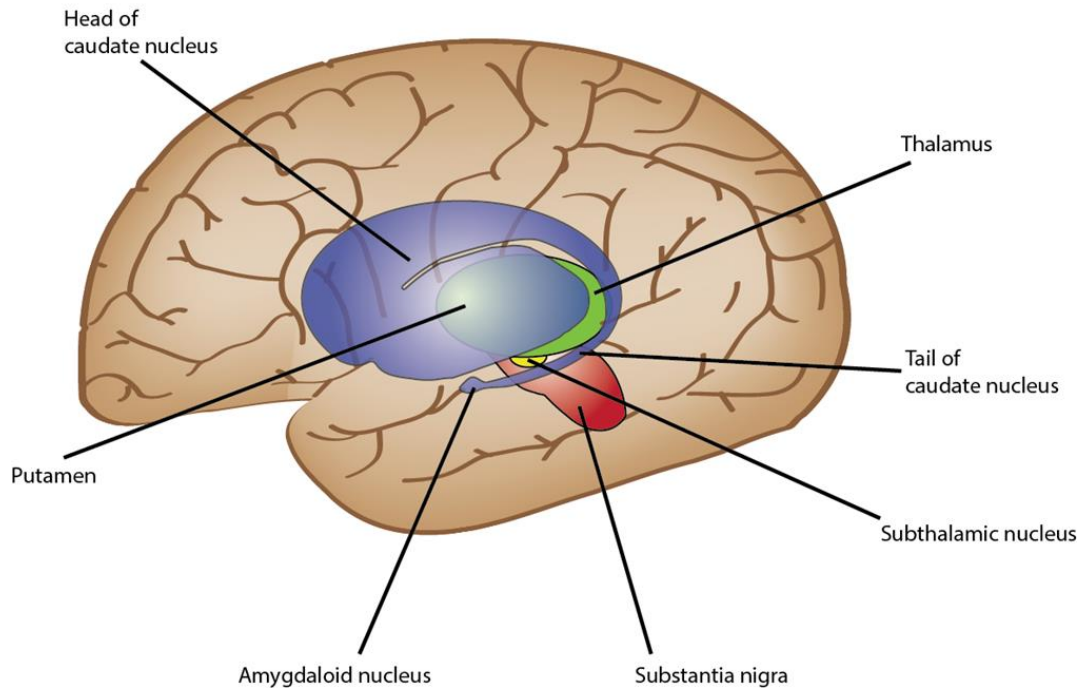


Figure 1.2: The basal ganglia in situ. The striatum (only caudate nucleus and putamen shown here) is located under the cerebral cortex and is anterior to the thalamus and substantia nigra. Adapted from Bradbury & Vehrencamp (2011)

The striatum receives inputs from the cortex and thalamus. More specifically, cortical input is predominantly from layer V of the cerebral cortex with secondary input from layers II, III and VI (Ferino et al., 1987, Jones et al., 1977, Royce 1982, Wilson 1987). The striatum also receives dopaminergic input from the midbrain (Bouyer et al., 1984). The input to the striatum from the midbrain predominantly synapses with the striatonigral neurons, with 59% of the tyrosine hydroxylase⁺ synaptic boutons, from the midbrain, synapsing on to the dendritic spines, and 35% on to the dendritic shafts of the striatonigral neurons (Freund et al., 1984). Midbrain input modulates the striatal response from cortical and thalamic input (Gerfen 1992). There are 3 types of synapses that form onto MSNs, those which contain round regular vesicles and synapse with spiny regions of dendrites (axo-spinous) (Hattori et al., 1970), some containing small vesicles of various shape and synapse with the cell body and dendrites, and synaptic boutons which contain large irregular shaped

vesicles which synapse with spines, dendrites and the soma (Wilson & Groves 1980).

Between 80 and 84% of rat MSNs are GAD⁺ (glutamic acid decarboxylase), staining with medium intensity, 3-5% of striatal neurons, smaller than MSNs with large invaginated nuclei stain intensely for GAD (Kita & Kitai 1988), therefore they are GABAergic and inhibitory on their targets of the globus pallidus, entopeduncular nucleus (Fonnum et al., 1978) and substantia nigra (Chevalier et al., 1985, Deniau & Chevalier 1985).

1.3.1 Types of Medium Spiny Neuron

There are two main efferent pathways from the striatum: striatonigral and striatopallidal, the striatonigral pathway has been demonstrated by applying glutamate to the striatum directly and recording the decrease in the substantia nigral neuronal firing (Chevalier et al., 1985, Deniau & Chevalier 1985). These pathways show differential expression of dopamine D1 α receptor or dopamine D2 receptor (Figure 1.3), dopamine D3 receptor is expressed in the striosomal patches of the nucleus accumbens and ventral putamen (Murray et al., 1994). The D1 receptor is localised to striatonigral neurons and the D2 receptor is expressed by striatopallidal neurons and this pattern of expression can be altered in a rat model of Parkinson's disease, where the nigrostriatal pathway is destroyed by excitotoxic treatment with 6-hydroxy dopamine (6-OHDA) (Gerfen et al., 1990). Here, the striatopallidal neurons increase the amount of D2 receptor mRNA and also enkephalin mRNA (another marker of striatopallidal neurons), this effect can be reversed using the D2 receptor agonist quinpirole (Gerfen et al., 1990). Excitotoxic treatment of the nigrostriatal pathway with 6-OHDA produces the opposite effect in the striatonigral neurons with a decrease of D1 receptor mRNA and substance P mRNA (another marker of striatonigral neurons), which is reversed when treated with the dopamine

D1 receptor agonist, SKF-38393, and this also increases the amount of dynorphin mRNA (a third marker specific to striatonigral neurons) (Gerfen et al., 1990).

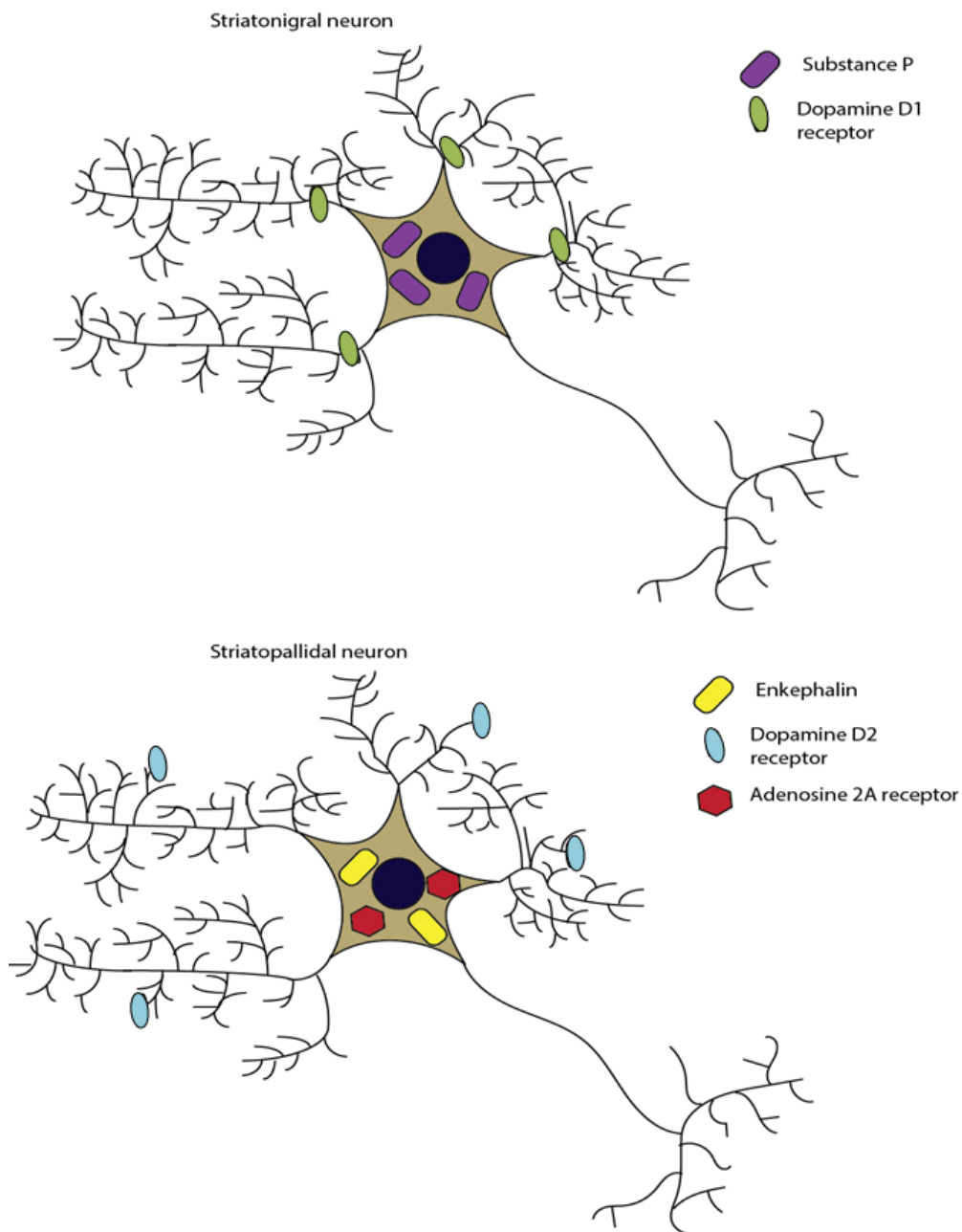


Figure 1.3: Schematic showing the types of medium spiny neuron in the striatum and their differential expression patterns. The top panel shows a striatonigral neuron which specifically expresses substance P and the dopamine D1 α receptor subtype. The expression of the dopamine receptor is localised to the dendrites of these neurons. Bottom panel shows the striatopallidal neuron, which expresses enkephalin, adenosine 2A receptor and the dopamine type 2 receptor subtype. The expression of the dopamine receptor in these neurons is localised to the spines of the neurons. Figure drawn using information in section 1.2.1

This dichotomy of the two pathways was confirmed by an electron microscope study of dopamine D1 and D2 receptor immunostaining in the rat striatum, where 53% of the medium spiny neurons stained for D1 receptor and 48% of the neurons were D2 receptor⁺, the main localisation of D1 receptor was on the dendrites with less in the spines and the D2 receptor was more localised to the spines than dendrites, also being observed in synaptic terminals whereas D1 receptor was not (Hersch et al., 1995). There was no co-localisation observed when performing dual staining for both receptors (Hersch et al., 1995). There has been some evidence of the dopamine D1 and D2 receptor mRNA not necessarily co-localising with substance P and enkephalin mRNA exclusively as 4% of both substance P⁺ and enkephalin⁺ neurons co-express either D2 receptors or D1 receptors, respectively. However D1 and D2 receptors did not co-localise (LeMoine & Bloch 1995). This was in contrast to what others have observed, using an *in vitro* fluorescent ligand to bind each of the receptor subtypes, D1 and D2 receptors co-localised on striatonigral neurons (Larson & Ariano 1994). In situ hybridisation studies in rat have shown a 26-27% co-localisation of D1 and D2 receptors in striatal neurons (Lester et al., 1993). Adora2a (adenosine A2 receptor) co-localises with the striatopallidal neurons that are dopamine D2 receptor⁺ and seldom seen in the D1⁺ neurons of the striatonigral pathway (Schiffman & Vanderhaegen 1993). Physiologically there was also a difference in the pathways. D1⁺ cells have a more hyperpolarised resting membrane potential and the cell capacitance is larger in D1⁺ neurons, reflected by an increased complexity when analysed using Sholl analysis (Gertler et al., 2008).

BAC transgenic mice, expressing GFP controlled either by dopamine receptor D1 promoter (*Drd1a EGFP* BAC mice) or the dopamine receptor D2 promoter (*Drd2 EGFP* BAC mice) have shown that GFP expression is localised to the medium spiny neurons. Retrograde labelling has demonstrated that all D1 receptor containing cells were synapsing in the substantia nigra, with less than 1% of D2 receptor cells

synapsing in the substantia nigra, D1 receptor cells would also project terminals to the lateral part of globus pallidus (Matamales et al., 2009). Another study utilising the *Drd1α EGFP* and *DRD2 EGFP* BAC transgenic mice profiled gene expression of the two separate populations by FACS sorting for the GFP⁺ cells and subsequent identification of differential gene expression between the two populations (Lobo et al., 2006). The striatonigral cells showed 8 genes were significantly up-regulated including *Ebf1* (early B cell factor 1, a transcription factor expressed in the developing striatum), *Zfp521* (a zinc finger protein which is an interacting partner of Ebf1), *Slc35d3* (solute carrier 35d3) and in the striatopallidal cells there were 23 genes specifically and significantly up-regulated including *Adora2a* (Lobo et al., 2006). They also showed that only the striatopallidal neurons expressed proenkephalin (Lobo et al., 2006). They also used a *Chrm4:EGFP* BAC transgenic mouse, which uses the promoter of μ opioid receptor 1 and is localised to the striatonigral neurons (Lobo et al., 2006). They crossed this with an *Ebf1*^{-/-} knockout mouse and showed there was a decrease in the number of striatonigral cells postnatally and determined it was a problem of synapse formation and not the inability of the cells to differentiate (Lobo et al., 2006).

1.3.2 Compartmentalisation of the Striatum

The striatum is also divided into two compartments, the striosomal patch and matrix compartments. The patches show an increased expression of μ opiate receptor (Herkenham & Pert 1981), and a diminished expression of acetylcholinesterase (Graybiel & Ragsdale 1978). The striatonigral and striatopallidal neurons arise from both areas as judged by substance P, dynorphin and enkephalin positivity and they are fairly evenly distributed ~45-60% of the neurons are positive for each of the markers of striatonigral and striatopallidal neurons in the patch and matrix compartments (Gerfen & Young 1988). A biocytin labelling study of neurons in the matrix compartment showed 3 types of neurons: striatopallidal cells which had the

most dense arborisations in the globus pallidus compared to the other types: a second type synapsing in the entopeduncular nucleus and substantia nigra pars reticulata with an axon collateral to the globus pallidus, and; a third type which synapsed with the substantia nigra with an axon collateral to the globus pallidus (Kawaguchi et al., 1990). Retrograde labelling of striatopallidal neurons in the non-human primate by horse radish peroxidase-wheat germ agglutinin and fluorescent dyes showed that striatopallidal neurons originate in the caudate and putamen with the majority arising from the matrix compartment (Giménez-Amaya & Graybiel 1990). Also a level of organisation was maintained from origin to target, efferent neurons leaving the rostral pole of the caudate and putamen synapse in the rostral portion of the globus pallidus and the same organisation was conserved along the dorsal/ventral axis (Giménez-Amaya & Graybiel 1990). The nucleus accumbens and olfactory tubercle were not labelled in the study and when the two different dyes were used in the external and internal segments of the globus pallidus, there was intermingling of neurons in the striatum (Giménez-Amaya & Graybiel 1990). Anterograde axonal tracing of neurons from midbrain to striatum has shown that neurons go to both the patch and matrix compartments and three types of neurons have been identified type A possess a large plexus of dendrites, with thin fibres and small varicosities; type B also have a large plexus of dendrites with thicker fibres and slightly larger varicosities, and; type C neurons are the minority of cells with larger fibres possessing larger varicosities (Gerfen et al., 1987a). Cells arising in the ventral tegmental area are dopaminergic type A neurons, which synapse in the dorsal MOR1⁻ matrix compartment of the striatum, cells of the dorsal tier of substantia nigra pars compacta are also dopaminergic type A cells and synapse in the MOR1⁻ matrix, the ventral tier of substantia nigra afferents are dopaminergic type B neurons and synapse with the MOR1⁺ patches, remaining cells from the substantia nigra are non-dopaminergic type C neurons which synapse in the matrix

(Gerfen et al., 1987a). The dopamine afferents that synapse in the patch compartment arrive first in the striatum during development as 6-hydroxy-dopamine injections into the new-born rat striatum leads to selective death of these cells which innervate the striosomal patch compartment, whereas the matrix-innervating dopaminergic cells are spared and survive (Gerfen et al., 1987b).

1.4 Development of the Striatum.

The central nervous system forms from the ectoderm layer of the three germ layers after gastrulation of the embryo. The ectoderm undergoes a process of neural induction to form neuroectoderm and then neurulation to form the neural tube. The neural tube lies dorsal to the notochord and prechordal plate, important ventral midline organising centres, in the embryo. Molecular patterning and folding of the neural tube gives rise to the prosencephalon, which lies most anteriorly and is subdivided into the most anterior telencephalon and diencephalon. Posterior to these structures is the mesencephalon and rhombencephalon. Here, I will focus on the development of the telencephalon, the anterior portion of neural tube that gives rise to the forebrain.

1.4.1 The Telencephalon

The telencephalon is divided into two main sections (Figure 1.4), the dorsally located pallium and the more ventrally located subpallium (Campbell 2003, Evans et al., 2012). The pallium forms the neocortex and the subpallium forms the striatum, globus pallidus and the origin of the olfactory bulb (Evans et al., 2012). The subpallium is divided into three substructures; the lateral ganglionic eminence (LGE), the medial ganglionic eminence (MGE), the caudal ganglionic eminence (CGE) and the septum. The LGE is the source of the MSNs, which locate ventrally and anteriorly populate the caudate and putamen of the striatum, nucleus accumbens and olfactory tubercle (Deacon et al., 1994, Evans et al., 2012,

Wichterle et al., 2001). In general, the cells from the caudal LGE, give rise to the MSNs of the nucleus accumbens and those of the dorsal anterior LGE; the olfactory bulb granule layer (Wichterle et al., 2001). The ganglionic eminences form as a result of cells being produced and migrating ventrally throughout the following zones during differentiation. Cells are produced from the ventricular zone (VZ), which lies on the border of the lateral ventricles, spanning the two ganglionic eminences (GEs), the second proliferative region the subventricular zone (SVZ) is more ventral to this and spans the VZ, the final region is non-proliferative and is where neural differentiation mostly occurs, the mantle zone (MZ), which spans the SVZ (Evans et al., 2012).

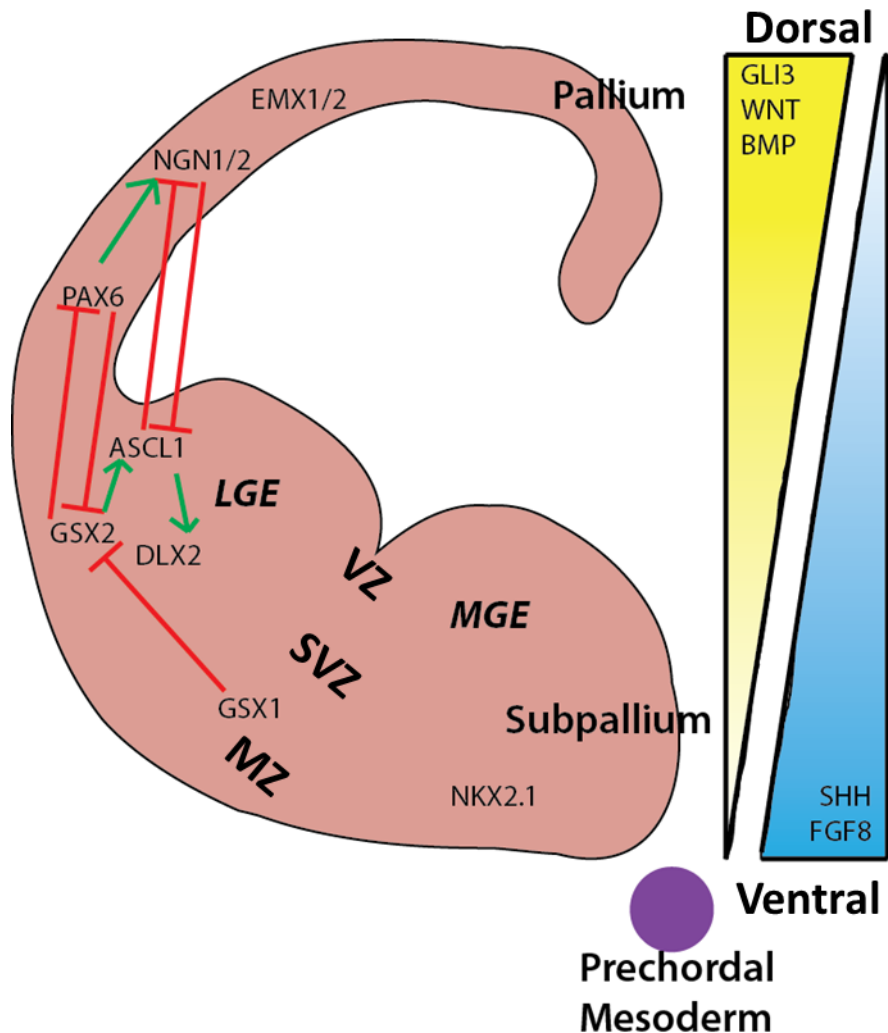


Figure 1.4: Molecule signalling and morphogen gradients in the developing telencephalon. A ventro-dorsal gradient of signalling molecules SHH and FGF8, and a dorso-ventral gradient of WNT, BMP and GLI3 is established in development and plays an important role of patterning development of the dorsal and ventral forebrain. The pallium will give rise to the cerebral cortex and the subpallium the striatum and globus pallidus. The LGE and MGE, which make up the subpallium, are indicated and the molecular interactions which take place between the regions of LGE and pallium are indicated on the diagram. VZ = ventricular zone, SVZ = subventricular zone, MZ = mantle zone (Adapted from Evans et al., 2012).

Unlike the rest of the CNS, the forebrain is not influenced by signals from the notochord, as it is not present and the prechordal plate adopts this role (Shimamura & Rubenstein 1997). The notochord and prechordal plate lie ventral to the developing neural tube and are involved in the patterning of the ventral neural tube. This was shown by the removal of the prechordal plate and the subsequent loss of *Nkx2.1* gene expression (a marker of the ventral telencephalon) in the MGE of the

developing telencephalon and ectopic expression of *Nkx2.1* laterally when the prechordal plate was transplanted to the lateral telencephalon (Shimamura & Rubenstein 1997). The anterior neural ridge (ANR) is also a source of patterning signals in the telencephalon and resides at the junction between the anterior neural plate and anterior non-neural ectoderm (Shimamura & Rubenstein 1997). The interactions between the following signalling pathways are an important factor for designing a differentiation protocol in order to derive ventral forebrain neural precursors. This is beyond the scope of this study and has been optimised by Joy et al., (unpublished data).

1.4.2 FGF8 signalling

The identity of the signalling molecule that originates from the ANR is FGF8, as identified by removing the ANR and replacing it with an FGF8 soaked heparin bead (Shimamura & Rubenstein 1997). Removing the ANR led to a loss of expression of *Foxg1* (Shimamura & Rubenstein 1997), a forebrain marker important for patterning the telencephalon (Section 1.4.6 The role of FoxG1), and this loss of expression has also been observed in the *Fgf8*^{-/-} mouse knockout, in addition to a decrease in cell proliferation and up-regulation of apoptosis (Storm et al., 2006). *Fgf8*^{-/-} knockout mice developed abnormally with a reduction in size of the telencephalon possessing only one ganglionic eminence and also showing aberrant expression of genes in the telencephalon (Storm et al., 2006). There was rostral and caudal expansion of *Otx2* and *Wnt8b* expression domains, *Bmp4* expression was absent from the rostro-dorsal midline at E9.5, and reduced expression of *Nkx2.1* and *Shh* in the ventral telencephalon concomitantly with ventral expansion of *Pax6* expression, a dorsal marker (Storm et al., 2006). In the zebrafish, *ace* (zebrafish *Fgf8* homologue) was required for the development of midline structures in the telencephalon and also for the differentiation of the basal telencephalon with the reduction of *nkx2.1b* (zebrafish *Nkx2.1* homologue), *lim1* and *lim6* expression observed in the *ace*^{-/-}

mutant (Shanmugalingam et al., 2000). In the *Fgfr* triple mutant mouse, targeted deletion of *Fgfr1*, *Fgfr2* and *Fgfr3* led to a total loss of FGF signalling in the forebrain, the telencephalon failed to develop with loss of expression at E12.5 of *Foxg1*, dorsal telencephalic marker *Emx1* and ventral markers; *Dlx2*, *Nkx2.1* and *Gli1* and *Shh* expression were downregulated implying that FGF signalling regulates *Shh* expression (Paek et al., 2009). The role of FGF signalling in the anterior neural plate seems to be in promoting survival and proliferation of the *Foxg1*⁺ cells (Paek et al., 2009). FGF15 was also observed to play a role in telencephalic development but its expression was repressed by FGF8 in the telencephalon and FGF15 is responsible for cortical maturation (Borello et al., 2008).

1.4.3 Sonic hedgehog signalling

Sonic hedgehog (SHH) acts as a morphogen and its signalling pathway is shown in Figure 1.5. The importance of SHH signalling in the development of the CNS and its expression from the notochord was established by Echelard et al., (1993). In the forebrain, the prechordal mesoderm was implicated (Shawlot & Behringer 1995) as the organiser of the ventral forebrain and the *cyclops* mutant zebrafish has demonstrated the role of the prechordal mesoderm as a continuation of the notochord (Hatta et al., 1994). The expression of SHH was adopted by the prechordal mesoderm (Shimamura et al., 1995) and this leads to the induction of *Nkx2.1* specifically in the forebrain, the expression of *Nkx2.1* was first observed at the 3 somite stage in the medial prosencephalic neural plate (Shimamura & Rubenstein 1997). *Nkx2.1* expression later is a marker of the MGE. *Shh* expression was identified as being limited to the MGE in development and co-expressed with *Nkx2.1* in the rat telencephalon from E11.5 onwards (Kohtz et al., 1998). SHH was required for the development of the LGE, but in lower concentrations than needed for the MGE, as observed in rat telencephalic explants, where there was a

generation of *Dlx⁺/Isl1⁺/Ikaros⁺* ventral-like cells (Kohtz et al., 1998). When these explants were cultured in the absence of SHH, there is the generation of dorsal progenitors as SHH represses the dorsal markers *Emx1* and *Tbr1* (Kohtz et al., 1998). *Shh* or activated *Smo* viral injections into the forebrain induced *Nkx2.1* expression medially or *Dlx2* and *Gsx2* more laterally (Rallu et al., 2002). Retroviral injections of *Shh* into mouse amniotic cavity (E8.5) or telencephalic ventricles (E9.0) led to an enlarged single telencephalic ventricle (Gaiano et al., 1999). *Nkx2.1* and *Crbp1* (cellular retinol binding protein 1) were expressed in *Shh* infected and adjacent cells whilst dorsal midline structures were lost and aberrant *Dlx2* expression was observed in the dorsal telencephalon (Gaiano et al., 1999). In the chick lateral neural plate explants, exogenous *Shh* was shown to induce *Nkx2.1* and *Isl1* (Ericson et al., 1995). In the *Shh^{-/-}* mouse, the notochord was degenerated and the ventral forebrain was lost resulting in a single vesicle present in the midline in the forebrain that is *Emx1⁺* (Chiang et al., 1996). Also, in the *Shh^{-/-}* mutant there was a lack of maintenance of *Fgf8* expression post developmental stage E9.0 (Chiang et al., 1996), there was no *Nkx2.1* expression but *Dlx2* and *Gsx2* expression persists at the ventral midline, implying that SHH is not necessary for their expression (Rallu et al., 2002). SHH also induced endogenous dopamine neurons with the help of FGF8 signalling in the developing telencephalon (Ye et al., 1998).

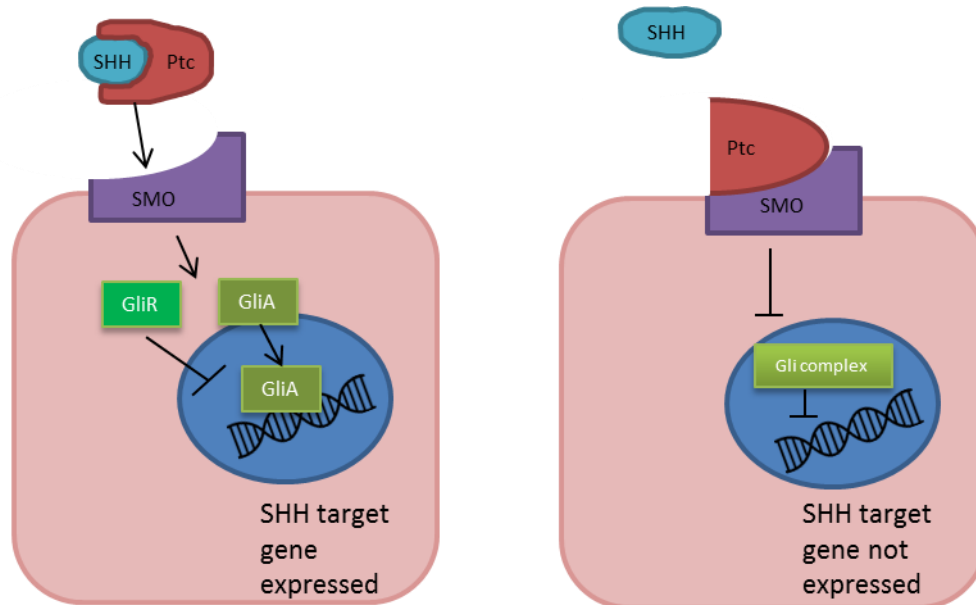


Figure 1.5: Schematic of the SHH signalling pathway. SHH, when present, binds to the molecule Patched (Ptc) and binds to the cell receptor Smoothened (SMO). This leads to downstream activation of the GLI family of transcription factors and target genes of SHH are expressed. When SHH is not present, Ptc binds SMO and inhibits the GLI complex of transcription factors therefore inhibiting the expression of SHH target genes. (Adapted from Evans et al., 2012)

As demonstrated in Figure 1.5 SHH acts by signalling via the GLI family of zinc finger transcription factors, by binding the receptor *Smoothened* (Evans et al., 2012). The *Foxg1^{Cre} Smo^{fl/fl}* mouse showed a loss of ventral telencephalon patterning, with a lack of *Nkx2.1*, *Gsx2*, *Ascl1* and *Dlx2* mRNA, plus *Pax6* and *Ngn2* expression was evident throughout the dorsal and ventral telencephalon and the other dorsal marker *Emx2* displayed a ventral expansion in expression, also the GEs failed to form and the other dorsal marker *Ngn2* was present throughout the VZ (Fuccillo et al., 2004). GLI3 was shown to repress *Shh* expression and vice versa (Rallu et al., 2002). The *extratoes* mouse mutant, *Gli3^{-/-}*, demonstrated that *Gli3* expression is complementary to that of *Shh*, as the pallium is completely lost and the basal ganglia occupy a dorsal position in the telencephalon with the dorsal markers *Emx1/2* were undetected (Theil et al., 1999). In the same mutant, the ventrally expressed *Isl1* and *Dlx2* expanded their expression into the dorsal telencephalon (Tole et al., 2000). In the *extratoes* mouse, that carries a naturally

occurring mutation in *Gli3*, there was also a failure of the telencephalic roof to invaginate and the dorsally located choroid plexus and cortical hem fail to form, which led to disruption in Wnt and BMP signalling (Tole et al., 2000, Grove et al., 1998, Theil et al., 1999). The double knockout mouse for *Shh*^{-/-};*Gli3*^{-/-} had a larger telencephalon than the *Shh*^{-/-} mouse, the ventral markers *Dlx2*, *Gsx2* and *Ascl1* were almost restored to wild type levels, *Pax6* was not co-expressed with *Gsx2* and there were low levels of *Nkx2.1* ventromedially and a small MGE-like structure formed (Rallu et al., 2002). Another GLI family member, *Gli1* usually expressed at the border between MGE and LGE was lost in the *Shh*^{-/-} mutant and *Shh*^{-/-}; *Gli3*^{-/-} mutant and *Ptch1* (*Ptc*), usually expressed in the MGE, was also lost in the *Shh*^{-/-} mutant but its expression was slightly retained in the *Shh*^{-/-}; *Gli3*^{-/-} double mutant (Rallu et al., 2002).

1.4.4 Retinoic acid signalling

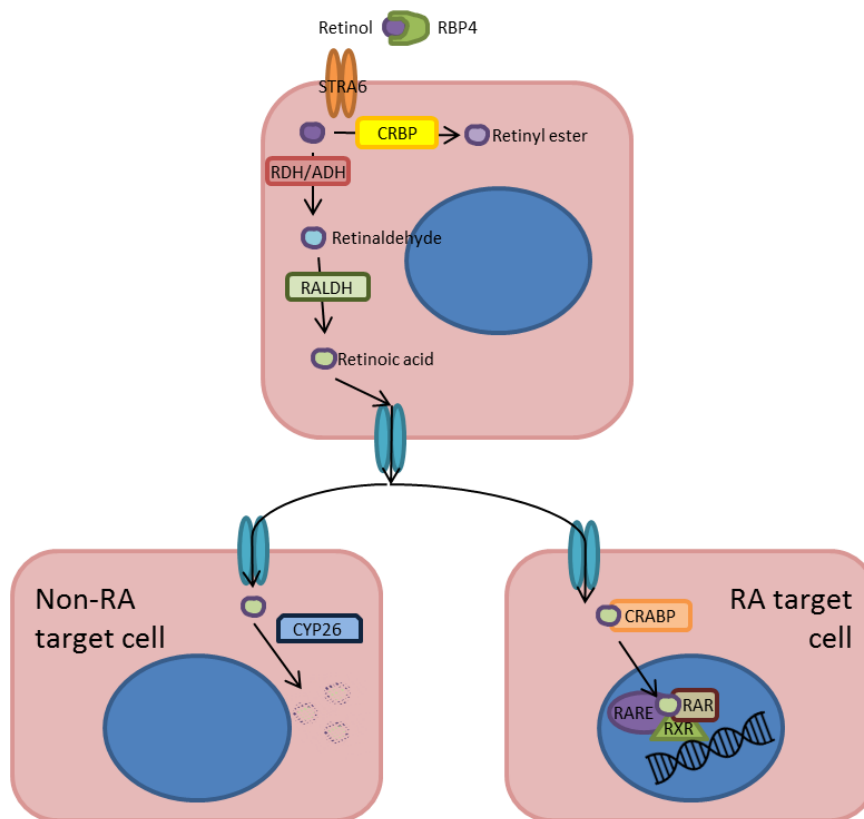


Figure 1.6: Retinol processing and the retinoic acid signalling pathway. Retinol is carried in serum by retinol binding protein (RBP4), which is secreted from the liver. Retinol enters the cell (top) via STRA6 receptor and inside the cell, either binds to cellular retinol binding protein (CRBP) and this facilitates the conversion of retinol to retinyl ester for storage, or in retinoic acid generating tissue, retinol becomes oxidised by alcohol/retinol dehydrogenase (ADH/RDH) to retinaldehyde. Retinaldehyde is then oxidised by retinaldehyde dehydrogenase (RALDH) to retinoic acid (RA). RA is then released to surrounding cells and when taken up by cells (left) that express cytochrome P450 (CYP26), RA is oxidised and therefore degraded. Some RA target cells (right) express cellular retinoic acid binding protein (CRABP), which facilitates RA uptake, and transports it to the nucleus where RA binds to retinoic acid receptor (RAR). The ternary complex of RA-RAR-RXR and retinoic acid response element (RARE) regulate transcription of RA targets.

The various stages involved in producing retinoic acid (RA) and how RA then acts on cells can be seen in Figure 1.6. MEIS2 is a marker of striatal progenitors in the intermediate telencephalon in the mouse and chick embryo and was required during striatal development (Toresson et al., 2000b, Marklund et al., 2004). In chick intermediate telencephalon explants harvested at progressively later stages of development, MEIS2 expression was upregulated, therefore was induced later *in vivo* (Marklund et al., 2004). RA was required for the specification of MEIS2⁺ cells in

the chick and RALDH3, an enzyme required for the formation of RA (Figure 1.6), was expressed at HH (Hamburger-Hamilton) stage 14 in the ventral and intermediate telencephalon in the chick (Marklund et al., 2004) and at E8.75 in the mouse frontonasal surface ectoderm and later at E12.5 in the LGE (Molotkova et al., 2007). In the *Raldh2^{-/-};Raldh3^{-/-}* mouse, there was no requirement of RA for the expression of *Meis2*, which was in disagreement with what was observed in the chick development (Molotkova et al., 2007). However, *Meis2* expression was up-regulated in P19 EC cells by the addition of RA and the LGE was shown to be a source of retinoids possibly via the radial glia which can provide migrating striatal cells with retinoids and aid striatal differentiation (Toresson et al., 1999).

Citral inhibited the synthesis of RA and when a citral-soaked bead was inserted into the HH stage 10 rostral margin of the forebrain in the chick, the whole telencephalon failed to form (Schneider et al., 2001). Using a retinoic acid receptor (RAR) antagonist soaked bead led to a loss of *fgf8* and *shh* expression in the forebrain only 12 hours post implantation and at 72 hours, there was a decrease in *foxg1*, *nkx2.1* and *dlx2* (Schneider et al., 2001). However, in the *Raldh2^{-/-};Raldh3^{-/-}* mouse, there was no effect on FGF8 and SHH signalling in the forebrain (Molotkova et al., 2007).

In *Raldh3^{-/-}* mutant mouse embryos, there was no loss of RA activity in the early forebrain but there was an absence of dopamine receptor D2 in the nucleus accumbens and depletion in RAR β in the striatum at E18.5 (Molotkova et al., 2007). There was also a decrease in the amount of GAD67⁺/TUJ1⁺ neurons produced *in vitro* from E14.5 *Raldh3^{-/-}* mouse mutant embryos (Chiatzi et al., 2011). The ectopic expression of RAR β 1 in cortical explant culture was shown to selectively up-regulate expression of DARPP32 (Liao & Liu 2005), and in the RAR β ^{-/-} mouse there was a depletion of DARPP32, tyrosine phosphatase (Liao et al., 2005), dynorphin, MOR1 and tyrosine hydroxylase (Evans et al., 2012).

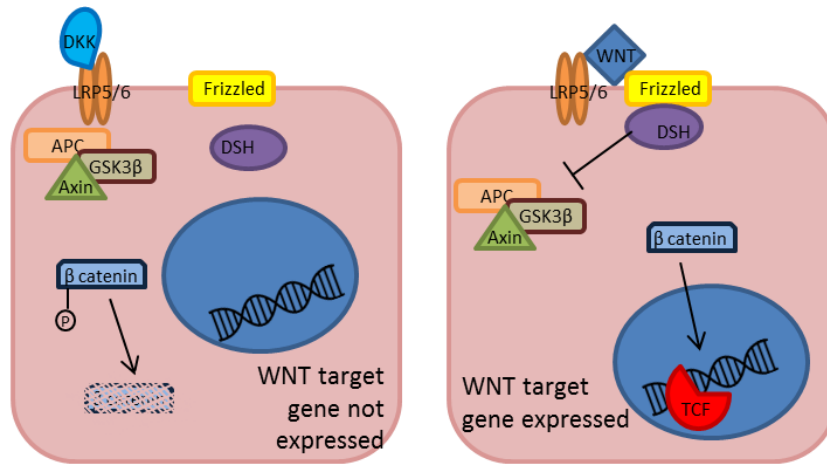


Figure 1.7: The canonical WNT signalling pathway. In the absence of WNT, its receptor Frizzled and co-receptor LRP5/6 are not bound and Dickkopf (DKK) binds LRP5/6, this allows glycogen synthase kinase 3 β (GSK3 β) to phosphorylate β -catenin which results in the degradation of β -catenin. When WNT is present, it binds the receptors Frizzled and LRP5/6 and Dishevelled (Dsh) is activated to repress GSK3 β , therefore preventing β -catenin phosphorylation, stabilising it and allowing β -catenin to translocate to the nucleus and induce transcription via the TCF/LEF family of transcription factors. (Adapted from Evans et al., 2012)

1.4.5 WNT and BMP signalling

WNT signalling is important for the patterning of the dorsal telencephalon, the canonical WNT pathway can be seen in Figure 1.7. A *frizzled* related WNT antagonist, TLC, is secreted from the anterior boundary of the neural plate in the zebrafish and promotes telencephalic gene expression in a concentration-dependent manner, and disruption of this gene leads to abnormal telencephalic development, a likely target of TLC is *Wnt8b* as it controls regional identity in the anterior neural plate (Houart et al., 2002). The expression of *tlc* was reduced in embryos lacking BMP signalling and in the *Bmp* knockout, implantation of *tlc* expressing cells led to restoration of *emx1* and *fgf8* expression (Houart et al., 2002). In explants of HH stage 8 chick dorsal neural fold combined with dorsal epidermal ectoderm, the dorsal telencephalic marker *emx1* was induced in culture (Gunhaga et al., 2003). Several *wnt* genes were candidates for controlling dorsal telencephalon development; *wnt1* and *wnt4* were expressed in dorsal epidermal ectoderm at HH stage 8 and *wnt8b* in the dorsal telencephalon at HH stage 10 chick

embryos (Gunhaga et al., 2003). Wnt3a blocked the differentiation of ventral telencephalic cells by inhibiting *nkx2.1* and it increased cell proliferation and *pax6* and *ngn2* expression, but *fgf8* was additionally required in order to express the other dorsal marker *emx1* (Gunhaga et al., 2003). The wnt antagonist, Frz receptor 8, blocked the expression of *pax6* and *emx1* in the developing chick telencephalon (Gunhaga et al., 2003). Inactivating the Wnt target, β -catenin, before neurogenesis led to a decrease in *Emx1/2*⁺ and *Ngn2*⁺ cells and an increase in the number of *Gsx2*⁺, *Ascl1*⁺ and *Dlx2*⁺ cells in the mouse pallium, and activating the canonical Wnt pathway in the subpallium decreased the expression of the ventral telencephalic markers and up-regulated dorsal markers (Backman et al., 2005). Using *lef1*, a wnt nuclear effector, morpholino in zebrafish knocked down wnt signalling and reduced the expression of the pallial markers *tbr1* and *lhx5* (Danesin et al., 2009).

BMP expression was also recorded as inhibiting ventral telencephalic fate and promoting a dorsal fate. BMP 2,4,5 & 7 were expressed in the pallium in the mouse and were important for the formation of the choroid plexus and expression of *Msx1* and *Hfh4*, *Foxg1* expression was excluded from BMP expression domains (Furuta et al., 1997). BMP 4 & 5 inhibited expression of subpallial markers: *nkx2.1*, *shh*, *dlx2*, and the neural tube displayed excessive cell death in the developing chick embryo when ectopically expressed in the chick neural tube (Ohkubo et al., 2002, Golden et al., 1999).

1.4.6 The role of FoxG1

FoxG1 is a forkhead-containing transcription factor belonging to the HNF3 family of transcription factors. Its expression was first isolated in the rat neural tube and was subsequently localised to the developing telencephalon (Tao & Lai 1992). In a later study, *Foxg1* was observed to be also expressed in the anterior optic vesicle, otic vesicle, facial and head ectoderm, olfactory epithelium, midbrain/hindbrain junction

and in the pharyngeal pouches (Hérbert & McConnell 2000). In the *Foxg1* null mutant mouse, there was a severe decrease in the size of the cerebral hemispheres with a 95% decrease in their mass at birth and a reduction in striatal and hippocampal volumes (Xuan et al., 1995, Eagleson et al., 2007). The development of the ventral telencephalon was impaired more than the dorsal telencephalon, with the main problem that there was a decrease in cell proliferation, as the cell cycle time increases (Martynoga et al., 2005). The cells of the telencephalon were specified too early, with an accumulation of post-mitotic neurons in the MZ and a doubling of the number of β III-tubulin⁺ cells in the SVZ, therefore depleting the progenitor population (Martynoga et al., 2005). The difference in phenotype, between wild type and *Foxg1* knockout, was noticed at E10.5 when the telencephalic vesicles were noticeably smaller and the cortex had an irregular and uneven surface (Xuan et al., 1995). The ganglionic eminences were not present at E12.5 and comprised of a neuroepithelial sheet and all of the telencephalic tissue was *Emx1/2*⁺/*Pax6*⁺, and *Dlx1/2* were undetectable (Xuan et al., 1995). In the *Foxg1*^{-/-} mouse, the expression of *Nkx2.1* was not observed in the prosencephalic neural plate of the prospective telencephalon at E8.5, but *Nkx2.1* was expressed in the prospective diencephalon, *Gsx2* and *Ascl1* (ventral telencephalon markers) were not expressed later in development and at E10.5 there was a decrease in *Fgf8* expression (Martynoga et al., 2005). Using *foxg1* morpholino knock down in zebrafish caused a deficiency of ventrally expressed genes including *dlx2* and *nkx2.1b* (the zebrafish *Nkx2.1*) and ventral expansion of *emx3* (Danesin et al., 2009). *Foxg1* in the zebrafish was shown to have a role of maintaining the dorsal/ventral boundary in the telencephalon and it also maintained ventral telencephalic progenitors, preventing them from aberrantly forming part of the hypothalamus, it also restricted the canonical *wnt* pathway to the dorsal telencephalon and was shown specifically to inhibit *wnt8b* (Danesin et al., 2009).

Foxg1 has been observed to act cell autonomously, as shown in chimeric mice, to ensure competence of the cells to respond to ventralising signals, as cells which were *Foxg1*^{-/-} in wild type mice did not express *Gsx2* and *Ascl1* in the ventral telencephalon but surrounding wild type cells did express these ventral markers and these *Foxg1*^{-/-} cells expressed dorsal markers including *Pax6* and *Ngn2* when in the dorsal telencephalon (Manuel et al., 2010). These *Foxg1*^{-/-} cells had lower rates of proliferation and the expression of *Pax6* (a cell cycle regulator) was lower in the dorsal telencephalon in these cells, overexpression of *Pax6* in a *Pax77* mouse line crossed with the *Foxg1*^{-/-} chimeric mice restored the levels of *Pax6* expression and increased cell proliferation in these mice, however proliferation was still below the levels seen in wild type mice, showing *Foxg1* to be a cell autonomous regulator of progenitor proliferation (Manuel et al., 2011).

1.4.7 The roles of *Dlx1/2*, *Gsx1/2* and *Ascl1*

Gsx2 is a dispersed homeobox gene resulting from a 2 kb transcript and was shown to be expressed in the ganglionic eminences of the telencephalon by *in situ* hybridisation (Hsieh-Li et al., 1995, Valerius et al., 1995). *Gsx2* is a downstream target of SHH, first detected in the neuroepithelium of the E9 telencephalic vesicle in the mouse and the *Gsx2* knockout showed a distinct decrease in the size of the LGE at E12.5-14.5, the striatal volume reduced by 55%, the expression of *Dlx2* was still present in the MGE at E12 but lost from the LGE and there was an expansion of the expression domain of dorsal markers into the LGE (Szucsik et al., 1997, Corbin et al., 2000, Toresson & Campbell 2001). At E12.5 in the *Gsx2*^{-/-} mouse there was also a decrease in *Ascl1*, *Ebf1* and *Gad67* expression and a decrease in *Raldh3* expression and retinoid production (Waclaw et al., 2004). Later, at E15.5, there was a partial rescue of molecular patterning but the striatum was smaller and gene expression levels did not reach the level seen in the wild type (Corbin et al., 2000). At later stages of development there was a decrease in the number of DARPP32

and ENK expressing cells in the nucleus accumbens and loss of DARPP32 expression in the striatum (Corbin et al., 2000). *Gsx2* has been shown to be an important gene involved in the formation of the pallio-subpallial boundary with *Pax6*, the expression of *Gsx2* led to the expression of *Ascl1* and *Dlx1/2*, *Pax6* induced expression of *Ngn1&2* and in the *Gsx2* and *Pax6* mutants, there was a ventral expansion of *Ngn1&2* expression or a dorsal expansion of *Dlx1/2* and *Ascl1* expression respectively (Toresson et al., 2000a, Waclaw et al., 2004). In the double *Pax6*^{-/-};*Gsx2*^{-/-} mouse mutant, this expression was improved along with cortical and striatal development (Toresson et al., 2000a, Waclaw et al., 2004). However, the diminished expression of *Raldh3* observed in the *Gsx2*^{-/-} mouse was not rescued (Toresson et al., 2000a, Waclaw et al., 2004). As early as E10.5 in mouse the pallio/subpallial boundary was observed through the differential expression of pallial *Tbr2*, *Ngn2* and of subpallial *Gsx2*, *Ascl1* and *Dlx2*. (Yun et al., 2001). In the *Gsx2*^{-/-} mouse there was a loss of the pallio-subpallial boundary and *Pax6* and *Ngn2* expression was observed in the VZ of the LGE at E12.5, but this was recovered by E15.5 (Corbin et al., 2000) and seemed to be due to the expansion in expression of *Gsx1* from the MGE into the LGE in the *Gsx2*^{-/-}. This compensation was confirmed with the exacerbated striatal defects observed in the double *Gsx1*^{-/-};*Gsx2*^{-/-} knockout mouse (Toresson & Campbell 2001). *Gsx1* is normally expressed at the boundary between the VZ and SVZ and has been shown to promote the maturation of the cells between the two zones (Pei et al., 2011). The *Gsx2*^{-/-} mouse also showed a reduction in DARPP32⁺ neurons but the matrix is relatively spared (Toresson & Campbell 2001).

Ascl1 is a proneural bHLH transcription factor and in the mutant mouse there was a pronounced reduction in the size of both of the GEs and in the number of BrdU⁺ proliferating cells in the VZ and SVZ (Casarosa et al., 1999). However, the differentiation potential of the LGE seemed unaffected (Casarosa et al., 1999). In

the *Ascl1* mutant mouse, there was a loss of *Dll1* expression (*Delta like*, a notch ligand) and loss of notch target *Hes5* expression, which was normally expressed in the VZ (Casarosa et al., 1999, Yun et al., 2002). Notch signalling regulated the normal expression of *Ascl1* in the VZ, and in *Ascl1* mutants SVZ and MZ markers were expressed earlier in the VZ and there was a loss of generation of mature neurons (Casarosa et al., 1999, Yun et al., 2002). In the *Dll1*^{-/-} mutant there was a decrease in expression of *Hes5* but the LGE retained the ability to make mature neurons, showing that *Ascl1* with Notch signalling controlled the progression of cells from the VZ to the SVZ and that ASCL1 was required cell autonomously to generate mature neurons (Casarosa et al., 1999, Yun et al., 2002). *Ascl1* was also shown to control cell cycle progression via genes such as *E2f1* and Notch signalling (Yun et al., 2002, Castro et al., 2011). In the *Dlx1/2*^{-/-} mouse, there was an increase in expression of *Dll1*, *Hes5* and *Ascl1* and the SVZ domain was expanded also there was a persistent expression of VZ markers; COUP-TF1 and GSX1/2 and a loss of OCT6 and DLX5/6 (SVZ markers) and even though mature neurons were produced, they lost their dopaminergic phenotype, losing DRD2 and DARPP32 expression (Yun et al., 2002). *Ascl1* was expressed ectopically in the *Ngn2*^{-/-} mutant mouse in the dorso-medial telencephalon at E12.5, but not in the *Ngn1*^{-/-} mouse, and in the *Ngn2*^{-/-} mutant mouse *Dlx1,2* and *5* were expressed in the cortex with *Ascl1* being required for the ectopic expression of *Dlx1* dorsally, both *Neurogenins* were normally expressed in the *Ascl1*^{-/-} mouse (Fode et al., 2000). Later in development, *Ascl1* was shown to control the expression of genes involved for differentiation and neurite outgrowth (Castro et al., 2011).

DLX2 (a homeodomain protein) was shown to be expressed in the VZ and SVZ of the forebrain and was co-expressed with *Ascl1* but not with the mature neuron marker MAP2 (Porteus et al., 1994, Liu et al., 1997). Porteus et al., (1994) described the presence of 4 populations of cells in the developing LGE. A study by

Yun et al., (2002) went further to suggest there was an additional population present in the VZ that was ASCL1⁺, and a DLX2⁺ neuronal population. *Dlx1/2* were also expressed with *Dlx5* in the SVZ and both *Dlx5/6* were highly expressed in the MZ (Liu et al., 1997). In the *Dlx1/2*^{-/-} double mutant there was absence of *Dlx5*, *Dlx6* and *Oct6* at E12.5 and at E14.5 a decrease in *Ctip2*, *Rarb*, *Ebf1* and *FoxP1*, but an increase in *Gsx1/2* and *Ascl1*, possibly to compensate for the loss of *Dlx1/2* (Anderson et al., 1997, Long et al., 2009). This change in expression of ventral markers was compounded with ectopic expression of cortical markers *Ebf3*, *Id2* and *Nhlh2* and there were defects in migration of later born cells to the MZ in the LGE with many proliferating cells present in the MZ (Anderson et al., 1997, Long et al., 2009). The *Dlx1/2*^{-/-} mouse showed a loss of matrix cells in the striatum. However, the striosomal patches formed fairly normally (Anderson et al., 1997). *Necdin* (a maternally imprinted gene which binds NRAGE) interacted with DLX2 or DLX5 with NRAGE and its overexpression increased the number of GABAergic, calbindin D-28k cells (Kuwajima et al., 2006).

As a result of the complex patterning and the fine balance that is needed in the telencephalon in order to obtain progenitors of the striatum, there needs to be a protocol which generates ventral-forebrain like neural precursors utilising these signalling pathways. This should mean that on transfection of the post-mitotically expressed transcription factors, genes such as *Gsx2*, *Ascl1*, *Dlx2* should already be expressed as a result of correct BMP and WNT inhibition, low levels of SHH signalling and FGF signalling during early differentiation *in vitro*. Currently a protocol has been optimised in the lab to produce these types of cells and follows these developmental instructions.

1.5 The Relevance of Transcription Factors in Striatal Development

1.5.1 EBF1

EBF1 (early B cell factor 1), also known as OLF1, is a transcription factor belonging to the COE family of transcription factors, which contain a non-basic helix loop helix domain, a novel zinc coordination motif responsible for DNA binding and when EBF1 binds to DNA it does so as a homodimer via the amino terminus (Figure 1.8) (Hagman et al., 1993, Hagman et al., 1995).

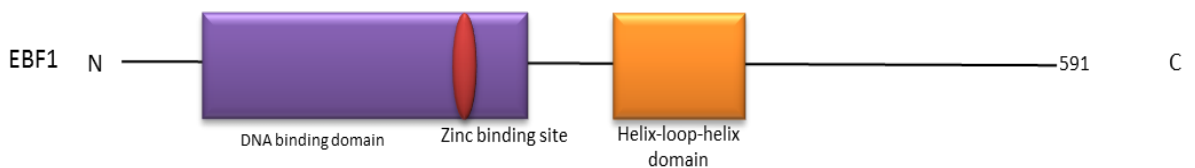


Figure 1.8: Schematic highlighting the important domains of human EBF1 protein. The N terminally located DNA binding domain encompasses a zinc binding site, upstream from the Helix-loop-helix domain

EBF1 is the only member of the COE family expressed in the lateral ganglionic eminence. At E12.5 in the mouse, EBF1 was expressed in the mantle zone of the LGE and not in the SVZ/VZ as observed by a lack of co-localisation with DLX1⁺ cells or the GBX2⁺ cells of the MGE mantle zone (Garel et al., 1997). In the chick embryo, EBF1 has the ability to promote early onset of neural differentiation and migration of neuroepithelial progenitors, and the cells exit the cell cycle when expressed ectopically in the chick neural tube (Garcia-Dominguez et al., 2003). Adhesion markers on chick neural progenitors changed when EBF1 is expressed ectopically, with a decrease of the N-cadherin molecule (expressed on neural progenitors) and an increased expression of R-cadherin which is observed in neurons (Garcia-Dominguez et al., 2003). *In situ* hybridization studies, in the mouse, have showed that *Ebf1* is expressed at E15.5 in a few cells of the LGE SVZ and in the mantle zone with a more caudal expression at the SVZ/MZ boundary on the

MGE, this expression is decreased from E17.5 (Garel et al., 1999). At P0 in the mouse, most of the MZ of the striatum expressed *Ebf1* mRNA and it is observed in the striatal matrix compartments as observed by lack of co-localisation with tyrosine hydroxylase staining of the patch compartments (Garel et al., 1999). In the *Ebf1*^{-/-} mutant mouse, the LGE developed normally with no stable change in size or morphology (Garel et al., 1999). However, the transition from the SVZ to the mantle zone was perturbed with the mantle markers CRABP1 (cellular retinoic acid binding protein 1), involved in retinoic acid metabolism (Boylan & Gudas 1992), and cadherin 8, a type II class cadherin expressed in neuroepithelial cells and radial glia cells (reviewed by Redies and Takeichi 1996) with a possible role in neuronal migration, were either absent or markedly reduced (Garel et al., 1999). This resulted in persistence of the SVZ markers, EphA4, RAR α , SCIP/Oct6 and Dlx5, in the mantle zone (Garel et al., 1999). These defects in expression of mantle and SVZ markers had an effect perinatally, with severe atrophy occurring in the striatum by E18.5 and also problems of axonal fasciculation and navigation of; internal capsule fibres, the posterior branch of the anterior commissure and thalamo-cortical fibres in and around the striatum (Garel et al., 1999). EBF1 was shown to interact with ZFP521, also known as EVI3, and they were both highly enriched in the striatonigral medium spiny neurons (Lobo et al., 2006). In the *Ebf1*^{-/-} co-expressing EGFP either from the *Chrm4* or *D2d* promoter mouse, the striatonigral MSNs were selectively lost postnatally as observed by a decrease in the number of GFP⁺ MSNs, the striatopallidal D2-EGFP⁺, enkephalin⁺ MSNs remain intact in the *Ebf1*^{-/-} knockout mouse (Lobo et al., 2006), *Ebf1* knockout also decreased the number of GFP⁺ neurons in the dorsal striatum of a *dopamine D1a receptor*-EGFP mouse line and a *solute carrier 35d3*-EGFP mouse line (Lobo et al., 2008), hence EBF1 is only required for striatonigral MSN development. It was also observed that a reduction of cells occurred in the matrix compartment, but the cells of the patch compartment still

remained which led to a decrease in the size of the matrix and the patches constituted a greater volume of the striatum (Lobo et al., 2008), so EBF1 is required for the development of the matrix, but not the striosomal patches of the striatum. ZFP521 is normally expressed in the mouse adult striatum (Lobo et al., 2008). However, in *Ebf1*^{-/-} knockout mice, there was a decrease to 43.9% of wild type mouse expression of ZFP521 in the striatum, but expression in the septum was not affected (Lobo et al., 2008). Therefore *Zfp521* is a specific EBF1 target in the striatum. HELIOS, a transcription factor involved in striatal development was expressed independently of EBF1 and *Ebf1* expression was independent of a related transcription factor IKAROS, which was also expressed during striatal development (Martín-Ibáñez et al 2010, Martín-Ibáñez et al., 2012). Therefore, there are other transcription factors required for the whole development of the striatum. As a result of the marked defects in striatal development observed in the various *Ebf1*^{-/-} mice with defects being limited to the striatonigral pathway and also the matrix compartment of the striatum, it is a suitable transcription factor to be used in transfections into neural stem cells in order to derive MSNs.

1.5.2 FOXP1

FOXP1 belongs to the forkhead box (Fox) family of transcription factors which all contain a ~100 amino acid winged helix/forkhead box DNA binding domain (Tang et al., 2012). The FOXP division of the transcription factor family also contain a zinc finger domain and a leucine zipper motif which is involved in transcriptional repression, these reside in the N-terminus of the protein and allow the transcription factors to form homo- and heterodimers with each other see Figure 1.9 (Tang et al., 2012, Li et al., 2004, Shu et al., 2001). *Foxp1* is widely expressed in E12.5 mice with high levels of expression in the lung, and lower levels expressed in intestinal, neural and cardiovascular tissue (Shu et al., 2001). There are at least four splice isoforms of *Foxp1* two of which have been detected in the brain which are; 3.2 kb

and 2.4 kb and are expressed at similar levels, the FOXP1 consensus binding site in promoter regions is TATTTG/AT (Wang et al., 2003).

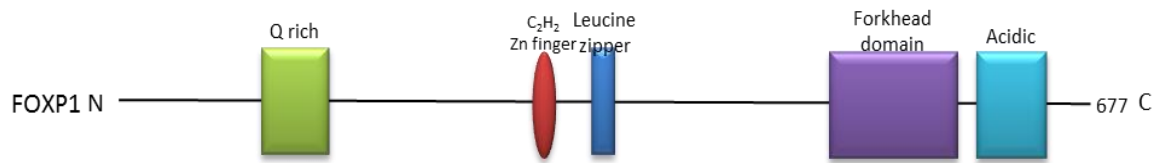


Figure 1.9: Schematic highlighting the important features in human FOXP1. An N terminal Glutamine rich domain and a centrally located C₂H₂ zinc finger and leucine zipper, and the C terminal Forkhead domain and acidic sequence

An alternative splice form of FoxP1 has been detected in human and mouse, which is expressed in pluripotent ES cells (Gabut et al., 2011). In human, exon 18 is substituted for exon 18b and in mouse exon 16 is substituted for 16b in the ES form; the expression of the “b form” of the exon decreases on differentiation, the splice variant alters the amino acid sequence of the forkhead domain affecting DNA binding (Gabut et al., 2011). *Foxp1* has been observed in the very early developing zebrafish from the one cell stage from the maternal transcript, decreasing in expression at the developmental stage of 30% epiboly and increasing again at 75% epiboly in the whole zebrafish embryo and at later stages localised to the developing midbrain, hindbrain and spinal cord (Cheng et al., 2007). There was a marked reduction of expression of *Foxp1* in a *Dlx1/2*^{-/-} mouse SVZ and MZ of the LGE and in maturing striatal neurones, suggesting that FoxP1 is an important transcription factor in later striatal development (Long et al., 2009). In the mouse, DLX5/6 were also expressed in the mantle zone and could induce the expression of *Foxp1* (Tamura et al., 2004).

At E12.5 in the mouse, *Foxp1* was shown to be expressed in the developing spinal cord motor neurons and possesses a similar expression pattern to Islet1 (Shu et al., 2001, Ericson et al., 1992, Tsuchida et al., 1994). However, its expression was observed later in the developing basal ganglia at E16.5 (Shu et al., 2001). Mouse *in*

situ hybridisation and immunohistochemistry showed FoxP1 protein and mRNA to be expressed in the SVZ of the ganglionic eminence at E14.5, therefore localised to the migratory/post-migratory neurons of the striatum (Ferland et al., 2003). Striatal expression of FOXP1 has been observed from later embryonic developmental stages right through to the adult mouse (Ferland et al., 2003). In the adult mouse, FOXP1 expression was observed elsewhere in the brain including the substantia nigra, the ventral striatum, anterior olfactory nucleus, olfactory tubercle, thalamus, pontine nucleus, inferior olive, deep layers of the superior colliculus and cortical layers III-V (Ferland et al., 2003). Tamura et al., (2003) performed *in situ* hybridisation in the mouse forebrain and detected *Foxp1* expression earlier at E13.5 in the post-mitotic neurons of the caudatoputamen. At E15.5, expression of *Foxp1* was also detected elsewhere including the paraventricular thalamic nucleus, lateral preoptic area and preoptic area (Tamura et al., 2003). At E17.5, the expression of *Foxp1* increased in the caudatoputamen and paraventricular thalamic nucleus, but decreased in the lateral preoptic area and preoptic area but was also detected in the CA1 region of hippocampus (Tamura et al., 2003). *Foxp1* mRNA was only expressed in MAP2⁺ neurons of the mouse striatum, with over two thirds of MSNs (DARPP32⁺/GluR2/3⁺) expressing *Foxp1* mRNA, and no *Foxp1* mRNA expressed in interneurons (Tamura et al., 2004). This expression pattern suggested *Foxp1* is more likely to be a matrix marker than a striosomal patch marker in mouse (Tamura et al., 2004). More recent findings by Martín-Ibáñez et al., (2012) have localised FOXP1 expression to the matrix in the mouse as it co-localises with HELIOS expression. However, FOXP1 has been shown to be expressed in both the striosomal patches and matrix compartments in the P3-20 rat striatum (Takahashi et al., 2003), indicating possible species variations in the location of FOXP1 expression in the striatum. *Foxp1* mRNA was first detected in the rat at E14 in the mantle zone of the LGE, at E16-20 *Foxp1* expression in the SVZ was lower than the

MZ, with low level expression in the primordium of septum and amygdala unlike the expression of the closely related transcription factor which was also striatally enriched, *Foxp2* (Takahashi et al., 2003). FOXP1 was detected in the 11 week old human fetus in the LGE in both precursors and differentiated medium spiny neurons (Delli Carri et al., 2013a).

FOXP1 overexpression in mouse striatal cells induced an increase in expression of *Follistatin*, *Fos* and *activating transcription factor 3* (Tang et al., 2012). siRNA mediated knockdown of *Foxp1* decreased their expression, suggesting these are targets of FoxP1 (Tang et al., 2012). FOXP1 overexpression also up-regulated genes involved in glutamate receptor function, GABA receptor signalling, G protein coupled receptor signalling and cAMP-mediated signal transduction (Tang et al., 2012). In total, there are currently 40 FoxP1 targets associated with the Huntington's disease signalling pathway, mainly involved in BDNF signalling, caspase activity and glutamate and calcium signalling (Tang et al., 2012). FOXP1 regulates its own expression as well as increasing expression of *Kcnp2* (Tang et al., 2012), KCNIP2 was significantly decreased in expression in human HD samples (Desplats et al., 2006). Interestingly, both FOXP1 and CTIP2 (another transcription factor involved in striatal development) showed a significant decrease in their expression in the striatum of an R6/1 HD transgenic mouse model compared to that of wild type littermates at 6 months of age (Desplats et al., 2006). The *Foxp1* promoter does not contain a CTIP2 binding site but *Foxp2* does (Desplats et al., 2008). However, *Ctip2* does possess many FOXP1 binding sites in its promoter region (Tang et al., 2012). It may become apparent on transfection that *Foxp1* transfection up-regulates *Ctip2* expression through direct activation of the promoter. FOXP1 may be involved in immunosuppression in the CNS and is predominantly expressed in the neurons as shown by co-labelling with NeuN, but has been detected in qRT-PCR analysis of activated microglia cultures (Tang et al., 2012). *In*

vivo, increased FOXP1 expression induced an increased expression of suppressor of cytokine signalling 5 (SOCS5), and so FOXP1 could be seen as being a neuro-protective transcription factor by counteracting glia activation (Tang et al., 2012). FOXP1 has been shown to regulate retinoic acid signalling in the developing lateral motor column of the spinal cord at brachial and lumbar levels (Rousso et al., 2008), and could be important in the developing striatum since retinoic acid signalling has been shown to induce expression of DARPP-32 (Liao et al., 2005, Liao & Liu 2005). In the mouse *Foxp1* knockout, there was a loss of the lateral motor column and an increased size of the medial motor column more laterally (Rousso et al., 2008). FOXP1 and ISLET1 are co-expressed in the lateral motor column (Rousso et al., 2008) and in the more caudal regions of the brachial and lumbar divisions of the lateral motor column, expression of OCT6, another transcription factor important for striatal development, has been observed (Dasen et al., 2005, Luria & Laufer 2007), and so there could be activation of *Foxp1* by OCT6 or vice versa and the same with *Foxp1* and ISLET1. The *Pitx3* gene promoter contains seven FOXP1 binding sites and FOXP1 is co-expressed in the *Pitx3*⁺ post mitotic midbrain dopamine neurons in the E12.5 mouse, *FoxP1* forced expression in mES cells led to expression of *Pitx3*⁺/*TH*⁺ dopamine neurons when differentiated in monolayer culture (Konstantoulas et al., 2010).

FoxP1 will be transfected into neural stem cells as it is important for MSN development as it is highly expressed in post-mitotic neurons of the developing striatum and co-localises in the developing and adult striatum with the MSN marker DARPP32. FOXP1 also co-localises with other transcription factors important for MSN development. The phenotype of FOXP1 transfected cells will need to be determined as there is disparity in the literature as to whether FOXP1⁺ cells correspond to matrix or a patch phenotype.

1.5.3 Islet1

Islet 1 (ISL1) is a LIM homeodomain containing transcription factor with 2 specialised zinc fingers functioning as the LIM domains, located N terminally of the homeodomain (Figure 1.10) (reviewed by Hobert & Westphal 2000).

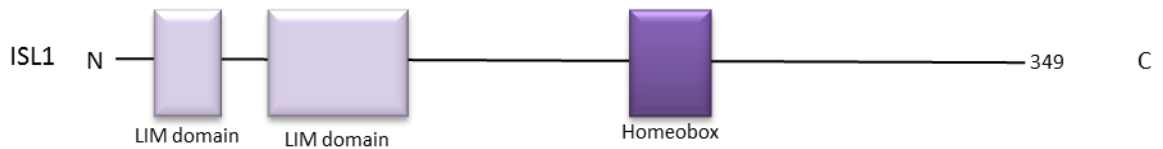


Figure 1.10: Schematic highlighting the important regions of the human ISL1 protein. The two N terminal LIM domains and the homeobox region

It is expressed mainly in the pancreas and motor neurons as seen in loss of function studies (Hobert & Westphal 2000, Pfaff et al., 1996). Additionally, a population of Engrailed⁺ interneurons failed to form in the embryonic *Isl1* mutant mouse (Pfaff et al. 1996). Mouse mutants for *Isl1* experienced arrested development around E9.5 with an abnormal dorsal aorta (Pfaff et al., 1996). *Isl1* is also highly expressed in the basal ganglia; the *Dlx1/2* mutation reduced *Isl1* expression to 86% of the wild type level in the basal ganglia more specifically in the SVZ and MZ of the developing LGE at E15.5 (Long et al., 2009). *Isl1* is also observed in the developing avian striatum (Abellan & Medina 2009) and ISL1 has been used in several studies to highlight the developing mouse striatum (Toresson et al., 2000, Toresson & Campbell 2001). ISL1 expression is co-localised with DLX1 expression and restricted to the ventral LGE SVZ and gives rise to striatal projection neurones (Stenman et al., 2003). More in depth work by Wang & Liu (2001) showed the expression of the Islet1 mRNA and protein in the developing striatum of the embryonic and postnatal rat with RT-PCR data that showed mRNA expression at E15 in the LGE and in the E20, P0 and adult striatum. ISL1 protein expression was observed from E13 with a thin layer of cells expressing ISL1 in the ventro-lateral telencephalon in the presumptive LGE (Wang & Liu 2001). At E15 there was a high

level of expression of ISL1 in the MZ of the mid and caudal LGE and by E18 a high to low medio-lateral gradient of ISL1⁺ cells in the mantle zone of the striatum, and a rostro-caudal gradient of ISL1⁺ cell expression from low to high (Wang & Liu 2001). By P0 the expression of ISL1 is starting to diminish with fewer cells showing positivity for ISL1 expression (Wang & Liu 2001). The majority of MAP2⁺ cells were ISL1⁺ and all DARPP32⁺ neurons were MAP2⁺, but there was little co-localisation of ISL1 with DARPP32, thus they hypothesised that ISL1⁺ precursors become DARPP32⁺ terminally differentiated neurons as ISL1 expression in the MAP2⁺ neurons decreased in the striatum during development and DARPP32 expression increased in terminal differentiation (Wang & Liu 2001).

More recent studies have highlighted the importance of ISL1 expression in the development of the striatonigral pathway and its role in repressing expression of striatopallidal genes, as striatonigral pathway development was impaired and the expression of striatopallidal genes was up-regulated in the *Nestin-Cre Isl1^{fl/fl}* mouse (Lu et al., 2014). A *Foxg1-Cre Isl1^{fl-exon1/fl-exon3}* mouse knockout with specific knockdown of *Isl1* in the striatum showed a similar failure of the striatonigral pathway to form with a decrease in the striatal size and also problems of axonal navigation in striatonigral cells through the internal capsule due to synapse in the substantia nigra (Ehrman et al., 2013).

The limited temporal expression of *Islet1* during development shows that it is important for embryonic development and not required postnatally, the expression of ISL1 in the developing LGE and the possible role for turning on DARPP32 expression in MSNs of the striatum, means that ISL1 expression is crucial for MSN development in the striatum. The important role that ISL1 has in the specification of striatonigral neurons is also of interest and will be investigated by monitoring of electrophysiological and morphological characteristics.

1.5.4 NOLZ1

Nolz1 is a transcription factor that belongs to the NET (Noc/Nlz, Elbow, Tlp1) family of zinc finger proteins (Nakamura et al., 2004). The family of proteins share a conserved Sp motif, buttonhead box domain and a C₂H₂ zinc finger see Figure 1.11 (Nakamura et al., 2004).

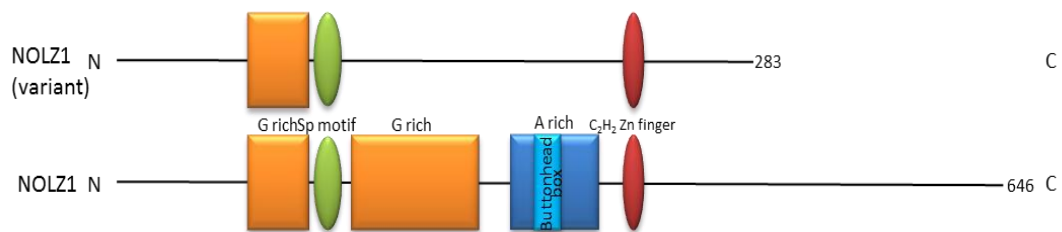


Figure 1.11: Alignment of the two versions of human NOLZ1 protein. The important regions of the proteins, showing conservation of a Glycine rich domain, the Sp motif and C₂H₂ Zinc finger

Amino acid alignment between several species has identified high sequence homology at the amino and carboxy termini with *Drosophila nocA* and zebrafish *nlz* and *Xenopus XNolz* (Chang et al., 2004). GSH2 has been shown to be required for *Nolz1* expression (Urbán et al., 2010). Nolz 1 mRNA and protein has been shown to be expressed throughout embryonic development in the developing mouse striatum and LGE before being down-regulated in the postnatal and adult striatum (Chang et al., 2004, Urban et al., 2010, and Ko et al., 2013). NOLZ1 protein expression was first detected in the E11.5 mouse LGE and Nolz 1 protein and mRNA co-localised with TuJ1⁺ neurons in the E12.5 SVZ and MZ and not Ki67⁺ cells of the SVZ (Chang et al., 2004, Ko et al., 2013). Nolz 1 mRNA and protein was not expressed in the mouse MGE, except for a caudal strip across the border between LGE and MGE which forms a corridor of NKX2.1⁻ cells and constitutes an axonal guidance pathway for thalamo-cortical projections (Chang et al., 2004, Ko et al., 2013). In the E16.5 SVZ and MZ many neurons co-expressed NOLZ1 and ISL1, at E18.5 many NOLZ1⁺ cells also expressed FOXP1 and FOXP2 (Ko et al., 2013). In the *Drd1-EGFP* and

Drd2-EGFP BAC transgenic mice NOLZ1⁺ cells were co-localised with the GFP⁺ cells of the dopamine D1 receptor and dopamine D2 receptor cells (Ko et al., 2013). *Nolz1* mRNA was co-expressed with DARPP32 protein in the MZ of the E18 and E20 rat striatum (Chang et al., 2004). In the developing rat striatum, 3 transcripts of *Nolz1* have been identified and were temporally regulated in their expression (Chang et al., 2004). The first was a ~3.5kb transcript highly expressed in the striatum and also a ~4.0kb transcript which was expressed to a lesser extent, both were expressed at E20 in the rat striatum, although the time of expression of the ~4.0kb transcript was limited to between E15 and P0 (Chang et al., 2004). A smaller transcript of ~3.0kb was detected postnatally in the rat striatum, the 3.5kb transcript was detected throughout striatal development before being down-regulated postnatally (Chang et al., 2004). NOLZ1 overexpression in primary neurosphere cultures has been shown to increase retinoic acid signalling by selectively up-regulating *Rarb* (Retinoic acid receptor beta) expression and also promoted cell cycle exit (Urbán et al., 2010). Premature expression of NOLZ1 in the developing LGE under the promoter of *Nestin* caused a decrease in cell proliferation, early cell cycle exit, aberrant apoptosis and premature differentiation and maturation of cells in the SVZ (Chang et al., 2013).

Nolz 1 has been selected as a candidate important for MSN development as NOLZ1 is expressed throughout striatal development but is down-regulated postnatally therefore the function of NOLZ1 is specific to development, in addition to this NOLZ1 is able to up-regulate *Rarb* and retinoic acid signalling is important in MSN development through its ability to turn on DARPP32 expression.

1.5.5 OCT6

OCT6 is a member of the POU domain of transcription factors. The POU domain consists of a POU specific domain and a POU homeodomain, these are connected

by an unstructured linker domain and this complex of domains is involved in DNA binding and protein-protein interactions see Figure 1.12 (Sturm & Herr 1988).



Figure 1.12: Schematic highlighting the important regions of the human OCT6 protein. The N terminally located Alanine rich, Glycine rich and Histidine rich domains and the C terminal POU domain and homeodomain

The role of OCT6 has been extensively characterised in Schwann cells, where it is involved in the conversion of promyelinating cells into differentiated myelinating cells and is also expressed following nerve transection (Jaegle & Meijer 1998, Monuki et al., 1989, Monuki et al., 1990, Jaegle, et al., 1996). Nuclear localisation of OCT6 has been shown to be dependent on its POU homeodomain, whereas the POU specific domain and POU homeodomain were both required for DNA binding (Sock et al., 1996). Importin $\alpha 2$ was bound to OCT6 in ES cells and localised it to the cytoplasm, on binding another importin α family member it was translocated to the nucleus (Yasuhara et al., 2013). *Oct6* was also detected in mouse brain, testis and F9 stem cells, specifically detected by *in situ* hybridisation at 10 days in the developing prosencephalon and at 12 days in the ventral portion of prospective striatum, at day 14 there were collections of *Oct6*⁺ cells in the ventral portion of the prospective striatum (Suzuki et al., 1990). OCT6 was also expressed at the late streak stage in the anterior half of the mouse embryo, and through gastrulation and neurulation (Zwart et al., 1996). OCT6 expression was restricted to the walls of the neural groove, when the neuropore closes and OCT6 was also expressed in the mid- and fore-brain (Zwart et al., 1996). At E9.5 in the mouse, OCT6 was expressed at the ventral midline of the secondary prosencephalon, later extending into the telencephalon (Zwart et al., 1996). *Oct6* was expressed in the SVZ of the LGE at E15.5 in the mouse, in the *Ebf1*^{-/-} mutant mouse, there was aberrant expression of

Oct6 in the mantle zone of the LGE (Garel et al., 1999) and is, therefore, a transcription factor that is required in early post-mitotic development. In the developing rat forebrain vesicle, *Oct6* mRNA was detected at E12 in the SVZ only of the telencephalon and completely excluded throughout development from the VZ (Alvarez-Bolado et al., 1995). *Oct6* expression remained high through to E13 and slowly decreased thereafter in the SVZ, being highly expressed in the E13 mantle zone and E14 striatum (Alvarez-Bolado et al., 1995). *Oct6* mRNA has also been shown to be expressed in the striatum of the adult rat and in the SVZ of the LGE at E13 and E15 (Frantz et al., 1994). OCT6 has been reported to be associated with the forebrain/midbrain (FM) enhancer region TAATTA in neural progenitor cells and in the embryonic forebrain and midbrain (Inoue et al., 2012). The human OCT6 protein lacks the first 50 amino acids of its mouse counterpart and has been shown to activate transcription via the octamer TATA minimal promoter (Tobler et al., 1993) with other OCT6 binding sites being TAATGARAT, TTAAAATTCA and CTCATGA (reviewed by Schöler 1991). POU transcription factors have been shown to activate the dopamine D1 receptor gene (Imafuku et al., 1996). The regulation of *Oct6* expression has been shown to be in part by 17 β -estradiol as this has enhanced *Oct6* expression in glia, this was due to an estrogen response element found ~5kb upstream of the *Oct6* mouse gene (Renner et al., 1996), consequently, OCT6 expression in cortex and hippocampus was observed earlier in development in females than in males (Ilia et al., 2003b). When another POU transcription factor, *Brn1*, was inserted into the *Oct6* gene locus in the mouse, the defect of Schwann cells in the peripheral nervous system of *Oct6*^{-/-} mice was rescued (Wolf et al., 2009). However, severe defects were observed in the developing forebrain of the *Oct6*^{Brn1} mouse, due to anterior expansion of cells expressing *Wnt1* and from E10.5-E18.5, there was severe truncation of the forebrain, in some cases the diencephalon and telencephalon were completely absent with the telencephalic

marker *Emx1* absent at E9.5 even though the cell proliferation rate remained normal (Wolf et al., 2009).

The Shh pathway has been shown, via GLI activators, to up-regulate the expression of *Oct6*, Shh is also required for striatal development (reviewed by Katoh & Katoh 2008). *Oct6* was expressed in both the cortex and basal ganglia, with a 2 fold higher expression in the basal ganglia; the level of expression in the basal ganglia was decreased to a quarter of its original level in the wild type compared to the *Dlx1/2^{-/-}* mutant (Long et al., 2009). DLX1/2 seemed to be two of the transcription factors responsible for inducing expression either directly or indirectly of *Isl1*, *Foxp1* and *Oct6* (Long et al., 2009). In adult mice OCT6 protein was detected in the striatum, cerebral cortex and hippocampus (Ilia et al., 2003a). OCT6 expression, in the mouse striatum, was present at postnatal week 12-18 before decreasing at 20 postnatal weeks (Ilia et al. 2003a).

Oct6 is being used in forced transcription factor expression in neural stem cells to drive differentiation in to MSNs due to the limited expression during development of the striatum as OCT6 is limited temporally in its expression in the LGE SVZ and in the striatum to embryonic and early postnatal expression only and so is important in MSN development. Another reason for choosing OCT6 is when other important transcription factors for MSN development are not expressed such as EBF1, and then OCT6 expression is altered. The expression of OCT6 is required to inhibit *Wnt1* expression which inhibits proper telencephalon development and so will be useful in preventing other more posterior fates of the neural tube development.

The relationship and timing of expression of the transcription factors utilised in this study can be seen in Figure 1.13

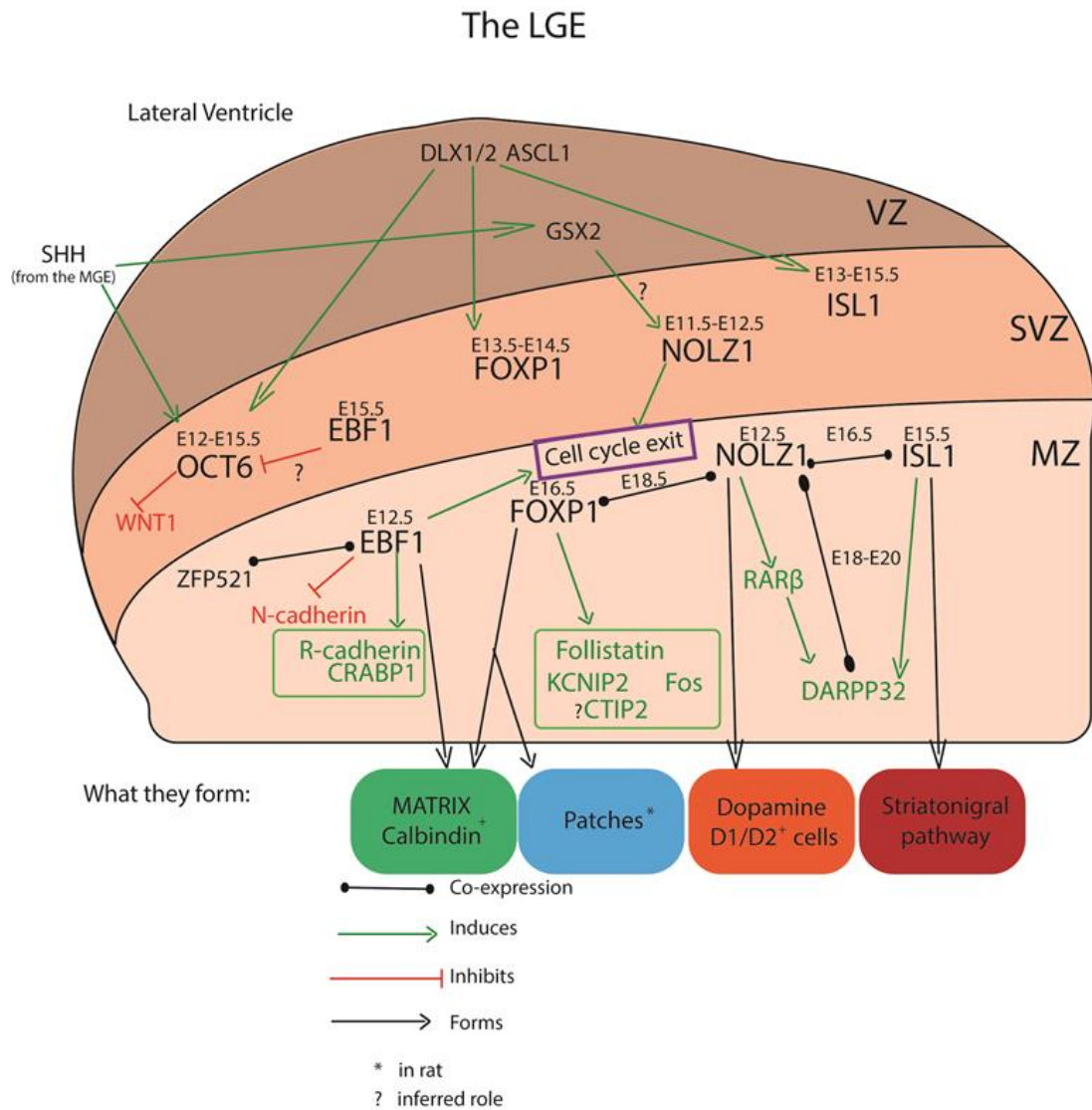


Figure 1.13: Location, relationship and timing of expression, in mouse, of the transcription factors used in this study. The relationship between the transcription factors utilised in this thesis for transfection of neural precursors. All of the transcription factors are expressed in the SVZ or MZ. Above each of the transcription factors indicates the approximate timing of expression in the mouse LGE. Some of the functional roles of the transcription factors are also documented and whether their expression contributes to cells of the different compartments and pathways of the striatum. Figure created from information in Sections 1.4.7 and 1.5.

1.6 Striatal neuronal differentiation *in vitro*

The advent of mouse ESC culture (Evans & Kaufman 1981) and the establishment of human pluripotent stem cell lines (Thomson et al., 1998, Takahashi et al., 2007) have meant that we can try and reproduce the development of different cell types *in vitro*. In order to emulate embryonic striatal development *in vitro*, stem cells need to

be exposed to the developmental cues which are present in the developing brain. Many studies have been carried out thus far with molecular programming which mimics to some extent the environment to which the cells of the neuroepithelium, telencephalon, and LGE are exposed. Several factors are repeated between studies, such as the inclusion of SHH/purmorphamine, DKK1 (dickkopf1- WNT pathway inhibitor), brain derived neurotrophic factor (BDNF), dbcAMP and VPA at time points which vary between studies. So far no-one has been able to achieve a pure population of MSNs or even close to achieving a population of cells which can be defined as mostly MSNs, the main focus of most studies is increasing the levels and numbers of positive cells of DARPP32 expression as this is highly expressed by neurons of the striatum (Ouimet et al., 1994).

1.6.1 Neural induction

Early differentiation of pluripotent stem cells into cells comparable to those seen in the developing neural tube, termed rosettes, with specification for the telencephalon has been carried out. Small molecules and morphogens were used that inhibit the TGF β /Activin/Lefty pathway and BMP signalling (Chambers et al., 2009). This suppressed BMP and Activin induced differentiation into mesoderm and endoderm and inhibited activin-dependent maintenance of pluripotency, and therefore allowed neuralisation to occur (Chambers et al., 2009). The morphogen, Noggin (BMP inhibitor) and small molecule, SB431542 (TGF β /Activin/Lefty inhibitor) were included in culture medium for dissociated human ES differentiation (Chambers et al., 2009). The ESCs lost OCT4 expression, a pluripotent marker, by day 5 of culture and expressed an epiblast marker FGF5 before expressing SOX1 and a population of >80% PAX6⁺ cells after 7 days of culture were generated that went on to express Nestin after 11 days (Chambers et al., 2009). These cells showed an anterior neural fate as judged by the expression of FOXG1, with apical ZO-1 expression (a tight-junction protein) and formed rosettes after passaging (Chambers

et al., 2009). Another method to force stem cells to undergo neural induction was by co-culture on murine stromal cells in 15% KSR (knockout-serum replacement) medium for 12 days then switched to a serum replacement medium, which produced neural rosettes 3 weeks post-induction that were Nestin⁺/PAX6⁺/FOXG1⁺ (Aubry et al., 2008). With the addition of the morphogen SHH, WNT inhibitor DKK1 and BDNF a neurotrophic factor, the rosettes were ventralised as shown by *DLX2* and *GSX2* mRNA expression after 1 week (Aubry et al., 2008). Another protocol utilising stromal cells and KSR containing medium later changed for N2-supplemented medium has been shown to produce neural rosettes within 2-3 weeks and the resulting rosettes were then cultured as embryoid bodies (EB) (Jeon et al., 2012). Detachment of ES cells to induce neuralisation by EB formation was also performed by several labs; a study by Joannides et al., (2007) maintained EBs in human neuralising medium and chopped the spheres every week, which led to extensive neural induction after 16 days. A method of culturing EBs in serum free media with SHH treatment at 3 days post induction led to the expression of *GSX2*, *GAD67* and *DLX2* and inhibited the expression of pallial markers (Danjo et al., 2011). In contrast to this, when a 20% serum containing media was used in EB culture, this produced a 95% yield of Nestin⁺ SOX1⁺ PAX6⁺ neural stem cells from HD iPS cell lines (Zhang et al., 2010). A protocol that utilised an N2 supplemented media on EBs for 7 days, then plated the cells on laminin formed PAX6⁺ neural stem cells, 12 days from induction (Ma et al., 2012). With the addition of SHH or its agonist purmorphamine for 2 weeks post induction, there was a high percentage induction of ventral telencephalic progenitors which were MEIS2⁺, ASCL1⁺ and the expression of *GSX2* mRNA was up-regulated (Ma et al., 2012). An amalgamation of two of the protocols has been shown by Delli Carri et al., (2013a&b) with neural induction by dual SMAD inhibition (noggin and SB431542 treatment) and ventralisation by SHHC-25II and DKK1, the resulting rosettes were over 50%

FOXG1⁺ and ~60% GSX2⁺ and expressed other rosette markers including *DACH1* *LIX1* *LMO3* and *MSX1* mRNA.

In order for the transfections of the transcription factors to produce the maximal benefit I needed to start with the correct neural stem cell population, dual SMAD inhibition seems to produce the best results along with subsequent WNT inhibition and SHH treatment, mimicking the *in vivo* situation and I have used an adaptation of these protocols to obtain neural rosettes of ventral forebrain character, which has been optimised by Joy et al., (unpublished data).

1.6.2 Terminal differentiation into MSN

The culture of primary mouse cells from different developmental time points has given clues as to the requirements of neuronal terminal differentiation in the striatum. The application of BDNF to culture of E13 and E17 mouse LGE and striatum, respectively, when cultured for 7 days, increased the proportion of DARPP32⁺/ARPP21⁺ cells from 25% to >50% DARPP32⁺ cells and from 10% to >29% ARPP21⁺ cells, the number of CALB1⁺ cells also increased (Ivkovic & Ehrlich 1999). In the BDNF null mouse, there was a decrease of DARPP32⁺ and ARPP21⁺ neurons present in the striatum at P0 and P10, and addition of 100 ng/ml BDNF to primary striatal cultures increased the expression of DARPP32 threefold after only 12 hours *in vitro* (Ivkovic & Ehrlich 1999, Ivkovic et al., 1997). Combining the effects of BDNF and NT3 and NT4/5 (neurotrophins 3 and 4/5) produced similar effects on DARPP32 and ARPP21 expression in primary culture, but the combinatorial action meant that the BDNF concentration could be reduced (Ivkovic & Ehrlich 1999). These studies showed that BDNF is required for the maturation of the MSN phenotype and increases the number of cells which undergo differentiation.

The addition of the SHH agonist, purmorphamine, to primary human striatal cells, increased neuronal differentiation as seen by an increase in DARPP32 expression

and it decreased the rate of proliferation and astrocyte formation compared to culture without purmorphamine (El-Akabawy et al., 2011). After 21 DIV, 7% of the cells were DARPP32⁺ and the number of CALB1⁺ cells doubled (El-Akabawy et al., 2011). The protocol utilised by Zhang et al., (2010), generated around 10% DARPP32⁺ neurons, which resulted from treatment of plated EBs with SHH, DKK1, BDNF and Y27632 (Rho kinase inhibitor to prevent cell death) and subsequent treatment with VPA (stimulated GABA neurogenesis), dbcAMP, BDNF and Y27632. In the two studies by Delli Carri et al., (2013a&b), mature neuronal proteins were detected from 45 days *in vitro* such as MAP2 and TAU, along with proteins of GABAergic phenotype: GAD65/67 and GABA, and striatal markers: CTIP2, calbindin, FOXP1, FOXP2, ARPP21 and DARPP32, with co-localisation of pairs of these striatal markers in a subset of neurons at 80 DIV. After 80DIV, from 15 DIV in N2 medium supplemented with B27 and 30 ng/ml BDNF, MAP2 expression was observed in 51% of cells and another 17% were expressing the immature neuronal marker β III-tubulin, a quarter of the cell population were GFAP⁺ astrocytes and the rest were Nestin⁺ neuroprogenitors (Delli Carri et al., 2013 a&b). DARPP32 was expressed in 10% of the total population of cells and co-localised with CTIP2, CTIP2 was also expressed in β III-tubulin⁺ neuronal cells that expressed dopamine receptor D2 (DRD2) (Delli Carri et al., 2013 a&b). The neurons were also functionally active, displaying fast inactivating K⁺ currents resembling type A K⁺ currents, and showed the presence of Na⁺ channels and were able to fire induced action potentials in response to a suprathreshold current step (Delli Carri et al., 2013 a&b). For terminal differentiation of cells in the Aubry et al., (2008) protocol, cells that mostly expressed DLX2 and/or GSX2 were plated at a low density (20-50,000 cells/cm²) with dibutyryl cAMP and VPA and at 63 days post neural induction, ~20% of the neurons were MAP2⁺ and ~50% of these possessed DARPP32. However, there were a majority of immature cells in the culture with ~70% of cells expressing

Nestin, and PAX6 was expressed in ~60% of cells. When 45 DIV cells were transplanted into the QA lesioned rat, they expressed DARPP32⁺ in 21% of the NeuN⁺ cells, the cells possessed a bipolar morphology and extensive neurite outgrowth (Aubry et al., 2008). However, there was a problem of graft overgrowth (Aubry et al., 2008), which was expected due to the large contamination of progenitors present in the culture which are still proliferating. In order for the transcription factor transfection to be successful and drive differentiation to an MSN phenotype, the cells should be post-mitotic to mimic the *in vivo* expression and also to avoid “contamination” of overgrowth of mitotic cells. Terminal differentiation of the EBs in the Jeon et al., (2012) protocol involved plating whole EBs on to poly-L-ornithine/fibronectin in DMEM media supplemented with BDNF and produced 27±1.7% DARPP32⁺ neurons and 19.1±2.1% Calbindin⁺ neurons, these neurons also affected a behavioural improvement in a rat model of HD (Jeon et al., 2012). In the study by Ma et al., (2012), ventral progenitors were plated at 26 days post induction in media supplemented with VPA for 1 week before withdrawal and addition of neurotrophic factors and cyclic AMP. At 47 DIV, over 90% of the cells were process-bearing neurons that expressed β III-tubulin and ~90% were GABAergic with 89.7±9.3% staining positive for DARPP32, which also expressed MEIS2 and had spiny processes on the dendrites (Ma et al., 2012). After 70 DIV, these cells were spontaneously active (Ma et al., 2012). At 40 DIV, cells were transplanted into the striatum of QA lesioned mice, which led to some functional recovery 4 months post-transplantation (Ma et al., 2012). Projections to the anterior substantia nigra were observed, and glutamatergic inputs were received from either the cortex, globus pallidus or thalamus, the grafts also had a >50% of cells expressing DARPP32, and synaptophysin was observed on MAP2⁺ dendrites (Ma et al., 2012). However, this protocol has yet to be replicated by other investigators and, where this has been attempted; the data do not indicate such high efficiency of

generating DARPP32⁺ neurones (E. Cattaneo, University of Milan, S. Joy, Cardiff University, C Svendsen, Cedars Sinai; all personal communication). Replication of ventral progenitor specification and terminal differentiation of the Aubry protocol and the use of BDNF, dbcAMP and VPA have been shown to produce 5% DARPP32⁺ neurons *in vitro* in long term differentiation (HD iPSC consortium 2012). Shin et al., (2012) obtained similar levels of DARPP32 expression with a monolayer method of differentiation using neurobasal medium supplemented with B27 that led to 30% of cells possessing β III-tubulin and of these, 90% were GABAergic and 32% of these cells were DARPP32⁺ in reality there was only approximately a 9% population of DARPP32⁺ neurons achieved *in vitro*. Around 65% of these neurons demonstrated induced action potentials and inward and outward currents on depolarisation and a level of spontaneous post synaptic currents (Shin et al., 2012), the cells also expressed dopamine receptor D1, DARPP32 and GAD67 when grafted into the striatum of a mouse model of HD, with more than 50% of NeuN⁺ cells expressing DARPP32 (Shin et al., 2012).

In order to obtain a higher percentage of MSNs, Danjo et al., (2011) used a *Foxg1:venus* cell line to FAC sort the fluorescent cells from the non-fluorescent cells at 9 days post induction, hence obtaining a pure *Foxg1* expressing culture. Subsequent SHH (10nM low concentration) treatment led to an emergence of a cell population that expressed NOLZ1/CTIP2 and when cultured in rat glial conditioned medium ~50% DARPP32⁺ neurons were obtained (Danjo et al., 2011). Four days after FAC sorting, cells were implanted in the P2 striatum and were observed to fasciculate with corticofugal fibres that projected ipsilaterally, the majority of implanted cells became DARPP32⁺ and no tumorigenesis was observed (Danjo et al., 2011).

The holy grail in the field of medium spiny neuronal differentiation, achieving differentiation of a population of cells into DARPP32⁺ MSNs, has not yet been met,

or if it has, it has not been able to be replicated. Increasing the number of DARPP32⁺ neurons *in vitro*, seems to require a pure population as shown by Danjo et al., (2011) and this needs to be considered for the cell populations which will undergo transfections and the cells afterwards, firstly does sorting of progenitors before transfection enable a better differentiation and secondly does removing all non-transfected cells do the same.

1.7 Directed differentiation by transcription factor expression

Multiple cell types and specification of neuronal cell types have been generated using forced transcription factor expression as a method of differentiating cells. The precursor cells also do not have to necessarily be pluripotent or multipotent as the use of fibroblasts and other differentiated cells have been used. Transcription factor driven expression for differentiation is not a new concept; one of the first studies utilised *MyoD1* mouse cDNA stably expressed in 10T1/2 fibroblasts in order to generate myogenic cells (Tapscott et al., 1988). Different regions of the MyoD1 protein could be deleted and the myogenic differentiation potential remained, however its nuclear localisation was disrupted, only 68 amino acids of the 318 amino acid protein were found to be required for MyoD1 protein nuclear localisation and myogenic differentiation properties (Tapscott et al., 1988). Further studies using MyoD1 have been carried out with retroviral infection of MyoD1 into dermal fibroblasts, chondroblasts, gizzard smooth muscle and pigmented retinal epithelial cells in order to trans-differentiate these cells into mononucleated striated myoblasts (Choi et al., 1990). These cells were contractile and formed myotubes and were equivalent to *in vivo* and *in vitro* myoblasts (Choi et al., 1990). Since then, others have utilised transcription factors important in differentiation/cell identity in order to induce a change of cell fate. The first induction of functional neurons by the basic helix loop helix transcription factors neurogenin 2 (*Ngn2*) and *Mash1* (*Ascl1*) in

astroglia formed neurons capable of firing action potentials (Berninger et al., 2007). *Ngn2* has also been expressed in postnatal cerebral cortical astroglia to induce them to become glutamatergic neurons, in the same study; *Dlx2* was used in order to produce GABAergic neurons (Heinrich et al., 2010). When *Ngn2* was expressed in hESC and hiPSC, the resulting neurons were shown to integrate, when transplanted, into the mouse brain (Zhang et al., 2013). The first induced neurons (iN) were produced from mouse fibroblasts by infection with the transcription factors *Ascl1*, *Myt1l* and *Brn2*, which produced functional neurons that were capable of firing induced action potentials and expressed the synaptic marker, synapsin (Vierbuchen et al., 2010). *Ascl1*, *Brn2* and *Myt1l* transcription factors were also expressed in human embryonic and postnatal fibroblasts; these cells formed neurons which fired action potentials in response to current injection (Pfisterer et al., 2011). In addition to these transcription factors, forced expression of the dopaminergic neuron specific transcription factors; *Lmx1a* and *FoxA2*, led to the formation of dopaminergic neurons (Pfisterer et al., 2011). When *NeuroD1* (another basic helix loop helix transcription factor) was added to the expression of *Ascl1*, *Brn2* and *Myt1l* in human fetal fibroblasts, the efficiency of conversion to iN cells was improved and spontaneous post synaptic currents were generated (Pang et al., 2011). iN generation efficiency was also improved by culturing fibroblasts in 5% O₂, post infection with the 4 transcription factors (*NeuroD1*, *Myt1l*, *Ascl1* and *Brn2*) (Davila et al., 2013). *NeuroD2* was expressed in N18-RE-105 neuroblastoma cells, which promoted neurite formation, increased synaptotagmin (a synaptic marker) and β III-tubulin expression along with an increased expression and redistribution of SNAP25 (a synaptic marker) to the cell membrane (Messmer et al., 2012). A microarray study, using single transcription factors expressed in mouse ESC lines, determined transcription factors which can induce cells into hepatocytes, blood cells, myocytes and neurons (Yamamizu et al., 2013). These neurons were

specified into neuronal subtypes and fired action potentials when induced, by 11 days post induction (Yamamizu et al., 2013). Oligodendrocytes were induced from rat and mouse fibroblasts by *Sox10*, *Olig2* and *Zfp536* forced expression, these oligodendrocytes were shown to be functional, ensheathing dorsal root ganglion cells and myelinating cells in the shiverer dysmyelinated mouse (Yang et al., 2013).

1.8 Aims & Objectives

As outlined in the aforementioned sections differentiation of stem cells into MSNs has had limited success. Forced transcription factor expression has had a positive effect on differentiation of cells in to other neuronal populations. The knowledge of embryonic development has enabled the selection of several transcription factors important for MSN development. This thesis aims, to use transcription factors important for MSN development in order to force differentiation of partially specified ventral forebrain-like neural progenitors and characterise the resulting cells after differentiation with the specific aims of:

- ❖ Clone transcription factors important for MSN development: and express them in a multicistronic plasmid.
- ❖ Validate the transcription factor protein expression from the plasmids in HEK293 cells.
- ❖ Characterise an additional protocol of neuronal maturation utilising protein expression of neurons.
- ❖ Use the plasmids in transfections to differentiate ventral forebrain-like neural progenitors into MSNs and to determine a few plasmids for further characterisation.
- ❖ Characterise the cells which have been differentiated with forced transcription factor transfection for protein markers of MSNs.
- ❖ Characterise the cells morphologically by Sholl analysis.

- ❖ Characterise the cells using electrophysiology for functional maturity and physiological markers of MSNs.

CHAPTER 2:
METHODS

2. Methods

2.1 Materials

Materials for experiments were purchased from various companies and more information can be obtained regarding catalogue numbers in the appendix.

2.2 Sourcing transcription factors

Plasmids containing the transcription factors of interest for cloning were purchased from PlasmID DNA resource core (Harvard, Boston, USA) or were cloned from total human fetal RNA (Amsbio, Abingdon, UK), or extracted from harvested sphere culture derived from human fetal WGE samples.

2.2.1 RNA extraction

Cells which had been harvested in buffer RLT (Qiagen, Hilden, Germany) with 143 mM 2-Mercaptoethanol (Sigma, Dorset, UK) were provided by Kelly C.M., and RNA extraction was performed with a QIAGEN RNeasy kit (Qiagen, Hilden, Germany) as per manufacturer's protocol. RNA was quantified using a Nanodrop Spectrophotometer ND1000.

2.2.2 cDNA synthesis

cDNA synthesis from RNA was performed using Superscript II[®] (Life Technologies, Paisley, UK). 3 µg of random primers and 25 mM dNTPs (final [0.5 mM]) (Promega, Hampshire, UK) were added to 1 µg of RNA and made up to 12 µl with DNase/RNase free H₂O (Life Technologies, Paisley, UK) in a 0.2 ml PCR tube (Amersham Biosciences, Bucks., UK). This was heated to 65°C for 5 minutes in a Techne TC512 thermocycler (Bibby Scientific Ltd., Staffordshire, UK) and subsequently chilled on ice. 5x first strand buffer was added for 1x buffer in total 20

µl volume, with 0.1 M DTT (final [10 mM]) and 40 U of RNase OUT (all Life Technologies, Paisley, UK) were added to the PCR tube and heated to 25°C for 2 minutes, then 200 U of Superscript II[®] (Life Technologies, Paisley, UK) was added and heated to 25°C for 10 minutes, 42°C for 50 minutes and 70°C for 15 minutes. Samples were frozen at -20°C or used for PCR at 1:50 dilution in H₂O.

2.3 Cloning of transcription factors and subcloning into multicistronic vectors

2.3.1 Cloning of transcription factors

Gene	Position	Restriction enzyme	Primer sequence (5'-3')	Annealing temperature
OCT6	5' section 5'-3' forward	BamHI	AACGGATCCATGGCCACCACCGCGCAGTACCTG	70°C
	3' section 5'-3' reverse	BamHI	AACGGATCCCTGCACTGAGCCGGGCAGTGT	67°C
	3' section 5'-3' forward	HpyCH4III	TACGGTAACGTGTTCTCGCAGACCACC	67°C
	5' section 5'-3' reverse	HpyCH4III	ACCGTAGAGCGTGCCACGCGCCAGCCC	70°C
FOXP1	5' end, forward	BamHI	AACGGATCCATGATGCAAGAATCTGGGACT	64.9°C
	3' end, reverse	BamHI	AACGGATCCCTCCATGTCCTCGTTTACTGGTTC	64.9°C
ISL1	5' end, forward	NheI	AACGCTAGCATGGGAGACATGGGAGATCCA	68.8°C
	3' end, reverse	NheI	AACGCTAGCTGCCTCAATAGGACTGGCTACCATGCT	68.8°C
EBF1	5' end, forward	NheI	AACGCTAGCATGTTTGGGATTCAGGAAAGCATC	67.6°C
	3' end, reverse	NheI	AACGCTAGCCATAGGAGGAACAATCATGCCAGA	67.6°C
NOLZ1	5' end, forward	BglII	AACAGATCTATGAGCACAGCGCCCTCGCTTCT	69.2°C
	3' end, reverse	BglII	AACAGATCTCTGATACCCAGCGCCGAGGCGGT	69.2°C

Table 2.1 Primer sequences used for cloning the transcription factors and optimised annealing temperatures.

2.3.1.1 PCR

Whole genes were cloned either from plasmids (PlasmID DNA resource core, Boston, MA, USA) or human fetal cDNA using primers designed to incorporate either a BamHI, BglII, NheI or XbaI restriction site at both the 5' and 3' ends of the

gene (Table 2.1). PCRs were performed using 0.5U Platinum[®] Taq polymerase (Life Technologies, Paisley, UK), in 2 mM MgSO₄, 1x buffer, 0.2 mM dNTPs 0.4 pmol primers, made up to 25 µl with DNase free H₂O, using annealing conditions optimal for the primers (Table 2.1) and following the Platinum[®] Taq standard protocol of initial denaturation 94°C for 1 minute and then 35 cycles of denature at 94°C for 30 seconds, anneal for 30 seconds, extension for 1 minute/kb of DNA at 68°C, for 35 cycles with a final extension at 68°C for 5 minutes.

2.3.1.2 PCR product purification

The PCR products were separated by gel electrophoresis at 80 V for 1 hour through a 0.8 % agarose 1x tris-acetate-ethylenediaminetetraacetic acid (TAE) gel (Melford Laboratories Ltd., Ipswich, UK & MP Biomedicals, Cambs., UK) (diluted with distilled H₂O from 50X stock of Tris Base 2M; Acetic acid 1M; Ethylenediaminetetraacetic acid (EDTA) 0.05 M) containing 1 mM guanosine (Sigma-Aldrich, Dorset, UK) to protect DNA from 312 nm UV-light damage (Gründemann & Schömig 1996) and 1:20000 dilution of SafeView nucleic acid stain (NBS Biologicals, Cambs, UK). Amplicons were visualised using a UV Transilluminator (Uvitec BTS-20-MS) at 312 nm, the PCR product of the expected size excised using a razor blade and purified by gel extraction using the GeneClean[®] kit (MP Bio Biomedicals, Cambs., UK), according to the manufacturer's protocol.

2.3.1.3 Ligation into pGEM T Easy vector

The PCR product of the gene of interest was ligated into the pGEM[®] T EASY vector (Promega, Hampshire, UK), using 3 U of T4 DNA ligase from the pGEM[®] T easy kit overnight at 4°C, using an PCR product:plasmid molar ratio of 1:1 in a 10 µl reaction, as per manufacturer's protocol in a 0.2 ml PCR tube. A background and positive control were also performed using no insert and the control insert (1:1) from the pGEM[®] T easy kit, respectively.

2.3.1.4 Transformation

Transformations of plasmid DNA were performed with either a vial of TOP10 (Life Technologies, Paisley, UK) *E.coli* or 50 µl of subcloning efficiency DH5α competent bacteria (Life Technologies, Paisley, UK) and 2 µl of the ligation reaction in a 1.5 ml microcentrifuge tube (Fisher Scientific, Loughborough, UK). These were incubated on ice for 30 minutes, heat shocked at 42°C for 20 seconds in a pre-heated water bath and incubated on ice again for 2 minutes, and subsequently grown in 950 µl of S.O.C medium (super optimal broth with catabolite repression) (Life Technologies, Paisley, UK) for 1 hour at 37°C in a shaker incubator (Jeio Tech SI-900) at 225 rpm. The transformed *E.coli* were grown as colonies by spreading 250 µl of the culture onto Luria-Bertani (LB) agar (Life Technologies, Paisley, UK) containing 50 µg/ml ampicillin (Sigma-Aldrich, Dorset, UK) in 100 mm Sterilin dishes (VWR, Leicestershire, UK) and inverted overnight at 37°C. The agar had been pre-treated with 40 µl of 20 mg/ml 5-bromo-4-chloro-3-indolyl-beta-D-galacto-pyranoside (XGAL) plus 40 µl 0.1 M isopropyl thiogalactoside (IPTG) (Melford Laboratories Ltd., Ipswich, UK) per 100 mm plate for blue/white colony selection.

2.3.1.5 Colony selection and DNA preparation

White colonies were selected with a sterile 200 µl pipette tip (VWR, Leicestershire, UK) and grown in 2 ml of LB broth (Life Technologies, Paisley, UK) containing 50 µg/ml ampicillin at 37°C overnight in a shaker 225 rpm. DNA was extracted from 1 ml of bacterial cultures using alkaline phosphatase lysis method (Sambrook et al., 1989). 1 ml of bacterial culture was pelleted at 16,000 *xg* and re-suspended in 100 µl of solution I (25 mM Tris pH 8.0 (Roche, Hertfordshire, UK); 10 mM EDTA pH 8.0 (Sigma-Aldrich, Dorset, UK); 50 mM Glucose (BDH Merck, Leicestershire, UK) in distilled H₂O), then 200 µl of fresh solution II (1% sodium dodecyl sulphate (SDS); 0.2 M NaOH (both Sigma-Aldrich, Dorset, UK) in distilled H₂O) and 150 µl of solution III added (3 M potassium acetate (Sigma-Aldrich, Dorset, UK); 11.5%

glacial acetic acid (Fisher Scientific, Loughborough, UK), in distilled H₂O) was added sequentially and mixed by inversion of the tube and incubated on ice for 5 minutes, this was then centrifuged in a Heraeus Biofuge Pico microcentrifuge at 16,000 *xg* for 3 minutes and the supernatant was pipetted into a clean microcentrifuge tube. 1 volume of phenol:chloroform (Sigma-Aldrich, Dorset, UK) was added and the solution, mixed and centrifuged at 16,000 *xg* for 3 minutes at RT. The aqueous (upper) phase was transferred to a new microcentrifuge tube and 2 volumes of 100% ethanol (Sigma-Aldrich, Dorset, UK) was added, mixed and incubated at room temperature for 5 minutes, then centrifuged for 5 minutes at 16,000 *xg*. The DNA pellet was washed with 150 µl of 70% ethanol and centrifuged for 1 minute at 16,000 *xg*. The DNA pellet was left to air-dry at room temperature for 5-10 minutes and was re-suspended in Tris-EDTA (10 mM Tris-HCl, 1 mM EDTA pH 7.4) (Sigma-Aldrich, Dorset, UK) containing 20 ng/ml bovine RNase A (Life Technologies, Paisley, UK), the remaining culture was used to make a glycerol stock using 99% glycerol (Sigma-Aldrich, Dorset, UK) in a 2:1 ratio with overnight broth culture, for a final concentration of 66% glycerol stock, these were stored at -80°C in 1.5 ml microcentrifuge tubes.

2.3.1.6 Verification of PCR product insertion

Restriction digests, utilising the sites which had been introduced through PCR (BamHI-HF, NheI-HF, BglII (NEB, Hertfordshire, UK)), were performed at 37°C for 30 minutes using a Techne TC-512 PCR machine. 10 µl of DNA, 10x buffer (NEB, Hertfordshire, UK) specific for the restriction enzyme, 100 µg/ml bovine serum albumin (BSA) (NEB, Hertfordshire, UK) (for NheI-HF restriction enzyme activity), and 10 U of restriction enzyme and made up to 25 µl with DNase free H₂O in a 0.2 ml PCR tube (Amersham Biosciences, Buckinghamshire, UK). The restriction digest DNA fragments were subsequently separated by gel electrophoresis in a 1% agarose TAE gel with 1:20,000 SafeView at 80 V, calibrating restriction digest

product size against 1 kb and 100 bp ladder (NEB, Hertfordshire, UK) on a BioRAD Gel Doc 2000.

2.3.1.7 Sequencing of PCR products

Samples with the correct size inserts, after digestion as determined by gel electrophoresis, were purified by DNA precipitation by adding ¼ volume of 1 M ammonium acetate (Fisher Scientific, Loughborough, UK) and 1 volume of 2-propanol (Sigma-Aldrich, Dorset, UK). The samples were incubated at room temperature for 30 minutes and then centrifuged at 15,500 xg for 10 minutes at 4°C in a Sigma 3K18 centrifuge, the DNA pellet was washed with 80% ethanol and centrifuged again. The DNA pellet was re-suspended in 50 µl of DNase free H₂O (Life Technologies, Paisley, UK), the DNA concentration verified using a Nanodrop Spectrophotometer ND1000 and then diluted to 100 ng/ml and sent for sequencing using the MWG Eurofins sequencing facility. Sequencing primers T7 and SP6 were used as well as product-specific primers, which were designed for larger genes (Table 2.2), to sequence from the middle to the ends of the gene. Sequences were compared to human sequences using NCBI Nucleotide BLAST.

Gene	Position (bp)	Forward	Reverse
OCT6	400	CTGTACGCGCAGGCGGCTACCCG	CGGGTAGGCCCGCCTGCGCGTACAG
FOXP1	500	CAGTTGGCTTTTCAGCAGCAGCTTTTA	-
FOXP1	1000	CTTGCAAAAGACAAAGAACGCCTGCAA	TTGCAGGCGTTCTTTGTCTTTTGAAG
FOXP1	1500	-	CCTGCCTAATTAAGATGCATATG
ISL1	500	CATCCAGCGCGGCCACTGCAAATGGC A	TGCCATTTGCAGTGGCCGCGCTGGAT G
EBF1	600	TGACATGCGGAGATTCCAGGTCGT	ACGACCTGGAATCTCCGCATGTCA
EBF1	1200	CCACACAACAACCAGGAAATCATT	AATGATTTCTGGTTGTTGTGTGG
NOLZ1	600	CCCTGCCTTCCACGCCGGTC	GGCAGGGGCTGCAGGTACTC
NOLZ1	1300	AGCCGGGCCAGACAGTGTTTC	CCCGGCTTGTAGGGTGACACG
NOLZ1	2000	ACCCAGCTCGTCGTCTCTGG	CCGTATGGGTCCGCAAGTGCC

Table 2.2 Primers used for sequence verification of transcription factor inserts.

2.3.2 Subcloning

Once the open reading frame sequences were verified, the pGEM[®] T easy plasmids containing the transcription factors and the p3x2ApMA-T multicistronic plasmid were digested with the relevant restriction enzyme for the incorporated restriction enzyme site on the ends of the transcription factors, either BamHI-HF, NheI-HF or BglII (all NEB, Hertfordshire, UK) (Figure 2.1). The restriction enzyme digestion of the p3x2ApMA-T plasmid was also incubated with 1.25 U thermo-sensitive alkaline phosphatase (TSAP) (Promega, Hampshire, UK) to remove the 5' phosphate groups from the ends of the linearised plasmid DNA in order to prevent re-circularisation and increase the likelihood of ligation to the insert. DNA products of the expected size were purified by gel extraction as per Section 2.3.1.2 and ligated using 400 U of T4 DNA ligase (NEB, Hertfordshire, UK), in a 20 µl reaction using the supplied 10X buffer and made to volume with H₂O. Varying insert:plasmid molar ratios were used, in order to optimise ligation, from 3:1 to 9:1. Ligation reactions were carried out for 12 hours at increasing temperatures from 16°C to 24°C in 2°C increments every 2 hours, with a final 2 hour step at 25°C. The ligation reaction was transformed into subcloning efficiency DH5α *E. coli* as per Section 2.3.14 and grown on 50 µg/ml ampicillin LB agar plates. Resulting colonies were grown up in LB broth containing 50 µg/ml ampicillin and the DNA purified as per Section 2.3.1.5. Diagnostic digests were carried out to verify insert orientation using specific restriction enzymes (Table 3.1 for a list of the restriction enzymes used and the fragments generated). *E.coli* colonies expressing constructs containing correctly orientated inserts were further cultured and midi prepped (Qiagen, Hilden, Germany) as per manufacturer's protocol and glycerol stocks were made as per 2.3.1.5. Then, either subsequent transcription factor gene insertions were performed using different restriction enzyme insertion sites in the multicistronic plasmid to create multi transcription factor plasmids, or the multicistronic section of the

plasmid, containing the transcription factor was subcloned into the pCAGG-IRES-EGFP vector using the *Sall* sites either side of the multicistronic section.

Sall-HF (NEB, Hertfordshire, UK) restriction enzyme digestion was used to isolate the transcription factor and flanking 3 x 2A sequences out of the p3x2ApMA-T plasmid and to linearise the pCAGG-IRES-EGFP plasmid, as above, the plasmid and insert were purified by gel extraction, ligated, transformed into subcloning efficiency DH5 α *E. coli*, grown up in LB agar and LB broth containing 50 μ g/ml kanamycin and then the DNA was purified as per Section 2.3.1.5. The orientation of the insert was checked by restriction digest (Table 3.1). Endo free maxi preps (Qiagen, Hilden, Germany) of plasmids, ready for transfection, were performed on positive clones as per manufacturer's instructions and glycerol stocks were made and stored at -80°C.

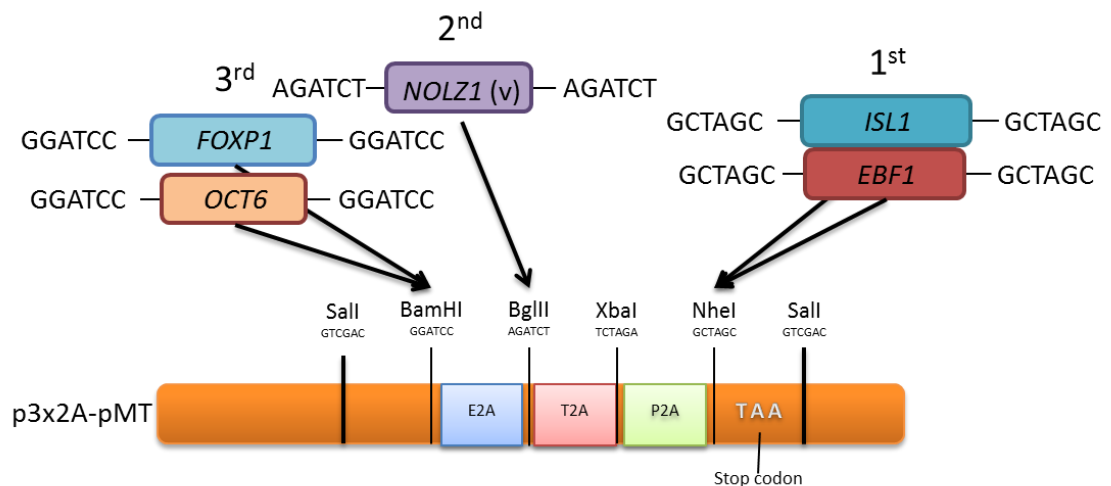


Figure 2.1: Schematic diagram showing the insertion sites for each of the cloned genes in the p3x2A-pMT multicistronic plasmid. Both *OCT6* and *FOXP1* are inserted into the BamHI restriction enzyme site, *NOLZ1* is inserted into the BglIII restriction site, *ISL1* and *EBF1* are inserted into the NheI site. The numbers demonstrate the order in which the genes are to be inserted in order to remain intact.

2.4 Cell culture

Unless otherwise stated, all cell culture reagents were supplied by Life Technologies, Paisley, UK.

2.4.1 Transfection of HEK293 cells

HEK293 cells were cultured in T25 flasks (BD Falcon, Oxford, UK) until 70% confluent in DMEM:F12 (1:1), supplemented with 10% FBS, 2 mM L-glutamine and 1% PenStrep at 37°C in 95% air/5% CO₂. Cells were washed with 1x phosphate buffered saline (PBS) pH 7.4 prior to dissociation with 1 ml of 0.05% trypsin-EDTA for 3 minutes at 37°C before being resuspended in 4 ml of culture medium, centrifuged at 230 *xg* for 3 minutes, washed with PBS, centrifuged again and re-suspended in 100 µl Nucleofector cell solution V (Lonza, Basel, Switzerland). 5 µg of plasmid DNA was added to the cells and then placed into a cuvette and nucleofected using Nucleofector II, programme Q001. After transfection, 900 µl of culture medium was added to the cuvette before being placed in a fresh tube and centrifuged for 2 minutes at 230 *xg*. The supernatant was removed and the cells re-suspended in culture medium for plating onto 13 mm coverslips (VWR, Leicestershire, UK) in a 24 well plate (Fisher Scientific, Loughborough, UK) and into a T25 flask. These cells were cultured for a further 48 hours in medium, as above. At 24 hours, the cells were observed on a fluorescent microscope (Olympus BX61, Southend-on-Sea, UK) and images of random fields of view were taken in order to determine transfection efficiency by calculating the number of GFP⁺ cells as a proportion of total cell number.

2.4.2 iPS cell culture

The control iPS cell line, referred to herein as 34D6, were a kind gift of Prof. Siddharthan Chandran, Edinburgh, UK and were generated as previously described (Bilican et al., 2012) iPS colonies were maintained at 37°C, 95% air/5% CO₂, in mTESR™1 complete media (Stemcell technologies, Manchester, UK) containing 1% Penstrep (Life Technologies, Paisley, UK), on Matrigel (hESC qualified) (VWR, Leicestershire, UK) coated, 60 mm Nunc dishes (VWR, Leicestershire, UK), diluted as per manufacturer's specifications in knockout DMEM at 37°C for 1 hour. Cells

were passaged every 3-4 days using 1 ml dispase (Stemcell technologies, Manchester, UK) with 10 μ M Y27632 dihydrochloride, the Rho kinase (ROCK) inhibitor, (Abcam, Cambridge, UK), for 15-20 minutes, until the colony edges began to lift. The colonies were washed off of the plates with knockout DMEM (Life Technologies, Paisley, UK) using a P1000, collected in a 15 ml tube (VWR, Leicestershire, UK) centrifuged at 230 xg for 3 minutes in a Rotanta 460R benchtop centrifuge (Hettich, Tuttlinge, Germany) and the cell pellet re-suspended in mTESR™1 medium and re-plated onto fresh Matrigel-coated plates; medium was changed daily (100%).

2.4.3 Early differentiation

iPS colonies were differentiated when they were at 70-80% confluency. mTESR™1 medium was removed, the colonies were washed with 1x PBS pH7.4 and the medium changed to SLI medium which contained Advanced DMEM/F12 (ADF) supplemented with 2 mM L-glutamine, 1% Penstrep, 2% Neurobrew 21 without vitamin A (Miltenyi, Surrey, UK), 10 μ M SB431542, (CHDI, Los Angeles, CA, USA), a TGF- β receptor kinase inhibitor, 1 μ M LDN 193189, (CHDI, Los Angeles, CA, USA) a BMP receptor ALK2 & ALK3 antagonist and 1.5 μ M IWR1, (CHDI, Los Angeles, CA, USA), an inhibitor of WNT signalling. This was defined as day 0 and the medium was fully changed daily. At day 4, when the cells were fully confluent, they were split 1:2. Cells were pre-treated with 10 μ M Y27632 dihydrochloride for 30 minutes before being washed with PBS pH 7.4 and treated with 1 ml neat Stempro® Accutase® containing 10 μ M Y27632 dihydrochloride for 5 minutes at 37°C. Cells were washed off of the plate with ADF containing 10 μ M Y27632 dihydrochloride using a P1000 pipette, collected into a 15 ml tube and centrifuged at 230 xg for 3 minutes; cells were re-suspended in SLI medium and re-plated on Matrigel-coated 60 mm Nunc dishes. At day 8, cells were split again 1:2 as above, and re-plated into LI medium (ADF supplemented with 2 mM L-glutamine, 1% Penstrep, 2%

Neurobrew 21 without RA, 0.2 μM LDN 193189 and 1.5 μM IWR1). Cells were cultured in LI medium, with daily medium changes, until day 16, when they were frozen in Cryostor CS10 (Stemcell technologies, Manchester, UK) with 10 μM Y27632 dihydrochloride after being dissociated from the dishes with Stempro[®] Accutase[®] containing 10 μM Y27632 dihydrochloride, as above, plated for terminal differentiation or transfected with the transcription factors (Section 2.4.4 & 2.4.5).

2.4.4 Terminal differentiation

Day 16 cells were either thawed or dissociated from the plates using Stempro[®] Accutase[®] with 10 μM Y27632 dihydrochloride, washed in ADF with 10 μM Y27632 dihydrochloride, centrifuged at 230 xg for 3 minutes, and re-suspended in 1 ml SCM1 medium (ADF supplemented with 2 mM L-glutamine, 1% Penstrep, 2% Neurobrew 21 with retinoic acid (Miltenyi, Surrey, UK), 2 μM PD 0332991 (CHDI, Los Angeles, CA, USA), a CDK4/6 inhibitor, 10 μM DAPT (CHDI, Los Angeles, CA, USA), an inhibitor of γ -secretase, 10 ng/ml brain-derived neurotrophic factor (BDNF, Miltenyi, Surrey, UK), 10 μM Forskolin (CHDI, Los Angeles, CA, USA), an adenylate cyclase activator, 3 μM CHIR 99021 (CHDI, Los Angeles, CA, USA), an inhibitor of glycogen synthase kinase 3 (GSK3), 300 μM γ -amino butyric acid (GABA, Tocris, Oxfordshire, UK), supplemented with CaCl_2 to final concentration of 1.8 mM (Sigma-Aldrich, Dorset, UK) and 200 μM Ascorbic acid (Sigma-Aldrich, Dorset, UK)). 10 μl of cells was added to 10 μl of trypan blue (Sigma-Aldrich, Dorset, UK) and were counted using a haemocytometer to allow accurate plating at 50,000 cells per well of a 24 well plate in 50 μl of medium on nitric acid etched/Poly-D-Lysine-/Matrigel-coated glass coverslips (Section 2.4.4.2) and allowed to settle for 90 minutes. A 50% medium change was performed on day 18 and 21, then fully changed on day 23 to SCM2 medium (1:1 ADF:Neurobasal A (Life Technologies, Paisley, UK) supplemented with 2 mM L-glutamine, 1% Penstrep, 2% Neurobrew 21 with retinoic acid, 2 μM PD 0332991, 10 ng/ml BDNF, 3 μM CHIR 99021, 1.8 mM CaCl_2 and 200

μ M Ascorbic acid). 1:1 medium changes continued for the remaining days: 25, 28, 30, 32, 35, 37 and 39. Occasionally, cells were maintained for a 4th week in SCM2, changing medium at 42 & 44 days.

2.4.4.2 Coverslip preparation for cell plating

Round 13 mm glass coverslips (VWR, Leicestershire, UK) were washed by treatment with nitric acid (Sigma-Aldrich, Dorset, UK) in a 50 ml centrifuge tube (VWR, Leicestershire, UK) on a Stuart mini see saw rocker SSM4 (Bibby Scientific Ltd., Staffordshire, UK) overnight at room temperature, 15 osc/min (as per Beaudoin et al., 2012). Coverslips were removed from the acid and washed 3 times with distilled water (Life Technologies, Paisley, UK) and a final wash in 70% ethanol before being spread in a borosilicate glass petri dish (Fisher Scientific, Loughborough, UK) and baked overnight in an oven (Swallow, LTE Scientific Ltd., Lancashire, UK) at 150°C. These coverslips were then placed into 24 well plates using ethanol-sterilised tweezers and the coverslips were coated with 50 μ l drops of 100 μ g/ml of Poly-D-Lysine (Sigma-Aldrich, Dorset, UK) in borate buffer pH 8.4 for 1 hour at room temperature and then washed with distilled water (Life Technologies, Paisley, UK) and coated with 50 μ l drops of Matrigel (as 2.4.1).

2.4.5 Transfection of plasmids for differentiation

At day 16, cells were transfected with pCAGG-TF-IRES-EGFP plasmids using nucleofection. The cells were pretreated with 10 μ M Y27632 dihydrochloride for one hour and then dissociated from the plate using Stempro[®] Accutase[®] containing 10 μ M Y27632 dihydrochloride. Cells were then washed off the dish with ADF containing 10 μ M Y27632 dihydrochloride into a 15 ml tube and then centrifuged at 230 xg for 3 minutes, washed with PBS pH 7.4, centrifuged again, then re-suspended in AMAXA Nucleofector mouse neural stem cell solution (Lonza, Basel, Switzerland) at 1×10^6 cells/100 μ l of solution per transfection, with 5 μ g of plasmid

DNA, in the AMAXA cuvette; provided and nucleofection was facilitated using programme A-033 on the Nucleofector II device (Lonza, Basel, Switzerland). Following nucleofection, 900 µl ADF containing 10 µM Y27632 dihydrochloride was added to the cell suspension, and then transferred into a 15 ml tube and centrifuged for 3 minutes at 230 *xg*. The cells were then re-suspended in 1 ml of SCM1 medium containing 10 µM Y27632 dihydrochloride and plated at 80,000 cells per well (as above, 2.4.4). Transfection efficiency was analysed 1 day later, by monitoring GFP expression microscopically on a Olympus BX61 epifluorescent microscope (Olympus, Southend-on-Sea, UK). Medium was changed, as detailed in section 2.4.4.

2.4.6 G418 Kill curve

After initial screening of plasmids by transfection for MSN differentiation, later transfections with fewer plasmids for more in depth analysis were treated with Geneticin[®] G418 to enrich the population for cells expressing the given plasmid. At 24 hours post plate-down of transfected cells, SCM1 medium was replaced with SCM1 medium containing G418 at 150 µg/ml, 300 µg/ml and 600 µg/ml or no G418 added. Media were changed then at the time points as described in Section 2.4.4 using medium containing G418. Cells were viewed every 48-96 hours and the proportion of GFP-positive cells was determined.

2.5 Protein analysis

2.5.1 Western blotting

At 48 hours post transfection, HEK293 cells were harvested by treatment with 1 ml of 0.05% trypsin-EDTA for 3 minutes at 37°C, resuspended in media and centrifuged at 120 *xg* for 2 minutes before re-suspension in radio-immunoprecipitation assay buffer (RIPA buffer) (Sigma-Aldrich, Dorset, UK)

containing one Complete Mini EDTA-free Protease Inhibitor Cocktail Tablet (Roche, Hertfordshire, UK)/10 ml and left on ice for 10 minutes. The lysate was centrifuged at 15,500 xg for 30 minutes at 4°C, after which the supernatant was aspirated and placed in to a fresh tube and frozen at -80°C.

Samples were thawed on ice in order to perform a bicinchoninic acid (BCA) assay (Thermo, Waltham, MA, USA) to determine the concentration of protein per sample. The microplate procedure was performed in a 96 well plate (Fisher Scientific, Loughborough, UK) as per manufacturer's instructions and protein concentration determined by plotting a protein concentration vs. absorbance at 562 nm calibration graph. Western blotting was performed using 1.5 mm polyacrylamide gel with a 10% resolving gel and 7.5% stacking gel (Table 2.3).

10% Resolving gel		7.5% Stacking gel		Transfer buffer	Running buffer
0.31 M	Tris pH 8.8	0.14 M	Tris pH 6.8	25 mM Tris base	25 mM Tris Base
10% (v/v)	Acrylamide	7.5% (v/v)	Acrylamide	192 mM Glycine	192 mM Glycine
0.002% (w/v)	SDS	0.002% (w/v)	SDS	20% (v/v) Methanol	0.1% (w/v) SDS
0.0003% (w/v)	Ammonium persulfate (APS)	0.001% (w/v)	APS	To 1 L with H ₂ O	To 1 L with ddH ₂ O
30 μ l TEMED		30 μ l TEMED			
ddH ₂ O to 21.03 ml		ddH ₂ O to 6.9225 ml			

Table 2.3 Composition of gels and buffers for Western blotting

Samples of 30 μ g protein were made up to 12.5 μ l with H₂O and added to 12.5 μ l of 2x Laemmli sample buffer (Sigma-Aldrich, Dorset, UK) in a 0.2 ml PCR tube and denatured at 95°C for 5 minutes in a Techne TC512 thermocycler (Bibby Scientific Ltd., Staffordshire, UK) before being loaded onto the gel. Novex protein ladder (Life Technologies, Paisley, UK) was used as a size marker and 6 μ l of this was loaded in an additional lane. Separation of proteins was performed by running the samples at 100 V until the dye front of the loading buffer reached the bottom of the stacking

gel and at 200 V for the dye front to reach the bottom of the resolving gel in 1x running buffer. The gel was removed from the glass moulds and placed between blotting paper (Sigma-Aldrich, Dorset, UK) and nitrocellulose membrane (Amersham Biosciences, Buckinghamshire, UK) to perform transfer of the protein from the gel to nitrocellulose and placed into a Mini-PROTEAN apparatus set-up as per manufacturer's instructions (BioRad, Hertfordshire, UK). Transfer of protein on to the nitrocellulose membrane was carried out at 100 V for 1 hour in transfer buffer (Table 2.3) from gel to nitrocellulose. The nitrocellulose membrane was then immersed in Ponceau S to check whether the transfer of protein from gel to nitrocellulose had been successful. Membranes were washed with transfer buffer and tris buffered saline (TBS, see appendix) before being placed in blocking solution for 1 hour at room temperature and then incubated with primary antibody (Table 2.4 for concentration of antibodies and specific blocking conditions). After incubation, primary antibodies were removed and stored at 4°C for future use. Membranes were washed 3 x 5 minutes in TBS/Tween and then incubated with the relevant secondary antibody (Table 2.5 for dilutions) for 1 hour at room temperature. The secondary antibody was then removed and the membranes were washed twice for 3 minutes in TBS, 3 x 3 minutes in TBS/0.1%Tween and twice for 3 minutes in TBS. The protein bands on the membrane were visualised by incubating with SuperSignal West Pico Chemiluminescent Substrate (Thermo Scientific, Waltham, MA, USA) or with SuperSignal West Dura Chemiluminescent Substrate (Thermo Scientific, Waltham, MA, USA) and exposed to X-ray film/Lumi-Film Chemiluminescent Detection Film (Roche, Hertfordshire, UK) in a Hypercassette (Amersham Biosciences, Buckinghamshire, UK) and the film was developed using an automatic developer (Xograph Compact X4).

Antibody	Species	Block	Dilution	Diluent	Incubation
2A peptide	Rabbit	5% Marvel PBS 0.1% Tween 0.05% Azide	1:1,000	1% block	Overnight 4°C
β-actin	Mouse	-	1:10,000	1% block	2 hours room temperature
Oct6	Rabbit	5% BSA 1% ovalbumin TBS 0.1% Tween 0.05% Azide	1:500	1% block	Overnight 4°C
FoxP1	Rabbit	5% BSA 1% ovalbumin TBS 0.1% Tween 0.05% Azide	1:5,000	1% block	Overnight 4°C
Islet1	Rabbit	5% BSA 1% ovalbumin TBS 0.1% Tween 0.05% Azide	1:10,000	1% block	Overnight 4°C
Nolz1	Rabbit	5% Milk TBS 0.1% Tween 0.05% Azide	1:1,000	1% block	Overnight 4°C
Ebf1	Rabbit	5% BSA 1% ovalbumin TBS 0.1% Tween 0.05% Azide	1:1,000	1% block	Overnight 4°C

Table 2.4: Antibody conditions and dilutions for western blotting of HEK293 protein samples.

Antibody	Host	Dilution	Diluent	Incubation
Rabbit	Donkey	1:20,000	TBS 0.1% Tween	2 hours room temperature
Mouse	Sheep	1:10,000	TBS 0.1% Tween	1 hour room temperature

Table 2.5: Secondary antibody dilutions and conditions for corresponding primary antibodies

2.5.2 Immunofluorescence

Cells on coverslips were washed with PBS and fixed with 4% paraformaldehyde, pH 7.4 (see appendix for recipe) for 10 minutes at room temperature. The cells were then washed with PBS before permeabilisation (Table 2.6 for specific conditions) and blocked for 1 hour at room temperature and then incubated with primary antibody overnight at 4°C. After removing the primary antibody, cells were washed 3 x 5 minutes with PBS and then incubated with secondary antibody (Table 2.7 for secondary antibodies and concentration used) in blocking solution for 2 hours at room temperature in the dark. The secondary antibody was removed and the cells were washed 3 x 5 minutes with PBS and incubated with Hoechst 33342 at 1:10,000 in PBS before being washed a further 3 x 5 minutes with PBS and mounted on glass slides (VWR, Leicestershire, UK) with Vectashield™ (Vector laboratories Ltd., Peterborough, UK) or Fluoromount-G® (Southern Biotech, Cambridgeshire, UK). Cells were viewed on an Olympus BX61 fluorescent

microscope (Olympus, Southend-on-Sea, UK) and digital images saved for later analyses. Cell counts were either performed manually in Image J (imagej.nih.gov/ij/), or nuclei and nuclear staining was performed using Cell Profiler v2.1.0 (Carpenter et al., 2006, <http://www.cellprofiler.org/citations.shtml>).

2.5.2.2 Quantification of DARPP32 immunofluorescence.

Cells were determined as positive for DARPP32 immunofluorescence by eye, with cytoplasmic localisation of staining. Initial GFP transfection efficiencies were used to determine induction efficiency of DARPP32 expression, by dividing the percentage of DARPP32⁺ cells by the percentage of GFP⁺ cells and this value was normalised to the CAG- transfected cells.

Antibody	Species	Permeabilisation	Block	Dilution	Incubation
2A peptide	Rabbit	0.25% Triton-X in PBS for 10 minutes	2% Goat serum, 3% BSA in 0.1% Triton-X PBS	1:500 in block	Overnight 4°C
OCT6	Rabbit	Methanol fixed	10% Goat serum 1% BSA 0.3M glycine 0.1% PBS Tween	1:200 in block	Overnight 4°C
FOXP1	Rabbit	0.25% Triton-X in PBS for 10 minutes	2% Goat serum, 3% BSA in 0.1% Triton-X PBS	1:500 in block	Overnight 4°C
FOXP1	Mouse	Ice cold ethanol 2 minutes	3% Goat serum, 3% BSA in 0.1% Triton-X PBS	1:500 in block	Overnight 4°C
ISL1	Rabbit	0.25% Triton-X in PBS for 10 minutes	2% Goat serum, 3% BSA in 0.1% Triton-X PBS	1:500 in block	Overnight 4°C
EBF1	Rabbit	0.25% Triton-X in PBS for 10 minutes	2% Goat serum, 3% BSA in 0.1% Triton-X PBS	1:500 in block	Overnight 4°C
MAP2	Rabbit	0.25% Triton-X in PBS for 10 minutes	2% Goat serum, 3% BSA in 0.1% Triton-X PBS	1:500 in block	Overnight 4°C
MAP2	Mouse	0.25% Triton-X in PBS for 10 minutes	2% Goat serum, 3% BSA in 0.1% Triton-X PBS	1:500 in block	Overnight 4°C
Synaptophysin	Mouse	-	2% Goat serum, 3% BSA in 0.05% Tween PBS	1:200 in block	Overnight 4°C
PSD-95	Rabbit	-	2% Goat serum, 3% BSA in 0.05% Tween PBS	1:100 in block	Overnight 4°C
S100β	Mouse	0.25% Triton-X in PBS for 10 minutes	2% Goat serum, 3% BSA in 0.1% Triton-X PBS	1:500 in block	Overnight 4°C
DCX	Goat	-	1% BSA in 0.3% Triton-X PBS	1:100 in block	Overnight 4°C
DARPP32	Rabbit	0.3% Triton-X in PBS for 10 minutes	2% Goat serum, 3% BSA in 0.1% Triton-X PBS	1:200 in block	Overnight 4°C
CTIP2	Rat	0.3% Triton-X in PBS for 10 minutes	2% Goat serum, 3% BSA in 0.1% Triton-X PBS	1:500 in block	Overnight 4°C
Calbindin	Rabbit	0.3% Triton-X in PBS for 10 minutes	3% Goat serum, 3% BSA in 0.1% Triton-X PBS	1:500 in block	Overnight 4°C
GFAP	Mouse	0.25% Triton-X in PBS for 10 minutes	2% Goat serum, 3% BSA in 0.1% Triton-X PBS	1:500 in block	Overnight 4°C
GFP	Chicken	0.25% Triton-X in PBS for 10 minutes	2% Goat serum, 3% BSA in 0.1% Triton-X PBS	1:1000 in block	Overnight 4°C

Table 2.6 Primary antibody dilutions and conditions for immunocytochemistry on cells.

Secondary antibody	Dilution
Alexa Fluor 594 goat α rabbit IgG (H&L)	1:500
Alexa Fluor 594 goat α mouse IgG (H&L)	1:500
Alexa Fluor 488 goat α rabbit IgG (H&L)	1:500
Alexa Fluor 488 goat α rat IgG (H&L)	1:500
Alexa Fluor 488 goat α mouse IgG (H&L)	1:500
Alexa Fluor 488 donkey α goat IgG (H&L)	1:500
Alexa Fluor 488 goat α chicken IgG (H&L)	1:1000
Alexa Fluor 350 goat α mouse IgG (H&L)	1:500
Alexa Fluor 350 goat α rat IgG (H&L)	1:500

Table 2.7 Secondary antibody dilutions and conditions for immunocytochemistry on cells

2.6 Sholl analysis

At day 23 and 30, coverslips of transfected cells were fixed with 4% PFA and the coverslips mounted with Fluoromount G[®] as per Section 2.5.2. Day 37 cells underwent a GFP immunocytochemistry in order to ensure GFP was still visible as per Section 2.3.2. GFP expressing cells were imaged on a confocal microscope Leica DM6000 (Leica, Milton Keynes, UK) taking a full z-stack throughout the cell every 0.6 μm . A 2D image was constructed using a maximum projection of each of the pixels on the image using the Leica LCS confocal software (Leica, Milton Keynes, UK). Images were stitched together, when required using Microsoft Image Composite Editor (Microsoft, Berkshire, UK). Images were converted to black and white by splitting the RGB channels of the image and the green channel selected for the axons and neurites to be traced using the simple neurite tracer plugin on Fiji software (http://fiji.sc/Simple_Neurite_Tracer). A line stack of the traces was created using the simple neurite tracer plugin, this was used for subsequent Sholl analysis. Data relating to neurite length and branching points was also obtained using the simple neurite tracer plugin. Sholl analysis was performed using the Sholl analysis plugin (http://fiji.sc/Sholl_Analysis) with a starting radius of 5 μm and final radius at the furthest point of the cell in increments of 1 μm .

2.7 Electrophysiology

Whole cell patch clamp was performed at 2 and 3 weeks post transfection for basic neuronal function by Dr Vsevelod Telezhkin (VT) and whole cell patch clamp for collecting data on GABA currents, and NMDA currents with dopamine D1 agonist enhancement and miniature synaptic currents was performed by Dr Christian Schnell (CS), who both provided the raw data files. All data analysis was performed by myself.

2.7.1 Electrodes

The patch electrode was silver/silver chloride wire (0.25 mm, Harvard Apparatus Ltd., Kent, UK), chloride coated using electrolysis of NaCl solution with a 9 V battery, and the bath/reference electrode was an Ag/AgCl pellet (Harvard Apparatus Ltd., Kent, UK) connected to the PC head stage.

2.7.2 Patch pipettes

Thin walled, filamented, borosilicate glass tubes (World Precision Instruments, Hertfordshire, UK) were pulled using a 2 stage pipette puller (PP-830, Naristige, Japan) to produce patch pipettes with a tip resistance of ~8-10 M Ω , when filled with standard pipette solution.

2.7.3 Whole cell patch clamp

Cells on glass coverslips which were at day 29-31 (termed week 2) and day 35-38 (termed week 3) were placed in the perfusion chamber on the stage of an inverted microscope (Olympus IX70 (VT), Olympus CK40 (CS), Olympus, Southend-on-Sea, UK) both with phase contrast and fluorescence optics. The microscope was mounted in a Faraday cage on an anti-vibration air table (Wentworth Laboratories, Oxfordshire, UK). Bath solution was perfused continuously in to the perfusion chamber using gravity flow at a rate of 2-4 ml/minute. A rapid solution changer

(RSC-160, Biologic, Claix, France) was utilised to perfuse other solutions onto the cells (Section 2.8.4.2), which was connected to parallel glass tubes with capillary tubing (Cole-Parmer, London, UK), which were positioned adjacent to the cells. A controlled flow rate from the RSC of 0.5-1.5 ml/minute and fully-automated switching of solutions allowed reproducible applications of various neurotransmitters. Waste solution was removed by vacuum suction through a flame-pulled glass tube into a Büchner flask.

Patch pipettes were filled with pipette solution (Table 2.8 for composition) through a 0.2 µm syringe filter (Sartorius Stedim, Surrey, UK) using a carbon-fibre flexible needle (Microfil, World Precision Instruments, Hertfordshire, UK). Pipettes were mounted on a CV 201AU headstage connected to an Axopatch 200B amplifier (VT), or Multiclamp 700A amplifier (CS) and DigiData 1322A A/D interface (Axon Instruments, Foster City, CA, USA). Recordings were digitized at 10 kHz and low-pass filtered using an 8-pole Bessl.

Cell bodies, which were accessible and GFP⁺ (suggesting transgene expression) were patched. The patch pipette was lowered using the macromanipulator (Burleigh PCS-PS60 (VT) (ThorLabs, Ely, UK), Scientifica Patchstar (CS) (Scientifica, East Sussex, UK)), when in the bath solution a seal test was performed using the pClamp 8.2 software (Molecular Devices, Sunnyvale, CA, USA), 10 mV for 10 ms at 50 Hz and the resistance between patch pipette and both electrodes calculated, pipette voltage offset was zeroed either manually (VT) or using MultiClamp commander software (CS, Molecular Devices, Sunnyvale, CA, USA). Micromanipulation of the patch pipette was used to lower the tip to the cell membrane until they touched and a decrease in amplitude of current was observed due to the increased resistance at the patch pipette due to touching the cell membrane. Negative pressure was applied to the patch pipette using a syringe, and the position of the patch pipette lowered by micromanipulation to improve the

membrane-pipette seal. A holding potential of -60 mV(VT)/-70 mV(CS) was applied across the membrane to prevent depolarisation of the cell upon whole-cell access. If the seal was $>1 \text{ G}\Omega$ the cell was used, the capacitance currents were compensated using fast and slow capacitance compensation either performed manually on the amplifier (VT) or with the MultiClamp commander software (CS).

Whole cell access was gained by applying negative pressure to the patch pipette until capacitance transients were observed from the seal test protocol and these were compensated as above. Series resistance was compensated 60-90%, cells with a leak current greater than 200 pA were rejected.

Voltage and current-clamp protocols were generated using pClamp 10 software (Molecular devices, Sunnyvale, CA, USA) and the recordings were taken online using pClamp 8.2 and analysed offline using Clampfit 10 (Molecular devices, Sunnyvale, CA, USA), Microsoft Excel and GraphPad Prism 6 (GraphPad Software, Inc., La Jolla, CA, USA). Basic electrophysiology properties were recorded using the standard pipette (Table 2.8) and standard bath solutions (Table 2.9).

Standard pipette solution (VT)		Pipette solution for NMDA/GABA currents (CS)	
Reagent	Concentration	Reagent	Concentration
KCl	117 mM	HEPES	40 mM
NaCl	10 mM	EGTA	10 mM
N-2-hydroxyethylpiperazine-N'-2-ethanesulfonic acid (HEPES)	11 mM	MgCl ₂	2 mM
Na ₃ -GTP	2 mM	Na ₃ -GTP	0.2 mM
Na ₂ -ATP	2 mM	Na ₂ -ATP	2 mM
Phosphocreatine	1.2 mM	N-Methyl-D-Glucamine (NMDG)	175 mM
MgCl ₂	2 mM	Phosphocreatine	12 mM
CaCl ₂	1 mM	Leupeptin	0.1 mM
Ethylene-glycol-tetra-acetic acid (EGTA)	11 mM		
pH adjusted to 7.2 with KOH		pH adjusted to 7.2 with H ₂ SO ₄	

Table 2.8 Composition of pipette solutions for whole cell patch clamp recordings

Standard bath solution (VT)		Bath solution for NMDA/GABA currents (CS)	
Reagent	Concentration	Reagent	Concentration
NaCl	135 mM	NaCl	127 mM
KCl	5 mM	HEPES	10 mM
MgCl ₂	1.2 mM	D-Glucose	12 mM
CaCl ₂	1.25 mM	CaCl ₂	2 mM
D-Glucose	10 mM	BaCl ₂	5 mM
HEPES	5 mM	CsCl	20 mM
		Tetrodotoxin	0.001 mM
		Glycine	0.02 mM
pH adjusted to 7.4 with NaOH		pH adjusted to 7.3 with NaOH	

Table 2.9 Composition of bath solutions for whole cell patch clamp recordings

2.7.4 Current clamp

2.7.4.1 Basic properties (VT)

Measurement of resting membrane potential (V_m) and monitoring the presence or absence of spontaneous action potentials in each cell was performed in fast current clamp with 0 pA current injection for 60-120 s. The V_m was determined by averaging a section of the trace containing no events. The membrane potential was also manipulated by manual variable current injection to obtain a membrane potential of -70 mV and see if cells were able to fire action potentials.

In order to analyse action potentials, a current clamp protocol involving variable current injection to hold the cell membrane potential at -70 mV and from this, specific current injection was applied for 1 second from -10 pA to 180 pA in 10 pA increments. The action potentials elicited were analysed in Clampfit 10.2 for parameters indicative of neuronal maturity and type. In order to determine the input resistance of the cells, the last 50 ms from up to the first 5 sweeps from the current clamp protocol without action potential attempts were averaged to create a linear I-V graph. The gradient of the linear regression equation is equal to the input resistance due to Ohm's law:

$$\text{Ohm's law: } V = \frac{I}{R} \text{ or } V = IG$$

$$\text{Linear regression: } y = mx + c$$

$$I = VR^{-1} + c$$

Where V=voltage, I=current, R=resistance, g=conductance

2.74.2 GABA & NMDA currents (CS)

2.7.4.2.1 GABA currents

Cells were held in current clamp mode at -40 mV, with 3 x 5 second applications of γ -amino butyric acid (GABA, 100 μ M) with a 90 second wash-out and recovery phase between each application. The average of the three sweeps was taken to determine the peak current.

The currents elicited were analysed by averaging the sets of three sweeps, then setting the baseline to the average current 2 seconds before GABA application and then measuring the peak current, which was positive-going for GABA

2.7.4.2.2 NMDA currents and dopamine D1 regulation

Investigation of dopamine enhancement of N-methyl-D-aspartic acid (NMDA, 100 μ M) was performed by 9 x 5 second applications, with 90 second recovery of 3 x NMDA alone applications, the second three applications were of NMDA with the dopamine D1 agonist SKF81297 (10 μ M) and the final three applications were of NMDA alone. The currents elicited were analysed by averaging the sets of three sweeps, then setting the baseline to the average current 2 seconds before NMDA application and then measuring the peak current, which was negative-going NMDA.

2.7.4.3 Mini excitatory post-synaptic currents (CS)

Cells were held in current clamp at -40 mV and recorded for 120 seconds as described in Flores-Hernández et al., (2002). The final 60 seconds of the recording were analysed for the presence of mini excitatory post-synaptic currents (EPSCs). Recordings were analysed using Mini Analysis 6.0.7 (Synaptosoft Inc., Decatur, GA, USA).

2.7.5 Voltage Clamp (VT)

Measurement of Na⁺ and K⁺ currents and voltage-dependent Na⁺ channel activation/inactivation was performed in voltage clamp. Cell membrane voltage was held at -70 mV before a voltage step for 200 ms from -120 mV increasing to 80 mV in 5 mV increments per sweep then a final voltage step to 0 mV for a further 200 ms. K⁺ currents were measured by averaging the last 50 ms of the variable section of the sweep. Na⁺ activation and inactivation currents were analysed from the initial 15 ms and 15 ms around the negative peak after the variable sweeps.

2.8 Statistical analysis

Analysis of data was performed using a suitable test for the data distribution and the hypothesis to be tested. Data were analysed in GraphPad Prism v 6.0 (GraphPad Software, Inc., La Jolla, CA, USA), and significant differences in data were analysed using one-way ANOVA with Tukey's multiple comparison, Kruskal-Wallis with Dunn's multiple comparison, unpaired two-tailed t-tests with Welch correction, Mann-Whitney U test.

CHAPTER 3:
TRANSCRIPTION
FACTOR CLONING &
PLASMID VALIDATION

3. Transcription factor cloning and plasmid validation

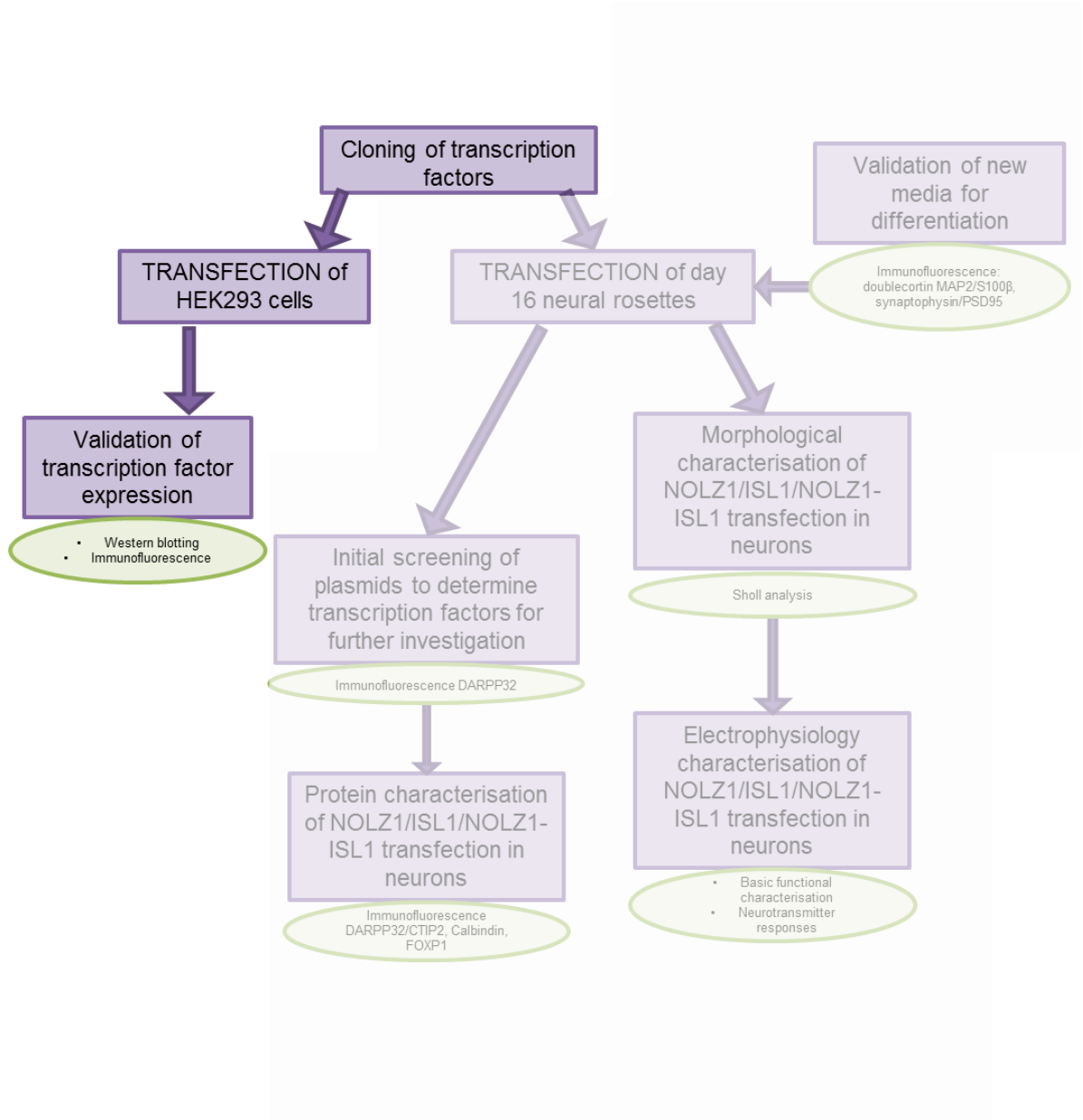


Figure 3.0: Summary of the data in chapter 3. In this chapter, is the cloning and validation of five transcription factors important for MSN development.

3.1 Introduction

The transcription factors EBF1, FOXP1, ISLET1, NOLZ1 & POU3F1 (OCT6), have been shown to play important roles in early striatal development and specification of

MSNs. In the *Ebf1* knockout mouse the transition of cells between the SVZ and MZ was disrupted and the postnatal mouse striatum was decreased in size (Garel et al., 1999). FOXP1 mRNA and protein were shown to be expressed from E14.5 to adult in the SVZ of the LGE (Ferland et al., 2004), ISLET1 mRNA and protein were shown to be expressed in the SVZ of the LGE throughout development (Stenman et al., 2003, Wang & Liu 2001), NOLZ1 mRNA and protein expression was observed during development of the early striatum before being downregulated postnatally (Chang et al., 2004, Urbán et al., 2010, Ko et al., 2013), and OCT6 mRNA and protein expression was seen in the SVZ of the LGE from E12 (Alvarez-Bolado et al., 1995), through to E15.5 (Garel et al., 1999) and in the adult (Frantz et al., 1994). Differential transcriptional profiling of the two MSN populations expressing either one of the two receptors; dopamine receptor D1a (*Drd1a*), the striatonigral population and dopamine receptor D2 (*Drd2*), the striatopallidal population, the results showed *Isl1* to be preferentially expressed in the striatonigral population and that the expression of *FoxP1*, *Nolz1* and *Ebf1* was upregulated in the striatum in comparison with the whole brain RNA (Heiman et al., 2008).

The developmental importance of these transcription factors, as highlighted above, due to their levels of expression during striatal development and the consequences of the absence of their expression are why these transcription factors have been chosen. These five key MSN-relevant transcription factors *ISLET1*, *NOLZ1* (*ZNF503*), *EBF1* (*OLF1*), *OCT6* (*POU3F1*) and *FOXP1*, were cloned from plasmids, which contained the protein coding sequences of the human genes, or from human brain cDNA. These transcription factors were then subcloned into a multicistronic plasmid. The multicistronic plasmid contains three 2A peptide cleavage sites separated and flanked by four different restriction enzyme sites. The 2A peptide is 18 amino acid residues in length terminating with a glycine, a 19 amino acid sequence was discovered to be sufficient in order to induce cleavage of the 2A

peptide at the C terminus in the foot and mouth disease virus (FMDV) (Ryan et al., 1991). The 2A peptide is followed by the 2B peptide, which is 19 amino acid residues long starting with a proline. The 2A peptides in the multicistronic plasmid originated from: i) the porcine teschovirus, termed P2A (Kim et al., 2011); ii) the equine rhinitis A virus, E2A; and; iii) insect virus *Thosea asigna*, T2A (Szymczak et al., 2004). These peptides induced self-cleavage by interacting with the exit tunnel of the ribosome during translation, this interaction induced a “skip” mechanism and as a result the peptide bond was not formed between the final residue of the 2A peptide (glycine) and the first residue of the 2B peptide (proline) (de Felipe 2004). The two peptides remained separate and the ribosome continues to translate the downstream sequence of the 2B peptide (de Felipe 2004). This means that the upstream proteins are tagged with a C terminal 18 amino acids and the downstream proteins are tagged with an N terminal proline residue, these have been shown to have a minimal effect on protein-protein interaction and activity, and have no effect on protein stability (de Felipe 2004).

This method was selected in order to express multiple genes in equal amounts, from a single promoter, and has advantages over other multicistronic transgene expression strategies such as the use of internal ribosomal entry sites (IRES) in which downstream genes are expressed at much lower levels, usually only at 50% of the upstream gene in the expression vector (Mizuguchi et al., 2000). Another method for multiple gene expression using Fusagenes, which contain enzyme target sites between genes e.g. furin, the Golgi endoprotease, relies on the presence of the enzyme and efficient cleavage with the translated protein, which may not always be possible (Gäken et al., 2000).

Once the genes had been cloned into this multicistronic plasmid, the entire insert was subcloned into a pCAGG-IRES-EGFP expression vector (created by E L Cope) for forced expression of these transcription factors in stem cell-derived neural

progenitors in an attempt to drive their differentiation towards a MSN phenotype. The fact that the plasmid contains GFP coding sequence for GFP expression means the cells which have been transfected can be identified for electrophysiological characterisation and Sholl analysis (Chapter 5). The plasmid also contains a neomycin resistance gene to allow for selection of transfected cells by G418 treatment, in order to try and increase the proportion of the cell population which is expressing the transcription factors.

3.2 Cloning, Subcloning & Plasmid Verification

Vector	Enzyme	Correct	Incorrect
p3x2ApMT- <i>ISLET1</i>	NcoI-HF	2683bp + 978bp	3241bp + 420bp
p3x2ApMT- <i>NOLZ1</i> (variant)	NcoI-HF	2675bp + 686bp	3156bp + 303bp
p3x2ApMT- <i>EBF1</i>	NcoI-HF	2629bp + 1748bp	3996bp + 388bp
p3x2ApMT- <i>OCT6</i>	NcoI-HF	2731bp + 1221bp + 12bp	137bp + 3325bp
p3x2ApMT- <i>NOLZ1</i> (variant)- <i>ISLET1</i> (<i>NOLZ1</i>)	NcoI-HF	2680bp + 1140bp + 686bp	2680bp + 1523bp + 303bp
p3x2ApMT- <i>FOXP1</i> - <i>NOLZ1</i> (variant)- <i>ISLET1</i> (<i>FOXP1</i>)	EcoRI-HF	4884bp + 1679bp	6113bp + 450bp
pCAGG- <i>ISLET1</i> -IRES-EGFP	XmnI	6649bp + 1032bp	6963bp + 718bp
pCAGG- <i>NOLZ1</i> (variant)-IRES-EGFP	NotI-HF	5791bp + 1699bp	5432bp + 2058bp
pCAGG- <i>NOLZ1</i> -IRES-EGFP	NheI-HF	7841bp + 735bp	7151bp + 1425bp
pCAGG- <i>NOLZ1</i> - <i>ISLET1</i> -IRES-EGFP (<i>NOLZ1</i>)	NheI-HF	7841bp + 1053bp + 753bp	7151bp + 1425bp + 1053bp
pCAGG- <i>EBF1</i> -IRES-EGFP	SmaI	6753bp + 1654bp	8027bp + 380bp
pCAGG- <i>OCT6</i> -IRES-EGFP	SmaI	6870bp + 861bp + 201bp + 59bp	7234bp + 497bp + 201bp + 59bp
pCAGG- <i>NOLZ1</i> (variant)- <i>ISLET1</i> -IRES-EGFP	SmaI	7043bp + 1490bp	7863bp + 670bp
pCAGG- <i>FOXP1</i> - <i>NOLZ1</i> (variant)- <i>ISLET1</i> -IRES-EGFP	SmaI	7082bp + 2018bp + 1490bp	7863bp + 2018bp + 709bp
pCAGG- <i>NOLZ1</i> (variant)- <i>ISLET1</i> -IRES-EGFP (<i>ISL1</i>)	PfIIM1	6735bp + 1136bp + 672bp	6735bp + 918bp + 890bp
pCAGG- <i>NOLZ1</i> (variant)- <i>ISLET1</i> -IRES-EGFP (<i>ISL1</i>)	XmnI	7514bp + 1029bp	8025bp + 518bp
pCAGG- <i>NOLZ1</i> - <i>ISLET1</i> -IRES-EGFP (<i>ISL1</i>)	PfIIM1	6735bp + 1136bp + 672bp	7824bp + 915bp + 890bp
pCAGG- <i>ISLET1</i> -IRES-EGFP (<i>ISL1</i>)	PfIIM1	6542bp + 1139bp	6788bp + 890bp

Table 3.1 The enzymes used to check the orientation of transcription factor insert in the p3x2ApMT vector and pCAGG-IRES-EGFP vector by restriction digest and the sizes of bands produced with the restriction enzymes

3.3 EBF1

EBF1 was selected to be cloned and used for forced expression in neural stem cells to impose a MSN phenotype because i) EBF1 is expressed in the SVZ and MZ of the LGE (Garel et al., 1997, Garel et al., 2003); ii) *Ebf1* overexpression forced cells to exit the cell cycle and undergo premature neural differentiation in the chick embryo (Garcia-Dominguez et al., 2003); iii) during development in the *Ebf1*^{-/-} mouse, there was a defect in the transition of cells from the SVZ to the MZ in the LGE (Garel et al., 1999), with a marked decrease in the expression of striatally enriched genes (Lobo et al., 2008).

1. Cloning of EBF1

Human *EBF1* was cloned from a plasmid clone ID: HsCD00296820 (PlasmID Harvard Medical School, Boston, U.S.A.), into the pGEM[®] T easy vector using PCR primers to incorporate NheI restriction enzyme sites onto the 5' and 3' ends of the gene (Figure 3.1a) and the stop codon omitted, the PCR product at ~1.7 kb can be observed as per Figure 3.1b. NheI sites were chosen for incorporation to insert the *EBF1* gene into the multicistronic plasmid as there are no NheI sites in the *EBF1* gene. White colonies were screened by restriction digestion using NheI, as insertion of the *EBF1* gene interrupts the *lacZ* gene of the pGEM[®] T easy vector. The restriction digest consisted of 2 DNA fragments of ~3kb and ~1.7kb (Figure 3.1c). Positive clones were sequenced at MWG Eurofins and verified by analysing the sequence on NCBI Nucleotide BLAST, the sequence homology was 100% with *Homo sapiens EBF1* (NM_024007.3), the 5' and 3' ends of the alignment as per Figure 3.2d (Appendix for full alignment).

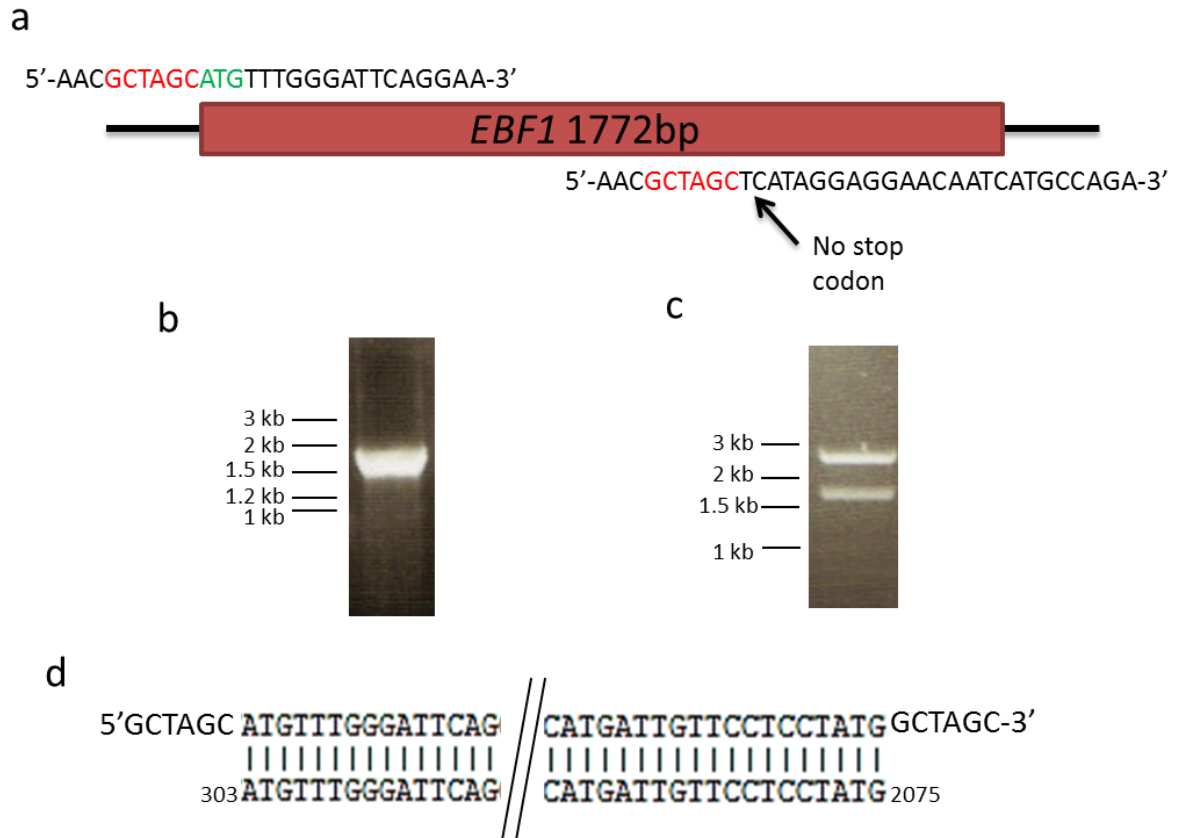


Figure 3.1: Cloning of *EBF1*. a) Schematic showing PCR primers incorporation of *NheI* sites (red) onto the 5' and 3' ends of *EBF1* and removing the stop codon. b) *EBF1* was cloned from Plasmid Harvard vector: HsCD00296820 by high fidelity PCR. The fragment was extracted and ligated into pGEM[®] T easy cloning vector, colonies were screened by utilising blue/white selection as a result of the *lacZ* gene being interrupted in the cloning vector. c) Restriction digest of a mini prep from a white colony to check that *EBF1* was inserted by *NheI* digestion, as seen by the pGEM[®] T easy vector backbone band at ~3kb and the insert at ~1.7kb. d) Alignment of *EBF1* sequencing data to NM_024007.3 100% homology.

2. Subcloning of *EBF1*

EBF1 was then subcloned into the p3x2A-pMT multicistronic plasmid with *NheI* (Figure 3.2a & 3.2b) and checked for orientation by restriction digest with *NcoI* to produce fragments of 2629bp and 1748bp (Table 3.1). *EBF1* in the multicistronic fragment was then subcloned into the pCAGG-IRES-EGFP plasmid (Figure 3.2c) with *Sall* and the orientation of the insert was verified with *SmaI* to produce fragments of 6753bp and 1654bp as per Figure 3.2e (Table 3.1).

3. Transcription factor cloning and plasmid validation

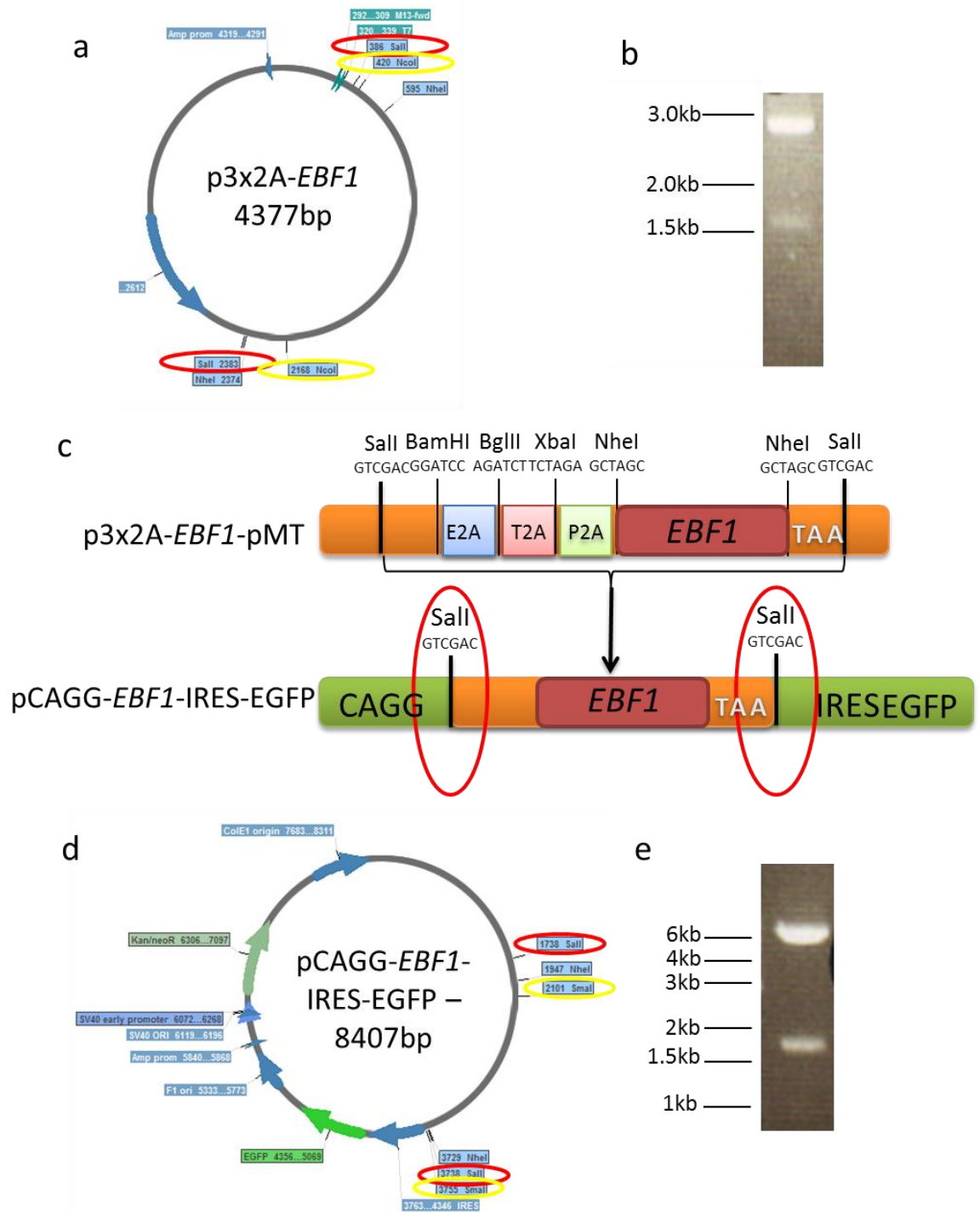


Figure 3.2: Plasmid design and formation of pCAGG-*EBF1*-IRES-EGFP. a) p3x2A-*EBF1* plasmid map highlighting important restriction enzyme sites for cloning strategy, red ringed sites correspond to those in a, NcoI sites ringed in yellow at 420 and 2168 were used for checking *EBF1* insertion orientation as seen in the gel in (b). b) NcoI digest producing fragments of p3x2A-*EBF1* producing bands of 2629bp and 1748bp c) Schematic showing the insertion of *EBF1* into the pCAGG-IRES-EGFP vector by Sall digestion. d) Plasmid map of pCAGG-*EBF1*-IRES-EGFP, red circles highlighting the Sall sites and SmaI sites ringed in yellow at 2101 and 3755 which were used for checking the orientation of *EBF1* insertion. e) SmaI digestion of pCAGG-*EBF1*-IRES-EGFP to check orientation producing fragments of 6753bp and 1654bp

3. Validation of EBF1 protein expression

In order to validate that the EBF1 protein was being expressed correctly, transient transfections of pCAGG-*EBF1*-IRES-EGFP into HEK293 cells were performed. Protein molecular weight was determined by western blot and immunocytochemistry was performed to determine cell localisation of EBF1 protein, which should be nuclear. The initial analysis of GFP expression from the pCAGG-*EBF1*-IRES-EGFP vector can be seen in Figure 3.3a and exemplifies the mean transfection efficiency of $13.2 \pm 1.1\%$ (N=1; n=3). Western blot and immunocytochemistry were unsuccessful, using two different antibodies for EBF1 expression as seen in Figure 3.3b with non-specific staining observed in the cytoplasm of the cells in both the empty plasmid control and EBF1 containing plasmid. The use of the anti-2A peptide antibody would not provide any signal as EBF1 is inserted into the final position in the multicistronic plasmid and therefore does not possess a 2A peptide tag.

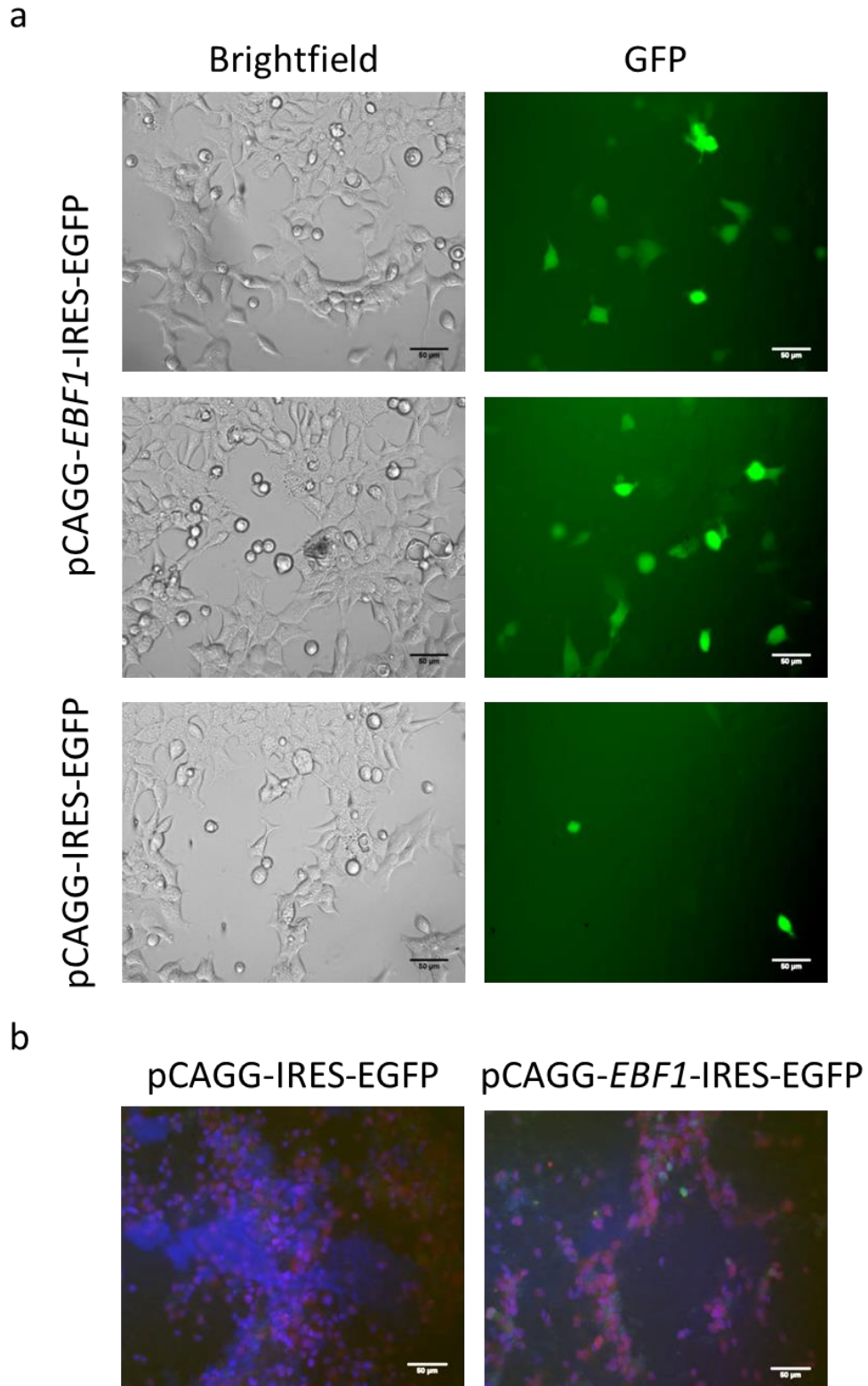


Figure 3.3: Analysis of protein expression in cells expressing pCAGG-EBF1-IRES-EGFP. HEK293 cells were transfected with pCAGG-EBF1-IRES-EGFP or pCAGG-IRES-EGFP (control). Images were taken 24 hours later. A) Bright field shown in left panels, GFP fluorescence of same field shown in right panels expression. Upper four panels show EBF1 plasmid, lower two panels show control plasmid. Transfection efficiency: $13.2\% \pm 1.1$.

Scalebar = 50 μ m b) Immunocytochemistry 48 hours post transfection of stem cell derived neural stem cells. Images of EBF1 expression in red and GFP expression from the plasmids in green, nuclei are stained blue. Scalebar = 50 μ m

3.4 ISLET1

ISLET1 was chosen to be utilised in transfections of neural stem cells as ISLET1 is an essential protein in striatal development and is highly expressed in the developing LGE and striatum (Wang & Liu 2001, Long et al., 2009, Stenman et al., 2003).

1. Cloning of ISLET1

ISLET1 was cloned from a plasmid clone ID HsCD00076385 (PlasmID) into the pGEM[®] T easy vector with primers incorporating the NheI restriction enzyme sites on to the 5' and 3' ends of the gene (Figure 3.4). NheI sites were chosen due to *ISLET1* being one of the two genes chosen which did not contain NheI sites in the protein coding sequence and as *ISLET1* did not contain XbaI, BglII and BamHI restriction sites (the other restriction sites for insertion in the p3x2A-pMT plasmid), *ISLET1* was the first gene to be inserted into the p3x2A-pMT vector before insertion of the other transcription factor genes. Colonies were screened by restriction digestion using NheI to check for insertion (Figure 3.4c). Positive clones were sequenced at MWG Eurofins and verified by NCBI Nucleotide (Figure 3.4d), where the sequence was identified as sharing >99% homology with *Homo sapiens ISLET1* (NM_002202.2), with a base substitution at position 1052 of an A to a G. Upon searching the SNP database (NCBI), it was confirmed to be a known SNP (Figure 3.4e) and did not result in a change of amino acid residue, with proline remaining intact.

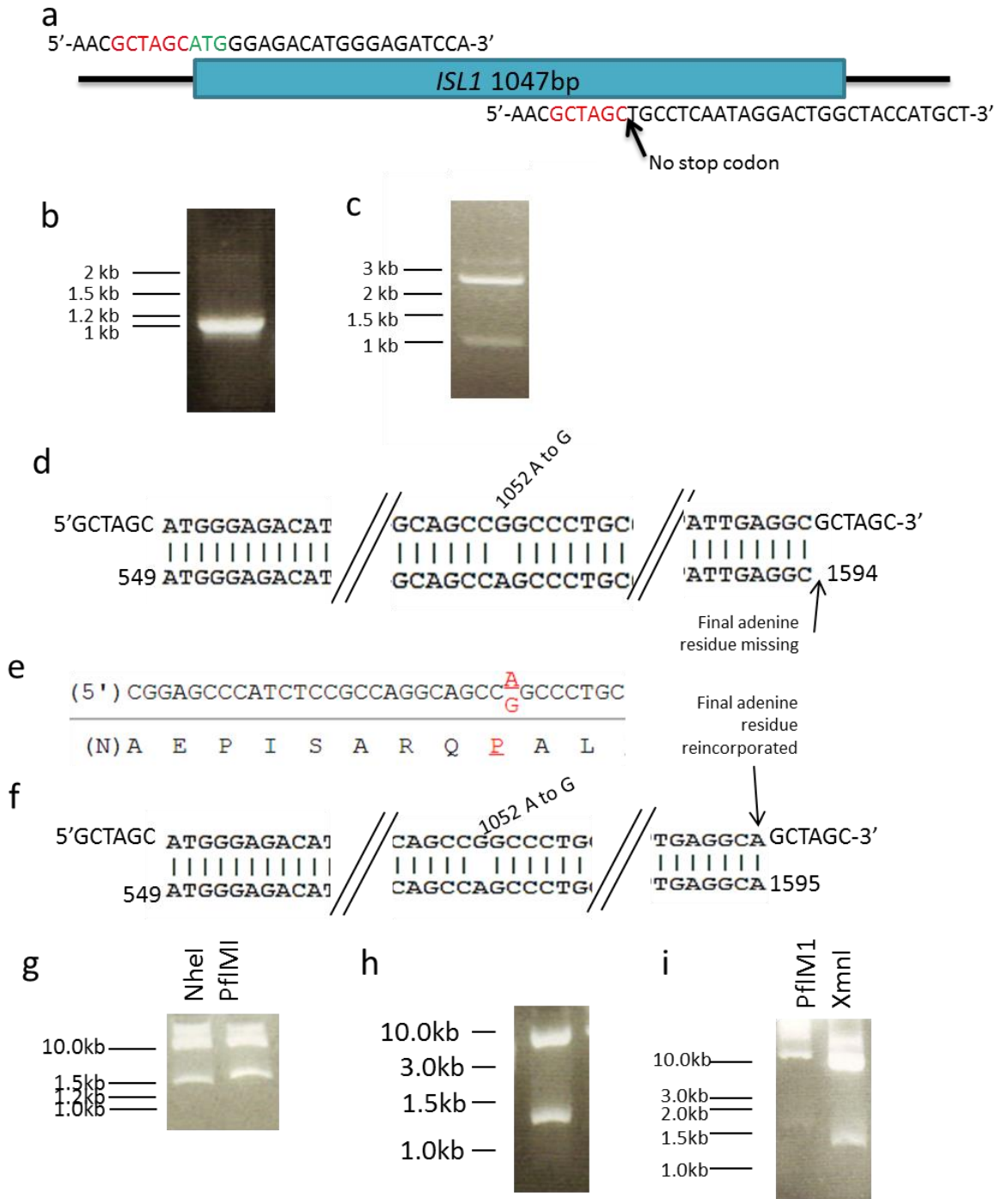


Figure 3.4: Cloning of *ISL1*. a) Schematic showing PCR primers incorporation of *NheI* sites (in red) onto the 5' and 3' ends of *ISL1* and removing the stop codon. b) *ISL1* was cloned from Plasmid Harvard vector: HsCD00076385 by high fidelity PCR. The fragment was extracted and ligated into pGEM® T easy cloning vector, colonies were screened by utilising blue/white selection as a result of the *lacZ* gene in the cloning vector. c) Restriction digest of a mini prep from a white colony to check that *ISL1* was inserted by *NheI* digestion, as seen by the pGEM® T easy vector backbone fragment at ~3kb and the insert at ~1kb. d) Alignment of *ISL1* sequencing data to NM_002202.2, 100% homology achieved apart from at base 1052 where a SNP was observed A to G, final adenine nucleotide missing on second inspection. e) Schematic to show that the resulting SNP still produces a proline residue. f) Alignment of re-cloned *ISL1* sequencing data to NM_002202.2, 100% homology

achieved apart from at base 1052 where a SNP was observed A to G, final adenine nucleotide incorporated. g) Restriction digest with NheI and PflM1 of a mini prep from a colony to check that *ISL1* was inserted by NheI digestion into the pCAGG-IRES-EGFP, as seen by the fragment at about 1.2kb with NheI digest. h) Restriction digest of a mini prep from a colony to check that *ISL1* was inserted by NheI digestion into the pCAGG-NOLZ1(variant)-IRES-EGFP, as seen by the PflM1 digest producing fragments of 6.7kb and 1.1kb . i) Restriction digest of a mini prep from a colony to check that *ISL1* was inserted by NheI digestion into pCAGG-NOLZ1-IRES-EGFP, as seen by the XmnI digest resulting in fragments of 7.8kb and 1.1kb and PflM1 digest of 6.7kb and 1.2kb.

2. Subcloning of *ISLET1*

ISLET1 was subcloned into the multicistronic p3x2A-pMT vector (insert:vector = 3:1) using NheI and checked for orientation by restriction digestion with NcoI to produce fragments of 2683bp and 978bp (Table 3.1 and Figure 3.5). *ISLET1* and the multicistronic section of the vector was subcloned into the pCAGG-IRES-EGFP vector by Sall digestion (insert:vector = 6:1) and checked for orientation by XmnI digestion producing fragments of 6649bp and 1032bp (Figure 3.5e).

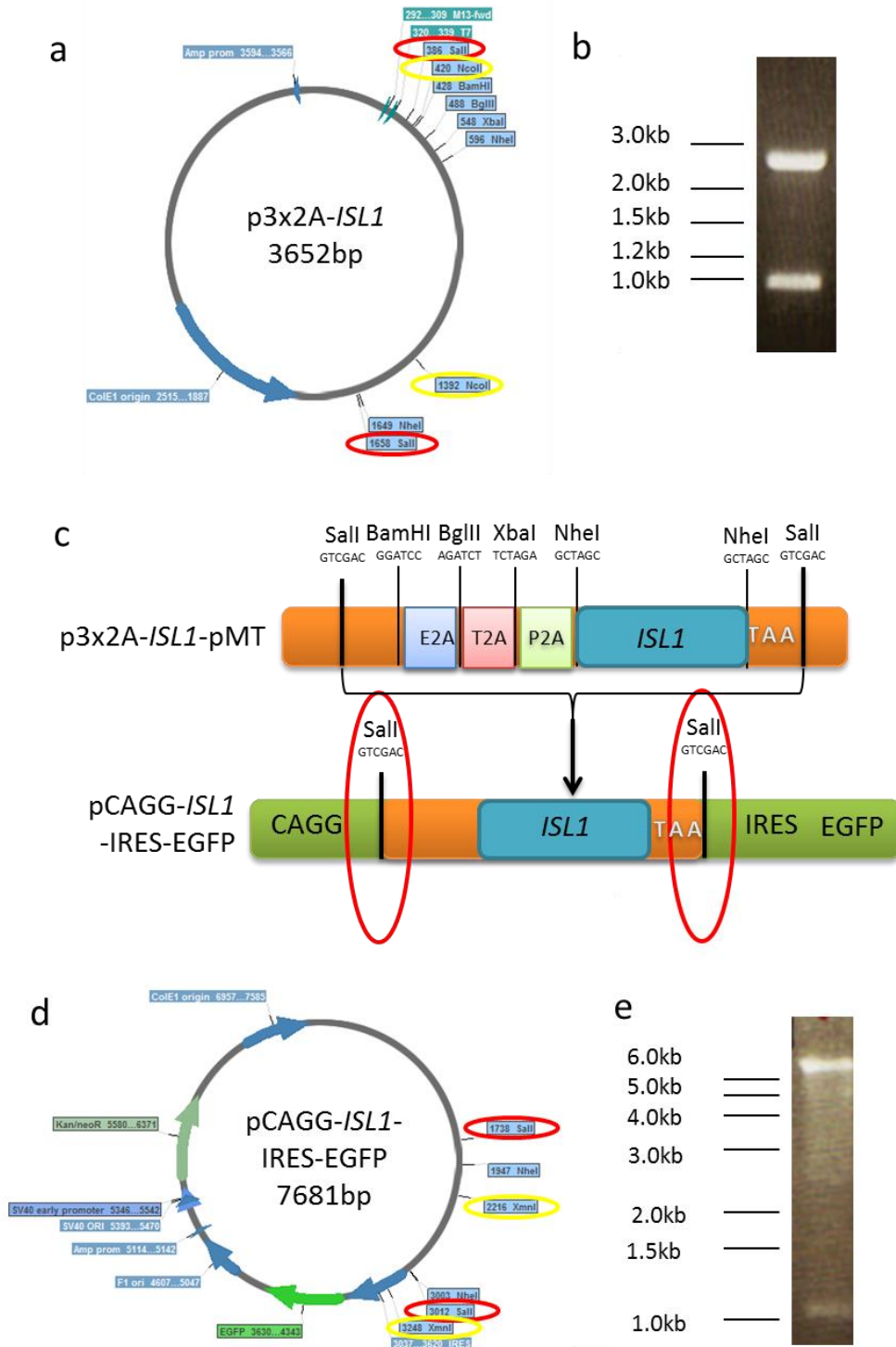


Figure 3.5: Plasmid design of pCAGG-*ISL1*-IRES-EGFP. a) p3x2A-*ISL1* plasmid map highlighting important restriction enzyme sites for cloning strategy, red ringed sites correspond to those on the schematic in a, *NcoI* sites ringed in yellow at 1392 and 420 were used for checking *ISL1* insertion orientation as seen in the gel in (b). B) *NcoI* digest producing fragments of p3x2A-*ISL1* producing fragments of 2683bp and 978bp c) Schematic showing the insertion of *ISL1* into the pCAGG-IRES-EGFP vector by *Sall* digestion. d) Plasmid map of pCAGG-*ISL1*-IRES-EGFP, red circles highlighting the *Sall* sites and *XmnI* sites ringed in yellow at 2216 and 3248 which were used for checking the orientation of *ISL1*

insertion. e) XmnI digestion of pCAGG-*ISL1*-IRES-EGFP to check orientation producing fragments of 6649bp and 1032bp

3. Validation of *ISLET1* protein expression

Once the vector had been validated by restriction digestion, it was grown up and purified for transfection into HEK293 cells. The GFP expression was monitored on a fluorescent microscope ~24 hours post transfection (Figure 3.6a), the transfection efficiency was $22.9 \pm 7.4\%$ (N=1; n=3). Cells were allowed to grow for a further 24 hours before being harvested for protein expression analysis by western blot and immunocytochemistry and the resulting protein expression as per Figure 3.6b. By western blot (Figure 3.7a) the protein was larger than the expected 39 kDa. Upon checking the DNA sequencing results, the final nucleotide adenine was seen to be missing (Figure 3.4d&f alignment). This produces a frame-shift mutation and results in a protein which is 368 amino acid residues and estimated at 41kDa, potentially explaining the larger band. This is as a result of the stop codon at the end of the multicistronic region being out of frame and a later stop codon being used to terminate translation. The primer sequence for cloning was checked and this was found to be the cause of the omitted nucleotide. *ISLET1* protein expression was restricted to the nuclei (Figure 3.7b). In order to overcome the error in *ISLET1*, the gene was re-cloned with a new set of primers to reintroduce the adenine at the 3' end of the *ISLET1* sequence. *ISLET1* was then subcloned into pCAGG-*ISLET1*-IRES-EGFP, pCAGG-NOLZ1-*ISLET1*-IRES-EGFP and pCAGG-NOLZ1(variant)-*ISLET1*-IRES-EGFP plasmids by NheI digestion removing the incorrect version of *ISLET1* and incorporating the correct version (Figure 3.5g-i) so the protein can be made appropriately and be used in future transfection studies. The new *ISL1* protein expression vector was verified by transfection into iPSC-derived neural stem cells (Figure 3.7b). Western blot analysis did not seem to show a difference in size between the old and new forms of the protein.

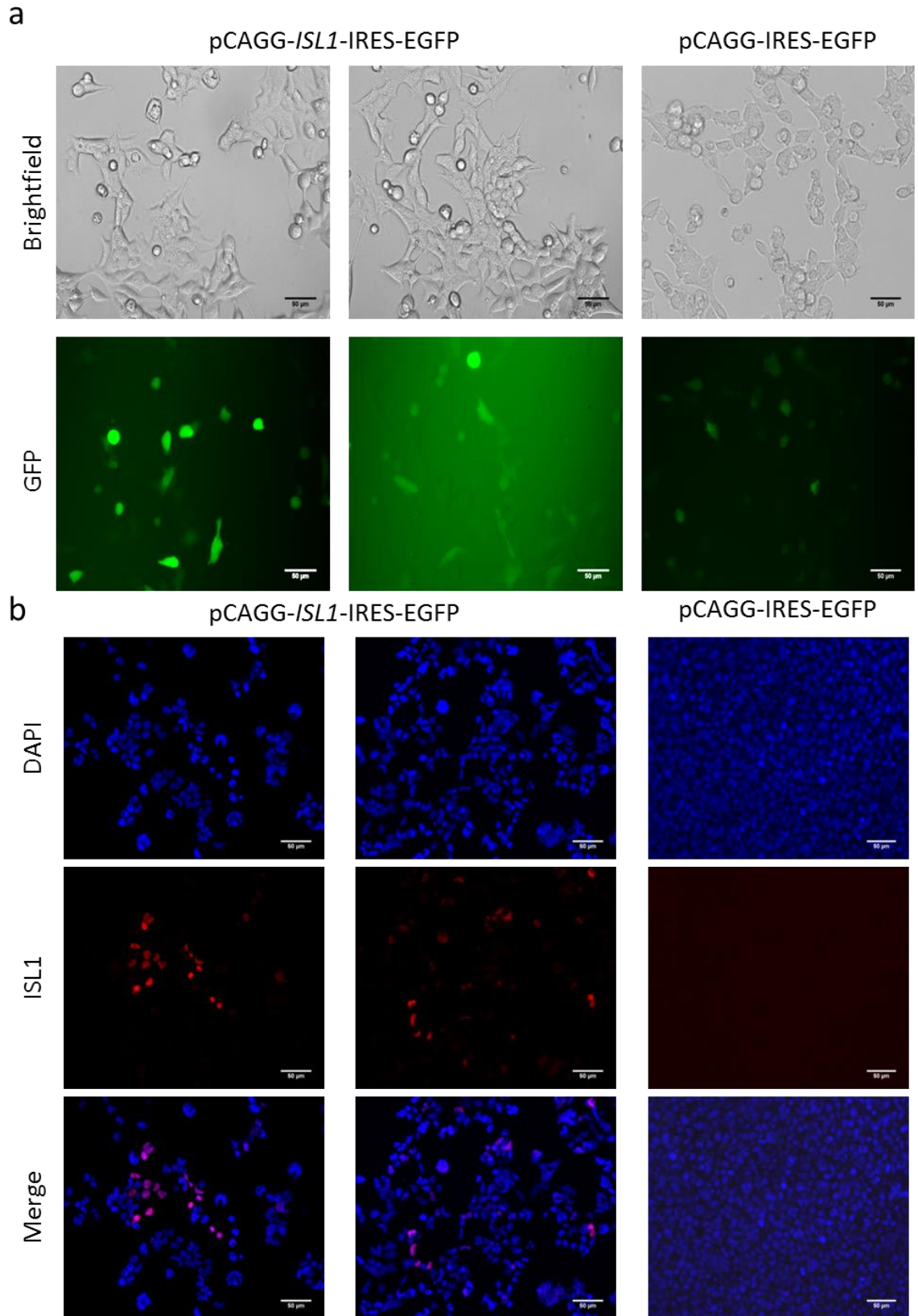


Figure 3.6: Analysis of protein expression in cells expressing pCAGG-*ISL1*-IRES-EGFP and pCAGG-IRES-EGFP. HEK293 cells transfected with pCAGG-*ISL1*-IRES-EGFP or pCAGG-IRES-EGFP (control). Images were taken 24 hours later. A) Bright field shown in

top panels and GFP fluorescence of same field shown in bottom panels. Left 4 panels show ISL1 plasmid and right 2 panels show control plasmid. Transfection efficiency: $22.89\% \pm 7.41$. Scalebar = 50 μm . b) Immunocytochemistry at 48 hours post transfection using Abcam ab109517 ISL1 antibody images showing nuclei in blue and ISL1 expression in red (α Rabbit IgG Alexa fluor 594 secondary antibody). Scale bars = 50 μm .

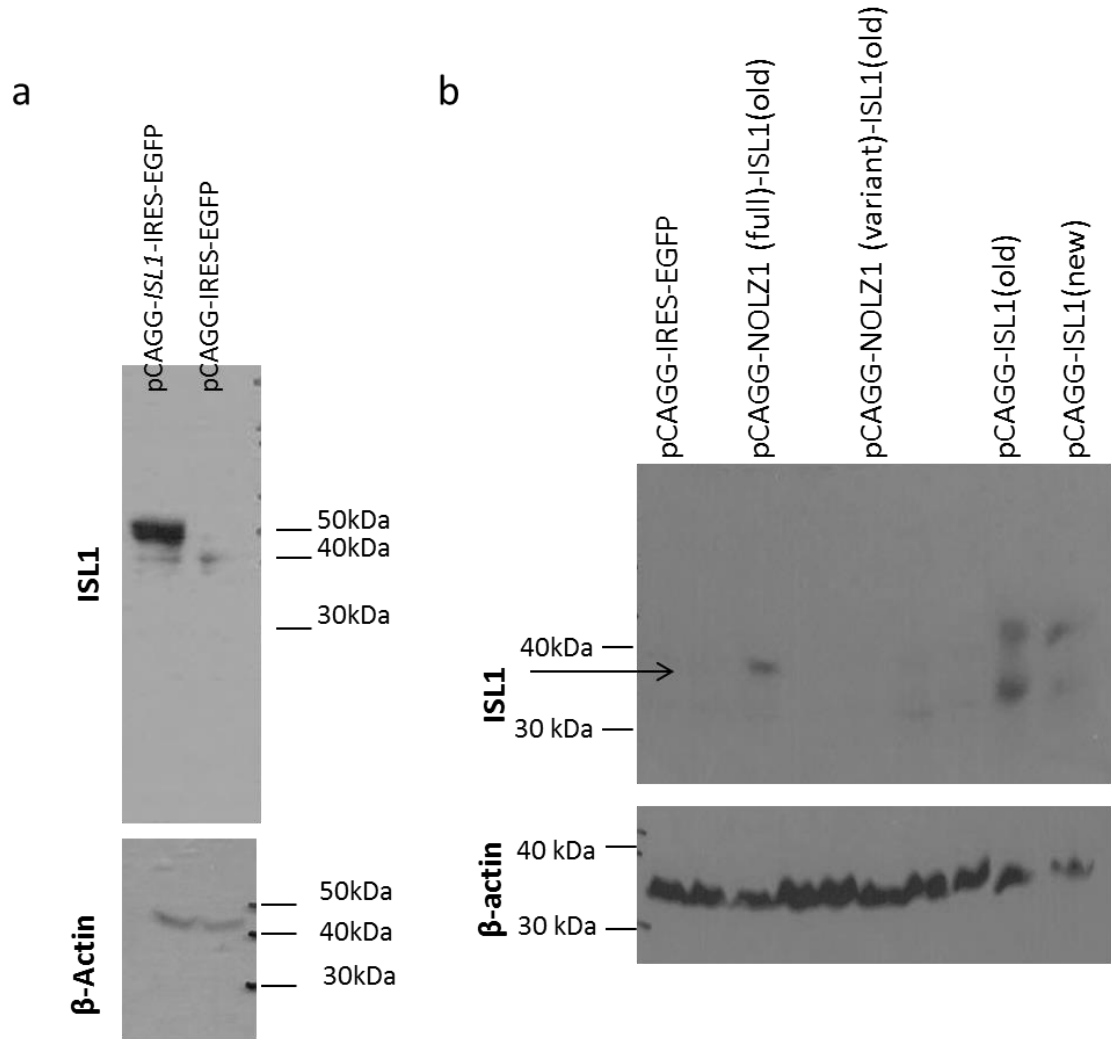


Figure 3.7: HEK293 cells transfected with pCAGG-ISL1-IRES-EGFP and pCAGG-IRES-EGFP a) Western blot to ISL1 on samples 48 hours post transfection showing a fragment of 39kDa for ISL1 and the bottom panel showing β -actin expression. b) Day 16 rosettes transfected with ISL1 containing plasmids. Western blot to ISL1 on samples 48 hours post transfection showing a fragment of 39kDa for ISL1 and the bottom panel showing β -actin expression

3.5 NOLZ1

NOLZ1 mRNA was shown to be expressed in developing striatum in the post-mitotic cells of the SVZ and MZ (Chang et al., 2004, Urbán et al., 2010, Ko et al., 2013) and has also been observed to be co-expressed with DARPP32 in rat striatum (Chang et al., 2004). *NOLZ1* overexpression upregulated retinoic acid signalling (Urbán et al., 2010), which is important in the striatum as it has been shown to be required for the expression of DARPP32 (Liao & Liu 2005). Consequently *NOLZ1* was chosen to be expressed in neural stem cells in an attempt to drive differentiation into MSNs *in vitro*.

1. Cloning of *NOLZ1*

Two versions of *NOLZ1* were cloned, incorporating BglII sites onto the 5' and 3' ends of the genes, one from human fetal 22 week diencephalon cDNA and human primary fetal (Swift REF:765) cDNA, referred to as *NOLZ1*(variant) (Figure 3.8a-c) and the other version from a plasmid provided by our collaborators in Barcelona (J.M. Canals), referred to as *NOLZ1* (full length)/*NOLZ1* (Figure 3.8e-g).

Once cloned into the pGEM[®] T easy vector, white colonies containing either gene were sent for sequencing at MWG Eurofins and were verified on NCBI Nucleotide, where it was found that the variant version of *NOLZ1* showed 100% homology to BC_007494.2 which had previously been cloned from skin, melanotic melanoma (Strausberg et al., 2002). *NOLZ1*(full length) showed 100% homology to NM_032772.4. *NOLZ1*(variant) was 849bp in length making a 283 amino acid protein, under half the size of the full length 646 amino acid *NOLZ1*. *NOLZ1*(full length) contained two exons running from nucleotide 1-651 and the second from 652-3182, the coding sequence was located from nucleotide 337-2277. The sequence homology of the variant to the full length version was 100% between nucleotides 1-729 and 1811-2542 of the gene and subsequent amino acid

sequence homology between 1-130 and 492-646 of the full length protein, therefore the variant form hasn't resulted from exon skipping. The zinc finger domain in NOLZ1 is between amino acid residues 514-542 and so the variant form of NOLZ1 contains the zinc finger domain, and also the Sp motif of the protein, but not the buttonhead box domain. Deletion of buttonhead box domain in the Sp1 protein led to a loss of activation of the LDL receptor promoter, and there was loss of stimulus for Sp1 DNA binding by the transcription factor; sterol regulatory binding element binding protein 1 (SREBP1) (Athanikar et al., 1997). Deletion of buttonhead box domain did not seem to affect Nlz1 self-association, HDAC binding, nuclear localisation of the protein nor gene repression of *krox20* in the developing zebrafish rhombomeres, whereas deletion of Sp motif leads to a disruption of *krox20* and *niz1* gene expression in rhombomeres 3-5 of the developing zebrafish embryo (Runko & Sagerström 2004). Therefore the variant form of the NOLZ1 protein should be able to function normally.

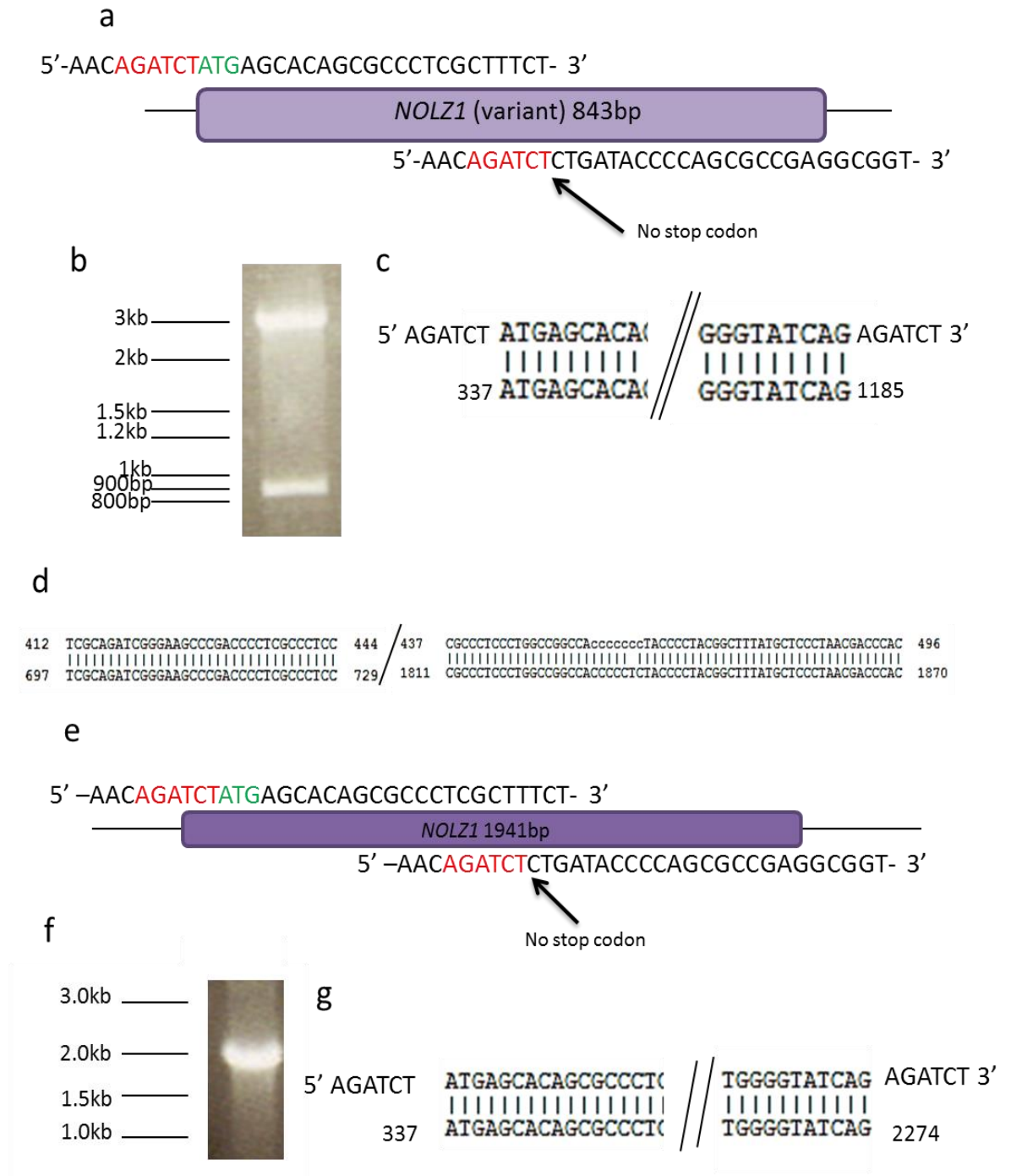


Figure 3.8: Cloning of *NOLZ1* (variant) and *NOLZ1*. a) Schematic showing insertion of BglIII restriction sites (in red) onto the 5' and 3' ends of *NOLZ1* and omission of a stop codon. b) *NOLZ1* (variant) cloned from human diencephalon cDNA into pGEM® T easy and a positive clone confirmed by BglIII digest *NOLZ1*(variant) insert at 849bp and pGEM® T easy vector backbone at ~3kb. c) Sequence alignment of *NOLZ1* (variant) of the 5' and 3' ends. d) The middle section of sequence alignment of *NOLZ1* (variant) aligned to the full length form of *NOLZ1*, 100% homology observed with the previously cloned version of *NOLZ1*(variant): BC_007494.2. e) Schematic showing insertion of BglIII restriction sites (in red) onto the 5' and 3' ends of *NOLZ1* and omission of a stop codon. f) Cloning of *NOLZ1* from pCAGG-*NOLZ1* vector (Barcelona) by PCR. g) Sequence alignment of *NOLZ1* of the 5' and 3' ends 100% homology observed to NM_032772.4 .

2. Subcloning of *NOLZ1*

The *NOLZ1*(variant) was subcloned into the p3x2A-pMT vector (Figure 3.9) and p3x2A-pMT-*ISLET1* (Figure 3.10) by BglIII digest and orientation was checked in both by NcoI digestion (Table 3.1), both these inserts were then subcloned into the pCAGG-IRES-EGFP vector using Sall digestion and the orientation of the insert was checked by restriction digest with NotI for pCAGG-*NOLZ1*(variant)-IRES-EGFP (Figure 3.9e) and SmaI for pCAGG-*NOLZ1*(variant)-*ISLET1*-IRES-EGFP (Figure 3.10g, Table 3.1).

NOLZ1 (full length) was subcloned into the pCAGG- *NOLZ1*(variant)-IRES-EGFP (Figure 3.11a-c) and the pCAGG- *NOLZ1*(variant)-*ISLET1*-IRES-EGFP (Figure 3.11d-f) with BglIII digestion, hence removing the variant form of *NOLZ1* from both vectors before insertion, and the orientation was checked of the full length *NOLZ1* was checked by restriction digest with NheI (Table 3.1).

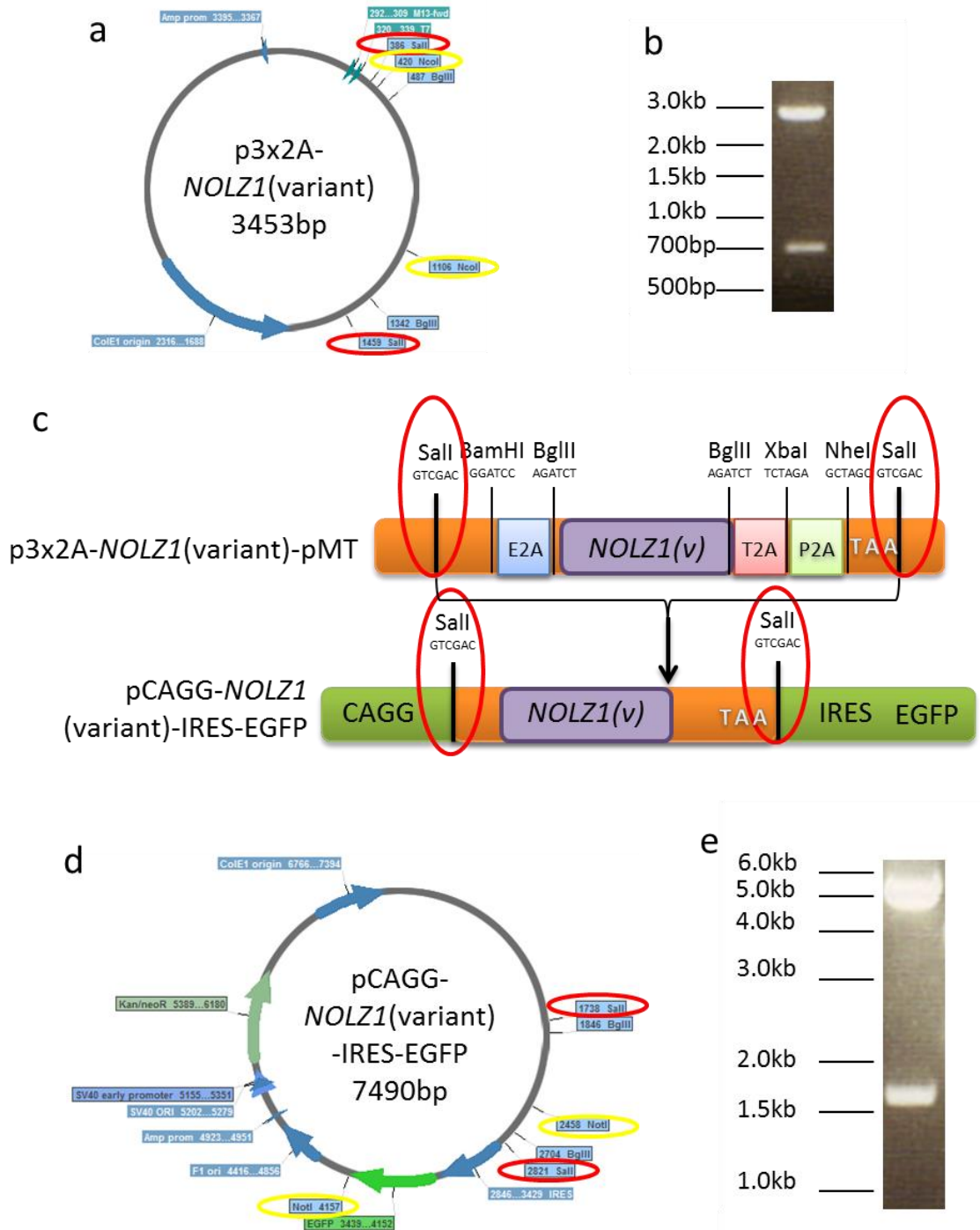


Figure 3.9: Plasmid design of pCAGG-*NOLZ1*(variant)-IRES-EGFP. a) p3x2A-*NOLZ1*(variant) plasmid map highlighting important restriction enzyme sites for cloning strategy, red ringed sites correspond to the *Sall* sites ringed red in (c), *NcoI* sites ringed in yellow at 420 and 1106 which were used for checking *NOLZ1* insertion orientation as seen in the gel in (b). b) *NcoI* digest producing fragments of p3x2A-*NOLZ1*(variant) producing fragments of 2767bp and 686bp. c) Schematic focussed showing the insertion of *NOLZ1*(variant) into the pCAGG-IRES-EGFP vector after *Sall* digestion. d) Plasmid map of pCAGG-*NOLZ1*(variant)-IRES-EGFP, red circles highlighting the *Sall* sites as in (a) and *NotI* sites ringed in yellow at 2458 and 4157 which were used for checking the orientation of

NOLZ1(variant) insertion. e) NotI digestion of pCAGG-*NOLZ1*(variant)-IRES-EGFP to check orientation producing fragments of 5791bp and 1699bp.

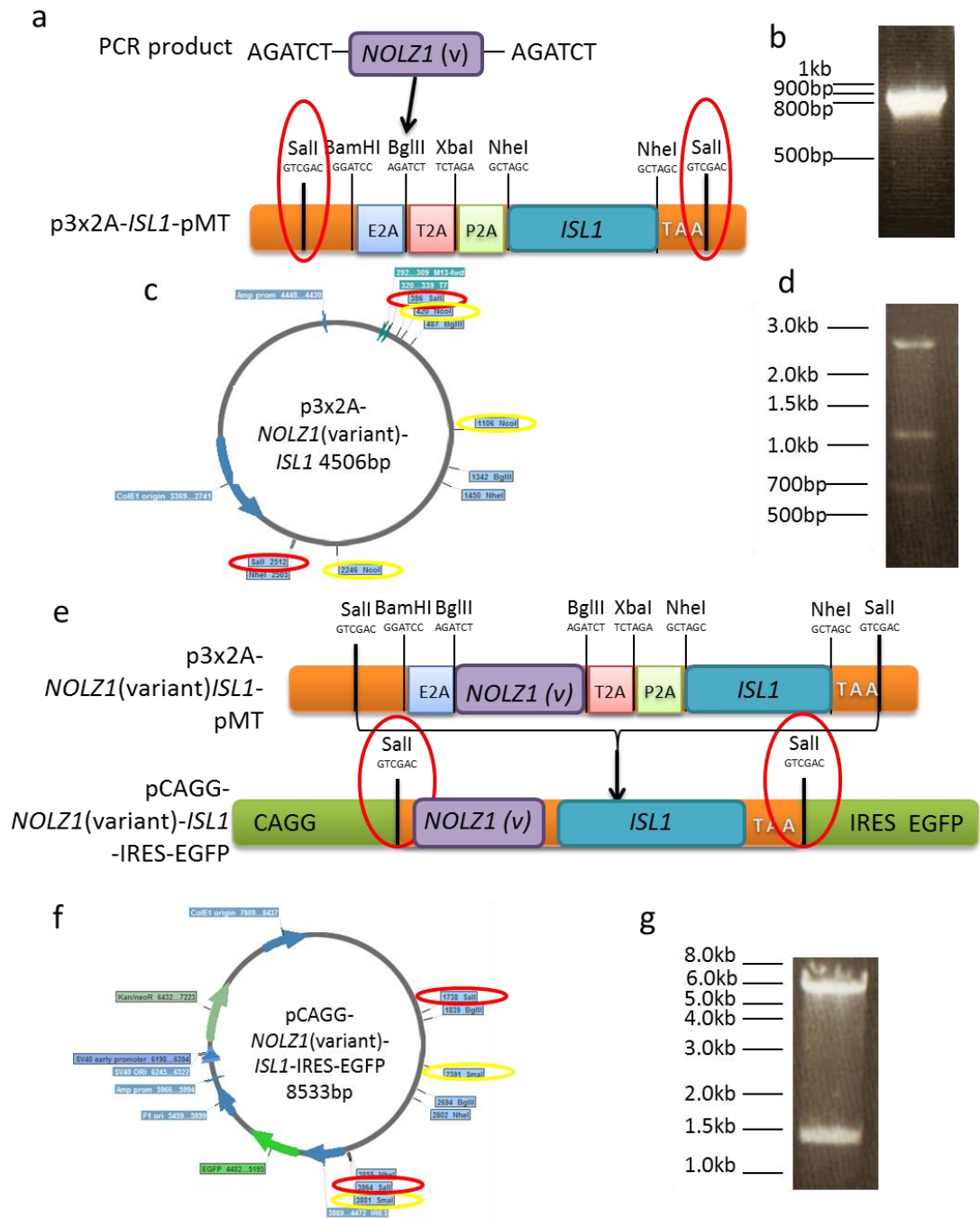


Figure 3.10: Plasmid design of pCAGG-*NOLZ1*(variant)-*ISL1*-IRES-EGFP a) Schematic to show important features of the p3x2A-*ISL1* vector and where the *NOLZ1*(variant) is inserted into the BglIII site showing the 2A cleavage sites and the incorporation of a final stop codon b) *NOLZ1*(variant) PCR fragment at 849bp cloned from human foetal diencephalon cDNA. c) p3x2A-*NOLZ1*(variant)-*ISL1* plasmid map highlighting important restriction enzyme sites for cloning strategy, red ringed sites correspond to those on the schematic in (a) and NcoI sites ringed in yellow at 420, 1106 and 2246 which were used for checking *NOLZ1* insertion orientation as seen in the gel in d) NcoI digest producing fragments of p3x2A-*NOLZ1*(variant)-*ISL1* producing fragments of 2680bp, 1140bp and 686bp e) Schematic

showing the insertion of *NOLZ1*(variant)-*ISL1* into the pCAGG-IRES-EGFP vector after *Sall* digestion f) Plasmid map of pCAGG-*NOLZ1*(variant)-*ISL1*-IRES-EGFP, red circles highlighting the *Sall* sites as in (a) and *SmaI* sites ringed in yellow at 2391 and 3881 used for checking the orientation of *NOLZ1*(variant)-*ISL1* insertion. g) *SmaI* digestion of pCAGG-*NOLZ1*(variant)-*ISL1*-IRES-EGFP to check orientation producing fragments of 7043bp and 1490bp

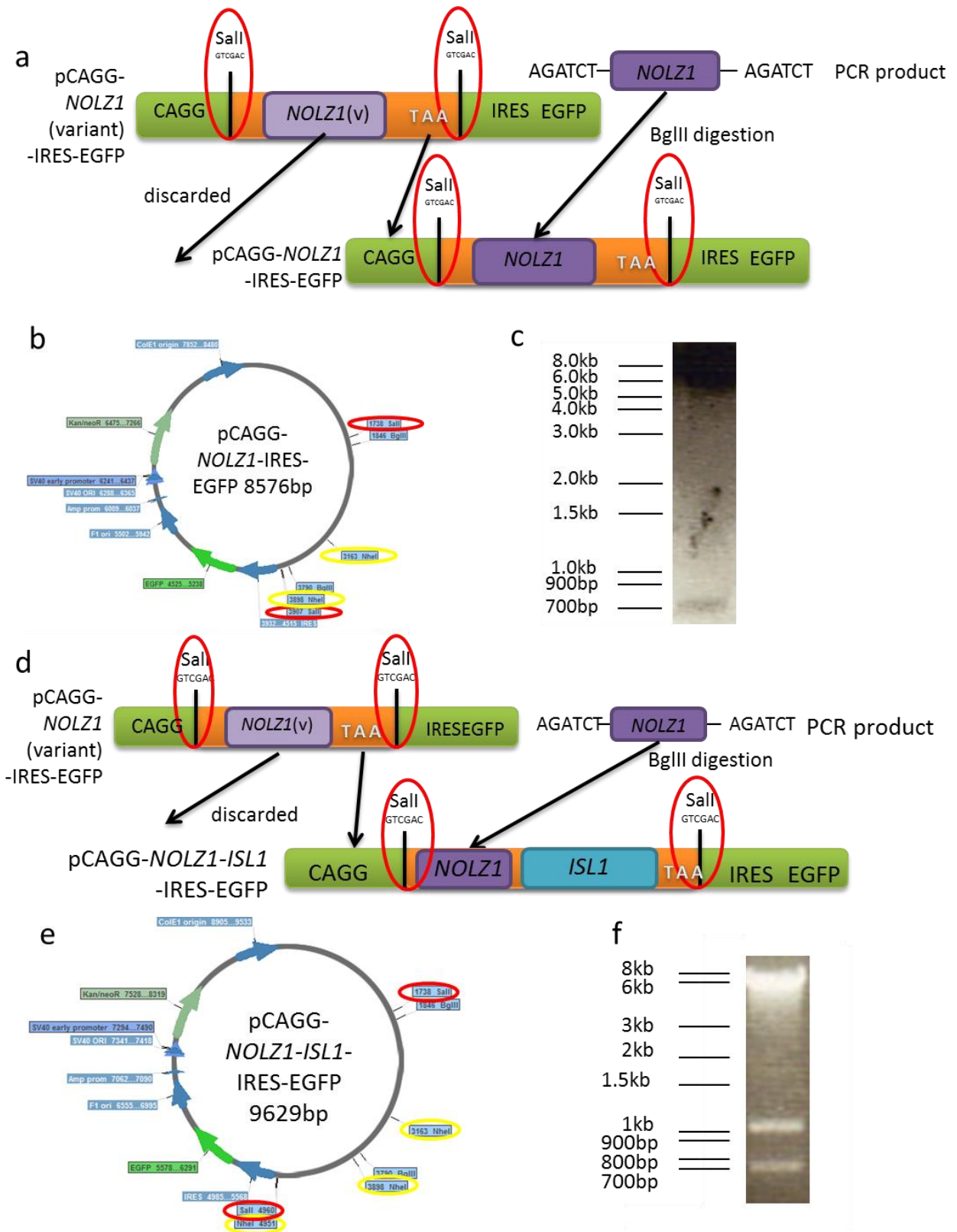


Figure 3.11: Plasmid design of pCAGG-NOLZ1-IRES-EGFP and pCAGG-NOLZ1-ISL1-IRES-EGFP. a) Schematic showing the insertion of *NOLZ1* into the pCAGG-IRES-EGFP vector after removal by BglIII digestion of *NOLZ1*(variant). b) Plasmid map of pCAGG-NOLZ1-IRES-EGFP, red circles highlighting the *Sall* sites as in (a) and *NheI* sites ringed in yellow at 3163 and 3898 used for checking the orientation of *NOLZ1* insertion. c) *NheI*

digestion of pCAGG-*NOLZ1*-IRES-EGFP to check orientation producing fragments of 7841bp and 735bp. d) Schematic showing the insertion of *NOLZ1* into the pCAGG-*ISL1*-IRES-EGFP vector after removal by BglII digestion of *NOLZ1*(variant). e) Plasmid map of pCAGG-*NOLZ1*-*ISL1*-IRES-EGFP, red circles highlighting the Sall sites as in (a) and NheI sites ringed in yellow at 3163, 3898 and 4951 which were used for checking the orientation of *NOLZ1* insertion. f) NheI digestion of pCAGG-*NOLZ1*-*ISL1*-IRES-EGFP to check orientation producing fragments of 7841bp, 1046bp and 735bp

3. Validation of *NOLZ1* protein expression

Once the orientation of the inserts in the pCAGG-IRES-EGFP vector were confirmed by digestion, the 4 vectors were then transiently transfected into HEK293 cells and subsequently observed under a fluorescent microscope at 24 hours post transfection to detect expression of the GFP from the expression plasmid, the transfection efficiency for the plasmids was *NOLZ1*: $41.5 \pm 0.76\%$ (N=1; n=2), *NOLZ1*(variant): $28.1 \pm 2.29\%$ (N=1; n=3) (Figure 3.12). The cells were then harvested 48 hours post transfection and processed for immunocytochemistry and western blot. There was not a commercially available antibody which will recognise the variant form of *NOLZ1*. Thus, this protein could only be detected using the 2A peptide tag, which shows nuclear staining (Figure 3.13a). Full length *NOLZ1* was detected by western blot (Figure 3.13b at ~65kDa).

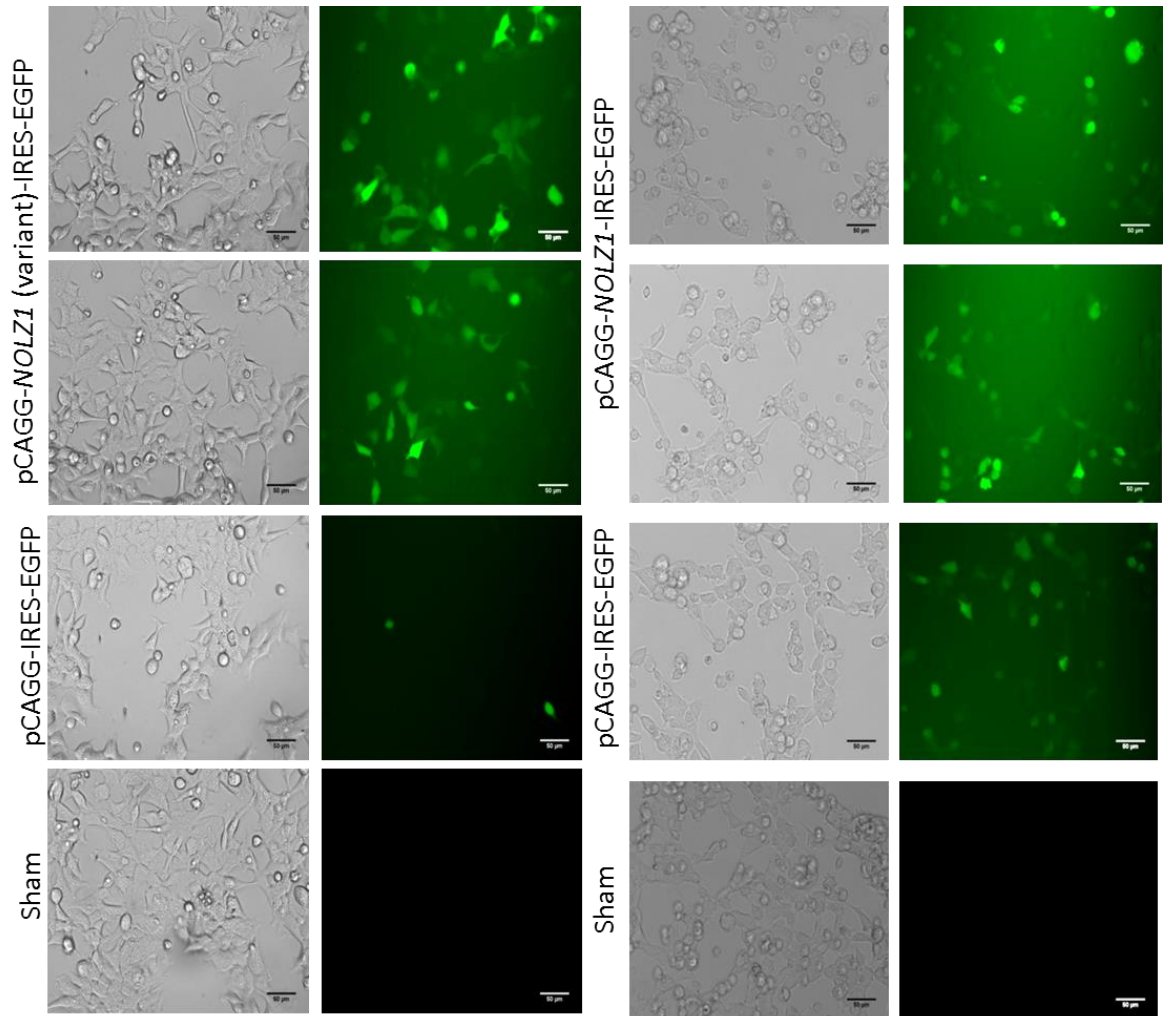


Figure 3.12: pCAGG-NOLZ1(variant)-IRES-EGFP, pCAGG-NOLZ1-IRES-EGFP, pCAGG-IRES EGFP control and sham transfected HEK293 cells 24 hours post transfection. Images of bright field in 1st and 3rd column and GFP fluorescence in the 2nd and 4th columns. Transfection efficiency: NOLZ1 (variant): 28.12% ± 2.29 control: 4.07% ± 1.28. NOLZ1: 41.5% ± 0.76 control: 49.08% ± 17.85 Scalebar = 50 µm

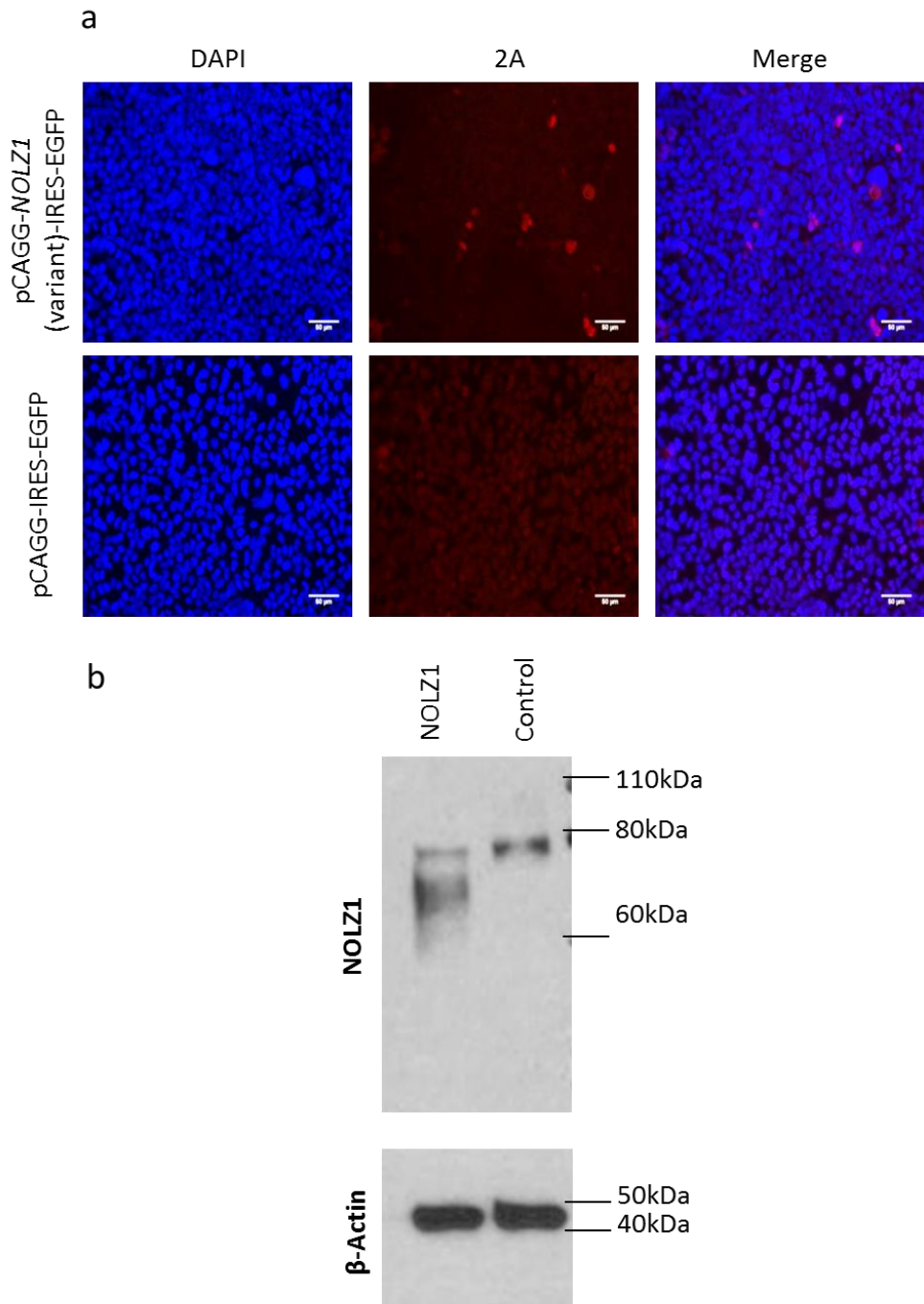


Figure 3.13: Analysis of protein expression in cells transfected with pCAGG-NOLZ1(variant)-IRES-EGFP, pCAGG-NOLZ1-IRES-EGFP and pCAGG-IRES-EGFP. a) Immunocytochemistry using Millipore ABS31 anti-2A antibody images showing nuclei in blue and 2A tagged NOLZ1(variant) expression in red (α Rabbit IgG Alexa fluor 594 secondary antibody). Left panels show nuclei, middle panels show 2A peptide expression and the right panels show the merge images. Upper 3 panels show Nolz1(variant plasmid, lower 3 panels show control plasmid. Scale bar = 50 μ m b) Protein was harvested 48 hours post transfection for western blot with NOLZ1 antibody showing a fragment of ~62kDa for full length NOLZ1 and the bottom panel showing β -actin expression as loading control.

3.6 FOXP1

FOXP1 was chosen to be used in this study due to its expression in the developing striatum (Ferland et al., 2003, Shu et al., 2001, Tamura et al., 2003), with over two-thirds of MSNs expressing this transcription factor (Tamura et al., 2004). Furthermore, *Foxp1* overexpression, in mouse striatal cells, has been demonstrated to increase the expression of striatally enriched genes (Tang et al., 2012). *FOXP1* was also shown to regulate retinoic acid signalling in the spinal cord (Rousso et al., 2008) and could be important for the same function in the striatum, as retinoic acid signalling was shown to be required for the induction of *DARPP32* expression (Liao & Liu 2005).

1. Cloning of *FOXP1*

FOXP1 was cloned (Figure 3.14) from a plasmid clone ID:HsCD00297105 (PlasmID), incorporating *Bam*HI restriction sites onto the 5' and 3' ends of the gene (Figure 3.14a&b). *Bam*HI restriction enzyme sites were chosen to insert *FOXP1* as the coding sequence contains *Bgl*III & *Nhe*I restriction sites and therefore would have been unsuitable to use *Bgl*III or *Nhe*I sites to insert *FOXP1* into the multicistronic plasmid. *FOXP1* was ligated into the pGEM[®] T easy vector and colonies were screened for the *FOXP1* insert by *Bam*HI digestion (Figure 3.14c). Positive clones were sent for sequencing at MWG Eurofins (Figure 3.14d and Appendix for alignment) and checked against NCBI Nucleotide database. The cloned *FOXP1* showed 100% homology to *Homo sapiens FOXP1* transcript variant 1 (NM_032682.5).

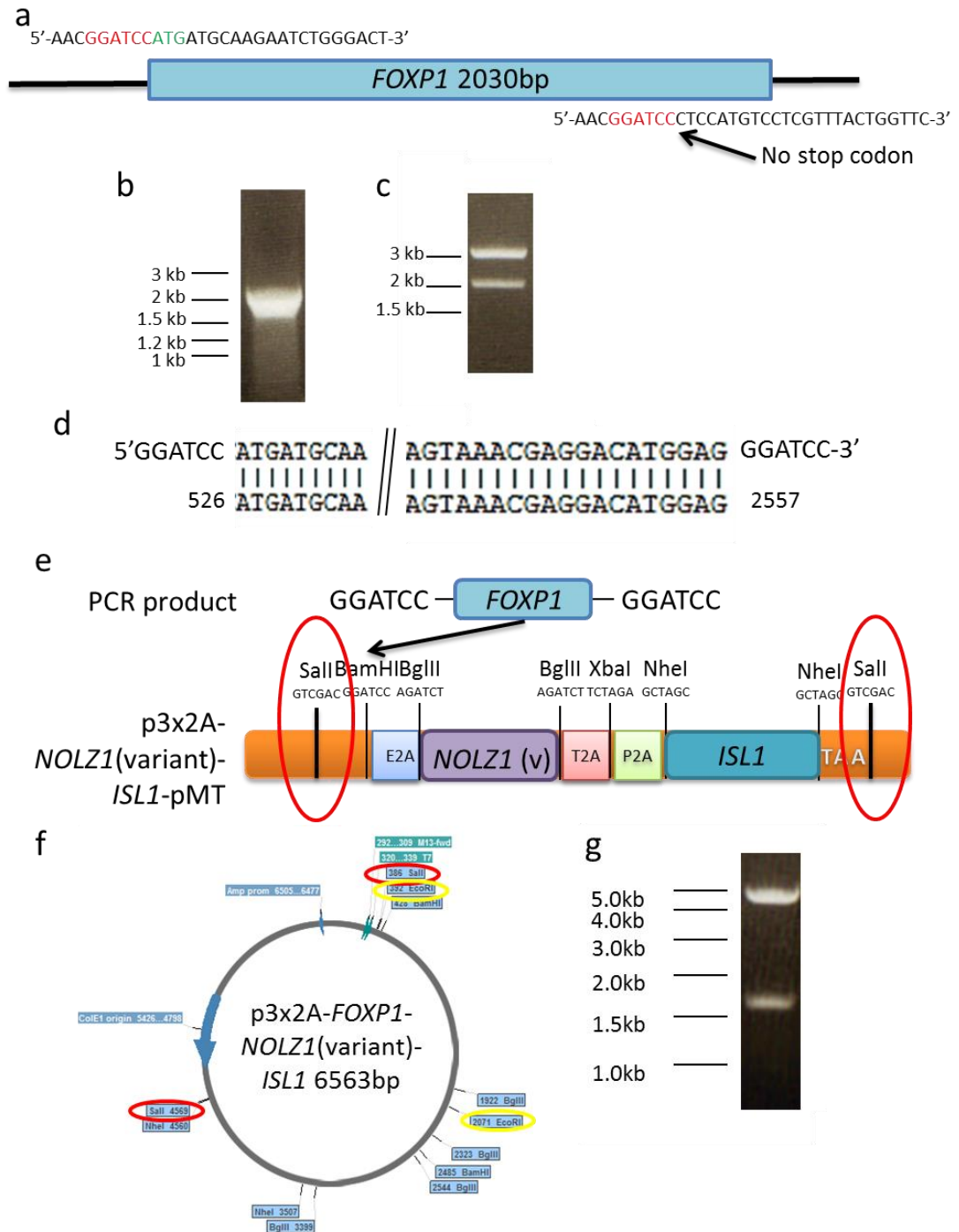


Figure 3.14: Cloning of *FOXP1*. a) Schematic showing PCR primers incorporation of BamHI sites (in red) onto the 5' and 3' ends of *FOXP1* and removing the stop codon. b) *FOXP1* was cloned from Plasmid Harvard vector: HsCD00297105 by high fidelity PCR. The fragment was extracted and ligated into pGEM® T easy cloning vector, colonies were screened by utilising blue/white selection as a result of the *lacZ* gene in the cloning vector. c) Restriction digest of a mini prep from a white colony to check that *FOXP1* was inserted by BamHI digestion, as seen by the pGEM® T easy vector backbone fragment at ~3kb and the insert at ~2kb. d) Alignment of *FOXP1* sequencing data to NM_032682.5 100% homology. e) Schematic to show important features of the p3x2A-*NOLZ1*(variant)-*ISL1* vector and where the *FOXP1* is inserted into the BamHI site showing the 2A cleavage sites and the incorporation of a final stop codon. f) p3x2A-*FOXP1*-*NOLZ1*(variant)-*ISL1* plasmid map

highlighting important restriction enzyme sites for cloning strategy, red ringed sites correspond to those on the schematic in (a) and EcoRI sites ringed in yellow at 392 and 2071 which were used for checking *FOXP1* insertion orientation as seen in the gel in (g). G) EcoRI digestion of p3x2A-*FOXP1*-*NOLZ1*(variant)-*ISL1* producing fragments of 4884bp and 1679bp

2. Subcloning of *FOXP1*

Subcloning of *FOXP1* into the p3x2A-pMT vector (Figure 3.14e-g) was performed by restriction digest with BamHI, ligated into the p3x2A-pMT vector and then the orientation of the insert checked by restriction digest with EcoRI to produce fragments of 2986bp and 1679bp (Table 3.1 and Figure 3.14g). Subsequent subcloning of *FOXP1* into the pCAGG-IRES-EGFP vector was unsuccessful. However, *FOXP1* was successfully subcloned into the p3x2A-pMT-*NOLZ1*(variant)-*ISLET1* plasmid. This was done by digestion of *FOXP1* and of p3x2A-pMT-*NOLZ1*(variant)-*ISLET1* plasmid by BamHI (Figure 3.15) and then ligated together, the orientation was checked by EcoRI digestion to produce fragments of 4884bp and 1679bp. The insert of *FOXP1*-*NOLZ1*(variant)-*ISLET1* was removed from the plasmid and the pCAGG-IRES-EGFP plasmid linearised by Sall digestion and subsequently ligated together. The resulting clones were checked for orientation by SmaI digestion to produce fragments of 7082bp, 2018bp and 1490bp (Figure 3.15c & Table 3.1).

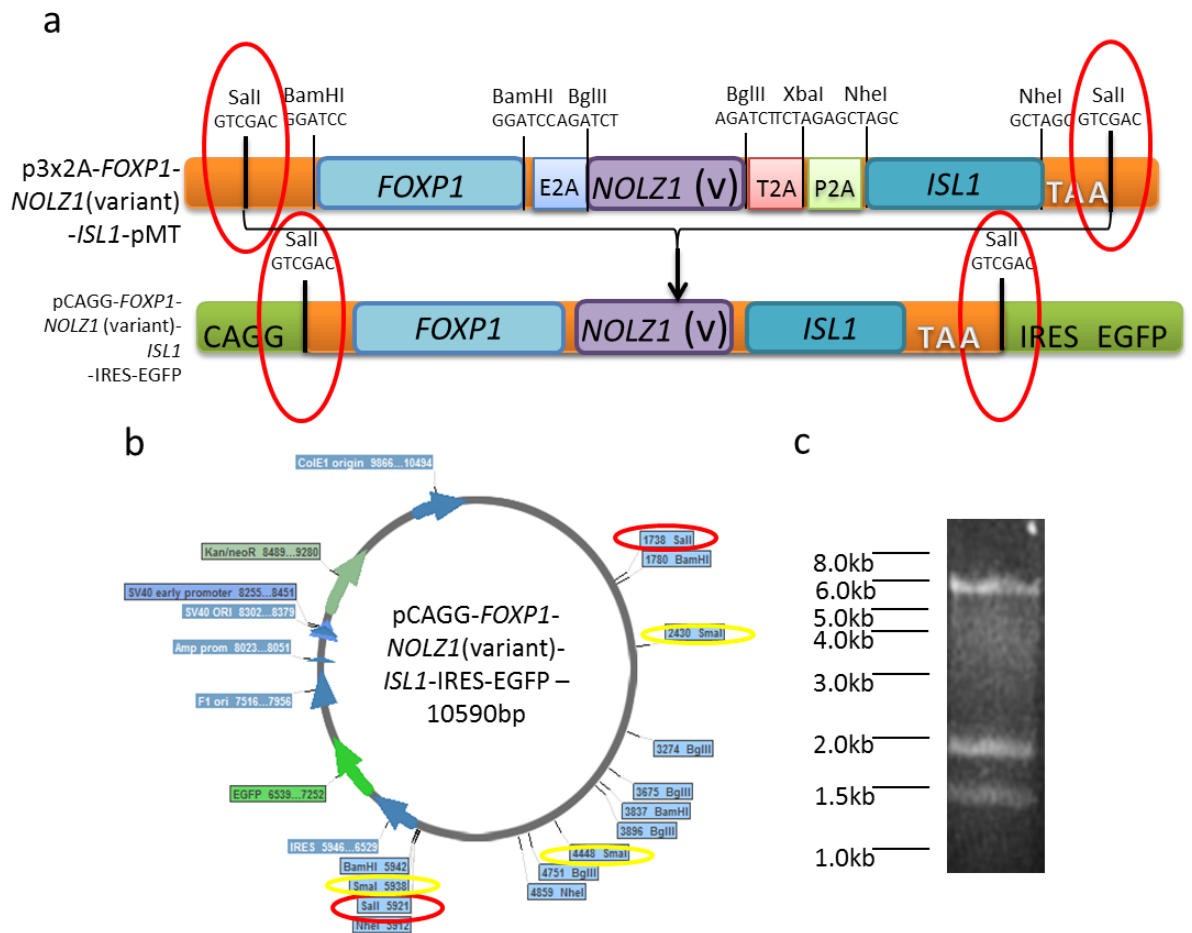


Figure 3.15: Plasmid design for pCAGG-FOXP1-NOLZ1(variant)-ISL1-IRES-EGFP a) Schematic showing the insertion of *FOXP1-NOLZ1(variant)-ISL1* into the pCAGG-IRES-EGFP vector by *Sall* digestion. b) Plasmid map of pCAGG-FOXP1-NOLZ1(variant)-ISL1-IRES-EGFP, red circles highlighting the *Sall* sites and *SmaI* sites ringed in yellow at 2430, 4448 and 5938 which were used for checking the orientation of *FOXP1-NOLZ1(variant)-ISL1* insertion. c) *SmaI* digestion of pCAGG-FOXP1-NOLZ1(variant)-ISL1-IRES-EGFP to check orientation of the insert producing fragments of 7082bp, 2018bp and 1490bp

3. Validation of *FOXP1* & *ISLET1* protein expression

The pCAGG-FOXP1-NOLZ1(variant)-ISLET1-IRES-EGFP plasmid was then transfected into HEK293 cells, transfection efficiency was determined at 24 hours post transfection (Figure 3.17a), which was $14.5 \pm 6\%$ (N=1; n=2). Cells were harvested for protein analysis at 48 hours post transfection. Immunocytochemistry of the HEK293 cells (Figure 3.16) shows *FOXP1* and *ISLET1* to be expressed in a

small number of cell nuclei corresponding with the low transfection efficiency (Figure 3.17a). Western blot analysis showed FOXP1 protein at ~53kDa and 80kDa to be expressed in both the empty vector and pCAGG-*FOXP1-NOLZ1*(variant)-*ISLET1-IRES-EGFP* vector transfection (Figure 3.17b), expression of ISLET1 protein was observed at ~39kDa. This means that HEK293 cells seem to express FOXP1 and ISLET1, however, in the case of FOXP1, this could be non-specific binding of the antibody as there is cytoplasmic staining in the empty plasmid control transfection (Figure 3.16). ISLET1 expression is lower in the empty plasmid control transfection by western blot and so the ISLET1 plasmid is increasing the levels of ISLET1 expression after transfection.

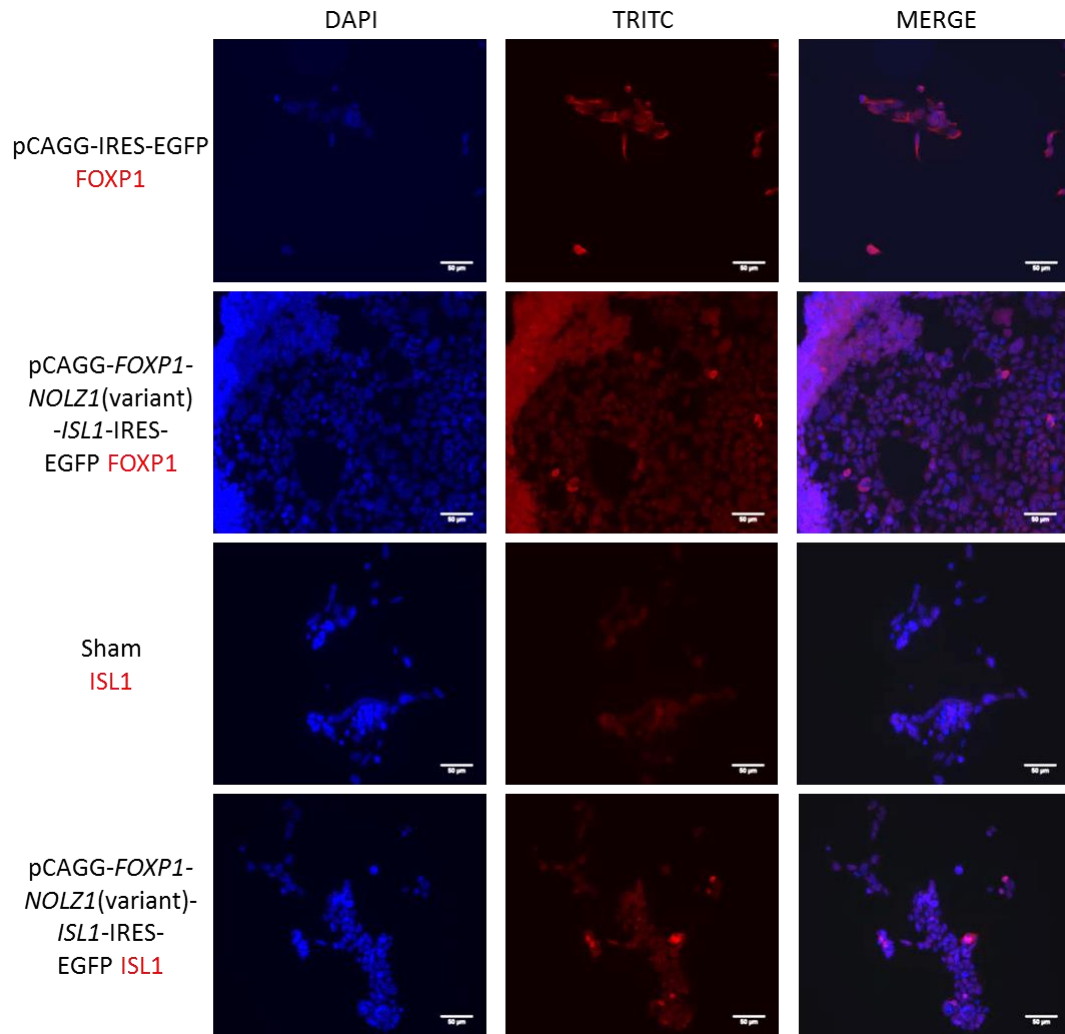


Figure 3.16: Analysis of protein expression of neural stem cells transfected with pCAGG-FOXP1-NOLZ1(variant)-ISL1-IRES-EGFP and pCAGG-IRES-EGFP. Immunocytochemistry for FOXP1 and ISL1 were performed 48 hours post transfection. Top 2 panels show expression of FOXP1 in the control plasmid (top panel) and *FOXP1-NOLZ1(variant)-ISL1* plasmid (second panel). The bottom two panels show ISL1 expression in the sham transfected (third panel) and *FOXP1-NOLZ1(variant)-ISL1* plasmid (bottom panel). Nuclei are stained blue and FOXP1 and ISL1 are stained red. Scalebar = 50 μ m

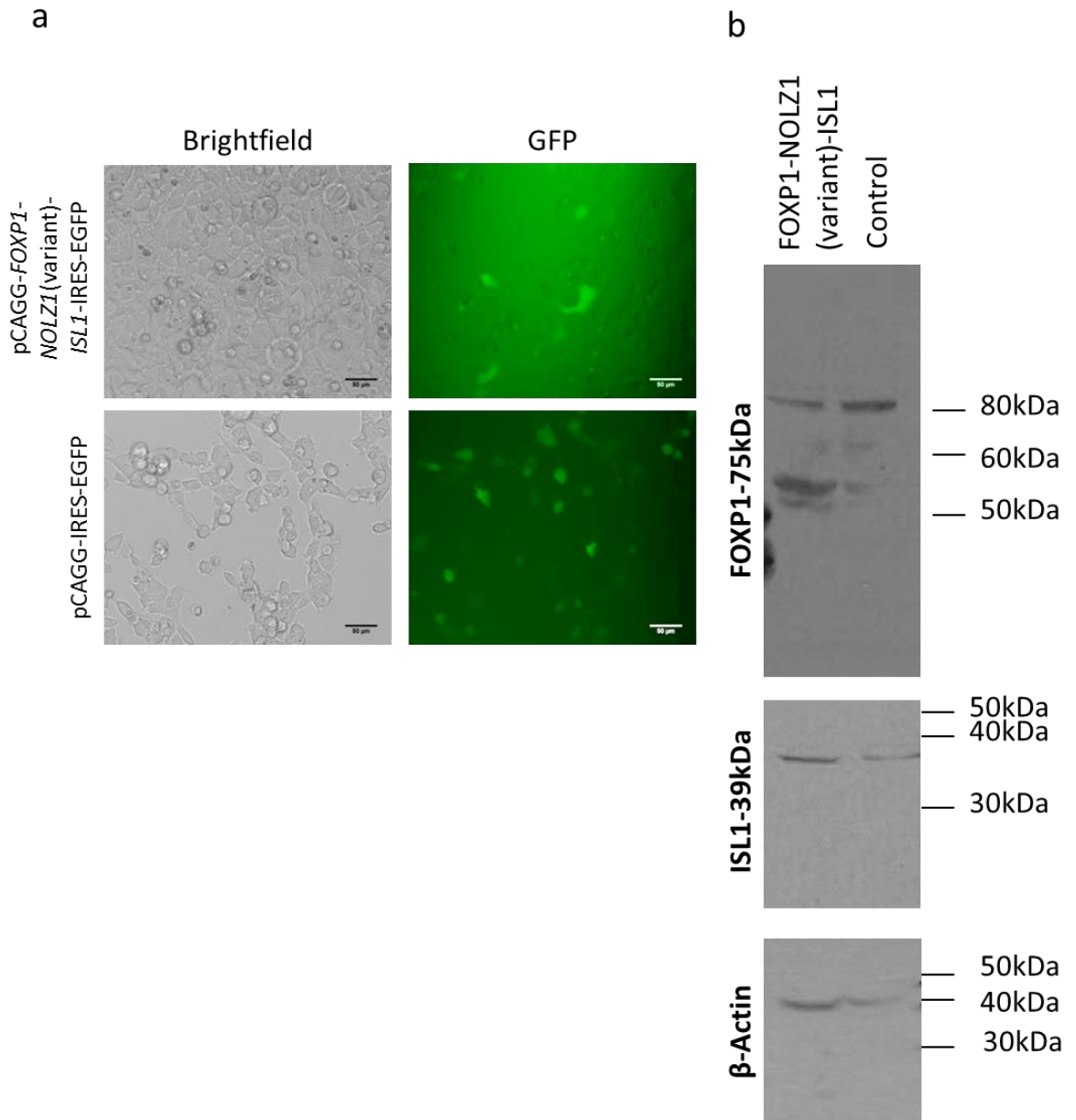


Figure 3.17: HEK293 cells transfected with pCAGG-FOXP1-NOLZ1(variant)-ISL1-IRES-EGFP and pCAGG-IRES-EGFP. a) Images of bright field (left panel) and GFP fluorescence of the same field (right panel) at 24 hours post transfection. Transfection efficiency: $14.52\% \pm 6.06$ Scalebar = 50 μm . b) Protein from HEK293 cells transfected with pCAGG-FOXP1-NOLZ1(variant)-ISL1-IRES-EGFP and pCAGG-IRES-EGFP harvested 48 hours post transfection western blot for FOXP1 (top panel) showing fragments at $\sim 53\text{kDa}$ and $\sim 80\text{kDa}$, western blot for ISL1 (middle panel) showing a fragment of $\sim 39\text{kDa}$ for ISL1 and loading control β -actin (bottom panel) $\sim 42\text{kDa}$

3.7 OCT6

OCT6 was chosen as one of the candidate genes for expression in neural stem cells to drive differentiation in to MSNs because OCT6 expression has been

detected in the developing striatum localised to the SVZ and MZ of the LGE (Suzuki et al., 1990, Garel et al., 1999, Alvarez-Bolado et al., 1995, Frantz et al., 1994). When *Oct6* was replaced with POU family member, *Brn2*, forebrain development was severely affected producing severe forebrain truncation (Wolf et al., 2009). *Oct6* expression, in the striatum, was down regulated several weeks after birth (Ilia et al., 2003a).

1. Cloning of *OCT6*

OCT6 was cloned from another plasmid, clone ID: HsCD00082889 (PlasmID), but unlike the rest of the genes, it was unable to be cloned as the full gene (possibly due to formation of primer dimer during PCR being more favourable to binding the template DNA). Therefore, primers were designed to clone the gene in two parts and then ligate them back together (Figure 3.18). The primers for the 5' and 3' ends of *OCT6* coding sequence incorporated BamHI restriction enzyme sites, the other primers were designed to bind midway through the gene itself, with an overlapping sequences (Figure 3.19d). The two sections of the gene named; *OCT6*-5' (855bp) and *OCT6*-3' (504bp), were cloned by PCR into the pGEM[®] T easy vector (Figure 3.19b&c) and white colonies were sent for sequencing at MWG Eurofins, the sequence was verified using NCBI Nucleotide. The start, end and overlap alignments as per Figure 3.19d, the full sequence alignment is in the appendix, the sequence was 100% homologous to *Homo sapiens POU3F1* NM_002699.3.

After this, the mid-section of the gene was digested out of the original plasmid using naturally occurring restriction enzyme sites NcoI and SphI (Figure 3.18) and ligated into the 3' end of the gene in the pGEM[®] T easy vector by cutting with the same enzymes. The 5' section of *OCT6* was then digested and ligated into the pGEM[®] T easy-*OCT6* middle & 3'section vector using XmnI and NarI restriction enzymes (Figure 3.18b), the full gene was checked for size by EcoRI digest (Figure 3.18c).

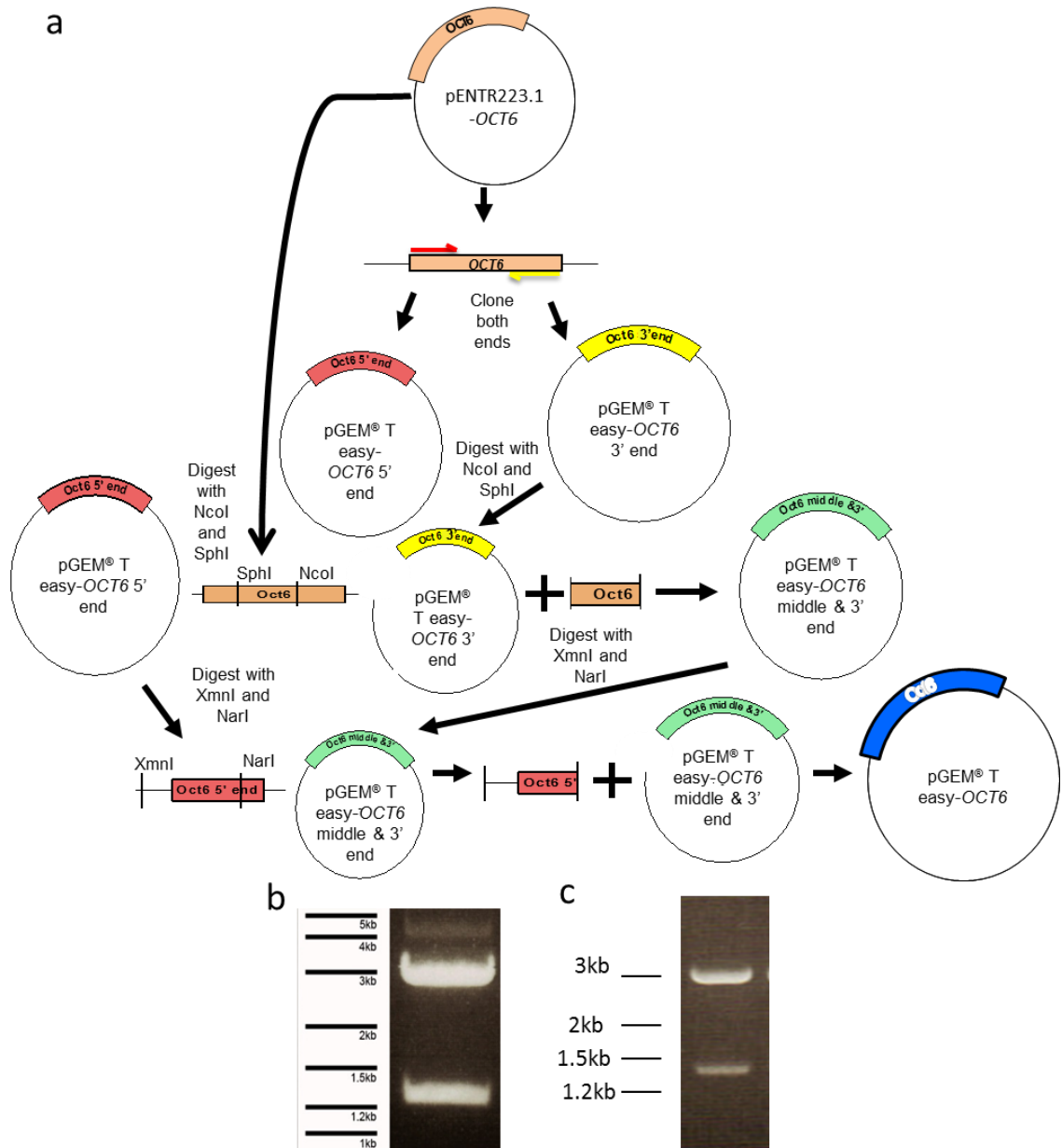


Figure 3.18: *OCT6* cloning diagram. A) Both the 5' and 3' ends are cloned by PCR to incorporate a BamHI restriction site at each end of the gene. These are cloned into pGEM[®] T easy vectors. The middle section of *OCT6* is then digested out of the original pENTR223.1 vector with SphI and NcoI, this is then inserted into the pGEM[®] T easy *OCT6*-3' end vector which has been cut with the same restriction enzymes. Finally the 5' end of *OCT6* is cut out of the pGEM[®] T easy vector with XmnI & NarI restriction enzymes, the pGEM[®] T Easy *OCT6* middle & 3' vector is cut with the same enzymes and ligated together. B) Subcloning of middle section of *OCT6* by digest with NcoI and SphI into pGEM[®] T easy-*OCT6*-3' vector checked for insertion with EcoRI. c) Subcloning of *OCT6* 5' into pGEM[®] T easy-*OCT6*-middle&3' end vector using XmnI and NarI and checked with EcoRI.

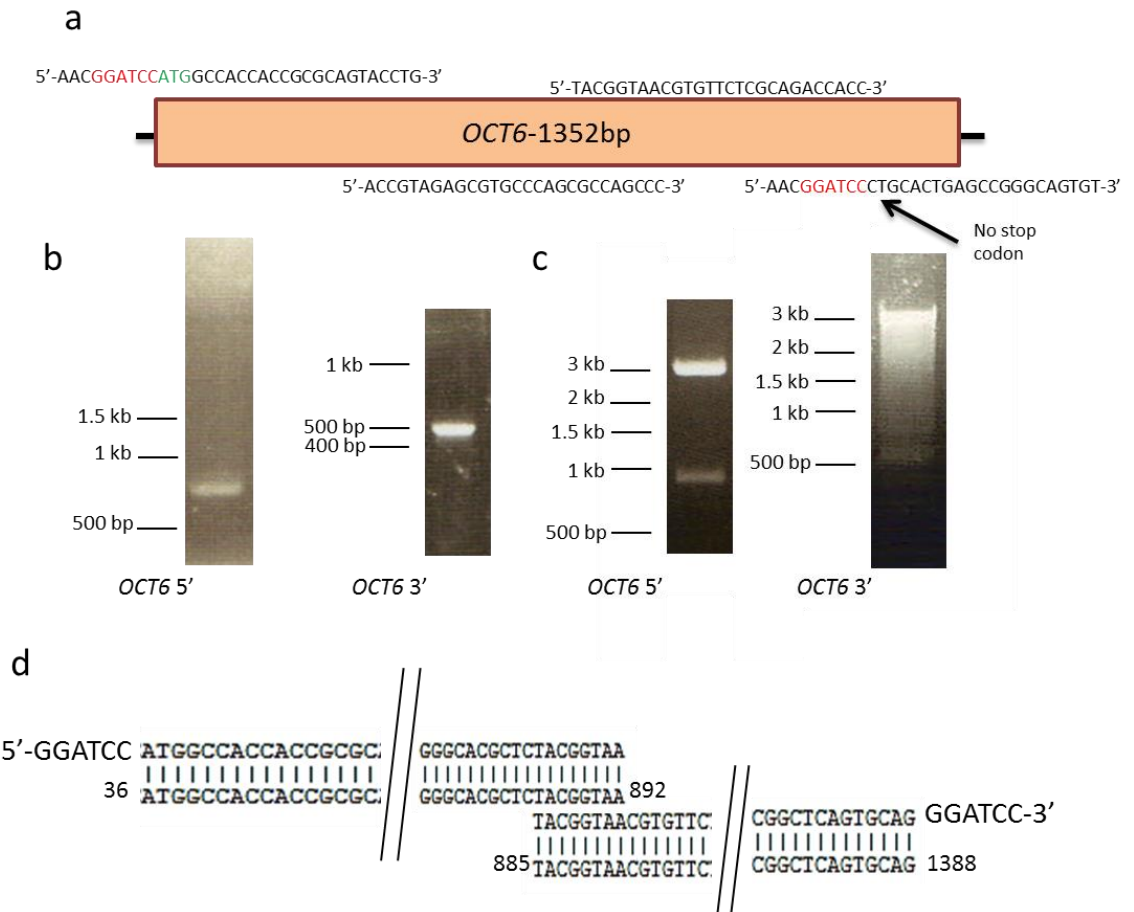


Figure 3.19: Cloning of *OCT6*. a) Schematic showing PCR primers incorporation of BamHI sites (in red) onto the 5' and 3' ends of *OCT6* and removing the stop codon. b) *OCT6* 5' and 3' sections were cloned from PlasmID vector: HsCD00082889 by high fidelity PCR. The fragments were extracted and ligated into pGEM[®] T easy cloning vector, colonies were screened by utilising blue/white selection as a result of the *lacZ* gene in the cloning vector. c) Restriction digest of a mini prep from white colonies to check that *OCT6* 5' and 3' sections were inserted by EcoRI digestion, as seen by the pGEM[®] T easy vector backbone fragment at ~3kb and the insert at 855bp (for 5' section) and 504bp (for 3' section). d) Alignment of *OCT6* 5' and 3' sequencing data to NM_002699.3 shows 100% homology.

2. Subcloning of *OCT6*

OCT6 was subcloned into the p3x2A-pMT vector using BamHI and checked for orientation with NcoI to produce fragments of 2731bp, 1221bp and 12bp (Table 3.1 and Figure 3.20). Then the *OCT6* gene and rest of the multicistronic section of p3x2A-pMT plasmid was subcloned into the pCAGG-IRES-EGFP plasmid using Sall (Figure 3.20c) and checked for orientation using restriction digest with SmaI to produce fragments of 6870bp, 863bp, 201bp and 59bp (Table 3.1 & Figure 3.20e).

3. Transcription factor cloning and plasmid validation

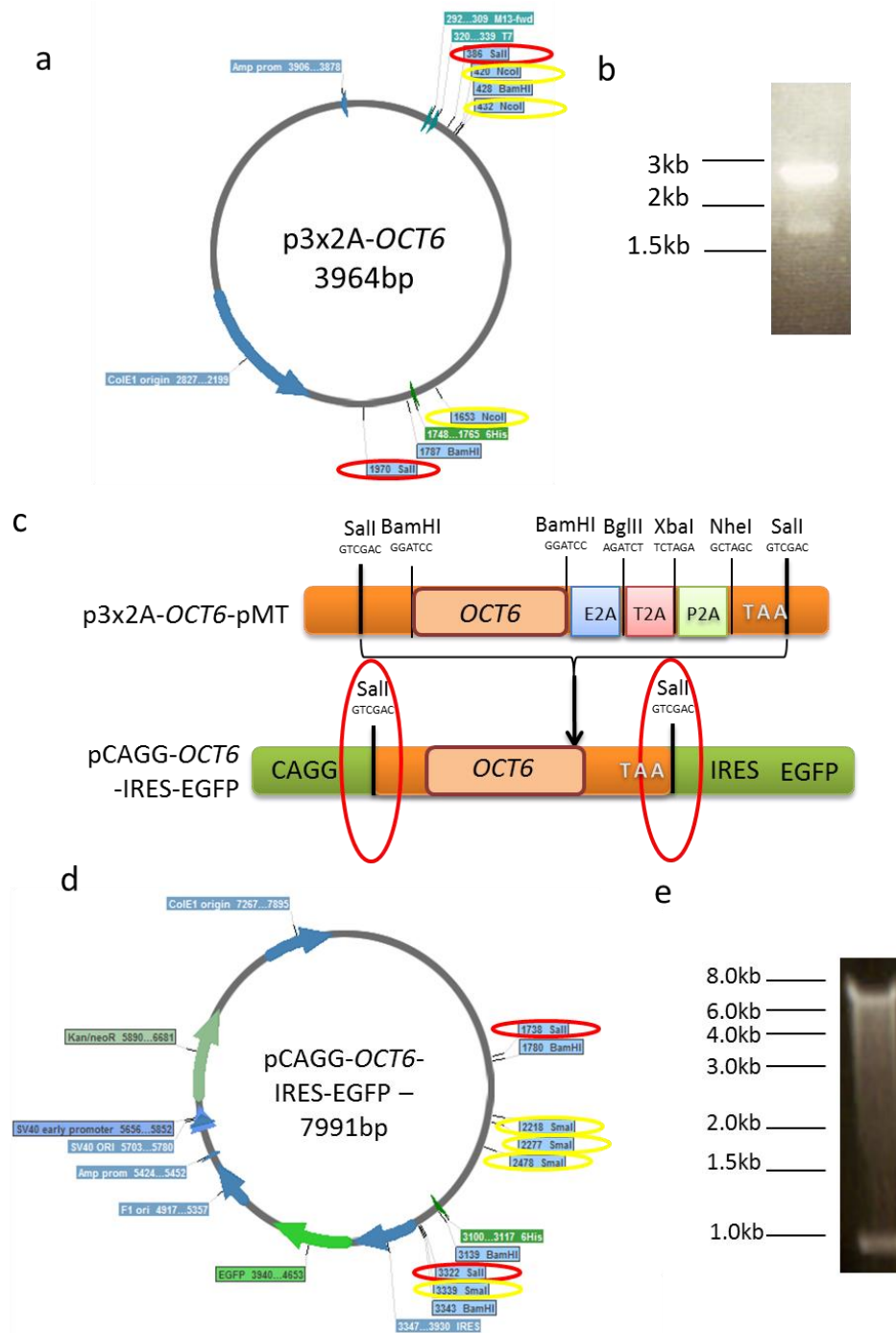


Figure 3.20: Plasmid design of pCAGG-OCT6-IRES-EGFP. a) p3x2A-OCT6 plasmid map highlighting important restriction enzyme sites for cloning strategy, red ringed sites are Sall sites and NcoI sites ringed in yellow at 420, 432 and 1653 were used for checking OCT6 insertion orientation as seen in the gel in (b). B) NcoI digest of p3x2A-OCT6 producing fragments of 2731bp and 1221bp (12bp unable to be detected). c) Schematic showing the insertion of OCT6 into the pCAGG-IRES-EGFP vector by Sall digestion. d) Plasmid map of pCAGG-OCT6-IRES-EGFP, red circles highlighting the Sall sites and SmaI sites ringed in yellow at 2218, 2277, 2478 and 3339 used for checking the orientation of OCT6 insertion. e) Digestion of pCAGG-OCT6-IRES-EGFP to check orientation producing fragments of 6,870 bp 861 bp (201 bp & 59 bp unable to be detected but unaltered between OCT6 orientation).

3. Validation of OCT6 protein expression

Once the orientation of *OCT6* insert was verified, the protein expression from the plasmid was determined by transfection of the pCAGG-*OCT6*-IRES-EGFP into HEK293 cells. GFP expression was monitored at 24 hours post transfection and protein analysis, using immunocytochemistry and western blot, was carried out at 48 hours. Although the GFP expression at 24 hours, $19.7 \pm 9.43\%$ (N=1; n=3), (Figure 3.21a) was lost in the process of fixing and subsequent immunocytochemistry, there are a number of cells which show *OCT6* protein expression (Figure 3.21b). The western blot for *OCT6* (Figure 3.22) has showed several bands, two of which could be considered possibilities for being *OCT6* as they have a higher level of expression and are not present in the empty plasmid control. However, neither is at the expected size of 45 kDa. It is noteworthy that the Abcam literature shows that the antibody detects a protein at 50 kDa but that this needs to be optimised, as protein bands are observed at ~42 kDa and ~58 kDa.

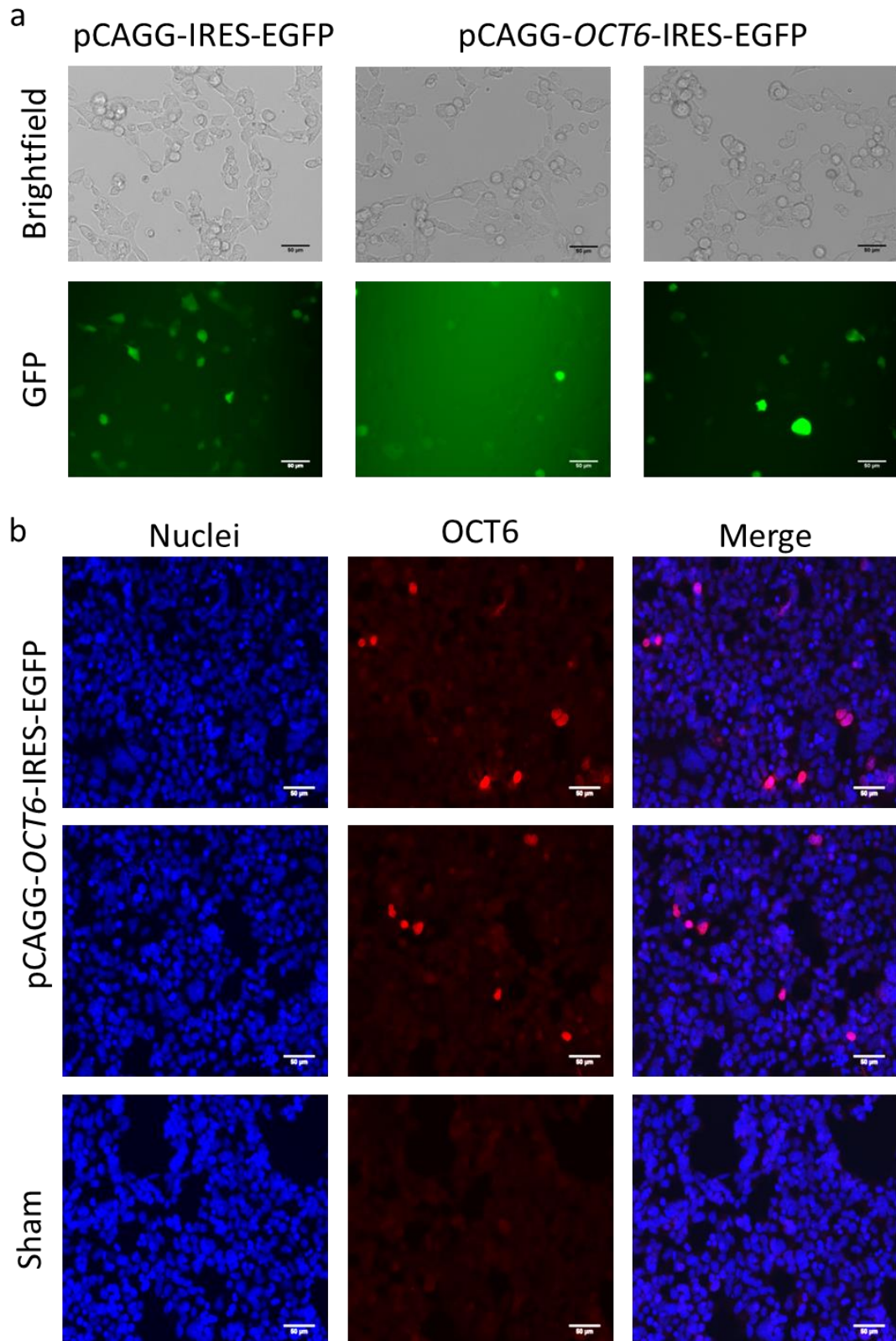


Figure 3.21: Analysis of protein expression of HEK293 cells transfected with pCAGG-OCT6-IRES-EGFP and pCAGG-IRES-EGFP. a) Images of bright field shown in top panel and GFP fluorescence for the same field in bottom panel, left panel shows control plasmid and right two panel show OCT6 plasmid at 24 hours post transfection. Transfection

efficiency: $19.71\% \pm 9.43$ Scalebar = 50 μm . b) Immunocytochemistry of HEK293 cells 48 hours after transfection with pCAGG-OCT6-IRES-EGFP (top 2 panels) and sham transfected control (bottom panel). OCT6 expression in red, nuclei stained blue. Scalebar = 50 μm

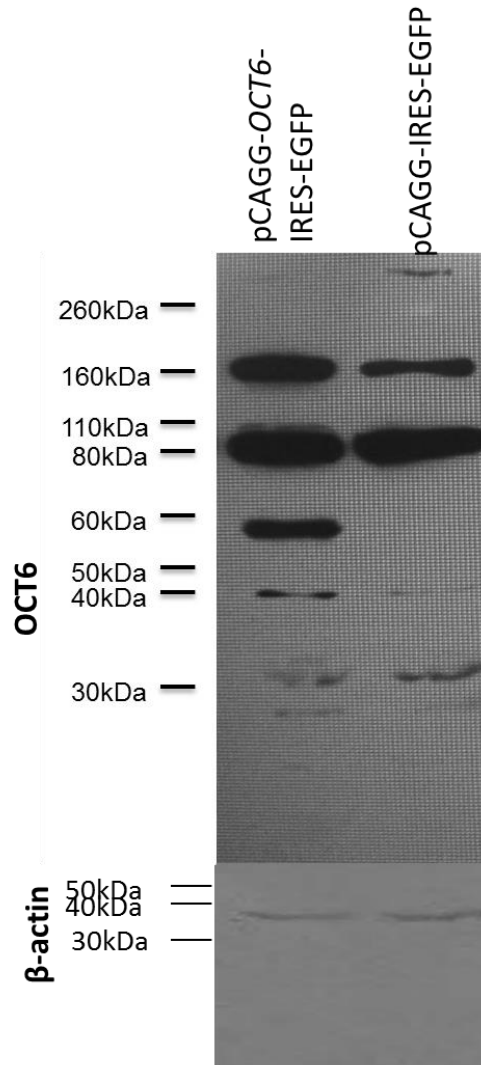


Figure 3.22: HEK293 cells transfected with pCAGG-OCT6-IRES-EGFP. Cells were harvested 48 hours post transfection. Top panel western blot with OCT6 antibody showing a fragment of ~57kDa and ~42kDa specific to OCT6 transfected cells and the bottom panel showing equal β -actin expression, as a loading control.

3.8 Conclusions

Single transcription factor plasmids	Multiple transcription factor plasmids
EBF1	NOLZ1-ISL1
ISL1	NOLZ1 (variant)-ISL1
NOLZ1	FOXP1-NOLZ1 (variant)-ISL1
NOLZ1 (variant)	
OCT6	

Table 3.2 Summary table of transcription factors and their combinations available for transfection in to neural stem cells

The plasmids (Table 3.2) have been validated by:

- i) Sequencing of each of the cloned genes using primers in the cloning plasmid and primers designed to sequence from within the transcription factor
- ii) Confirming the orientation of the inserted gene by restriction digestions
- iii) Confirming the proteins: expression of GFP and each of the specific transcription factors by immunocytochemistry or western blot or both.

3.8.1 The transcription factors

Which transcription factors were selected and then cloned were determined by their biology, particularly their documented importance during striatal development *in vivo*. Thus, EBF1 and OCT6 are expressed in the developing LGE SVZ and MZ, (Garel et al., 1997, Suzuki et al., 1990, Garel et al., 1999, Alvarez-Bolado et al., 1995, Frantz et al., 1994); the *Ebf1* knockout mouse shows a defect of SVZ to MZ transition (Garel et al., 1999). ISL1 has also been shown to be an important transcription factor in the development of the LGE and striatum (Wang & Liu 2001, Long et al., 2009, Stenman et al., 2003) and more specifically the striatonigral pathway (Lu et al., 2014, Ehrman et al., 2013). NOLZ1 seems to activate indirectly downstream expression of DARPP32 via its action on RAR β (Liao & Liu 2005, Urbán et al., 2010) and is therefore likely to be an important transcription factor of MSN development. Here, a variant form of NOLZ1 was cloned from the human

WGE and diencephalon, which had only been previously cloned from a skin melanotic melanoma (Strausberg et al., 2002). This was an interesting discovery which suggested that variant forms of NOLZ1 protein might be expressed differentially in different regions during development and postnatally. As the full length form of NOLZ1 could not be cloned successfully from human WGE or diencephalon cDNA, this particular short variant form may be the version which is expressed in the WGE *in vivo* early in striatal development. FOXP1 was cloned and expressed in a plasmid with NOLZ1 (variant) and ISL1 as it was unable to be sub-cloned into the plasmid as a singular transcription factor. FOXP1 is important during MSN development and is expressed in two-thirds of MSNs (Tamura et al., 2004) and up-regulates the expression of striatally enriched genes (Tang et al., 2012).

3.8.2 Plasmid design features

The use of the multicistronic p3x2A-pMT plasmid has allowed the expression of multiple transcription factors in HEK293 cells in order to validate their protein expression. The use of the 2A peptide has allowed the expression of multiple transcription factors, all in an equal amount. The 2A peptide allows the separation of the transcription factors during translation by self-cleavage (de Felipe 2004). This has allowed exploitation of the highly efficient CAGG promoter (Miyazaki et al., 1989) for the equal expression of up to three genes (in the case of FOXP1-NOLZ1(variant)-ISL1 plasmid) from one promoter within a single plasmid.

With the GFP being expressed downstream of an IRES, the levels of expression of the GFP (as a reporter of transfection efficiency) will be up to 50% lower than the level of expression of the transcription factors themselves (Mizuguchi et al., 2000). This means that any determination of transfection efficiency using GFP will most likely underestimate the transfection efficiency and levels of the transcription factors themselves. With only up to three of the four insertion sites being utilised for the expression of transcription factors in the multicistronic plasmid, the GFP could

possibly be inserted into the final restriction site, which is XbaI, in order to gain a more accurate, live readout of transcription factor expression. However, this was not possible with the current pCAGG-IRES-EGFP plasmid, as there are two extra XbaI sites in the plasmid, therefore XbaI restriction digestion would lead to the disintegration of the plasmid. However, such a strategy would be made possible by employing the p3x2A-pMT multicistronic plasmid. Other sites in the plasmid, including BglII (where NOLZ1/NOLZ1(variant) were inserted) and NheI (where EBF1/ISL1 were inserted) could be utilised for insertion of other transcription factors of interest, either for MSN development or perhaps to drive cortical neuronal differentiation; the resulting neurons could be used in co-culture with the developing iPS-MSN neurons, since co-culture with other neuronal types has been shown to be beneficial for specification and maturation (Penrod et al., 2011, Segal et al., 2003). The GFP in the plasmid could be switched for an alternate fluorescent protein colour and therefore allow identity of the separate populations, but selection for both with G418 due to the neomycin resistance..

The transfection efficiency was variable between the plasmids, and was relatively poor in some cases, meaning that the percentage of cells expressing the transcription factors will be always limited by this low efficiency. In the future, and beyond the scope of this study, the use of viruses to infect neuroprogenitors with the transcription factor constructs would ultimately result in a higher percentage of positively expressing cells and neurons.

However, in the following chapters, the neomycin resistance gene in the pCAGG-IRES-EGFP plasmid backbone was exploited as a way to obtain a more pure population of cells by G418 treatment of the cells post-transfection. These plasmids were transfected into neural progenitors derived from iPS cells, in order to drive differentiation into medium spiny neurones. Firstly, an initial screen of plasmids was performed in order to narrow down the number of plasmids to be used for full

analysis. This involved transfection of the neural stem cells with the plasmids and subsequent analysis of DARPP32 protein expression, a protein enriched in MSNs (Ouimet et al., 1984).

3.8.3 Limitations of the methods

In order to validate the expression of the protein, the methods of immunofluorescence and western blotting were used. The limitations of these methods mean they need to be used in conjunction as both size of protein and the nuclear localisation of the transcription factor have to be shown. The problem with western blotting with the low transfection efficiencies means that protein expression of the transcription factors was harder to visualise, therefore the immunofluorescence validation of the protein was more likely to show protein expression. Separation of the proteins was observed by cleavage of the 2A peptide tag, for example, in the case of NOLZ1-ISL1 transfections and so the 2A self-cleaving peptides worked in the system employed herein.

***CHAPTER 4: PROTEIN
CHARACTERISATION OF
DIFFERENTIATION
PROTOCOL***

4. Protein characterisation of differentiation protocol

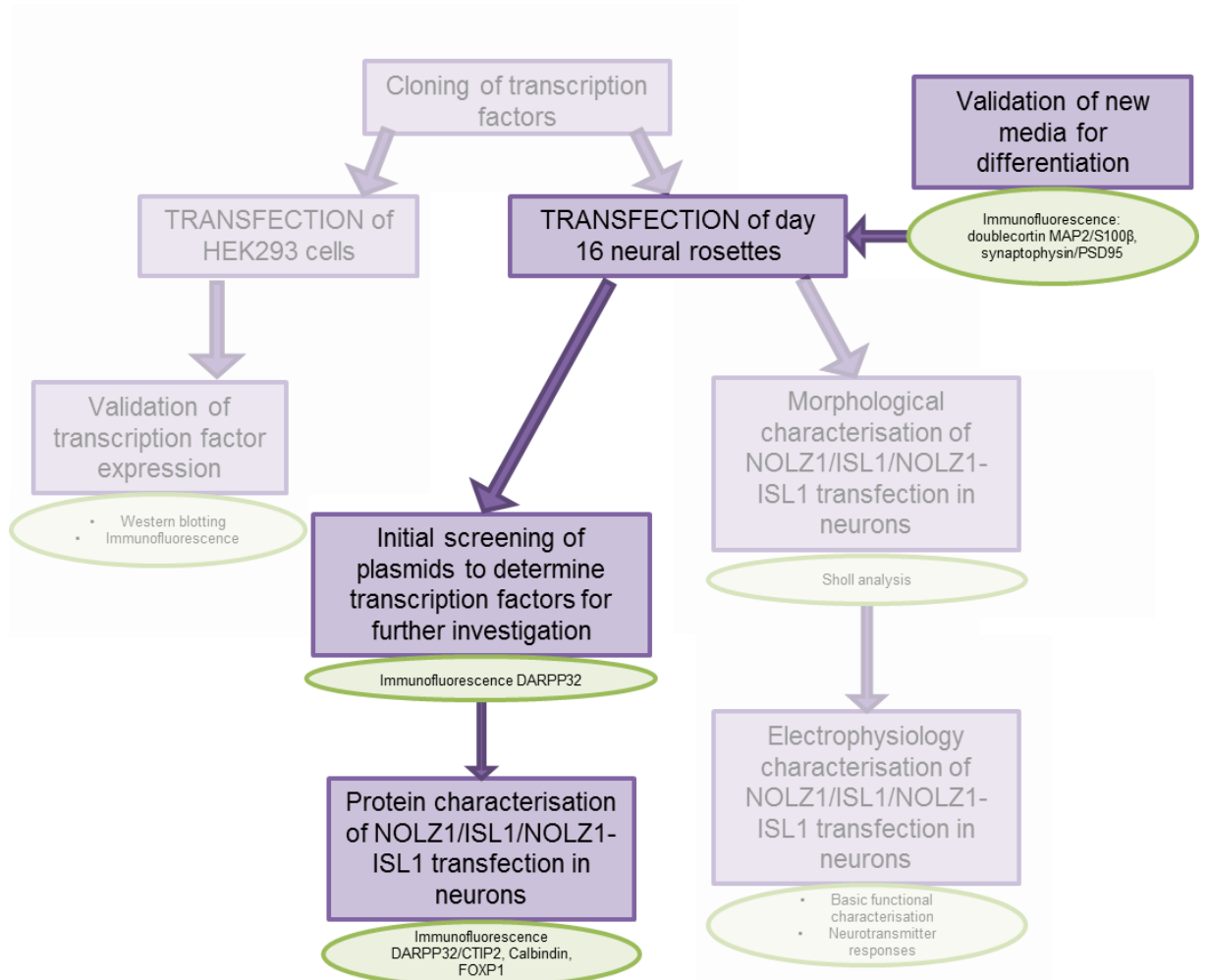


Figure 4.0: Summary of the data in chapter 4. In this chapter, is the characterisation of the SCM1/2 differentiation protocol, which was subsequently used for further protein characterisation of neurons that have been transfected with NOLZ1, ISL1 or NOLZ1-ISL1 combined.

4.1 Introduction

In order to produce functionally mature neurons, our lab generated a new protocol for differentiation of neural stem cells into mature neurons. However, the neurons were not specified to be a certain neuronal subtype, but the precursors have been patterned to be ventral forebrain-like. The medium has been formulated based on several previous papers, to include several compounds with specific roles; firstly N-[N-(3,5-Difluorophenacetyl)-L-alanyl]-S-phenylglycine t-butyl ester (DAPT), a Notch signalling inhibitor targeting γ -secretase, a molecule that delays G1/S phase transition in the cell cycle, caused cell cycle exit, committing cells to neurogenesis (Borghese et al., 2010). Cell cycle arrest has also been targeted by the compound PD 0332991, a cyclin dependent kinase 4 & 6 inhibitor which arrests the cell cycle at G1 (Fry et al., 2004, Toogood et al., 2005). A compound added in order to promote neuronal maturation was forskolin (an adenylate cyclase activator); this compound activates presynaptic release of neurotransmitters and increases the frequency of spontaneous mini EPSCs (Robbe et al, 2001; Chen and Regehr, 1997; Chavez-Noriega and Stevens, 1994). Foskolin also induces the phosphorylation of methyl CpG binding protein 2 (MeCP2) *in vivo* which, *in vitro* induces phosphorylation of the protein kinase A target, CREB at Ser133 (Hutchinson et al., 2012). The medium also contains brain-derived neurotrophic factor (BDNF), which in combination with phosphorylated CREB has been postulated to induce DARPP32 expression in medium spiny neurons (Keilani et al., 2012). A recent study has also shown that the addition of Ca^{2+} and γ -amino butyric acid (GABA, a neurotransmitter) mimics the effects of culturing with astrocyte conditioned medium by maturing neurons, so that they fire spontaneous action potentials and the resting membrane potential is decreased significantly (Rushton et al., 2013).

The new protocol mostly aimed to improve maturation, whereas for specification to MSNs, utilising the method of forced transcription factor expression (as per Section

1.7). As part of the new protocol, the validation of expression of mature neuronal proteins and synaptic markers was carried out. This has been further extended to be utilised in conjunction with the transcription factor transfection of 8 different plasmids plus the empty plasmid control in order to try and improve levels of DARPP32 expression in the neurons, 4 weeks post transfection. Once these were analysed, the transcription factors which improved the proportion of DARPP32 expression, were further analysed for protein expression which are observed in MSNs.

4.2 Immunofluorescence of differentiation

The new protocol for differentiation was validated for making mature neurons. This was done by immunofluorescence in order to analyse the expression of MAP2 (a mature neuronal marker), S100 β (an astrocyte marker), synaptophysin and PSD95 (pre- and post-synaptic proteins, respectively) and doublecortin (an early marker of neurogenesis, usually expressed for approximately 2 weeks of differentiation).

Cells were differentiated for 16 days to form forebrain specified neural progenitors, these were plated for differentiation following the SCM protocol and were harvested for immunofluorescence at fixed time points over the following 20 days in order to characterise the cell expression of the immature neurogenesis protein; doublecortin, the mature neuronal protein; MAP2, the astrocyte marker; S100 β and the synaptic proteins; synaptophysin and PSD95.

4.2.1 Doublecortin expression

Immunofluorescence for doublecortin was performed throughout from day 18 of the experiment. The percentage of cells that expressed doublecortin is approximately 90% at day 18 (Figure 4.1) as expected, indicating these cells were undergoing neurogenesis. The level of expression of doublecortin remained at a similar level throughout differentiation.

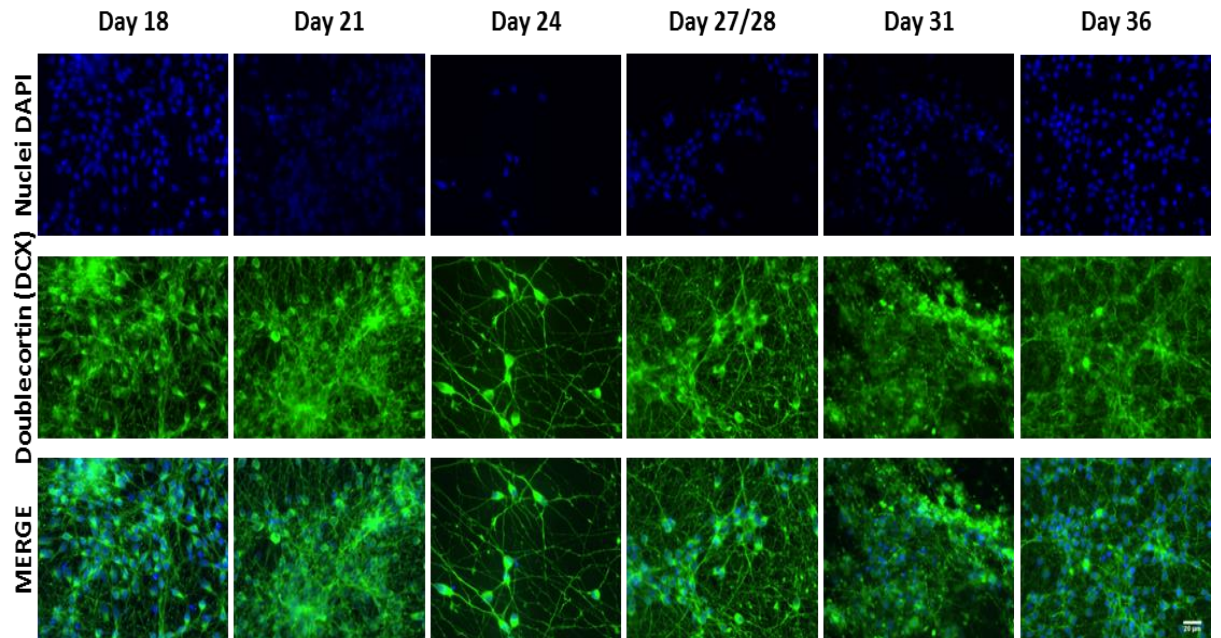


Figure 4.1: Doublecortin expression during differentiation of 34D6 iPS from day 18 to day 36 of neuronal differentiation. iPS cells were differentiated to neural progenitors for 16 days, then plated as progenitors for neuronal differentiation. Cells were fixed at the time points indicated (every 3-5 days) and immunofluorescence performed for doublecortin (DCX) using goat DCX (1:100 sc8066) in block overnight @ 4 °C. Scale bar = 20 μ m N=3; n=9

4.2.2 MAP2/S100 β expression

Immunofluorescence for both MAP2 and S100 β were performed throughout from day 18 of the experiment. As shown in Figure 4.2 and 4.3, the majority of cells expressed MAP2 (Figure 4.2). The numbers of MAP2⁺ cells steadily increased during differentiation and reached 89.9% \pm 3.05 by day 36 (Mean \pm SEM across N=3; n=9), the proportion of S100 β ⁺ cells was 2.60% \pm 2.43 at day 36 (N=3; n=9). This suggests that the population of cells generated was neuronal and contained few astrocytes.

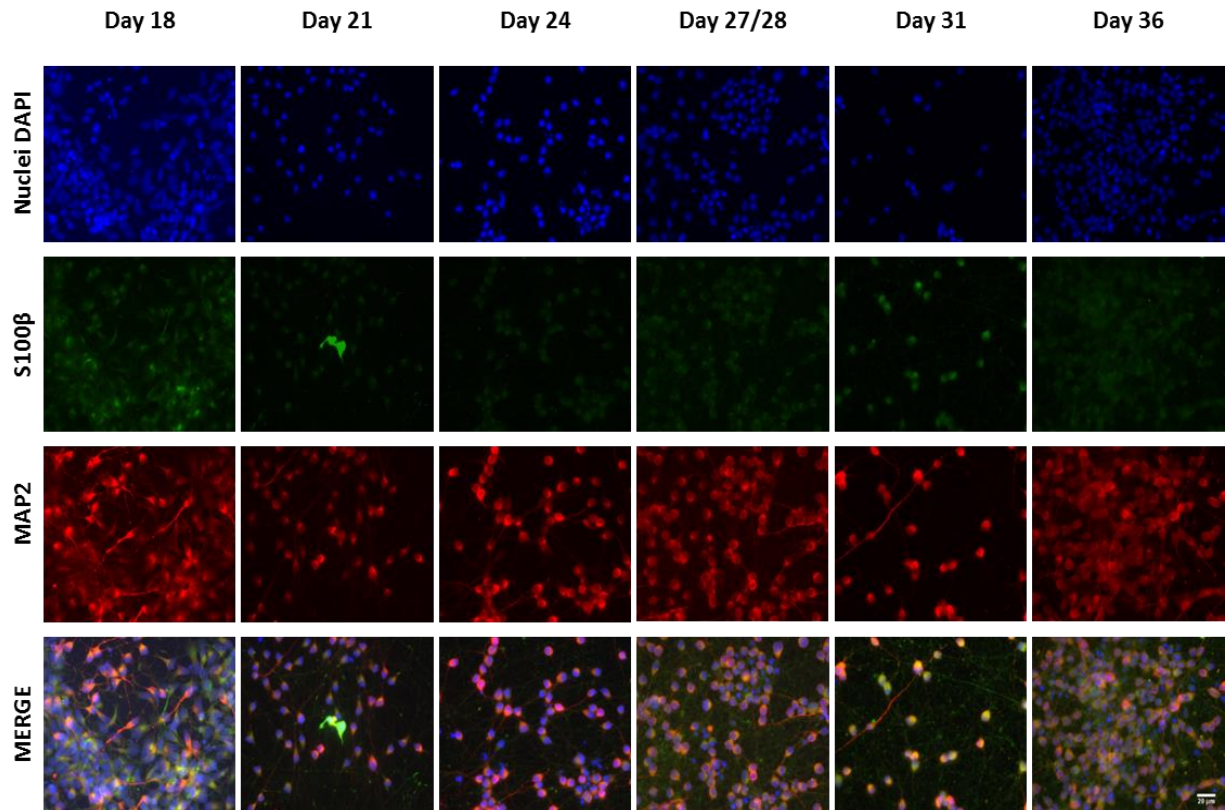


Figure 4.2: MAP2 and S100 β expression during differentiation of 34D6 iPS from day 18 to day 36 of neuronal differentiation. iPS cells were differentiated to neural progenitors for 16 days, then plated as progenitors for neuronal differentiation. Cells were fixed at the time points indicated (every 3-5 days) and immunofluorescence performed for MAP2 using rabbit α MAP2 (1:500) and S100 β using mouse α S100 β (1:500 S2532) in block overnight @ 4 °C. Scale bar = 20 μ m N=3; n=9

4.2.3 MAP2/synaptophysin expression

Immunofluorescence for both MAP2 and synaptophysin were performed from day 18 of the experiment and are shown in Figure 4.3. As per Figure 4.2, the majority of cells expressed MAP2 and the levels of expression of synaptophysin steadily increased throughout the differentiation, peaking at around day 27/28. This co-staining was performed in order to determine localisation of synaptophysin to the axons, due to the punctate nature of the staining, making sure that it stained the cells and was not background staining. The localisation of synaptophysin to the axons was apparent from the staining, and highlights the formation of presynaptic terminals through the length of the axon. Co-staining with PSD-95 confirmed both pre- and post-synaptic boutons are developing, indicating the formation of functional

synapses (Figure 4.4 and 4.5).

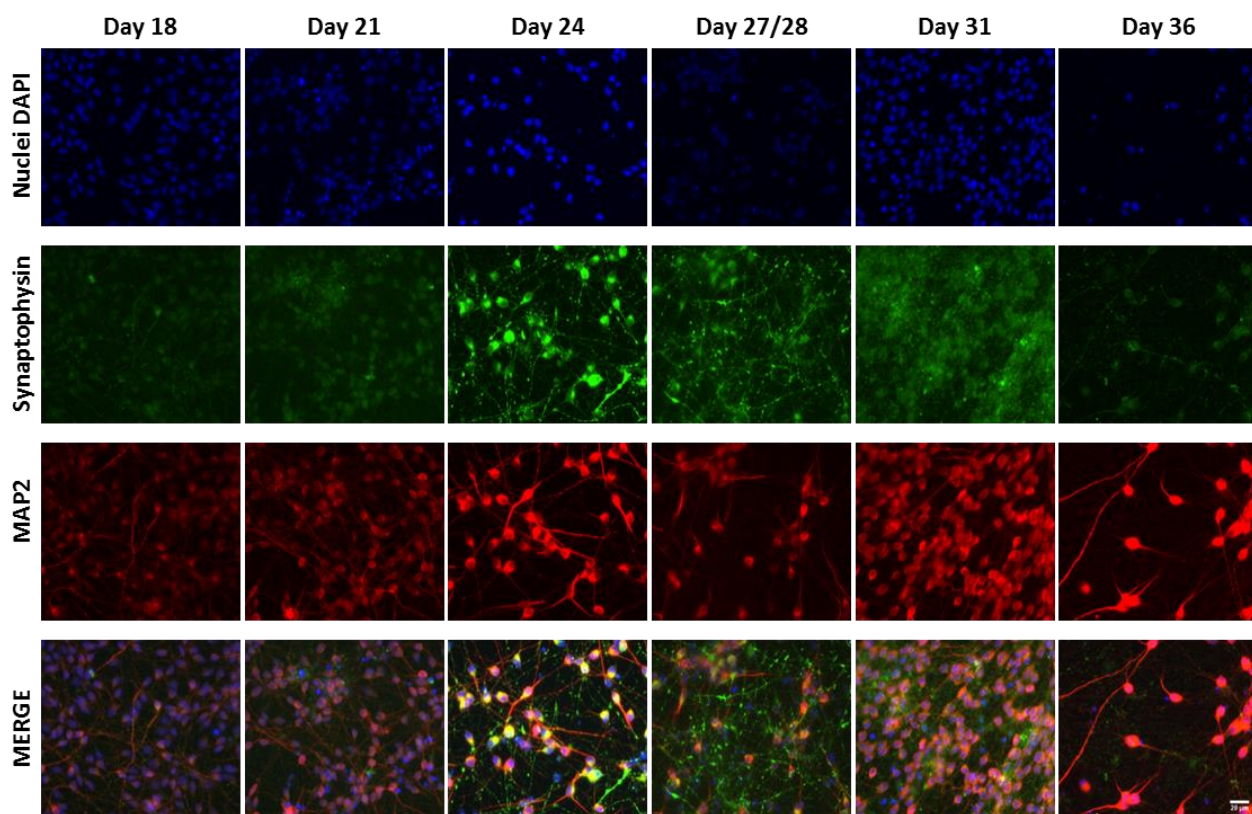


Figure 4.3: MAP2 & synaptophysin expression during differentiation of 34D6 iPS from day 18 to day 36 of neuronal differentiation. iPS cells were differentiated to neural progenitors for 16 days, then plated as progenitors for neuronal differentiation. Cells were fixed at the time points indicated (every 3-5 days) and immunofluorescence performed for rabbit α MAP2 (1:500 ab32454), mouse α synaptophysin (1:200 ab8049) in block overnight @ 4°C. Scale bar = 20 μ m N=3; n=9

4.2.4 PSD95/Synaptophysin expression

Co-localisation of PSD95 and synaptophysin was determined throughout the time course of the experiment, using immunofluorescence (Figure 4.4). As seen above (Figure 4.3), the levels of expression of synaptophysin steadily increased throughout the differentiation, and peaked at around day 27/28. The localisation of PSD95 started in the cell bodies at day 21 where it appeared to remain throughout differentiation. However, there was evidence of axonal staining at day 27/28, coinciding with the peak expression of synaptophysin. Confocal microscopy images of day 31 cells can be seen in Figure 4.5. These were taken in order to confirm the

co-registration of synaptophysin and PSD95, which can be clearly observed (indicated by the white arrows) these data suggest that the differentiating iPSCs are beginning to form synapses by 27/28 DIV.

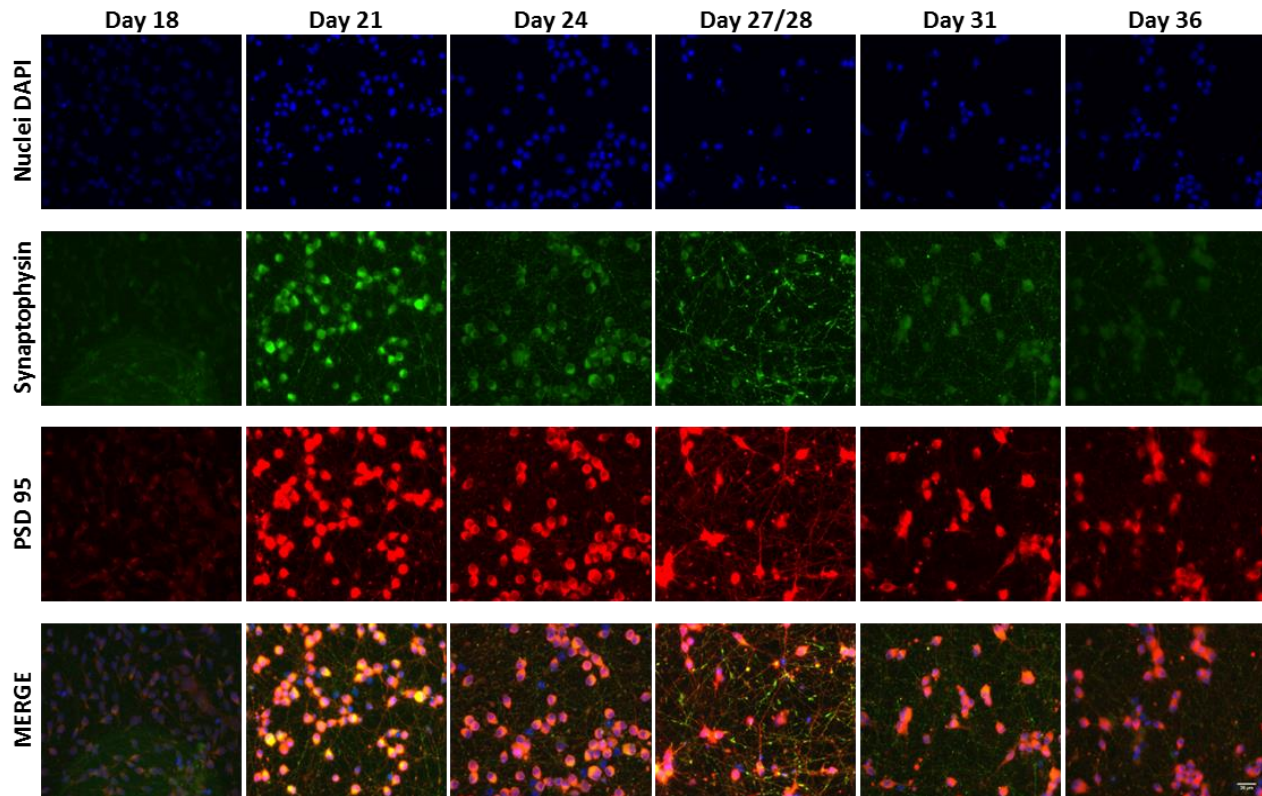


Figure 4.4: Synaptophysin & PSD95 expression during differentiation of 34D6 iPSC from day 18 to day 36 of neuronal differentiation. iPSC cells were differentiated to neural progenitors for 16 days, then plated as progenitors for neuronal differentiation. Cells were fixed at the time points indicated (every 3-5 days) and immunofluorescence performed for rabbit α PSD95 (1:100 ab18258), mouse α synaptophysin (1:200 ab8049) in block overnight @ 4°C. Scale bar = 20 μ m N=3; n=9

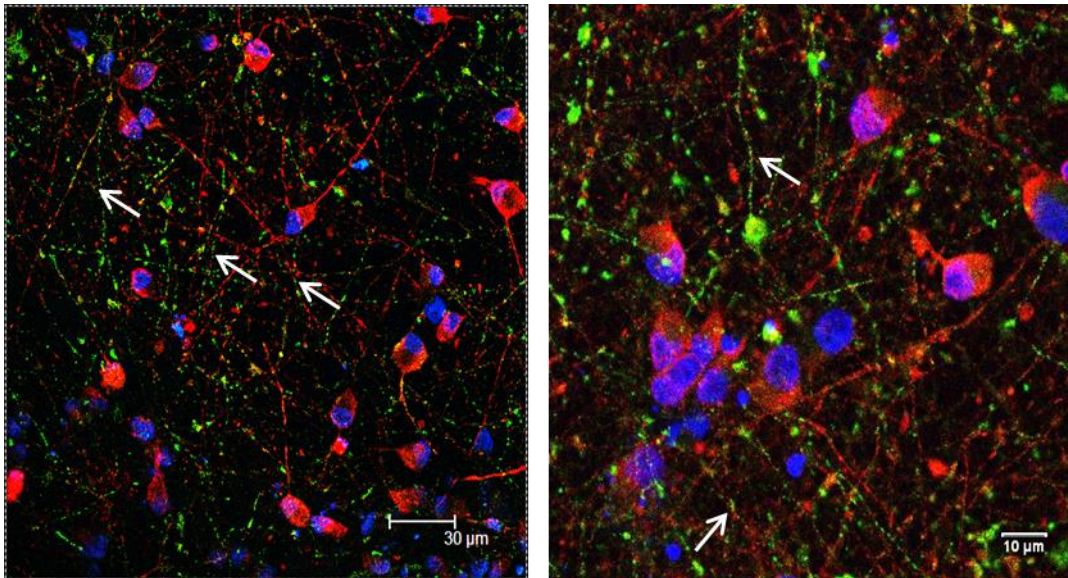


Figure 4.5: Confocal images of immunofluorescence of synaptophysin and PSD95 on 34D6 iPS derived neurons, 31 days post neuronal induction. The co-localisation of synaptophysin and PSD95 puncta can be observed. Rabbit α PSD 95 (1:100 ab18258) in red, mouse α Synaptophysin (1:200 ab8049) in green, blue nuclei. Arrows indicate areas where co-localisation of synaptophysin and PSD95 are seen and therefore indicating possible synapses

4.3 Initial transfection of the 9 plasmids for driven differentiation of neural stem cells

In order to select transcription factor vectors for detailed analysis their ability to differentiate neural progenitors into MSNs was tested by transfecting each of the 9 plasmids described in Chapter 3 into day 16 neural progenitors. At 1 day post transfection, the transfection expression/efficiency of each plasmid was determined by GFP expression (Figure 4.6 for example pictures and transfection efficiencies). The transfection efficiencies varied depending on the plasmid used. The plasmids which produced the higher transfection efficiencies were CAG- (24.9% \pm 1.70 N=3; n=9), ISL1 (22.8% \pm 0.70 N=3; n=9), NOLZ1 (variant) (22.5% \pm 2.66 N=3; n=9) and NOLZ1(variant)-ISL1 (19.1% \pm 1.79 N=2; n=6). Lower transfection efficiencies were observed for NOLZ1-ISL1 (11.0% \pm 3.55 N=3; n=9), OCT6 (10.9% \pm 2.15 N=3; n=9), FOXP1-NOLZ1(variant)-ISL1 (10.9% \pm 1.24 N=3; n=9), EBF1 (8.57% \pm 2.41 N=3; n=9), with the lowest efficiency observed for NOLZ1 transfected cells (5.96% \pm

2.21 N=3;n=9). The cells were differentiated in the SCM1/2 media until 4 weeks post transfection, when the cells were fixed for DARPP32 immunofluorescence.

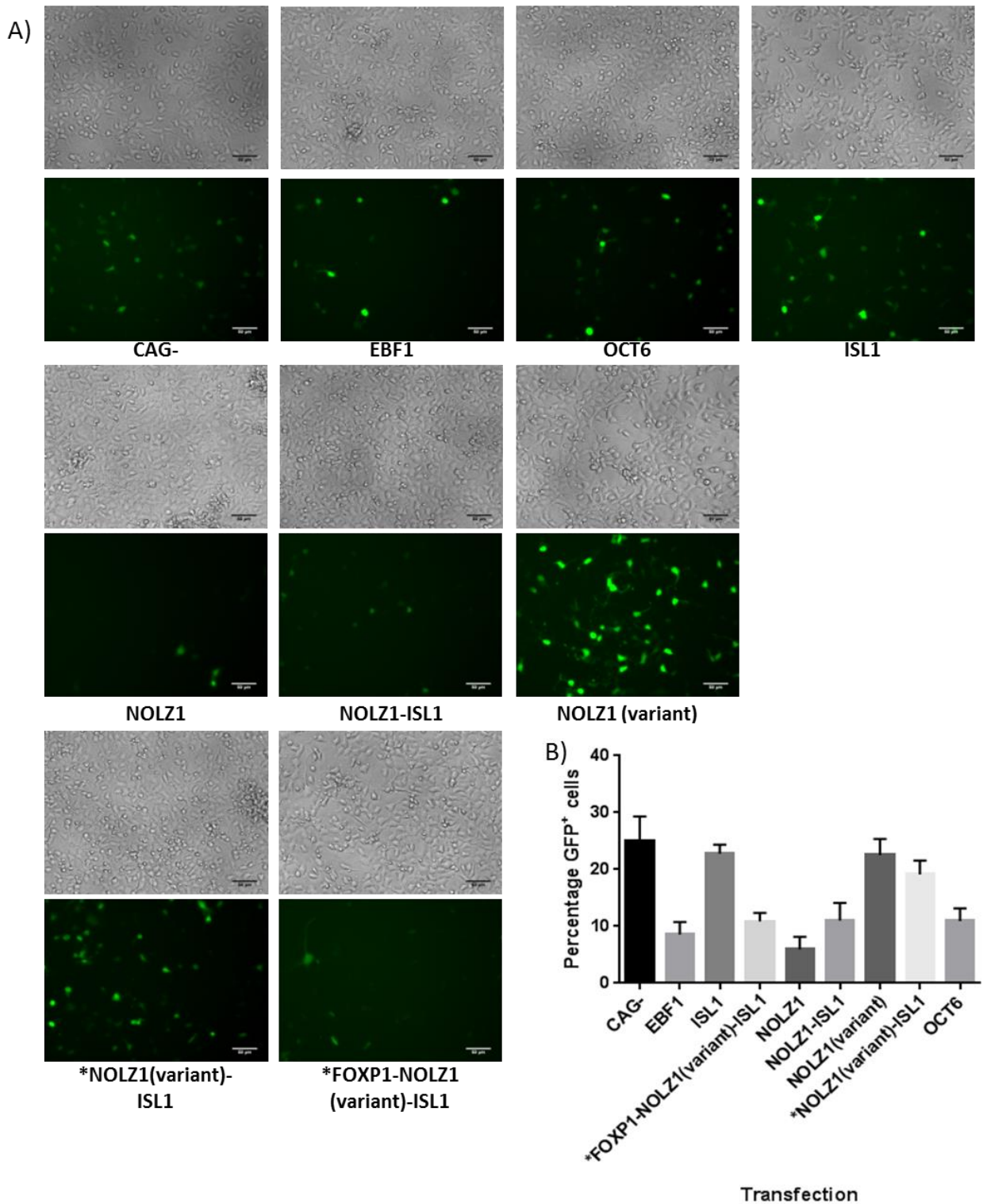


Figure 4.6: GFP expression in 34D6 D17 cells 1 day post transfection. Transfections were performed on 34D6 iPS derived day 16 neural progenitors with the pCAGG-Transcription Factor-IRES-EGFP plasmid, using nucleofection. These cells were then

imaged 1 day post transfection in order to determine the transfection efficiency. A) Example images of the brightfield and FITC channel of cells 1 day post transfection with each of the 9 plasmids. These images were used in order to calculate the transfection efficiencies of the individual plasmids, scale bars = 50 μm . B) Mean transfection efficiencies generated by counting the number of GFP⁺ cells compared to total number of cells. The efficiencies were calculated by counting cells in at least 3 fields of view were captured per transfection per biological replicate (N), N=2;n=6 where * otherwise N=3;n=9. Mean \pm SEM across each field of view.

The percentage of DARPP32 expressing cells resulting from each plasmid transfection was determined (Figure 4.7 for example images). The expression efficiency of the plasmids and the percentage of DARPP32 expression for each of the plasmids can be seen in Figure 4.8a and 4.8b, respectively. The transfection efficiency varied between the plasmids and as the levels of GFP were unable to be determined at the 4 week time point for all the plasmids, transfection efficiency at the beginning of the experiment was used to determine efficiency of DARPP32 induction. The percentage of DARPP32 expression in control cultures transfected with empty vector was 14.62% \pm 2.59% (N=3; n=9) which was comparable to previous studies of differentiated hPSCs (Zhang et al., 2010, El-Akabawy et al., 2011, Delli Carri et al., 2013a&b, Aubry et al., 2008, Shin et al., 2012). Cultures transfected with the NOLZ1(variant)-ISL1 plasmid had a higher percentage of DARPP32 expressing neurons than those with empty vector at 18.7% \pm 3.33% (N=2; n=8). The remaining transcription factors did not produce a cell population expressing DARPP32 in greater proportion, than the negative control.

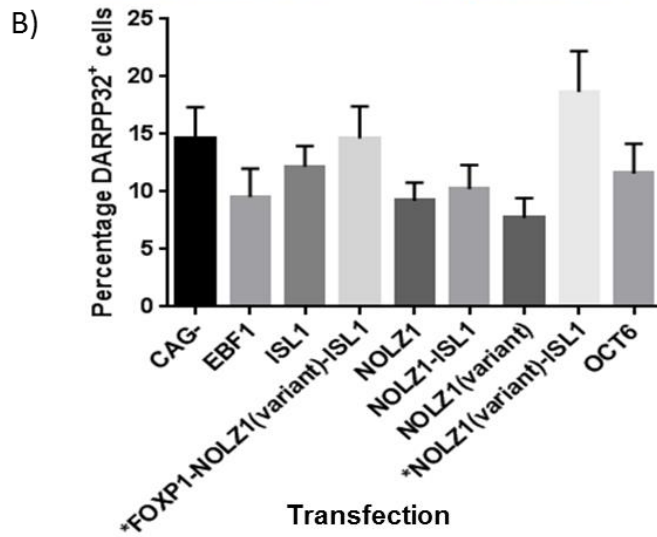
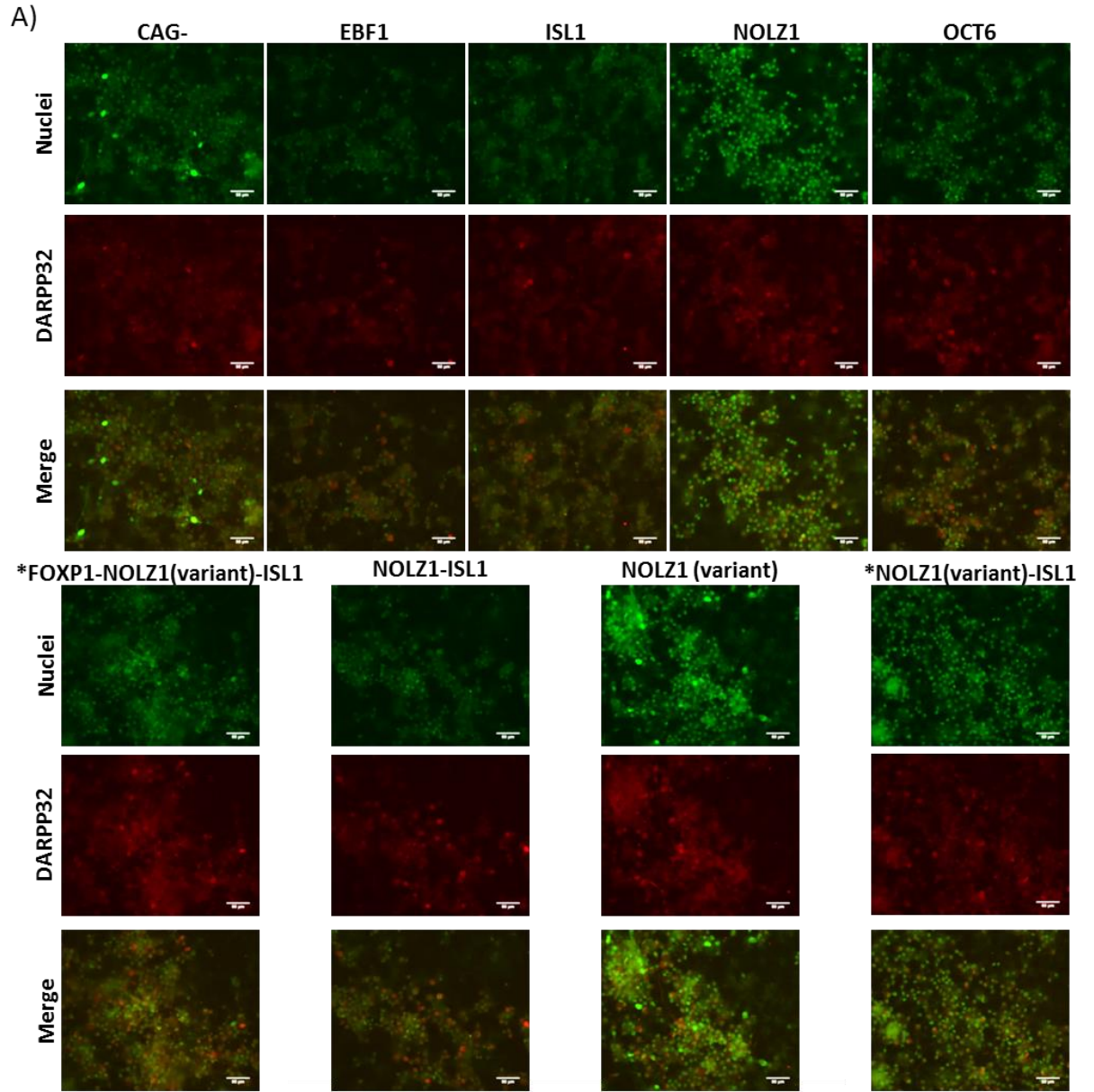


Figure 4.7 (above): DARPP32 expression in 34D6 iPS-derived neurons 4 weeks post transfection. 34D6 iPS derived neural stem cells were transfected at 16 days post neural induction with the 8 pCAGG-Transcription factor-IRES-EGFP plasmids & the negative control. These cells were differentiated for a further 4 weeks in SCM1/2 media. Cells were harvested for immunofluorescence of DARPP32 using rabbit α DARPP32 antibody (abcam ab40801 1:200) @ 4°C overnight in block. A) Example images from the DARPP32 immunofluorescence, nuclei stained green with SYTO16 nuclear stain and DARPP32 stained red with Alexa-fluor 594 goat α rabbit IgG. Scale bar = 50 μ m. B) Bar graphs showing the percentage of DARPP32 expression in the total number of cells, calculated from at least 4 fields of view per biological replicate (N), N=3;n=12 unless marked with *N=2;n=8. Error bars showing SEM of mean across each field of view.

The levels of DARPP32 expression were normalised to transfection efficiency of the plasmids and subsequently to the normalised value for DARPP32 expression level of the negative control (Figure 4.8c for graph of DARPP32 induction efficiency). The transcription factors which had an efficiency of DARPP32 induction of greater than 1 (i.e. above the control transfection level) were all of the transcription factors excluding ISL1 alone and NOLZ1 (variant), with NOLZ1 having the highest induction efficiency of DARPP32 out of all the transcription factors of 2.96.

In summary, it has been determined that NOLZ1 transfection induces the expression of DARPP32 with the greatest efficiency. As a result of the initial transcription screen in Section 4.3, NOLZ1 was used as a transcription factor to be expressed in day 16 rosettes and the resulting cells analysed for molecular (Section 4.4), morphological and physiological (Chapter 5) characteristics. A recent study has also revealed that premature expression of Nolz1 *in vivo* under control of the Nestin promoter stimulates cell cycle exit and differentiation of neural stem cells, in the mouse ventricular zone of the lateral ganglionic eminence (Chang et al., 2013). The other transcription factor that was investigated further was ISL1, although it was determined to not have a high efficiency of DARPP32 induction, the ISL1 plasmid used in this experiment was the incorrect form, missing the final nucleotide of the coding sequence, as this was discovered after the experiment. This may have impaired the functionality of ISL1 with the frame shift mutation causing an elongation of the protein due to the stop codon at the end of the multicistronic

section of the plasmid being out of frame and the resulting protein being 19 amino acids larger than it should be, with no understanding how this affects the transcription factor's function. The sequence data was re-analysed after the ISL1 protein was judged to be larger than expected by Western blotting (chapter 3) and as a result of two recent papers supporting its role with regard to striatonigral medium spiny neuron development (Ehrman et al., 2013). ISL1 promotes striatonigral pathway development of medium spiny neurons and represses striatopallidal fate as seen when *Isl1* is conditionally knocked out in the striatum (Lu et al., 2014).

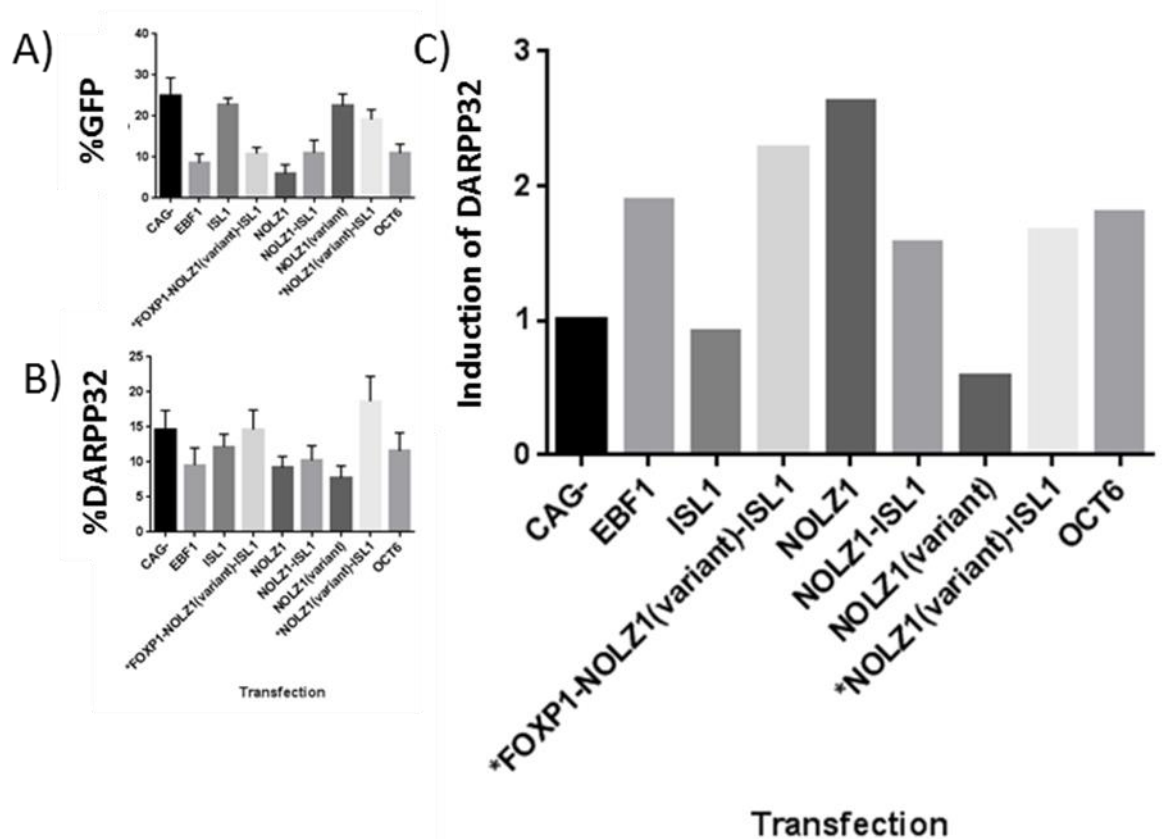


Figure 4.8: Induction efficiency of the transcription factors of DARPP32 expression. GFP expression was used as a determinant of transcription factor expression and therefore the proportion of cells which were expressing the transcription factor. The levels of DARPP32 were determined at 4 weeks. The DARPP32 proportion of expression was divided by the percentage of GFP expression, then each of the transcription factor transfections were normalised to the CAG- transfected cells. A) Transfection efficiency graph from 4.6B. B) Percentage of DARPP32 expressing cells graph from figure 4.7B. C) Bar graph showing induction of DARPP32 expression. N=3;n=12 unless marked with *N=2;n=8. Mean \pm SEM across each field of view.

4.4 Further investigation into the use of NOLZ1 and ISL1 transfection for differentiation

4.4.1 G418 kill curves

In order to enrich the population of neurons expressing the transcription factor that had been transfected, cells were selected with G418, as the expression vector also conferred G418 resistance. Obtaining an enriched population was more important for the molecular characterisation than the morphological or physiological characterisation of transfected neurons as cells could be selectively patched or imaged for Sholl analysis based on their GFP expression.

Initial transfections were conducted with a short selection of cells with G418 at 800 µg/ml, at 2 days post transfection, for 1 day, following a protocol developed by Sali Bagabir. This was then followed by re-plating of the selected cells for differentiation. This proved to be unsuccessful with cells not surviving the second plating. This was possibly due to the changed initial protocol which the cells had been differentiated with, as the cells under selection were starting to form neurons, rather than remain as progenitors, even at high density. This meant they did not survive re-plating and therefore a new protocol was required, without a second re-plating.

Cells were transfected at day 16 with each of the 4 plasmids to be used in further study: empty plasmid control (CAG-), NOLZ1, ISL1 and the NOLZ1-ISL1 combined plasmid. These were allowed to recover for 1 day before being changed to SCM1 medium supplemented with G418 at, 150 µg/ml, 300 µg/ml and 600 µg/ml, or no G418 added. These were then imaged every 2 days and the percentage of GFP expression and the total number of cells calculated per field of view was recorded. At 7 days post transfection, half of the cultures exposed to 300 µg/ml G418 treatment were changed to medium without G418 to see if this could improve survival whilst increasing the percentage of GFP⁺ cells *in vitro*.

For all transfections, G418 treatment increased the percentage of GFP⁺ cells by the final time point, 600 µg/ml G418 treatment increased the percentage of GFP⁺ cells the most, by the final time point the percentage of GFP⁺ cells varied from 45% to 80% depending on the transfection, but as a result of the initial transfection efficiency being fairly low (1.30% for CAG- to 14.7% for ISL1) the percentage of GFP expression still increased. The number of cells that were still alive and attached was also very low after treatment with 600 µg/ml G418 varying, on average, from 3 to 10.3 cells per field of view, an 8 fold decrease from the numbers observed without G418 treatment (Figure 4.9). In conjunction with this analysis, cells underwent basic electrophysiological characterisation by Dr. Vsevelod Telezhkin, which showed cells selected at 150 µg/ml G418 to be the most neuronal with spontaneous activity at 2 weeks post transfection and were comparable to those without G418 treatment (data not shown). Cells treated with 600 µg/ml G418 were not viable to be analysed by whole cell patch clamp at 2 weeks post transfection. Cells treated with 300 µg/ml G418 also showed deterioration in their ability to be analysed by whole cell patch clamp.

An enrichment of GFP⁺ cells was beginning to be observed with 150 µg/ml G418 treatment at 11 days post transfection, initial transfection efficiencies of 1.30% (CAG-), 14.7% (ISL1), 11.2% (NOLZ1) and 7.54% (NOLZ1-ISL1) were raised to levels of expression of GFP in the cell population of 2.80% (CAG-), 15.5% (ISL1), 18.8% (NOLZ1) and 13% (NOLZ1-ISL1) by 11 days post transfection. With further analysis being undertaken at 14 days and 21 days post transfection, cell viability was important and as a result ruled out 600 µg/ml G418 treatment as an option of enrichment of cells expressing the plasmid, as cell density was at $6.07 \pm 1.74\%$ (N=4; n=12) of the 0 µg/ml G418 treated cells. The number of cells per field of view compared to 0 µg/ml G418 treated cells, across all transfections, was at $50.2 \pm 6.82\%$ (N=4; n=12) with 150 µg/ml G418 treatment as opposed to $20.9 \pm 9.17\%$

(N=4; n=12, 300 µg/ml G418 treatment for the whole experiment) or $22.2 \pm 4.68\%$ (N=4; n=12, 300 µg/ml G418 for up to 1 week post transfection). This showed that the viability was decreased at higher concentrations of G418 selection, which was to be expected, but with the variable transfection efficiencies, the cells are not necessarily comparable between the transfections.

As a result of; the deterioration in electrophysiological properties, the improvement of GFP⁺ cells apparent at 11 days post transfection and the cell density/viability, 150 µg/ml G418 selection was used in order to enrich the population of cells for GFP⁺ expression in further experiments.

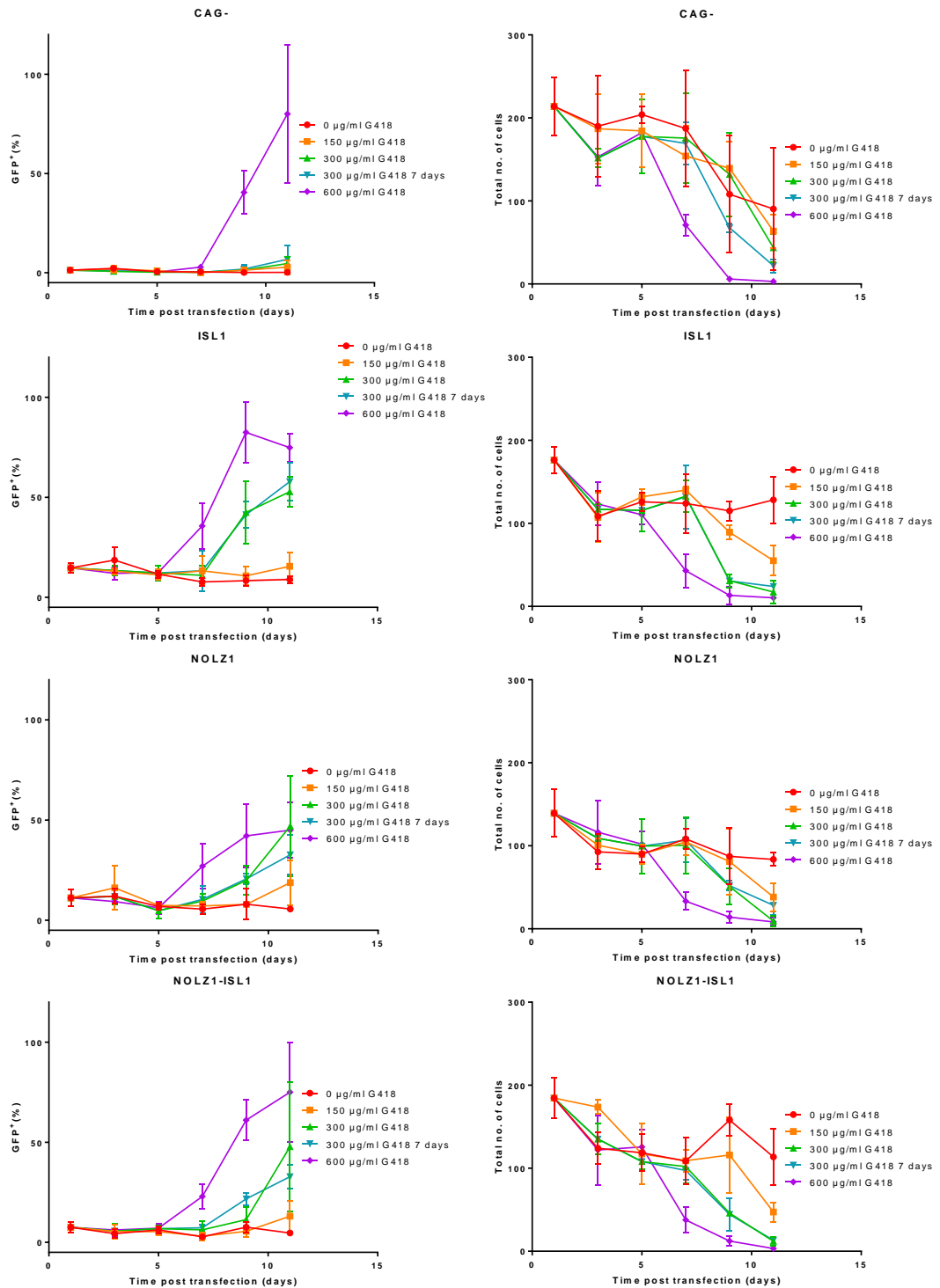


Figure 4.9: G418 kill curves of cells transfected with pCAGG-IRES-EGFP plasmids. 34D6 D16 neural rosettes were transfected with the four plasmids, CAG- control, NOLZ1, ISL1 and NOLZ1-ISL1. At 1 day post transfection, the cells were imaged and placed in media containing various G418 concentrations, no G418, 150 µg/ml, 300 µg/ml for whole experiment, 300 µg/ml until 7 days and 600 µg/ml. Left column shows percentage of GFP⁺ cells. Right column shows total number of cell bodies per field of view. From top to bottom,

CAG- control, ISL1, NOLZ1, and NOLZ1-ISL1 transfected cells. Mean \pm SEM across the fields of view (N=1, n \geq 3)

4.4.2 Characterisation of transfections by immunofluorescence

Cells were fixed with paraformaldehyde (4%) at 3 weeks post transfection; the cells had received treatment with 150 μ g/ml G418 for 6 days, in order to enrich the population of cells expressing the plasmids. In conjunction with G418 selection, a GFP antibody was used for immunofluorescence to co-localise any GFP expression observed with the expression of the protein of interest in order to characterise these cells. However, this did not account for cells which had been transfected with the plasmid but had stopped expressing it and therefore ceased expression of GFP, prior to analysis by immunofluorescence. The transfection efficiency in the cells was higher in CAG- (28.9% \pm 1.56 N=2;n=9) and NOLZ1 (33.5% \pm 4.27 N=2;n=9) transfected cells than ISL1 (25.5% \pm 3.41 N=2;n=9) and NOLZ1-ISL1 cells (11.5% \pm 1.37, N=2;n=9).

4.4.2.1 Calbindin expression

One of the proteins investigated was calbindin-28K (Figure 4.10A), a calcium binding protein expressed in the projection neurons of the matrix compartment which has been shown to be expressed in the medium sized-spiny neurons of the rat striatum (Gerfen & Wilson 1996, Bennett & Bolam 1993). The proportion of calbindin expression in GFP⁺ cells (Figure 4.10B) did not change significantly between CAG- (95.0% \pm 1.44), ISL1 (85.0% \pm 3.79), NOLZ1 (88.8% \pm 3.27) or NOLZ1-ISL1 (82.5% \pm 4.42) (Kruskal-Wallis statistic=3.28, p=0.35 (N=2, n=30)).

When considering the total population, (Figure 4.10C), the proportion of calbindin expressing cells was 17.6% \pm 1.13 in CAG- transfected cells, which is the highest observed, ISL1 (15.6% \pm 0.91), NOLZ1 (12.8% \pm 1.43) and NOLZ1-ISL1 (13.8% \pm 1.56) transfections lead to slightly lower percentage of calbindin expression. Calbindin expression in the CAG- control was significantly greater than NOLZ1

(Kruskal-Wallis statistic=10.4, Dunn's multiple comparison $p=0.02$ $N=2$, $n=30$). As transfections with the NOLZ1-ISL1 plasmid resulted in the lowest transfection efficiency, this in turn resulted in the highest level of cell death during selection with G418. Therefore, the NOLZ1-ISL1 transfected cells were at a lower density, relative to the other transfections during differentiation. This lower density during differentiation could have adversely effected neuronal maturation and therefore resulted in the lower levels of calbindin expression.

With calbindin expression at a similar proportion in all transfections, when considered as a percentage of GFP⁺ cells, it may be likely the continued expression of the plasmid in the cells does not have an effect on calbindin expression.

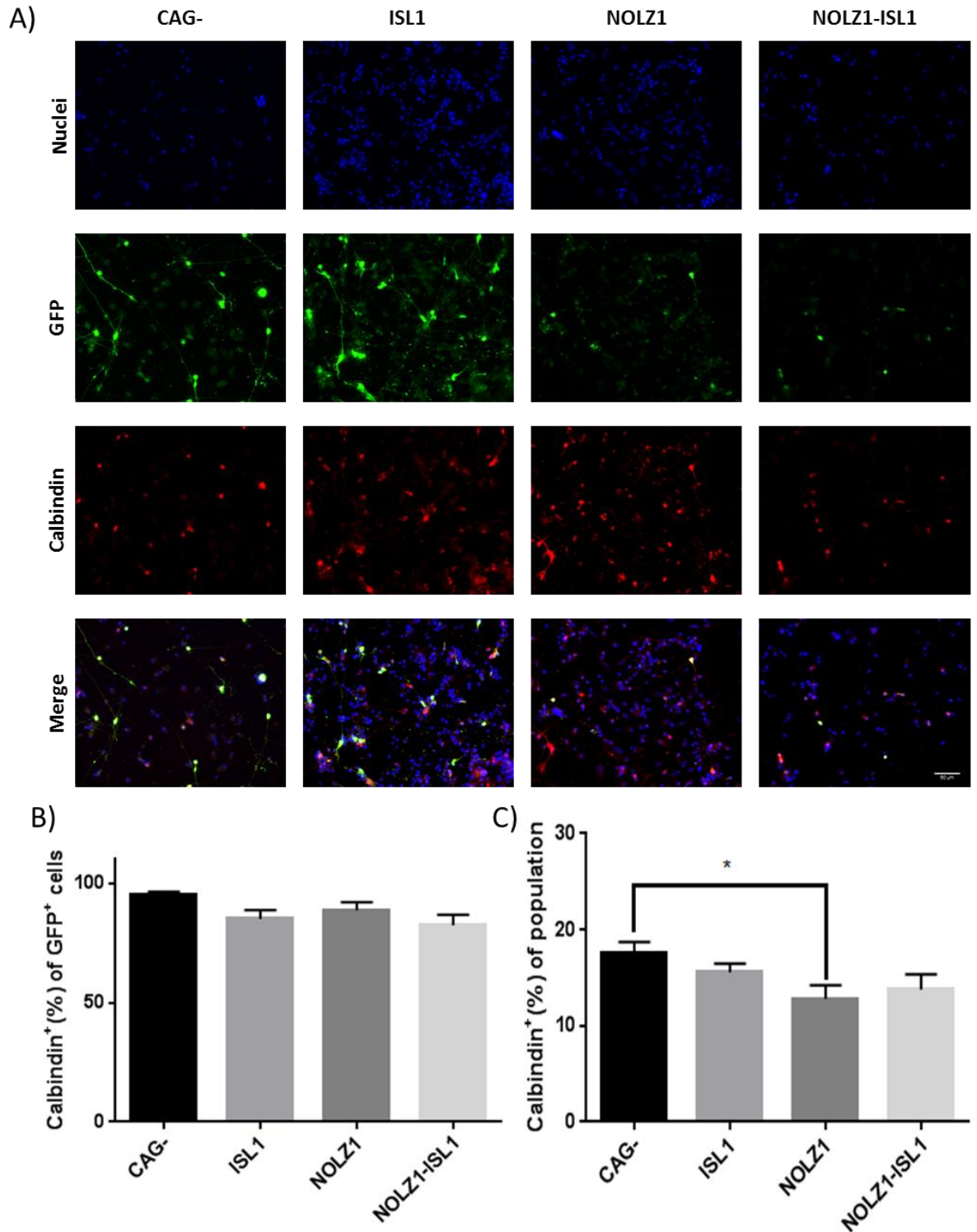


Figure 4.10: Calbindin and GFP expression in neurons 3 weeks post transfection. Neural progenitors differentiated from 34D6 iPS cells for 16 days were transfected with 1 of the 4 plasmids either CAG-, ISL1, NOLZ1 or NOLZ1-ISL1. 1 day later they were placed into 150 $\mu\text{g/ml}$ G418 selection media until 7 days post-transfection and then differentiated for a further 2 weeks. Cells were fixed for immunofluorescence at 3 weeks post transfection and stained with anti-GFP and anti-calbindin antibodies. A) Example images captured on an epifluorescent microscope showing GFP (green) and nuclei (blue), calbindin (red) and the merged image at the bottom. Scale bar for all images in bottom right image=50 μm . B)

Percentage of calbindin expressing cells at 3 weeks post transfection calculated as percentage of the number of GFP⁺ cells (N=2, n=30). C) Percentage of calbindin expressing cells at 3 weeks post transfection calculated as percentage of the total number of cells, (N=2, n=30). Error bars on all graphs displaying standard error across the field s of view. N= biological replicates, n = field of view

4.4.2.2 FOXP1 expression

The expression of the transcription factor, FOXP1, was analysed by immunofluorescence at 3 weeks post transfection (Figure 4.11A). The percentage of GFP⁺ cells expressing FOXP1 at 3 weeks post transfection (Figure 4.11B) was not significantly different between transfections (Kruskal-Wallis Statistic=5.31, p=0.15 (N=2, n=30, except ISL1 N=1, n=15)). However, ISL1-transfected cells (83.7% ± 2.75) had a slightly higher percentage of FOXP1 expression than the other transcription factor transfected cells (CAG-=80.2% ± 2.67, NOLZ1=74.2% ± 6.01, NOLZ1-ISL1=69.1% ± 4.52). The percentage of the total population of cells expressing FOXP1 (Figure 4.11C), was not significantly different between transfections (Kruskal-Wallis Statistic=3.88, p=0.28 (N=2, n>29, except ISL1 N=1, n=15)), the NOLZ1 transfected cell population had the highest percentage of FOXP1 expressing cells (19.1% ± 3.38) and the ISL1 transfected cell population had the lowest proportion of FOXP1⁺ cells (11.0% ± 0.96), with CAG- transfected cells (17.4% ± 2.22) and NOLZ1-ISL1 transfected cell population (15.4 ± 1.16) between the two other transfections. The proportion of total cells expressing FOXP1 in ISL1 transfected cells seems to counter the data seen when considering the GFP⁺ population, however ISL1 transfections had lower transfection efficiency, so as a proportion of total cells less expression is seen.

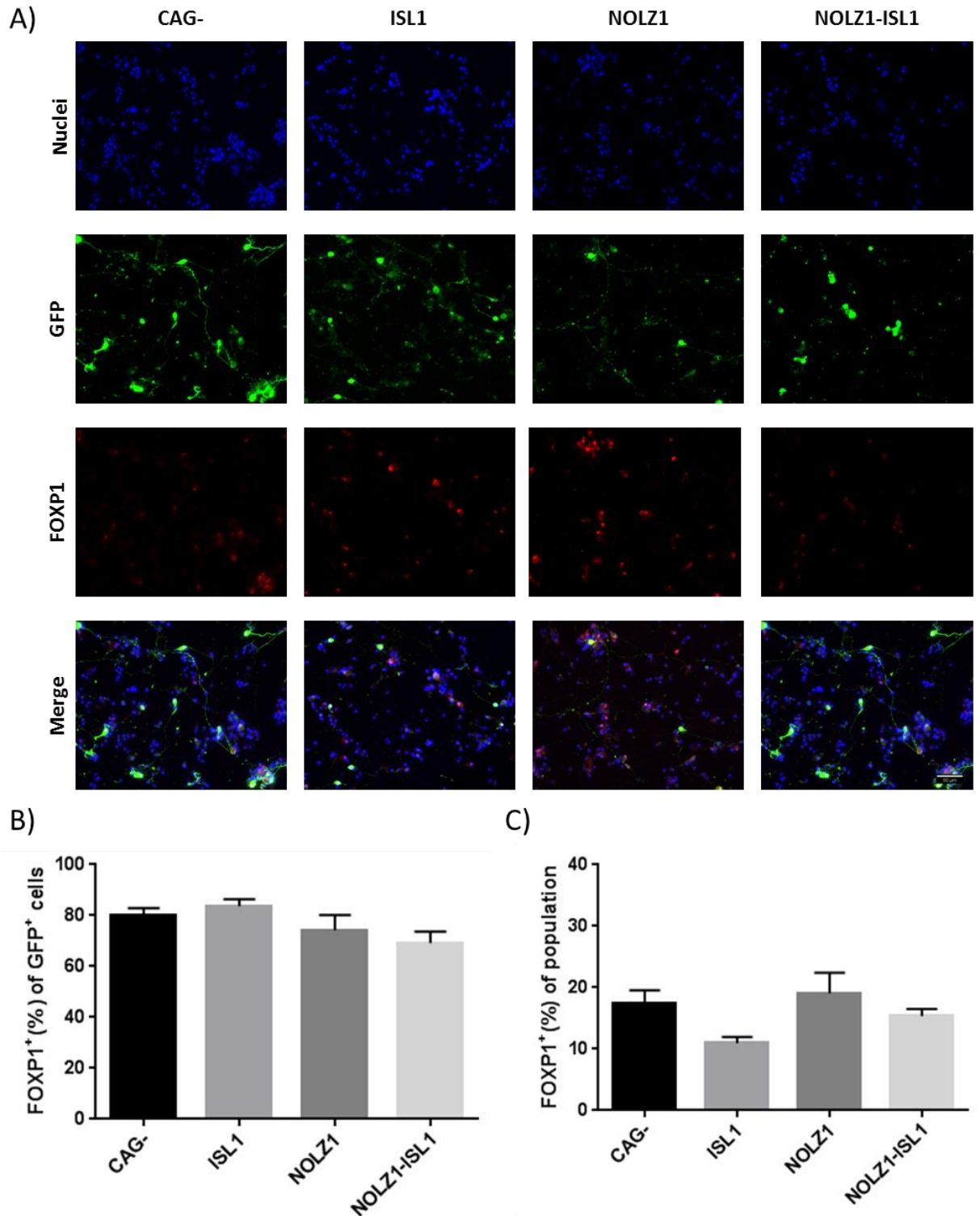


Figure 4.11: FOXP1 and GFP expression in neurons 3 weeks post transfection. Neural progenitors differentiated from 34D6 iPS cells for 16 days were transfected with 1 of the 4 plasmids either CAG-, ISL1, NOLZ1 or NOLZ1-ISL1. 1 day later they were placed into 150 μ g/ml G418 selection media until 7 days post-transfection and then differentiated for a further 2 weeks. Cells were fixed for immunofluorescence at 3 weeks post transfection and stained with anti-GFP and anti-FOXP1 antibodies. A) Example images captured on an epifluorescent microscope showing GFP (green) and nuclei (blue), FOXP1 (red) and the merged image at the bottom. Scalebar for all images in bottom right image = 50 μ m. B)

FOXP1 expression at 3 weeks post transfection calculated as percentage of the number of GFP⁺ cells. C) FOXP1 expression at 3 weeks post transfection calculated as percentage of the total number of cells. (N=2, n>29, except ISL1 N=1, n=15). Error bars on all graphs displaying standard error across the data set. N= biological replicates, n = field of view.

4.4.2.3 DARPP32/CTIP2 expression

Analysis of DARPP32 and CTIP2 protein expression was carried out on terminally differentiated cells (Figure 4.12A & 4.13A), analysed separately and for co-expression, as although both are striatally enriched proteins, their co-expression is reported to be specific to the striatum (Delli-Carri et al., 2013 a). The percentage of GFP⁺ cells which were CTIP2⁺ at 3 weeks post transfection with G418 selection (Figure 4.12B) was not significantly different between transfections (one-way ANOVA $F(3,56)=1.14$, $p=0.34$ (N=1, n=15)). ISL1 transfected cells (70.8% \pm 7.37) had a slightly higher proportion of CTIP2 expression than CAG- (66.5% \pm 6.69), NOLZ1 (56.4% \pm 9.51) and NOLZ1-ISL1 (52.3% \pm 8.53) transfected cells. The percentage of GFP⁺ cells expressing DARPP32 (Figure 4.12C) at 3 weeks post transfection showed no significant difference between transfections NOLZ1 transfected cells had the highest proportion of DARPP32 expression (66.1% \pm 9.54) with CAG- plasmid (64.1% \pm 5.50) and NOLZ1-ISL1 (64.0% \pm 9.14) and ISL1 (58.1% \pm 7.86) transfected cells only having slightly lower DARPP32 expression (one-way ANOVA $F(3,56)=0.18$, $p=0.91$ (N=1, n=15)). ISL1 transfected cells had a slightly higher proportion of DARPP32⁺/CTIP2⁺ cells (54.7% \pm 7.53, figure 4.12D), but there was no significant difference between ISL1, CAG- (51.5% \pm 5.39), NOLZ1 (53.2% \pm 10.2) and NOLZ1-ISL1 (50.1% \pm 8.95) in the proportion of GFP⁺ cells co-expressing DARPP32 and CTIP2 (Kruskal-Wallis statistic = 0.36, $p=0.95$ (N=1, n=15)).

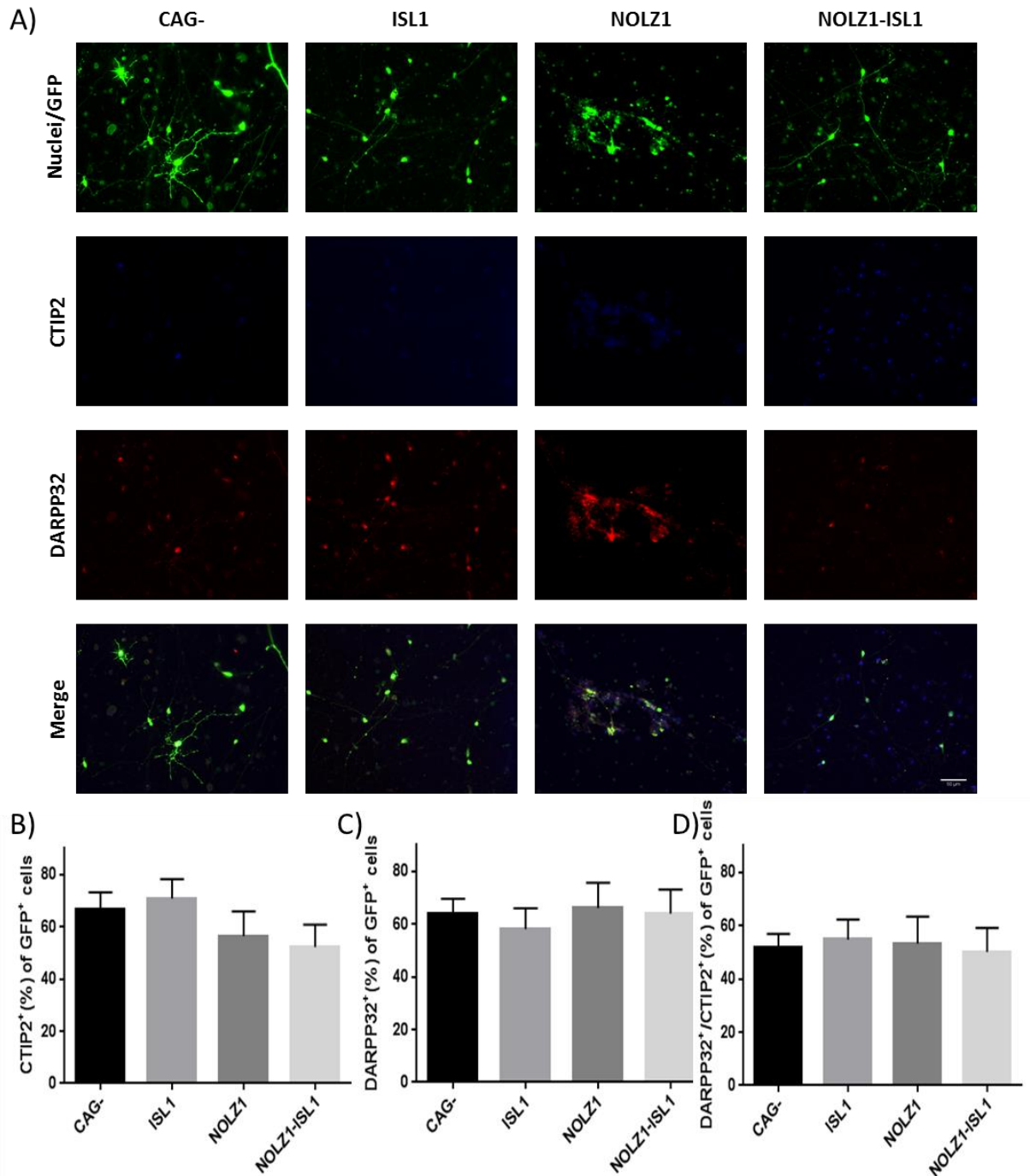


Figure 4.12: DARPP32 CTIP2 and GFP expression in neurons 3 weeks post transfection. Neural progenitors differentiated from 34D6 iPS cells for 16 days were transfected with 1 of the 4 plasmids either CAG-, ISL1, NOLZ1 or NOLZ1-ISL1. 1 day later they were placed into 150 μ g/ml G418 selection media until 7 days post-transfection and then differentiated for a further 2 weeks. Cells were fixed for immunofluorescence at 3 weeks post transfection and stained with anti-CTIP2 and anti-DARPP32 antibodies. A) Example images captured on an epifluorescent microscope showing GFP and nuclei (green), CTIP2 (blue), DARPP32 (red) and the merged image at the bottom. Scale bar for all images in bottom right image = 50 μ m B) CTIP2 expression at 3 weeks post transfection calculated as percentage of GFP⁺ cells (N=1, n=15) C) DARPP32 expression at 3 weeks post transfection calculated as percentage of GFP⁺ cells (N=1, n=15). D) DARPP32/CTIP2 co-expression cells at 3 weeks post transfection calculated as percentage of GFP⁺ cells. (N=1, n=15). Error bars on

all graphs displaying standard error across the data set. N= biological replicates, n = field of view

The percentage of the total population of cells, which were expressing CTIP2 at 3 weeks post transfection (Figure 4.13B), was not significantly different between transfections (Kruskal-Wallis statistic=3.30, $p=0.35$ ($N=2$, $n \geq 24$)), ISL1 transfected cells ($45.5\% \pm 10.8$, $n=25$) had the highest percentage of cells expressing CTIP2 and CAG- ($29.3\% \pm 4.30$ $n=25$), NOLZ1 ($19.9\% \pm 3.47$ $n=24$) and NOLZ1-ISL1 ($24.1\% \pm 4.59$ $n=25$) transfected cells had a lower proportion of cells that expressed CTIP2. The percentage of cells expressing DARPP32 (Figure 4.13C) at 3 weeks post transfection, showed no significant difference between transfections (Kruskal-Wallis statistic=6.64, $p=0.08$ ($N=2$, $n \geq 24$)), ISL1 transfected cells ($12.2\% \pm 1.98$ $n=25$) showed a higher proportion of DARPP32 expression than CAG- ($9.89\% \pm 0.99$ $n=25$), NOLZ1 ($6.92\% \pm 0.82$ $n=24$) and NOLZ1-ISL1 transfected cells ($7.98\% \pm 1.30$ $n=25$).

The proportion of DARPP32⁺/CTIP2⁺ cells (Figure 4.13D) at 3 weeks post transfection showed a significant difference between transfections (Kruskal-Wallis statistic=10.2, $p=0.02$, Dunn's multiple comparison ($N=2$, $n \geq 24$)). The ISL1 transfected cell population ($9.99\% \pm 1.74$ $n=25$) showed a significantly increased percentage of co-expression of DARPP32 and CTIP2 compared to NOLZ1 ($4.37\% \pm 0.64$ $n=24$ $p=0.04$) and was higher than their expression in CAG- control ($7.44\% \pm 0.89$ $n=25$) and NOLZ1-ISL1 transfected cells ($5.94\% \pm 0.96$ $n=25$).

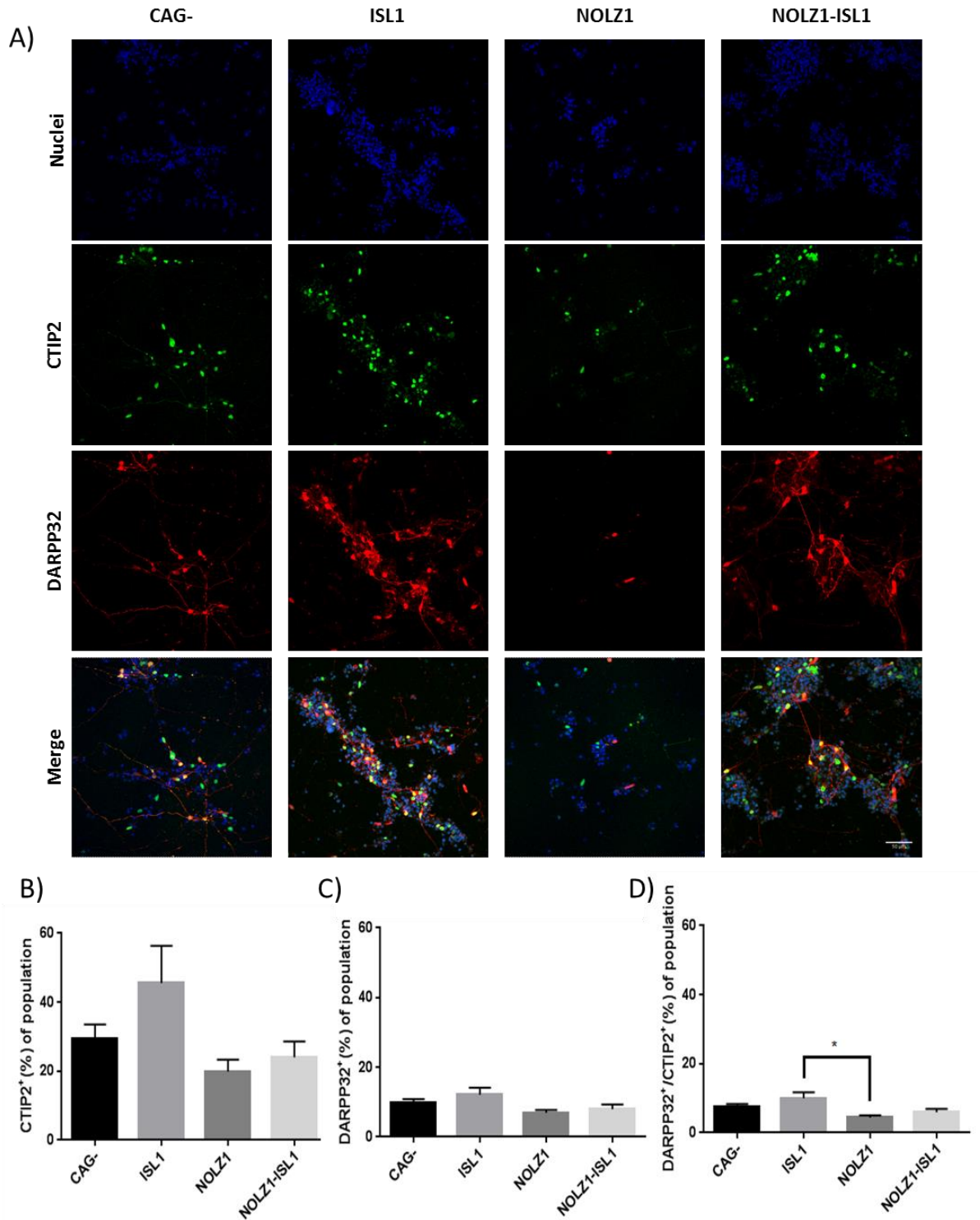


Figure 4.13: DARPP32 and CTIP2 expression in neurons 3 weeks post transfection G418 selected. Neural progenitors differentiated from 34D6 iPS cells for 16 days were transfected with 1 of the 4 plasmids either CAG-, ISL1, NOLZ1 or NOLZ1-ISL1. 1 day later they were placed into 150 μ g/ml G418 selection media until 7 days post-transfection and then differentiated for a further 2 weeks. Cells were fixed for immunofluorescence at 3 weeks post transfection and stained with anti-CTIP2 and anti-DARPP32 antibodies. A) Example images captured on a confocal microscope showing nuclei (blue), CTIP2 (green), DARPP32 (red) and the merged image at the bottom. Scale bar for all images in bottom right image = 50 μ m

B) CTIP2 expression cells at 3 weeks post transfection calculated as percentage of the total number of cells (N=2, n>24). C) DARPP32 expression at 3 weeks post transfection calculated as percentage of the total number of cells, (N=2, n>24). D) DARPP32/CTIP2 co-expression at 3 weeks post transfection calculated as percentage of the total number of cells (N=2, n>24). Error bars on all graphs displaying standard error across the fields of view. N= biological replicates, n = field of view

4.5 Conclusions

Protein characterisation of the SCM1/2 protocol showed that the majority of cells ~90% were neuronal, expressing MAP2 from early in differentiation and then during differentiation, the synaptic markers were increased in expression and co-localised. In order to concentrate on a few transcription factors, an initial screen of plasmids was carried out, and highlighted NOLZ1 as a candidate for inducing DARPP32 expression.

Further characterisation was then carried out with NOLZ1, ISL1 and NOLZ1-ISL1 plasmids in comparison with control transfections. Immunofluorescence for calbindin, FOXP1, CTIP2 and DARPP32 expression were performed. This showed that ISL1 induced the most MSN-like phenotype with an increased expression of CTIP2, FOXP1 and combined DARPP32/CTIP2 expression, in comparison to the control and other transcription factor transfections.

4.5.1 Protein characterisation of the SCM1/2 protocol

Previous studies have utilised different methods to obtain neurons from pluripotent stem cells, most involving the formation of embryoid bodies (EB) and inclusion of basic fibroblast growth factor (bFGF) in the medium (Okabe et al., 1996, Li et al., 1998, Bain et al., 1995, Jones-Villeneuve et al., 1982). These generate a relatively high percentage of neurons, with 50% of the proliferative (SOX2⁺) cells producing MAP2⁺ neurons with expression of the synaptic marker, synapsin I (Li et al., 1998). Exposure of EBs to retinoic acid also aids the neural induction process, and with subsequent dissociation, increases neuronal markers such as β III-tubulin and neurofilament M (Bain et al., 1995, Jones-Villeneuve et al., 1982). However, EB

formation often results in a non-uniform differentiation, with different areas of the EB being subjected to different signalling cues and varied concentration gradients of medium supplements/growth factors/drugs, which can result in incomplete differentiation into different germ layers or cell types. Other methods of neural induction have involved the use of undefined signalling by co-culture with other cell types *e.g.* stromal cells (Perrier et al., 2004, Kawasaki et al., 2000) or conditioned medium from human hepatocellular carcinoma cells (Shin et al., 2006).

The use of monolayer differentiation culture in mouse ESCs by Ying et al., (2003), resulted in more rapid differentiation, with neural tube like rosettes forming after only 4 days. The expression of the mature neuronal protein marker, Tau, was switched on in these cultures from day 5 (Ying et al., 2003) and the mature neuronal marker, MAP2 was observed from day 18 (although since nearly all cells were expressing the protein and earlier time points were not investigated, it seems likely that MAP2 was activating rather earlier in the protocol). A monolayer protocol employing retinoic acid and bFGF in serum-free medium generated similar data and, although rosettes were mechanically dissociated before re-plating, >90% of cells expressed MAP2, synaptophysin and neurofilament protein at 30 days post-induction (Baharvand et al., 2007). Throughout this thesis, a monolayer differentiation protocol was utilised, where re-plating of early differentiating neural progenitors was carried out at day 4, and which resulted in the formation of neural rosettes from day 5 onwards. This protocol was comparable to other protocols in terms of protein expression of mature neuronal markers and synaptic proteins.

The data suggest that the cells are undergoing neurogenesis, evidenced by the fact that approximately 90% of the cell population stained positive for the neurogenesis marker, doublecortin, from day 18 onwards (Figure 4.1). The data also suggest that the majority of cells were neurons as nearly 90% of the population stained positive for MAP2 and less than 3% of the cells stained positive for the astrocyte marker,

S100 β (Figure 4.2). Finally, expression and localisation of the synaptic markers; synaptophysin and PSD95 showed how they gradually increased in expression during differentiation, with a peak at 27 days post neural induction (Figure 4.4). These proteins are co-localised throughout differentiation (Figure 4.5), implying that synapses begin to form almost as soon as the neural rosettes are plated at day 16 post neural induction.

Once able to generate neurons, the objective of this chapter was to specify the neurons to MSNs. The forced expression of five transcription factors, important in MSN development, was carried out in ventral forebrain-like neural progenitors, in order to try and specify a DARPP32+ MSN phenotype (Figure 4,7). The data showed that NOLZ1 had the highest efficiency of DARPP32 induction (Figure 4.8). G418 kill curves were also performed to determine the best concentration of G418 for selection after transfection (Figure 4.9).

4.5.2 ISL1 is a likely candidate for specifying a MSN phenotype

Of all the transfection manoeuvres, ISL1 transfection seemed to result in differentiation into neurons with a phenotype most similar to MSNs.

Calbindin expression in GFP⁺ cells (Figure 4.10) was similar between transfections with the various transcription factors and so more biological replicates may be required to show a significant change. The general trend is that the CAG- control transfected cells produce the highest percentage of calbindin⁺ neurons, but this is only a slight increase from that seen with the transcription factor transfections. This may be a result of calbindin not being a downstream target of NOLZ1 or ISL1 and so is not affected by their transfection. It may also be that as calbindin is a matrix marker in the striatum (Pickel & Heras 1996, Gerfen & Wilson 1996), it is possible with ISL1 specifying cells of the striatonigral pathway (Ehrman et al., 2013, Lu et al., 2014), which is neither limited to or excluded from the matrix compartment of the

striatum (Gerfen & Young 1988) that ISL1 does not play a role in switching on calbindin expression.

There also needs to be analysis of whether the calbindin⁺ population are interneurons, by investigating expression of somatostatin/parvalbumin or analysing for co-expression with CTIP2 (Delli Carri et al., 2013b). Although from separate coverslips, the fact that the overwhelming majority of cells which were GFP⁺ were calbindin⁺ and 55% of GFP⁺ cells after ISL1 transfection were CTIP2⁺, indicated the ISL1 transfections were not necessarily generating just calbindin⁺ interneurons.

FOXP1 (Figure 4.11) was also increased by ISL1 transfections. FOXP1 is an important transcription factor in the developing striatum and has been implicated in the switching on of glutamate receptor genes and GABA receptor signalling genes, when overexpressed (Tang et al., 2012). Furthermore, FOXP1 is co-expressed with GluR2/3 in two-thirds of mouse MSNs (Tamura et al., 2004), supporting its role in switching on expression of glutamate receptors, which are required by MSNs to receive glutamatergic input from the cortex (Ferino et al., 1987, Jones et al., 1977, Royce 1982, Wilson 1987). FOXP1 is also co-expressed with ISL1 in the spinal motor column (Ericson et al., 1992, Tsuchida et al., 1994, Shu et al., 2001, Dasen et al., 2005, Luria & Laufer 2007). With the co-expression of FOXP1 and ISL1 observed in other regions, and the induction of expression observed in this chapter, speculation arises as to whether FOXP1 is a target of ISL1, a previously undefined role.

CTIP2 (Figure 4.12, 4.13) is an important transcription factor of MSN development and is first detected at E12.5 in the mouse LGE (Arlotta et al., 2005), MSN neurogenesis occurs from E13.5 and persists in the adult mouse and CTIP2 expression increases in cells during MSN migration, but is restricted to the mantle zone, therefore only expressed in postmitotic neurons (Arlotta et al., 2008). In the developing human, CTIP2 is expressed in the striatal anlage of the 11 week brain

(Delli Carri et al., 2013a). In this chapter, data pointed towards ISL1 being the most efficient inducer of this MSN marker. Interestingly, CTIP2 may have a role of transcriptional repression of NOLZ1 and ISL1 as in the mouse, there are 3 CTIP2 binding sites in the 1kb promoter region upstream of the translation start site of *Isl1* and 1 site in *Nolz1* promoter region (Desplats et al., 2008). Due to the limited time of expression of these transcription factors (Wang & Liu 2001, Chang et al., 2004), this could be a role for CTIP2, but needs further investigation.

CTIP2 protein co-localises with DARPP32 and FOXP1 in the MSNs of the mouse striatum and is excluded from the interneurons (Arlotta et al., 2008). In the 11 week old human fetal striatum, the CTIP2⁺ cells of the caudate nucleus also express DARPP32 (Delli Carri et al., 2013a). In this chapter ISL1 (Figure 4.12, 4.13) has also induced the highest levels of DARPP32/CTIP2 co-expression. NOLZ1 transfection had a positive influence on DARPP32 expression, but not CTIP2 expression and therefore did not induce co-expression of the two striatal markers as well as ISL1.

4.5.3 NOLZ1-ISL1 co-expression in the differentiation

The co-expression of NOLZ1 and ISL1 in the neural progenitors did not yield the expected improvement of MSN specification, perhaps because they may not specify the same types of MSN *in vivo* (Ko et al., 2013, Lu et al., 2014, Ehrman et al., 2013). However, NOLZ1 and ISL1 are co-expressed at E16.5 in the SVZ and MZ of the mouse LGE (Ko et al., 2013), so they are likely to play a complimentary role in MSN specification. The likely cause of the unexpected result is the transfection efficiencies between the plasmids varied according to plasmid size, with the largest plasmid, NOLZ1-ISL1, resulting in the lowest transfection efficiencies (~11%). With G418 selection, the dramatically reduced cell density may not have been optimal for effective differentiation. This may have masked any beneficial effects of this particular co-transfection strategy; co-expression of DARPP32⁺/CTIP2⁺ in the GFP⁺

cells was around 50%, compared to 51% observed for the CAG- control. Therefore, if the reduction in cell density was having a detrimental effect on differentiation, it may have led to the decrease in the expression of markers of differentiation, in comparison to the single transfections.

In summary, ISL1 transfection improved the proportion of FOXP1, CTIP2 and DARPP32/CTIP2 combined expression in cells differentiated utilising the SCM1/2 protocol.

4.5.4 Limitations of the methods in this chapter

Immunofluorescence was utilised to determine a molecular phenotype of the neurons generated. Semi quantitative methods were used to compare the different transfections and quantify the protein expression in the GFP⁺ cells and in the total population. Due to the method chosen, definitive quantification couldn't be performed due to the limitations of not being able to analyse the entire population, but analyse a proportion of the population. The levels of protein expression could also be measured using western blotting, but would only be able to account for the whole population and not differentiate between the GFP⁺ cells and the rest of the population. Another method for protein quantification that could be used was flow cytometry; however this could be more troublesome to perform with neurons, due to their morphology. The mRNA could be quantified with qRT-PCR, which would allow accurate quantification of the mRNA, but as with western blotting, the total population would be analysed and would not allow differentiation between the GFP⁺/GFP⁻ cells.

***CHAPTER 5:
MORPHOLOGICAL &
ELECTROPHYSIOLOGICAL
CHARACTERISATION OF
TRANSFECTED NEURONS***

5. Morphological and electrophysiological characterisation of transfected neurons

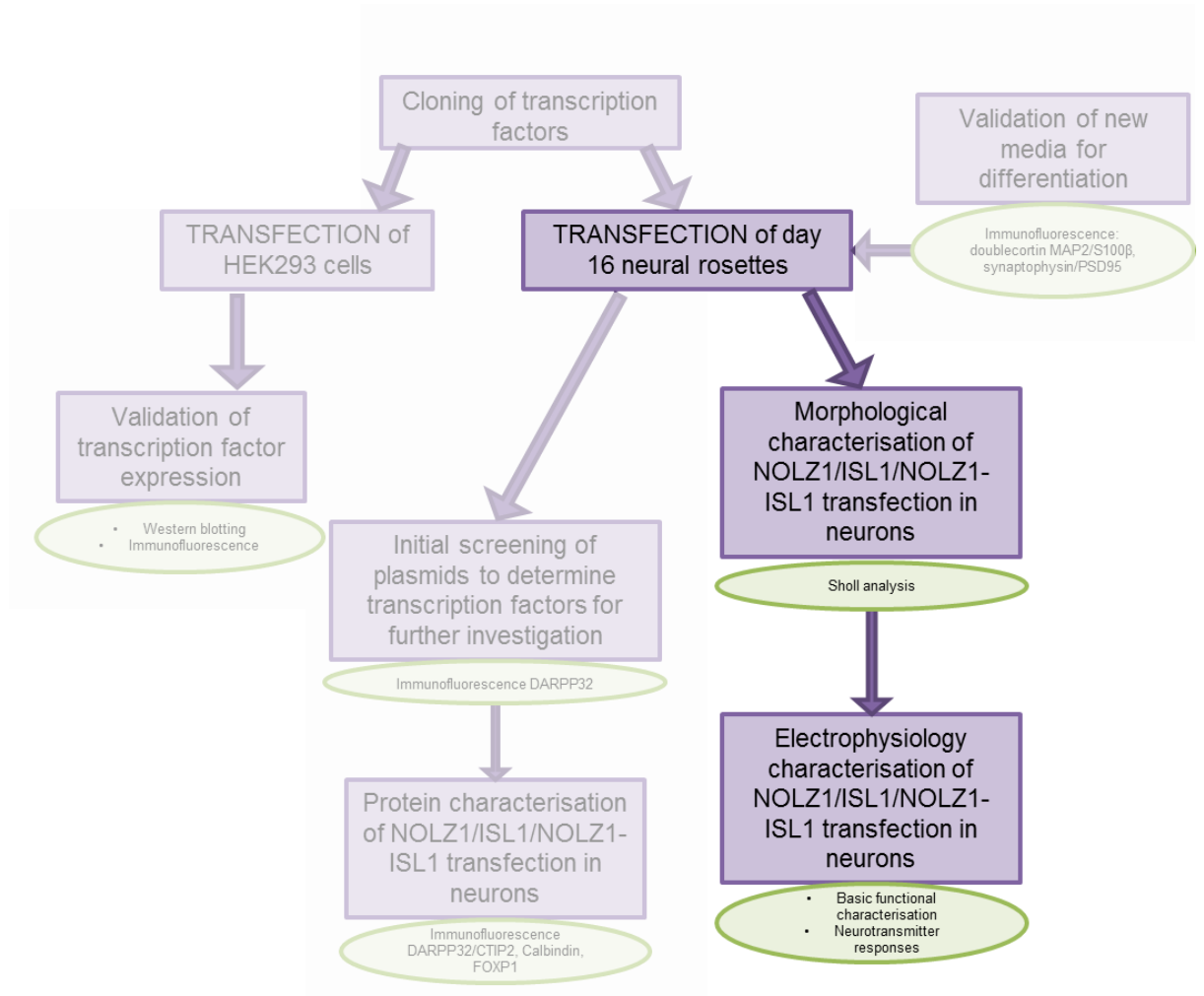


Figure 5.0: Summary of the data in chapter 5. In this chapter, is the characterisation of the morphological and physiological phenotype of the neurons, which have been transfected with NOLZ1, ISL1 or NOLZ1-ISL1 combined.

5.1 Introduction

Characterisation of neuronal maturity and phenotype can be performed by looking at the morphological characteristics, such as dendrite complexity, number and length, and investigating physiological properties such as ability to fire action potentials, responses to certain neurotransmitters and presence of particular ionic currents.

Sholl analysis was first introduced in 1953, looking at the complexity of neurons in the visual and motor cortices in the cat, by using concentric circles centred on the cell body of the neuron and at each circle, counting the number of intersections by the neuron (Sholl 1953). Sholl analysis has been used to investigate the complexity of neurons in a HD knock-in mouse, and it demonstrated that as the disease progressed, the neurons of the striatum decreased in dendritic complexity (Lerner et al., 2012). This suggests that Sholl analysis would be a useful tool for modelling the disease *in vitro*. BAC transgenic mice with eGFP expressed from the dopamine D1 or D2 receptor has allowed electrophysiological and morphological data to be acquired of cells of the different striatal efferent pathways (Gertler et al., 2008). There is a morphological difference between the D1⁺ and D2⁺ neurons, with more intersections by Sholl analysis, longer dendritic length and more primary dendrites in D1⁺ MSNs in comparison to D2⁺ MSNs (Gertler et al., 2008). Passive electrical differences are also observed, with dopamine D1 receptor expressing MSNs having a larger capacitance, indicating a larger cell surface area than D2⁺ MSNs, supporting the morphological data (Gertler et al., 2008). The D1⁺ MSNs also show a greater rheobase current, the current injection required to elicit an action potential (Ashley et al., 2005), reflected in a right-ward shift in the current injection against action potential spike frequency graph, and a sign of decreased excitability (Gertler et al., 2008). Another electrophysiological characteristic of MSNs, which is lacking in DARPP32^{-/-} mice, is dopamine D1 enhancement of NMDA currents and attenuation

of GABA currents, suggesting this is a function of DARPP32 (Flores-Hernández et al., 2002).

To elucidate the morphological and electrophysiological characteristics of the neurons transfected at day 16 with either empty CAG- plasmid, NOLZ1, ISL1 or the combination of NOLZ1-ISL1, neurons were analysed by Sholl analysis to determine morphological complexity at 1, 2 and 3 weeks and by whole-cell patch clamp to determine the electrophysiological properties of the neurons at 2 and 3 weeks post-transfection.

5.2 Morphological analysis of differentiated neurons

Cells which had been differentiated for 16 days to form neural progenitors were transfected with the 4 different plasmids pCAGG-IRES-EGFP (CAG-), pCAGG-NOLZ1-IRES-EGFP (NOLZ1), pCAGG-ISL1-IRES-EGFP (ISL1), pCAGG-NOLZ1-ISL1-IRES-EGFP (NOLZ1-ISL1), and differentiated for up to 3 weeks on coverslips, then harvested for analysis at 1, 2 and 3 weeks post transfection. Cells which were harvested at 1 and 2 weeks post transfection were selected with 150 µg/ml G418 from 24 hours post transfection in order to enrich the population of cells which had been transfected, cells which were differentiated for 3 weeks were un-selected with G418 as electrophysiological characterisation showed this treatment to be detrimental to the cells.

5.2.1 Week 1

Cells harvested at 1 week post transfection were analysed for total neurite length, total number of branches, Sholl analysis and then a linear regression of branch number against neurite length, in order to classify the neurons based on morphological characteristics (Figure 5.1). At 1 week, the CAG-control and ISL1 neurons showed more complex dendrites, closer to the soma, than the NOLZ1 and NOLZ1-ISL1 neurons; NOLZ1 and NOLZ1-ISL1 were less complex closer to the

soma, and more complex at the end of the axon (Figure 5.1B&C). Further from the cell soma at 50 μm , NOLZ1-ISL1, ISL1 and NOLZ1 transfected cells were less complex than the control transfection (Figure 5.1C). This could have resulted from the fact that the distance from the soma reached by CAG- transfected cells is shorter than the other neurons after transfection (Figure 5.1B) and the increased number of branches observed for CAG- transfected neurons (Figure 5.1D). Further from the cell soma (230 μm) the complexity of NOLZ1-ISL1 was increased compared to the CAG- transfected neurons (Figure 5.1C).

The mean number of branches per cell at 1 week post transfection, was comparable between CAG- (31.1 ± 8.64 N=3; n=47), ISL1 (26.0 ± 3.52 N=3; n=51) and NOLZ1-ISL1 (28.8 ± 8.54 N=3;n=49) transfected cells, all three were greater than NOLZ1 transfected cells (18.1 ± 3.30 N=3; n=46), but this was not significant (Figure 5.1D).

The mean total neurite length of the cells was also comparable between the 4 transfections: CAG- ($686.0 \mu\text{m} \pm 140.1$ N=3; n=47); ISL1 ($701.6 \mu\text{m} \pm 85.8$ N=3;n=51); NOLZ1 ($560.2 \mu\text{m} \pm 55.5$ N=3; n=46), and; NOLZ1-ISL1 ($675.4 \mu\text{m} \pm 69.8$ N=3; n=49) (Figure 5.1E). The cells were each plotted onto a scatter graph, in order to determine the types of neurons being formed (Figure 5.1F). Cells in the top left of the graph are longer with fewer branches, cells in the top right are longer and more branched, cells in the bottom left are shorter with fewer branches and cells in the bottom right are shorter with more branches. NOLZ1-ISL1 produced more cells which were long & branched neurons, ISL1 transfections produced the more cells that were long & basic neurons and CAG- transfected neurons produced the most short & basic neurons. Most of the cells were long & branched, with fewer cells in each of the other classifications.

5. Morphological and electrophysiological characterisation of transfected neurons

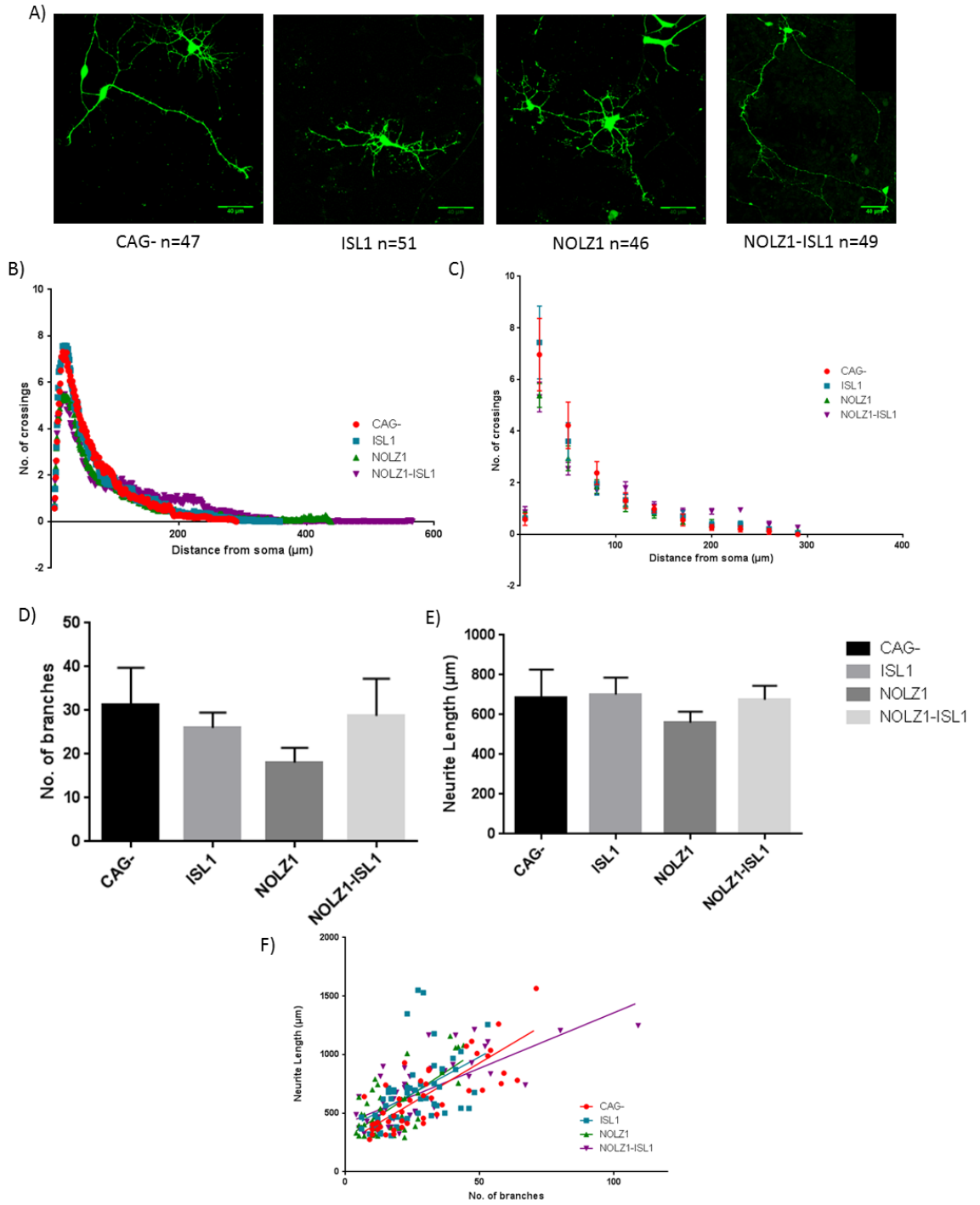


Figure 5.1 (above): Sholl analysis of cells 1 week post transfection. Neural progenitors were transfected after 16 days of differentiation with each of the 4 plasmids and further differentiated for 1 week, under selection, before being harvest for Sholl analysis. A) Example images of neurons at 1 week post transfection, captured for Sholl analysis and the number of cells used for each group stated underneath, scale bar= 40 μm . B) Scatter plot of the mean of the Sholl analysis from each transfection, no significant difference was observed between transfections, two way ANOVA repeated measures $F=1.34$, $DF=3,189$ $p=0.26$. C) Scatter plot showing selected data points analysed for differences between transfections, samples taken at 5 μm , 20 μm and then every 30 μm thereafter. There was no significant difference at any point between the transfections. D) Bar charts showing the mean number of branches on the neurons, with the number of branches being higher in CAG- and NOLZ1-ISL1 transfected neurons. E) Bar chart showing mean neurite length, which was highest in ISL1 and NOLZ1-ISL1 transfected neurons F) Scatter plots showing the branch number plotted against neurite length for each cell in order to determine whether cells are longer and branched, or more basic with fewer branches. Lines show linear regression. CAG- cells tended to be shorter and more branched, NOLZ1-ISL1 were longer and more branched. Data mean \pm SEM across the biological replicates $N=3; n \geq 46$

5.2.2 Week 2

Cells at 2 weeks post transfection were harvested and analysed for the same parameters as cells at week 1. Sholl analysis revealed differences between transfections (Figure 5.2B). CAG- transfected cells were more complex closer to the cell soma at 20 μm . ISL1 transfected cells were consistently more complex than CAG- transfected cells further from the cell soma. Both NOLZ1 and NOLZ1-ISL1 transfected cells showed an increase in complexity further from the cell soma compared to CAG- transfected cells (Figure 5.2B&C). At 230 μm there was a significant difference between all transfections in complexity (Kruskal-Wallis $=7.72$, $p=0.02$, figure 5.2B) ISL1 was more complex than CAG- cells but this was not significant (Dunn's multiple comparisons $p=0.08$).

The number of branches was increased between ISL1 and NOLZ1-ISL1 cells (ISL1 = 19.2 ± 3.00 $N=3; n=52$ and NOLZ1-ISL1 = 13.2 ± 0.75 , $N=3; n=46$), which could have resulted from the decreased transfection efficiency of NOLZ1-ISL1 plasmid into cells ($9.28 \pm 2.47\%$ $N=3; n=18$) in comparison to ISL1 plasmid ($24.1 \pm 2.90\%$, $N=3; n=18$). This decrease in transfection efficiency would have subsequently resulted in a decrease in cell density in NOLZ1-ISL1 cells under selection with G418, and could have led to a negative effect on cell complexity as there were fewer cells available with which to make synaptic connections. The number of

branches in CAG- (17.1 ± 4.30 N=3; n=49) and NOLZ1 (15.4 ± 1.36 N=3; n=43) transfected cells were comparable and in between that observed for ISL1 and NOLZ1-ISL1 ISL1 transfected cells. ISL1 transfected cells ($645.4 \mu\text{m} \pm 93.9$, N=3;n=52) had longer total neurite length in comparison to CAG- ($441.6 \mu\text{m} \pm 83.8$, N=3;n=49) and NOLZ1-ISL1 transfected cells ($493.9 \mu\text{m} \pm 46.6$, N=3;n=46), both NOLZ1 ($546.7 \mu\text{m} \pm 49.2$, n=43) and NOLZ1-ISL1 had a greater neurite length than CAG- transfected but this was not statistically significant (figure 5.2E). When the cells were plotted on a scatter plot, the majority of cells from all transfections were long & branched cells, with ISL1 and NOLZ1 transfected cells having more cells, CAG- control transfections had a higher proportion of short cells with a comparable number of branches and so may not induce a complex cell phenotype (Figure 5.2F) and also may be responsible for the increased complexity of cells closer to the cell soma as seen from the Sholl analysis. The intercept of the regression line showed a significant difference between transfections ($F=5.99$, DF3, 185, $p<0.001$), therefore a variation in the number of branches between transfections.

5. Morphological and electrophysiological characterisation of transfected neurons

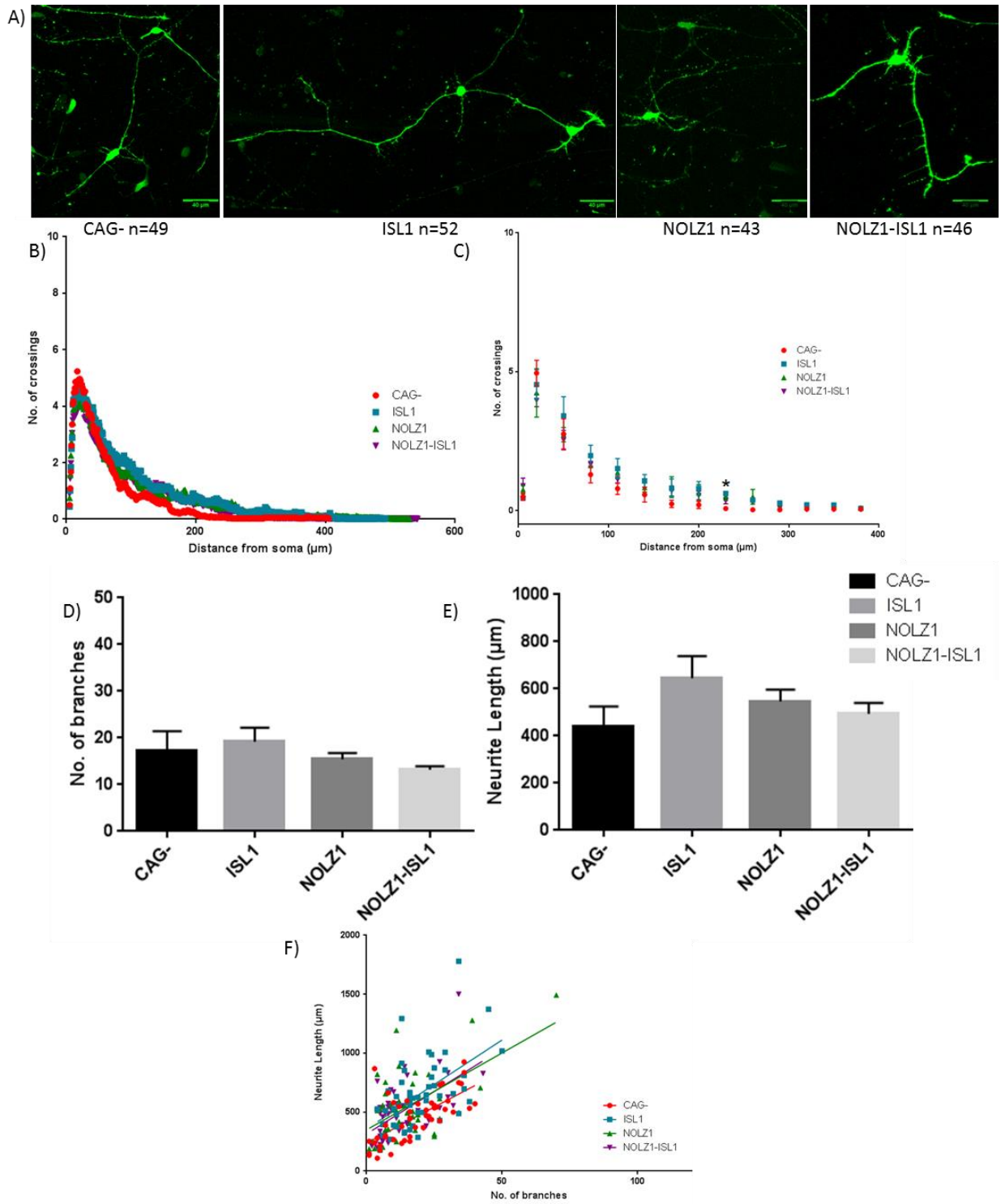


Figure 5.2 (above): Sholl analysis of cells 2 weeks post transfection. Neural progenitors were transfected after 16 days of differentiation with each of the 4 plasmids and further differentiated for 2 weeks, under selection, before being harvested for Sholl analysis. A) Example images of neurons captured for Sholl analysis and the number of cells used for each group stated underneath, scale bar= 40 μm . B) Scatter plot of the mean of the Sholl analysis from each transfection, CAG- and ISL1 transfected cells were more complex closer to the cell soma, then the transcription factor transfected cells were more complex than the CAG- transfected cells further from the soma. C) Scatter plot showing selected data points analysed for differences between transfections, samples taken at 5 μm , 20 μm and then every 30 μm thereafter. There was a significant difference in complexity at 230 μm from the cell soma with ISL1 transfected cells being more complex than CAG- transfected cells, Kruskal-Wallis=7.72, $p=0.02$, Dunn's multiple comparison CAG- vs ISL1 $p=0.08$. D) Bar charts showing the mean number of branches on the neurons, ISL1 transfected cells have more branches than the other transfections. E) Bar chart showing mean neurite length, ISL1 had the longest neurites observed between the transfections F) Scatter plots showing the branch number plotted against neurite length for each cell in order to determine whether cells are longer and branched, or more basic with fewer branches. Lines show linear regression. ISL1 neurons tend to be longer than the rest, and CAG- cells being the shortest. Data mean \pm SEM across the biological replicates $N=3$; $n\geq 43$.

5.2.3 Week 3

Cells at 3 weeks post transfection were harvested after no G418 treatment. This was done in order to determine changes in cell complexity between transfections when at the same density and also as a result of improved electrophysiology of cells when not under selection (Section 5.3 onwards). NOLZ1-ISL1 has the greatest number of intersections and therefore more complex at the peak of the Sholl analysis curve (figure 5.3B), but further from the cell soma, CAG- control transfected neurons are significantly more complex than NOLZ1 at 80 μm (Kruskal-Wallis=11.4, $p<0.01$ Dunn's multiple comparisons $p=0.02$, $N=1$; $n=20$) and NOLZ1-ISL1 at 80 μm from the cell soma ($p=0.04$ $N=1$; $n=20$). Further from the cell soma at >100 μm , ISL1 transfected neurons become more complex than CAG- control and NOLZ1 transfected cells. NOLZ1-ISL1 transfected neurons were more complex than NOLZ1 transfected neurons (Figure 5.3B).

The number of branches (Figure 5.3D) and total neurite length (Figure 5.3E) were greater in the neurons transfected with NOLZ1 (neurite length: 1186.9 ± 240.2 μm $N=1$; $n=20$, branches: 16.9 ± 2.01 $N=1$; $n=20$), ISL1 (1095.6 ± 116.9 μm $N=1$; $n=18$, 22.5 ± 3.72 $N=1$; $n=18$) or the combination of the two genes (1355.7 ± 186 μm $N=1$; $n=20$, 18.2 ± 2.32 $N=1$; $n=20$) compared to control transfected cells (968.8 ± 104.3 μm $N=1$; $n=20$, 16.3 ± 1.67 $N=1$; $n=20$), but was not statistically significant for either

the number of branches or the neurite length. ISL1 cells tended to have more short cells with more branches (Figure 5.3F) and NOLZ1-ISL1 cells possessed longer neurites with a slightly more branched phenotype.

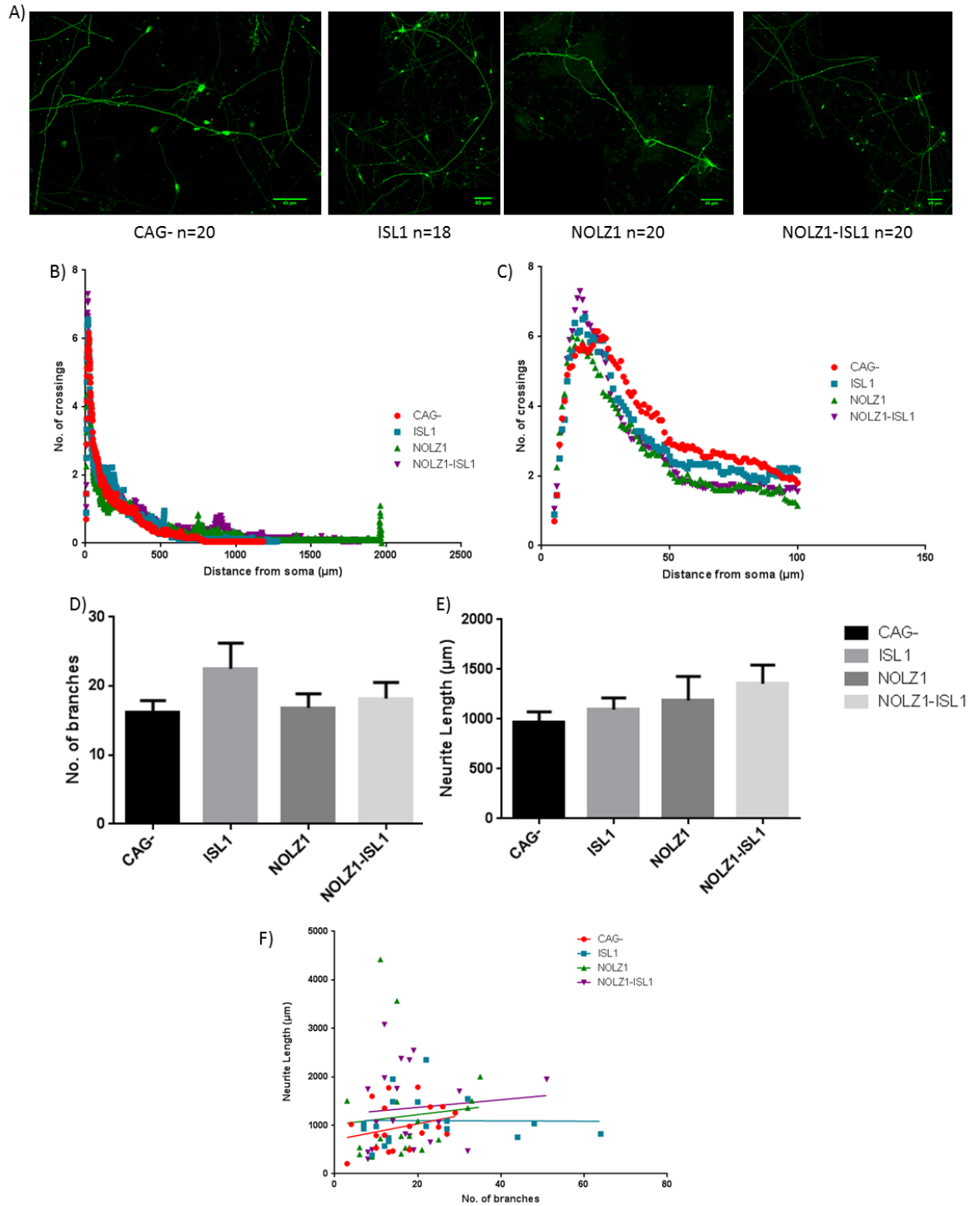


Figure 5.3 (above): Sholl analysis of cells 3 weeks post transfection. Neural progenitors were transfected after 16 days of differentiation with each of the 4 plasmids and further differentiated for 3 weeks, without selection, before being harvested for Sholl analysis. A)

Example images of neurons captured for Sholl analysis and the number of cells used for each group stated underneath, scale bar= 40 μm . B) Scatter plot of the mean of the Sholl analysis from each transfection, no significant difference between transfusions was observed. C) A zoomed in section of B from 5 to 100 μm D) Bar charts showing the mean number of branches on the neurons, there was no significant difference between the transfusions, which is increased in ISL1 and NOLZ1-ISL1 transfected cells. E) Bar chart showing mean neurite length, no significant difference between the transfusions, but is increased on transfection with transcription factors in comparison to control-. All error bars represent SEM. N=1;n=20 (except ISL1 n=18)

5.3 Basic electrophysiological characterisation.

The electrophysiological properties of transfected neurons were assessed at 2 and 3 weeks post-transfection using whole cell patch clamp. In early experiments, cells were selected with 150 $\mu\text{g/ml}$ G418 in an attempt to obtain a higher proportion of transfected cells within the population. However, it became clear that this selection resulted in a drastically reduced success rate for seal formation. As a consequence, all electrophysiological experiments described herein did not use G418 selection.

5.3.1 Passive properties of transfected neurons

No significant differences were observed in mean resting membrane potential (V_m) values across multiple transfusions at either time point (Figure 5.4A, week 2: Kruskal-Wallis=7.43 $p=0.06$, $n>14$, week 3: Kruskal-Wallis=3.00, $p=0.39$, $n>15$). However, the V_m for CAG- control transfected cells became modestly, but significantly hyperpolarised between 2 ($-22.7 \text{ mV} \pm 1.38$ $n=15$) and 3 weeks ($-27.5 \text{ mV} \pm 1.13$ $n=22$, unpaired two-tailed t-test Welch correction $t=2.73$, $DF=29.98$, $p=0.01$). The V_m values were not significantly changed between weeks 2 and 3 for NOLZ1 ($-30.2 \text{ mV} \pm 2.17$ $n=22$, $-29.9 \text{ mV} \pm 1.81$ $n=20$), ISL1 ($-25.4 \text{ mV} \pm 1.55$ $n=26$, $-27.2 \text{ mV} \pm 3.00$ $n=16$) and NOLZ1-ISL1 ($-28.4 \text{ mV} \pm 1.69$ $n=24$, $-29.2 \text{ mV} \pm 2.31$ $n=20$).

The cell capacitance, which is a measure of membrane surface area, was determined in voltage clamp by iterative elimination of transient current caused by the charging and discharging of the cell membrane, elicited by a 10 mV, 10 ms

voltage step (Figure 5.4B). The cell capacitance data broadly support the Sholl analysis at week 3 (Figure 5.3 D&E) in that the capacitance tended to increase when cells transfected with a transcription factor, as opposed to control, and the cells were morphologically more complex. However, there were no significant differences between CAG- and any of the transcription factors at either week. Cell capacitance was increased at week 2, in cells transfected with ISL1 ($17.8 \text{ pF} \pm 1.98$ $n=18$), NOLZ1 ($19.0 \text{ pF} \pm 2.75$ $n=18$), and NOLZ1-ISL1 ($16.0 \text{ pF} \pm 2.27$, $n=17$) compared to CAG- ($14.9 \text{ pF} \pm 3.87$ $n=9$) and at week 3, ISL1 ($23.0 \text{ pF} \pm 3.94$ $n=11$) and NOLZ1-ISL1 transfected cells ($24.4 \text{ pF} \pm 3.41$ $n=18$) have a greater capacitance than the CAG- transfected cells ($18.1 \text{ pF} \pm 1.96$ $n=14$). NOLZ1-ISL1 transfected cells have a significantly greater capacitance than cells transfected with NOLZ1 ($14.4 \text{ pF} \pm 1.66$ $n=16$, one way ANOVA $F=2.79$ $DF=3$, 55 $p<0.05$ Tukey's multiple comparison: NOLZ1 vs NOLZ1-ISL1 $p<0.05$).

The input resistance (R_{in}) is a measure of the cells permeability to ions when at rest. The input resistance for the cells as per Figure 5.4C. There was no significant difference between the transfection conditions, the exception was at week 2 where the R_{in} was increased in cells transfected with ISL1 ($0.59 \text{ G}\Omega \pm 0.11$ $n=22$), NOLZ1 ($0.85 \text{ G}\Omega \pm 0.13$ $n=22$) or both ($0.93 \text{ G}\Omega \pm 0.12$ $n=22$) compared to CAG- control transfected cells ($0.45 \text{ G}\Omega \pm 0.08$ $n=14$, one-way ANOVA $F=3.20(3,76)$ $p=0.03$). By contrast, at 3 weeks this was reversed and CAG- transfected cells ($1.05 \text{ G}\Omega \pm 0.15$ $n=18$) have a greater input resistance compared to the cells transfected with ISL1 ($0.68 \text{ G}\Omega \pm 0.15$ $n=14$), NOLZ1 ($0.71 \text{ G}\Omega \pm 0.16$ $n=18$) or both ($0.63 \text{ G}\Omega \pm 0.10$ $n=18$), although this was not significant. The input resistance of CAG- transfected cells is significantly increased from week 2 to week 3 post transfection (Mann-Whitney $U=45$, $p=0.002$).

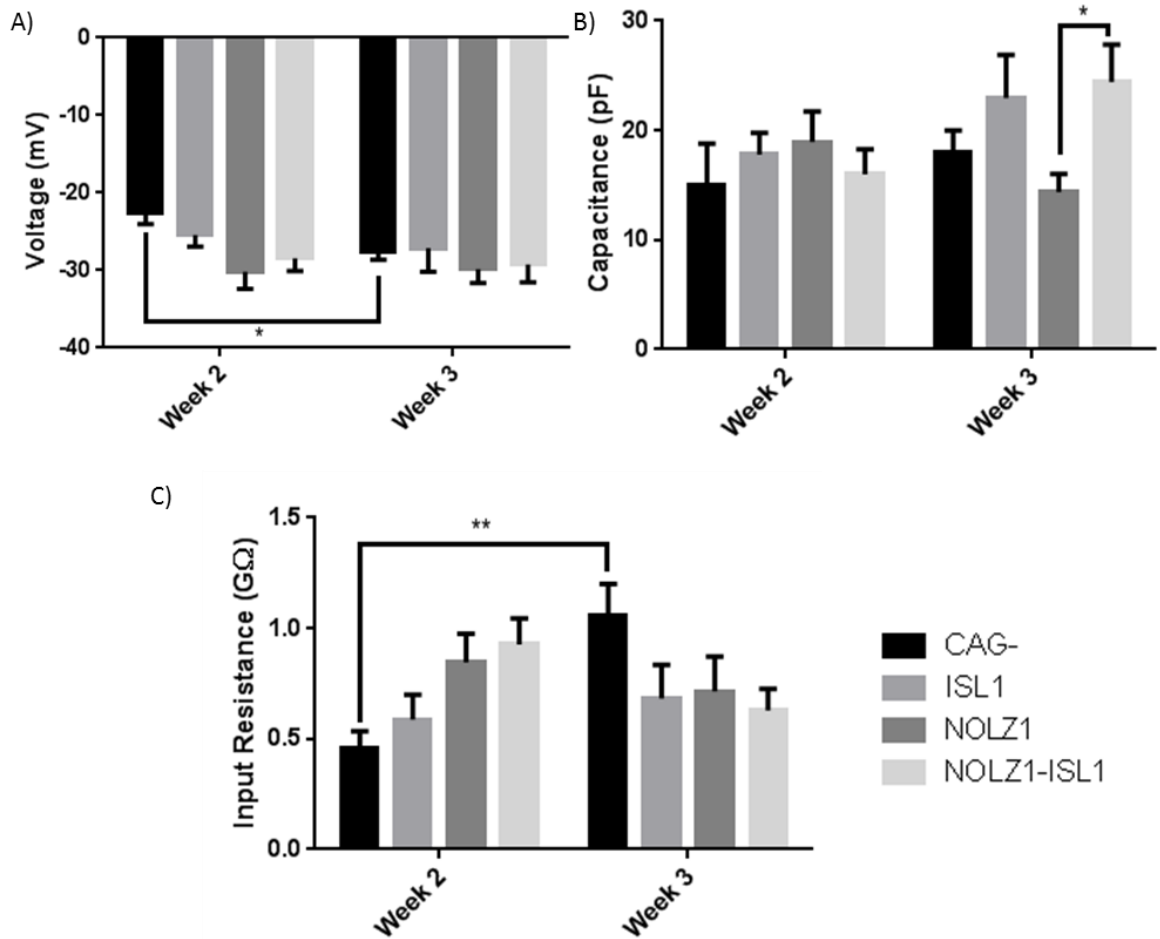


Figure 5.4: Bar graphs showing the passive properties of cells. Whole cell patch clamp recordings were performed at 2 and 3 weeks post transfection. A) Bar graph showing the mean resting membrane potential of neurons, analysed from a current clamp protocol of $I=0$. There was no significant difference in resting membrane potential between transfection conditions at each time point but there was a significant hyperpolarisation between week 2 and week 3 CAG- transfected cell's V_m unpaired two-tailed t-test Welch correction $t=2.73$, $DF=29.98$, $p=0.01$ $n>13$. B) Bar graph showing the mean cell capacitance of neurons. Data obtained from voltage clamp of cells analysing the charging and discharging of the cell membrane. There was no significant difference in cell capacitance between transfection conditions. At week 3, there was a significant difference between transfections one way ANOVA $F=2.79$ $DF=3$, 55 $p<0.05$ Tukey's multiple comparison: NOLZ1 vs NOLZ1-ISL1 $p<0.05$, $n>6$ for each condition. C) Bar graph showing the input resistance of neurons. Data were obtained from current clamp recordings, analysing the final 50 ms of the first 5 sweeps. There was no significant difference in input resistance between transfection conditions except at week 2 one way ANOVA $F=3.2$, $DF=3$, 76 $p=0.03$, significant difference between CAG- at week2 vs week 3 Mann-Whitney U test= 45 $p=0.002$. All graph error bars = SEM.

5.3.2 Induced action potentials and trains

A crucial property of neurons is the ability to fire action potentials. To induce action potentials in the differentiated neurons, cells were hyperpolarised using continuous current injection (to remove inactivation of Na⁺ channels) then a 1 second current injection was applied to depolarise the cell membrane, which increased with each successive sweep.

5.3.2.1 Proportion of cells firing action potentials & frequency of the action potentials

In order to generate current-frequency (I-F) scatter plots, the number of action potentials generated during a single 1s current step were counted and plotted against injected current. All conditions resulted in a time-dependent increase in the proportion of cells which were able to produce trains of action potentials, as exemplified in figure 5.5. At 2 weeks, NOLZ1 (59.1%) and NOLZ1-ISL1 transfected cells (54.6%) had the highest proportion of cells which fired trains of action potentials in comparison to the ISL1 (9.09%) and CAG- (20%) transfected neurons. At 3 weeks post transfection, all NOLZ1-ISL1 transfected cells fired induced action potentials, mostly as trains of action potentials, this proportion was increased from week 2, as was seen for the other transfections CAG- 27.8%, ISL1 61.5%, NOLZ1-ISL1 83.3%, except for NOLZ1 (50%), which decreased slightly. The other two transfections, NOLZ1 and ISL1 individually, both gave rise to neurons which were more excitable than the CAG- transfected cells at 3 weeks post transfection. Thus, NOLZ1-ISL1 co-transfection was most beneficial in terms of facilitation of the generation of neurons capable of firing repetitive trains of action potentials. Furthermore, the excitability of cells (Figure 5.6) which generated trains of action potentials within each transcription factor group was different from the control group (although not significant). NOLZ1 (Figure 5.6 C&G) and NOLZ1-ISL1 (Figure 5.6

D&H) transfected cells showed a similar pattern of neuronal firing frequency, where both showed a higher number of action potentials fired at lower current injection where by comparison the ISL1 (Figure 5.6 B&F) transfected cells remained firing when a higher current injection is delivered at a similar rate. Interestingly, the ISL1 transfected neurons have a similar action potential firing pattern to dopamine D1 receptor-positive striatonigral neurons, with a rightward shift in the I-F curve, therefore firing trains of a higher number of action potentials at higher current injection (Gertler et al., 2008). Also importantly, this is seen as a more mature marker of neurons as the cells decrease in excitability (Mongiati et al., 2009).

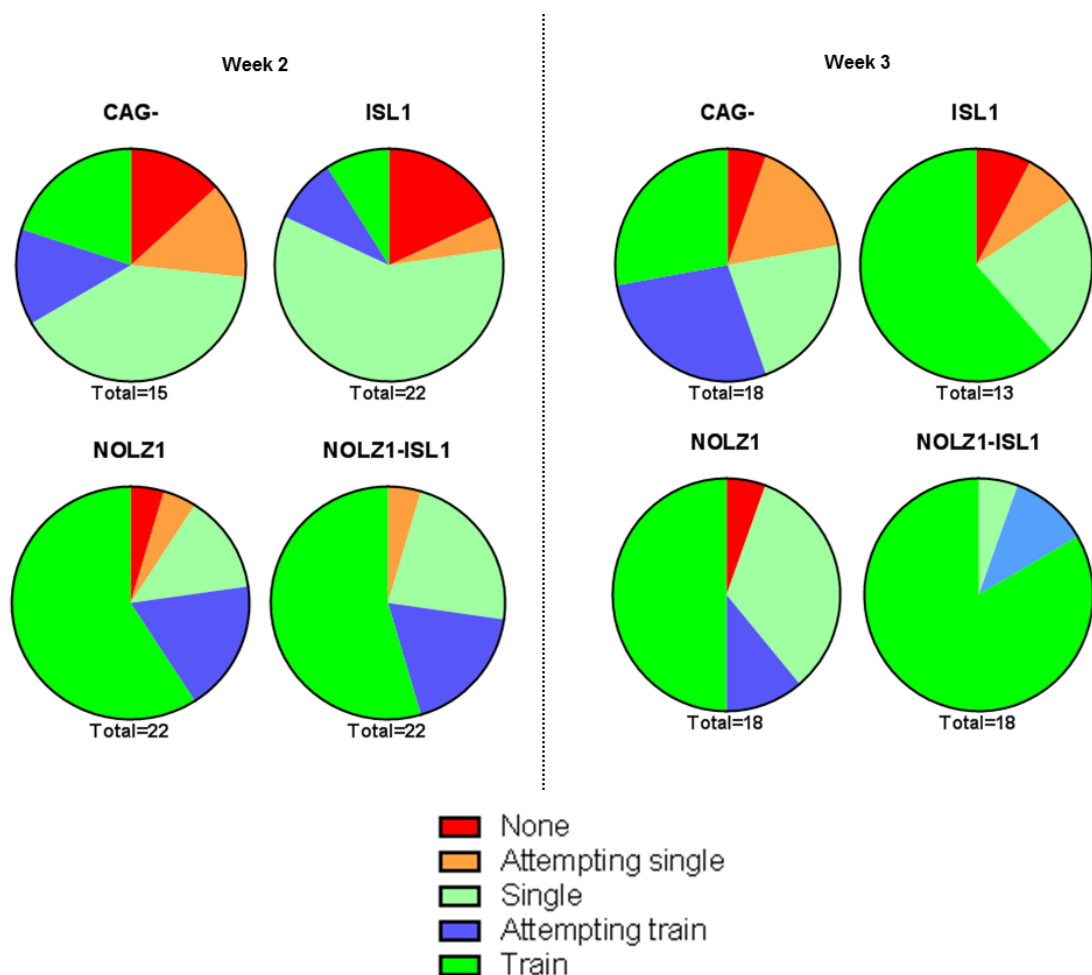


Figure 5.5: The proportions of neurons producing induced action potentials. Cells were recorded in current clamp mode at 2 and 3 weeks post transfection. Pie charts representing the proportions of cells which show induced action potentials left panel = week 2, right panel = week 3. Key for all pie charts is below the figure. n is below each pie chart. N=2

5. Morphological and electrophysiological characterisation of transfected neurons

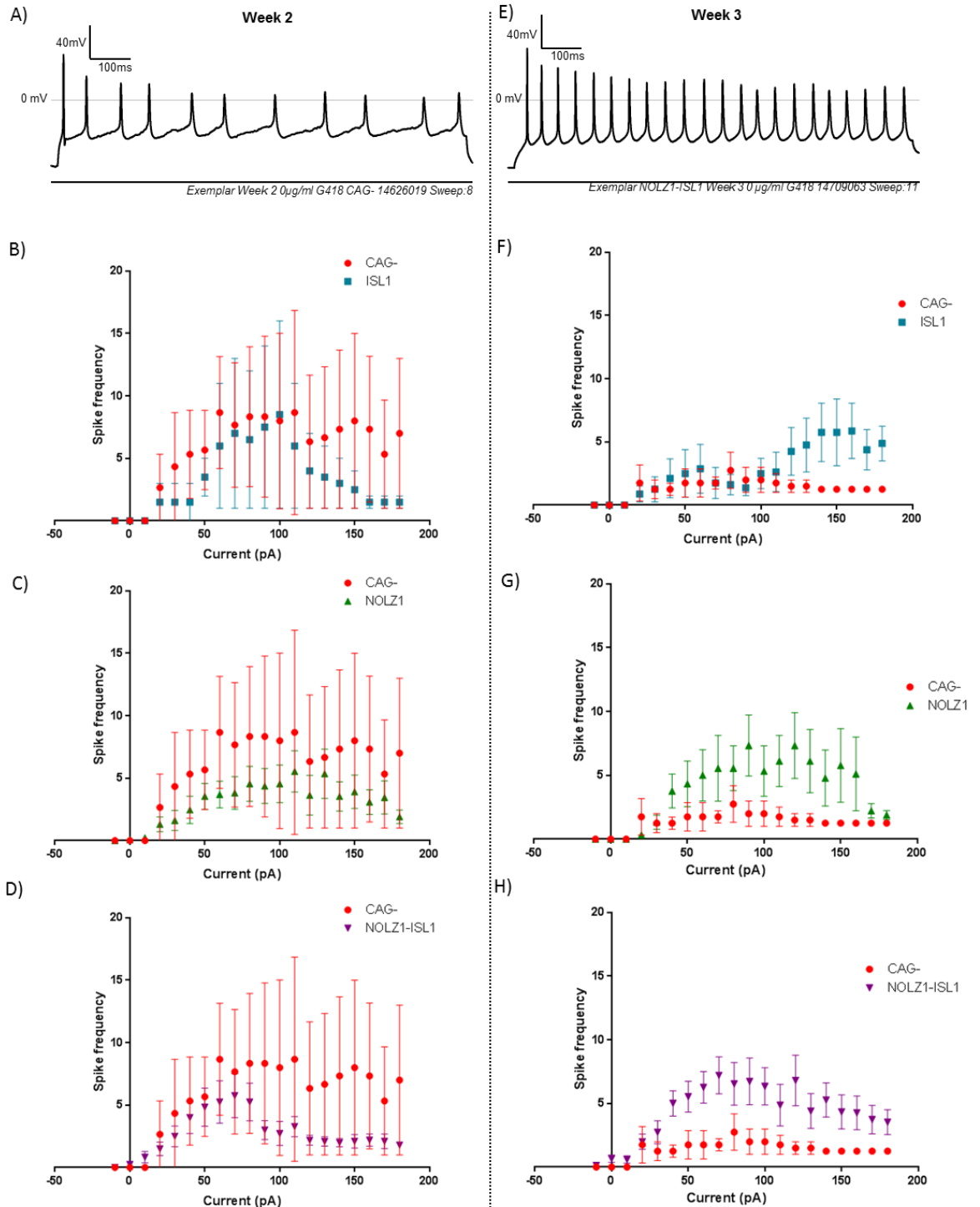


Figure 5.6: Spike frequency of induced action potential trains of neurons at 2 and 3 weeks post transfection. Cells were recorded in current clamp mode at 2 and 3 weeks post transfection A) An exemplar trace from a CAG- transfected neuron 2 weeks post transfection in whole cell patch clamp when there was a 60 pA current injection for 1 second, showing induction of a train of action potentials. B) Scatter plot showing mean spike frequency of trains of action potentials of CAG- (n=3) and ISL1 (n=2) transfected neurons at 2 weeks post transfection against current injected, ISL1 cells were not as excitable as control at increased current steps. C) Scatter plot showing mean spike frequency of trains of action potentials of CAG- and NOLZ1 (n=11) transfected neurons at 2 weeks post transfection against current injected, NOLZ1 cells were not as excitable as control. D) Scatter plot showing mean spike frequency of trains of action potentials of CAG- and NOLZ1-ISL1 (n=11) transfected neurons at 2 weeks post transfection against current injected, NOLZ1-ISL1 cells were not as excitable as control. E) An exemplar trace from a NOLZ1-ISL1 transfected neuron 3 weeks post transfection in whole cell patch clamp when there was a 60 pA current injection for 1 second, showing induction of a train of action potentials. F) Scatter plot showing mean spike frequency of trains of action potentials of CAG- (n=3) and ISL1 (n=2) transfected neurons at 3 weeks post transfection against current injected, ISL1 cells were more excitable than control at increased current steps. G) Scatter plot showing mean spike frequency of trains of action potentials of CAG- and NOLZ1 (n=11) transfected neurons at 3 weeks post transfection against current injected, NOLZ1 cells were more excitable than control. H) Scatter plot showing mean spike frequency of trains of action potentials of CAG- and NOLZ1-ISL1 (n=11) transfected neurons at 3 weeks post transfection against current injected, NOLZ1-ISL1 cells were more excitable than control.

Scatter plot showing mean spike frequency of trains of action potentials of neurons at 2 weeks post transfection of CAG- and NOLZ1-ISL1 (n=10) against current injected, NOLZ1-ISL1 cells were not as excitable as control at higher current steps. E) An exemplar trace from a neuron 3 weeks post transfection in whole cell patch clamp when there was a 90 pA current injection for 1 second, showing induction of a train of action potentials. F) Scatter plot showing mean spike frequency of trains of action potentials of CAG- (n=4) and ISL1 (n=8) transfected neurons at 3 weeks post transfection against current injected, ISL1 cells were comparable to control at smaller current steps, but ISL1 cells fired increased numbers of action potentials at higher current steps. C) Scatter plot showing mean spike frequency of trains of action potentials of CAG- and NOLZ1 (n=9) transfected neurons at 3 weeks post transfection against current injected, NOLZ1 cells were more excitable than control and comparable to the cells at week 2. D) Scatter plot showing mean spike frequency of trains of action potentials of neurons at 3 weeks post transfection of CAG- and NOLZ1-ISL1 (n=15) against current injected, NOLZ1-ISL1 cells were not as excitable as control at higher current steps, and comparable to the cells at week 2.

5.3.2.2 Anatomy of the action potential

The different parameter contribution to the anatomy of the action potentials (Figure 5.7A) generated by the current clamp protocol were measured for each of the different transfected cells at each of the time points, as discussed in Bean (2007).

The threshold voltage (figure 5.7B) was calculated as the maximum of the third differential of the rate of change in voltage versus time. The threshold voltages did not significantly change between the transfection conditions or between time points (one-way ANOVA, week 2: $F=1.06$, $DF=3$, 65 , $p=0.37$ $n>10$ and week 3: $F=2.63$, $DF=3$, 56 , $p=0.06$, $n>10$). At 2 weeks post transfection, the threshold voltage was more hyperpolarised in the CAG- transfection (-30.3 mV \pm 2.88 $n=11$), compared to the cells transfected with ISL1 (-24.5 mV \pm 1.64 $n=17$), NOLZ1 (-27.1 mV \pm 1.62 $n=20$) or both (-27.0 mV \pm 2.11 $n=21$). At 3 weeks, there was a more pronounced difference between control transfected cells (-23.2 mV \pm 2.47 $n=14$) and NOLZ1 (-30.6 mV \pm 2.09 $n=17$), ISL1 (-24.4 mV \pm 2.80 $n=11$) or NOLZ1-ISL1 transfected cells (-30.8 mV \pm 2.55 $n=18$) with threshold voltage becoming more hyperpolarised. Threshold voltage becomes more depolarised during maturation (Mongiat et al., 2009, Pirchio et al., 1997), which was seen for the control and ISL1 transfected cells between week 2 and week 3 post transfection but not for NOLZ1 and NOLZ1-ISL1 transfected cells.

The overshoot of the action potential was calculated by measuring the peak of the action potential (Figure 5.7A). The overshoot of the action potential (figure 5.7C) increased between week 2 and week 3 post transfection for the control ($16.2 \text{ mV} \pm 6.23$ $n=11$ and $18.3 \text{ mV} \pm 5.78$ $n=14$ respectively) and significantly increased for ISL1 ($9.62 \text{ mV} \pm 2.32$ $n=17$ and $33.6 \text{ mV} \pm 5.16$ $n=11$, respectively, unpaired two-tailed t-test Welch corrected: $t=4.25$ $DF=14.1$ $p=0.0008$) and NOLZ1-ISL1 transfected cells ($19.9 \text{ mV} \pm 3.43$ $n=21$ and $31.1 \text{ mV} \pm 4.19$ $n=18$ respectively, unpaired two-tailed t-test Welch corrected: $t=2.05$ $DF=34.3$ $p=0.05$), ISL1 and NOLZ1-ISL1 transfected cells had the greatest overshoot at 3 weeks post-transfection. There was a significant difference in overshoot, only at week 2 between ISL1 (see above) and NOLZ1 transfected cells ($30.1 \text{ mV} \pm 4.00$ $n=20$, Kruskal-Wallis statistic= 14.1 $p=0.0027$, Dunn's multiple comparison $p<0.01$).

The afterhyperpolarisation of the action potential was calculated as the lowest voltage which was achieved immediately after the action potential (figure 5.7A). The afterhyperpolarisation of the action potential (Figure 5.7D) remained consistent from week 2 to week 3 and between transfection conditions.

The spike height was calculated as the difference between the overshoot and afterhyperpolarisation voltages (Figure 5.7G). There was significant difference in spike height between NOLZ1 ($81.8 \text{ mV} \pm 4.76$ $n=20$) and ISL1 ($53.0 \text{ mV} \pm 3.63$ $n=17$) transfected cells at 2 weeks (Kruskal-Wallis= 14.3 $p<0.005$ Dunn's multiple comparison $p<0.01$). The ISL1 transfected cells showed a significant increase in spike height from week 2 (see above) to week 3 ($81.3 \text{ mV} \pm 7.40$ $n=11$, unpaired two-tailed t-test Welch corrected: $t=3.42$, $DF=14.9$, $p<0.01$) and there was a slight increase for NOLZ1-ISL1 transfected cells (week 2: $70.4 \text{ mV} \pm 5.78$ $n=21$ week 3: $83.7 \text{ mV} \pm 6.01$ $n=18$). There was a slight increase in spike height in CAG- (week 2: $64.4 \text{ mV} \pm 9.47$ $n=11$, week 3: $64.7 \text{ mV} \pm 6.63$ $n=14$) and in contrast, a decrease in NOLZ1 transfected cells spike height (week 3: $75.2 \text{ mV} \pm 7.11$ $n=17$). ISL1, NOLZ1

and NOLZ1-ISL1 transfections increased spike height at 3 weeks in comparison with control transfected cells; therefore more likely forms a more mature neuron than the control (Johnson et al., 2007).

The depolarisation rate (Figure 5.7E) and repolarisation rate (Figure 5.7F) were determined for each of the action potentials, a faster rate of depolarisation and repolarisation tends to show a more mature neuron (Mongiat et al., 2009). At week 2, NOLZ1 ($85.8 \text{ mV/ms} \pm 10.9$ $n=20$) had a significantly increased rate of depolarisation than ISL1 transfected cells ($44.5 \text{ mV/ms} \pm 5.63$ $n=17$, one-way ANOVA $F=3.95$, $DF=3,65$, $p=0.02$, Tukey's multiple comparison, ISL1 vs NOLZ1 $p=0.01$), and NOLZ1-ISL1 transfected cells ($58.6 \text{ mV/ms} \pm 8.28$ $n=21$) had a higher rate of depolarisation than control ($51.9 \text{ mV/ms} \pm 11.9$ $n=11$) and ISL1 transfected cells. At 3 weeks post transfection, the rate of depolarisation increased from week 2 in NOLZ1-ISL1 ($115.8 \text{ mV/ms} \pm 19.9$ $n=18$) and significantly increased in ISL1 transfected cells ($98.2 \text{ mV/ms} \pm 16.5$ $n=11$, unpaired two-tailed t-test Welch corrected $t=3.08$, $DF=12.4$, $p<0.01$, $n>10$), but decreased for NOLZ1 ($73.3 \text{ mV/ms} \pm 12.2$ $n=17$) which was greater than the depolarisation rate of CAG- transfected cells ($52.3 \text{ mV/ms} \pm 9.73$ $n=14$).

There was a significant difference in repolarisation rate between transfections at 2 weeks, NOLZ1 ($-63.2 \text{ mV/ms} \pm 5.48$ $n=20$) had a greater rate of repolarisation than CAG- ($-44.1 \text{ mV/ms} \pm 9.18$ $n=11$), ISL1: $-43.4 \text{ mV/ms} \pm 5.52$ $n=17$ and NOLZ1-ISL1: $-46.7 \text{ mV/ms} \pm 5.30$ $n=21$, Kruskal-Wallis= 8.31 , $p=0.04$). At 3 weeks post-transfection, NOLZ1-ISL1 transfected cells ($-63.8 \text{ mV/ms} \pm 8.74$ $n=18$) had the fastest rate of repolarisation of the action potential, compared to the other transfections. NOLZ1 ($-57.7 \text{ mV/ms} \pm 8.59$ $n=17$) and ISL1 transfected cells ($-62.2 \text{ mV/ms} \pm 7.39$ $n=11$) had an increased rate of repolarisation in comparison to control cells ($-39.9 \text{ mV/ms} \pm 8.84$ $n=14$). At 3 weeks post transfection, the rate of

repolarisation increased from week 2 in ISL1 and NOLZ1-ISL1 transfected cells, but decreased for NOLZ1 and CAG- control transfected cells.

The half-width was calculated for the action potential by measuring the time taken to reach 50% of the height of the action potential, using afterhyperpolarisation as the base-line (Figure 5.7A). The half-width of the action potential decreases with neuronal maturity (Johnson et al., 2007). At week 2 (figure 5.7H), NOLZ1 ($3.11 \text{ ms} \pm 0.32$ $n=20$) and NOLZ1-ISL1 transfected cells ($3.55 \text{ ms} \pm 0.33$ $n=21$) had a smaller half-width than the CAG- transfected cells- ($3.99 \text{ ms} \pm 0.42$ $n=11$). There was also a significant decrease between ISL1 ($4.92 \text{ ms} \pm 0.48$ $n=17$) and NOLZ1 transfected cells in half-width (Kruskal-Wallis=11.6, $p<0.01$ Dunn's multiple comparison: ISL1 vs. NOLZ1 $p<0.01$). At 3 weeks there was a decrease in half width for NOLZ1 ($1.92 \text{ ms} \pm 1.56$ $n=17$) and NOLZ1-ISL1 transfected cells ($2.95 \text{ ms} \pm 0.41$ $n=18$), and a significant decrease in half-width for ISL1 transfected cells ($2.72 \text{ ms} \pm 0.40$ $n=11$, Mann-Whitney $U=31$, $p<0.01$). The half-width is decreased for all the transfections in comparison to CAG- transfected cells at 3 weeks post-transfection ($4.65 \text{ ms} \pm 0.60$ $n=14$) an increase from 2 weeks, therefore implying a more neuronal phenotype (Johnson et al., 2007) when transfected with any of the transcription factors.

5. Morphological and electrophysiological characterisation of transfected neurons

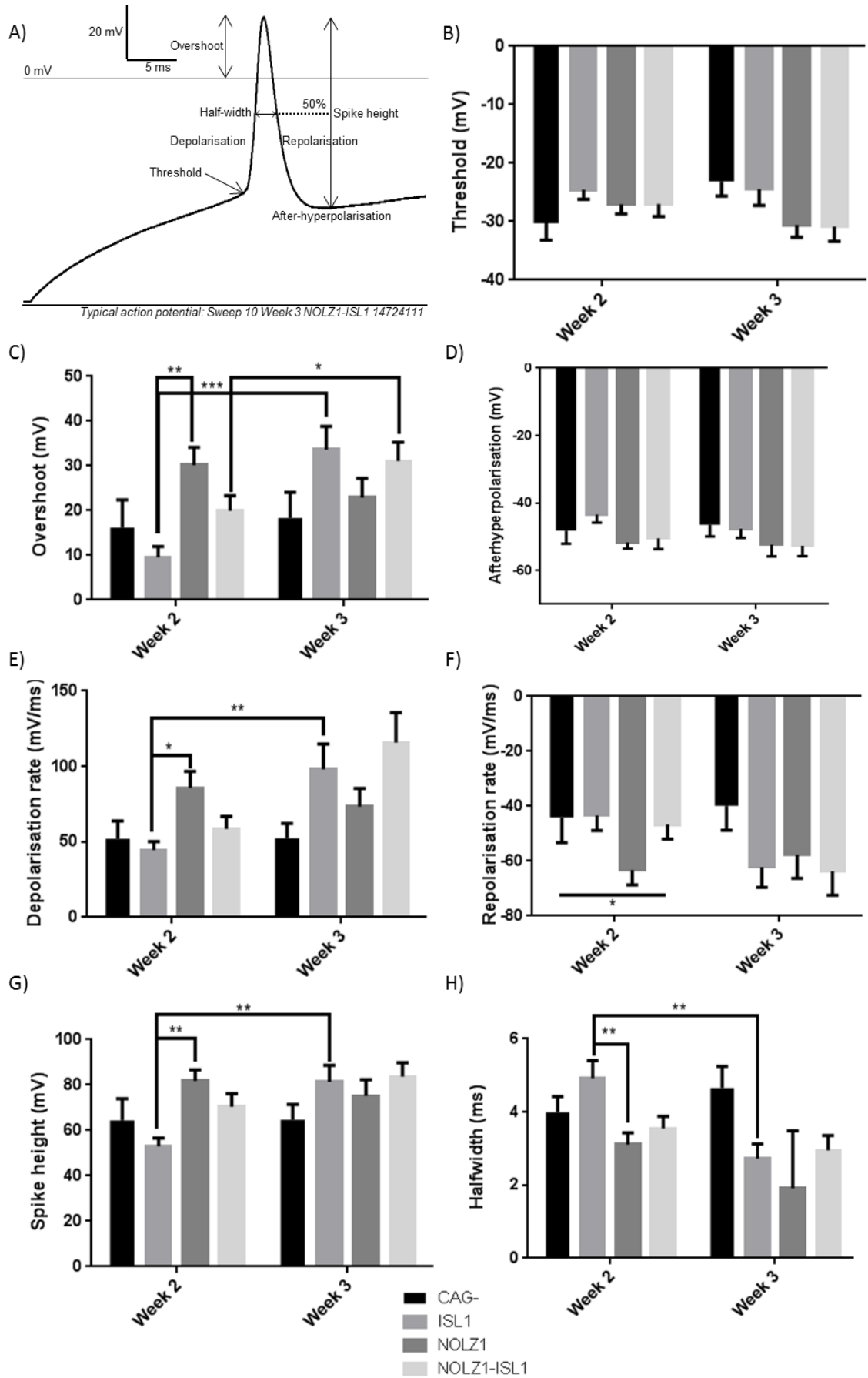


Figure 5.7 (above): Properties of the induced action potential. Cells were recorded in current clamp mode at 2 and 3 weeks post transfection. The analysis was performed on the first trace which elicited the action potential type for the cell, i.e. either singular action potential, attempting train, or train of action potentials. A) A typical induced action potential with the different properties which were measured marked on the action potential trace. B) Bar graph showing the mean threshold voltage at which action potentials were initiated in neurons. There was no significant difference between the transfections at either of the time points. C) Bar graph showing the mean overshoot of the action potentials of the neurons. There was no significant difference in overshoot between transfection conditions, except at week 2 Kruskal-Wallis test=14.12 $p=0.0027$, NOLZ1 increased compared to ISL1 Dunn's multiple comparison $p<0.01$. Overshoot was significantly increased between 2 and 3 weeks for NOLZ1-ISL1 $t=2.06$, $DF = 34.3$, $p<0.05$, and ISL1 $t=4.25$, $DF=14.1$, $p<0.001$ both unpaired two-tailed t tests Welch corrected. D) Bar graph showing the mean afterhyperpolarisation of the action potentials of the neurons. Afterhyperpolarisation generally increased from week 2 to week 3 and was increased in cells transfected with NOLZ1 plasmids. E) Bar graph showing the mean depolarisation rate of action potentials in neurons, there was a significant increase between the NOLZ1 and ISL1 transfections at 2 weeks one-way ANOVA $F=3.95$, $DF=3,65$, $p=0.02$, Tukey's multiple comparison, $p=0.01$. There was a significant increase between ISL1 transfected cells at 2 and 3 weeks post transfection unpaired two-tailed t-test Welch corrected $t=3.08$, $DF=12.4$, $p<0.01$ F) Bar graph showing the mean repolarisation rate of the action potentials of the neurons. There was a significant difference in repolarisation rate between transfection conditions at 2 weeks, Kruskal-Wallis test=8.31, $p=0.04$. G) Bar graph showing the mean spike height of the action potentials of the neurons. There was no significant difference in spike height between transfection conditions except there was an increase between NOLZ1 and ISL1 at 2 weeks post transfection, Kruskal-Wallis test=14.3 $p<0.005$ Dunn's multiple comparison NOLZ1 vs. ISL1 $p<0.01$. Between 2 and 3 weeks post transfection there was a significant increase for ISL1 transfected cells, unpaired two-tailed t-test $t=3.42$, $DF=14.9$, $p<0.01$. H) Bar graph showing the mean half width of the action potentials of the neurons. There was a significant decrease in half-width between ISL1 and NOLZ1 at 2 weeks post transfection Kruskal-Wallis test=11.6, $p<0.01$ Dunn's multiple comparison: ISL1 vs. NOLZ1 $p<0.01$. There was also a significant decrease in ISL1 transfected cells between 2 and 3 weeks post transfection Mann-Whitney U test =31, $p<0.01$, also there was a significant difference observed between G418 treatment at 2 weeks post transfection in NOLZ1-ISL1 transfected cells Mann-Whitney U test =51, $p=0.02$. All graph error bars = SEM $n>9$ for each condition. Key for all graphs at bottom of figure.

5.3.3 Spontaneous activity of transfected cells

A crucial property of mature neurons is the ability to fire action potentials spontaneously. In order to determine if the cells which had been transfected and differentiated were spontaneously active, recordings were obtained by current clamp at $I=0$ for approximately 1 minute. They were classified into three groups depending on the types of action potentials observed either non action potentials (Figure 5.8A), or whether they attempted to fire action potentials, but they didn't reach 0 mV (Figure 5.8B) or if they were in fact firing action potentials which fired over 0 mV (Figure 5.8C). The proportions of cells which fitted into these categories were calculated and plotted as pie charts (Figure 5.8D).

At 3 weeks post transfection, the proportion of cells with spontaneous activity was increased by transfection with NOLZ1 (from week 2 9.09% to week 3 10%) or ISL1 (from 0% to 12.5%), compared to CAG- transfection (from 13.3% to 0%). This was increased further with the transfection of NOLZ1-ISL1 (from 8.33% to 35%), where less than half the cells showed no attempt at spontaneous activity.

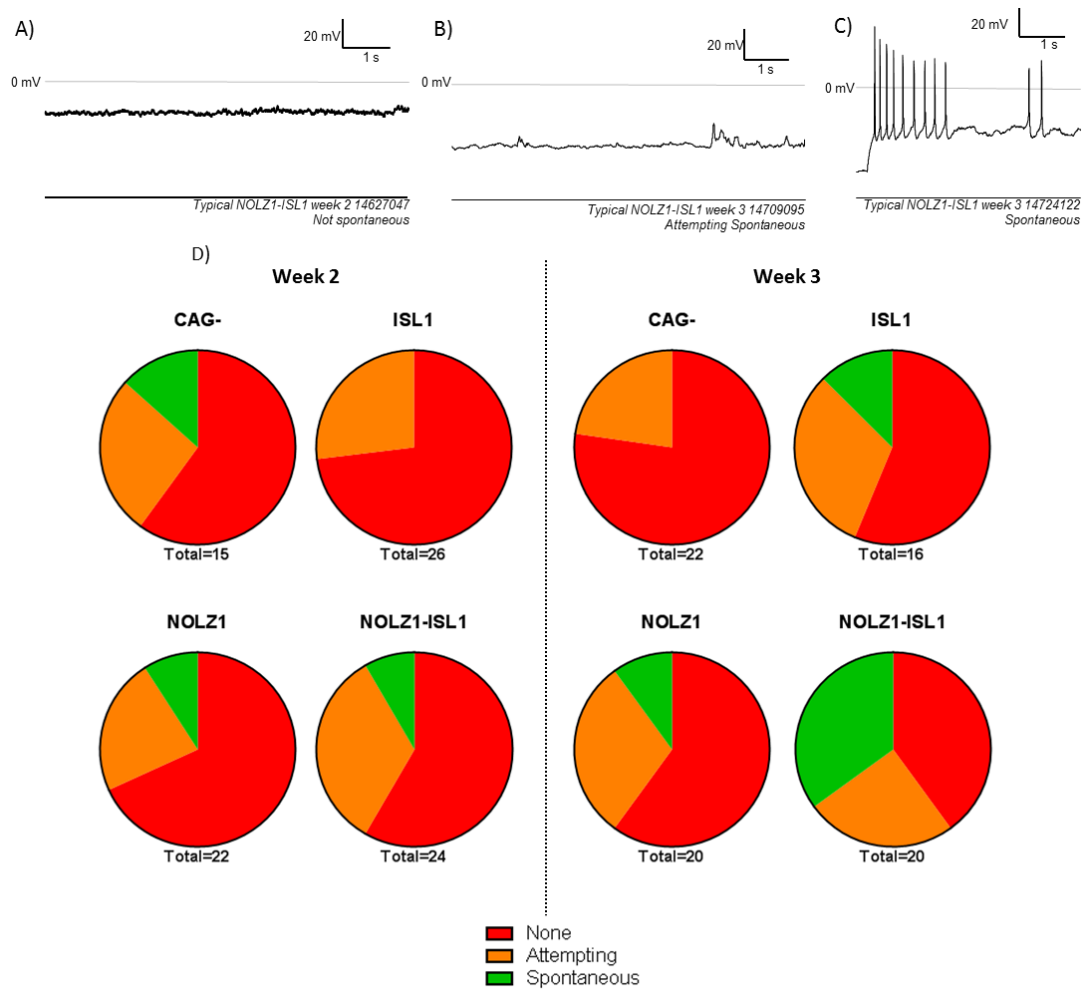


Figure 5.8: The proportions of neurons producing spontaneous action potentials. Cells were analysed in gap free protocol in current clamp $I=0$ at 2 and 3 weeks post transfection. A) A typical trace from a neuron in whole cell patch clamp when there was 0 pA current injection, showing no spontaneous activity, B) A typical trace from a neuron in whole cell patch clamp with 0 pA current injection, showing attempts at spontaneous activity, but the action potential not reaching 0 mV C) A typical trace from a neuron in whole cell patch clamp with 0 pA current injection, showing spontaneous activity. D) Pie charts representing the proportions of cells which show no spontaneous activity as in trace A (red), attempts at spontaneous activity as in trace B (orange) or spontaneous activity as in trace C (green). Left panel representing the different transfections at week 2, right panel representing the different transfections at week 3. n is below each pie chart. N=2

Recordings were also performed in current clamp following current injection to hyperpolarise the membrane potential to approximately -70 mV (Figure 5.9). This allowed us to discriminate between cells which could not generate spontaneous activity at all, and cells which did not generate spontaneous activity because the V_m had inactivated the Na^+ current. This artificial hyperpolarisation increased the proportion of cells firing action potentials which reached 0 mV (figure 5.9). Consistent with results using their native V_m , the NOLZ1-ISL1 transfected cells produced the highest proportion of cells which fired action potentials (week 2: 75%, week 3: 89.5%). NOLZ1 (week 2: 68.2%, week 3: 68.4%), and ISL1 (week 3: 56.3%), individually transfected cells had a higher proportion of cells which fired action potentials compared to the CAG- transfected cells (week 2: 46.7%, week 3: 33.3%) except for ISL1 transfected cells at 2 weeks (30.8%).

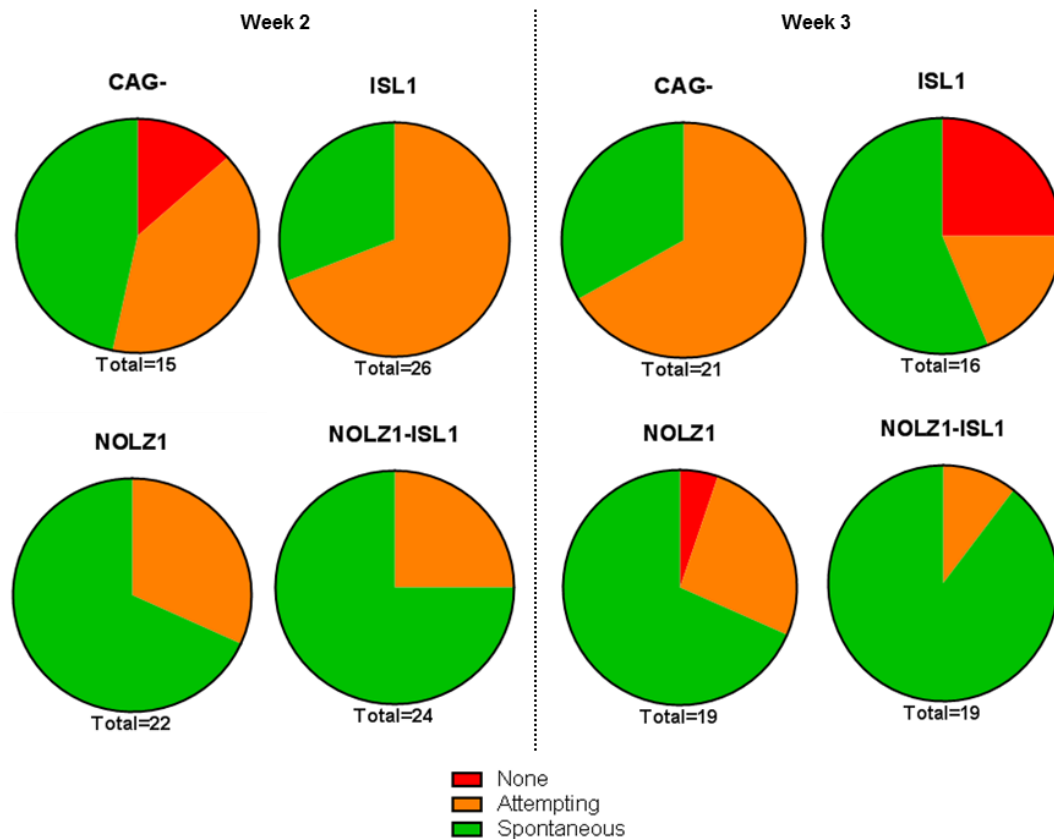


Figure 5.9: The proportions of neurons producing spontaneous action potentials when V_m was hyperpolarised. Cells were analysed in gap free protocol with an artificially hyperpolarised membrane potential to approx. -70 mV by variable current injection at 2 and

3 weeks post transfection. Pie charts representing the proportions of cells which show no spontaneous activity as in trace 5.5A (red), attempts at spontaneous activity as in trace 5.5B (orange) or spontaneous activity as in trace 5.5C (green). Left panel representing the different transfections at week 2, 0 µg/ml G418, right panel representing the different transfections at week 3, 0 µg/ml G418. n is below each pie chart. N=2

5.3.4 Na⁺ and K⁺ currents

A voltage clamp protocol was employed to evoke voltage activated currents. From a holding voltage of -70 mV a 200 ms voltage step was applied, starting at -120 mV and increasing to +80 mV in 5 mV increments per sweep. Voltage gated Na⁺ channels were activated at approximately -35 mV generating rapidly activating inward (depolarising) current which then rapidly inactivated. The K⁺ channels activated around 0 mV, with slower activation kinetics than Na⁺ current and which did not inactivate significantly during the test pulse (Figure 5.10A&B). The resulting currents were firstly corrected for leak current and then converted to current density. Leak current is the flow of ions through leak channels and the seal resistance, and was determined by the linear regression of the initial linear section. The calculated slope and offset for the linear regression were used to subtract leak currents from the voltage-activated currents. Current densities were calculated by dividing the currents, corrected for leak current, by the cell capacitance, in order to normalise current to the cell membrane surface area, therefore normalising to the number of voltage gated channels present per unit of membrane area.

At week 2 (Figure 5.10C), CAG- transfected cells (-282.8 pA/pF ± 121.8 n=8) had a greater Na⁺ maximal current density than the other transfected cells (NOLZ1-ISL1: -202.2 pA/pF ± 41.0 n=15), ISL1 (-121.9 pA/pF ± 40.0 n=14) and NOLZ1 (-248.4 pA/pF ± 40.3 n=16) with a significant increase in Na⁺ current density between NOLZ1 and ISL1 (Kruskal-Wallis=9.28, p=0.03, Dunn's multiple comparison p=0.02). At 3 weeks post transfection, the maximal Na⁺ current density of the neurons was greater in the cells which have been transfected with NOLZ1 (-321.0

pA/pF \pm 99.3 n=12), ISL1 (-428.9 pA/pF \pm 187.8 n=4) and was significant in NOLZ1-ISL1 transfected cells (-431.2 pA/pF \pm 74.4 n=17) compared to CAG- (-139.1 pA/pF \pm 30.2 n=10, Kruskal-Wallis=10.3, $p=0.02$, Dunn's multiple comparison CAG- vs. NOLZ1-ISL1, $p<0.01$), with NOLZ1-ISL1 having the largest Na⁺ current density which was significantly increased from week 2 (Mann-Whitney U=53, $p<0.005$). The Na⁺ current density-voltage curves (Figure 5.10E) represent the maximal data, at 2 and 3 weeks post transfection.

The maximal K⁺ current density (Figure 5.10D) at 2 weeks post-transfection, showed an increase in CAG- transfected cells (306.3 pA/pF \pm 52.3 n=8) compared to NOLZ1 (262.7 pA/pF \pm 38.4 n=16) and ISL1 (235.9 pA/pF \pm 67.5 n=14). NOLZ1-ISL1 transfected cells (330.8 pA/pF \pm 37.5 n=15) had a greater maximal K⁺ current density than CAG- transfected cells. From week 2 to week 3 post-transfection there was an increase in maximal K⁺ current density for NOLZ1 (361.7 pA/pF \pm 74.7 n=12), ISL1 (430.4 pA/pF \pm 79.5 n=4) and NOLZ1-ISL1 transfected cells (417.2 pA/pF \pm 49.6 n=17), but a decrease for CAG- transfected cells (232.7 pA/pF \pm 37.6 n=10). ISL1 transfected cells had the greatest maximal K⁺ current density. The CAG- transfected cells having a greater K⁺ current density at week 2, then having the smallest K⁺ current density at week 3 was observed in the IV curves (Figure 5.10E).

5. Morphological and electrophysiological characterisation of transfected neurons

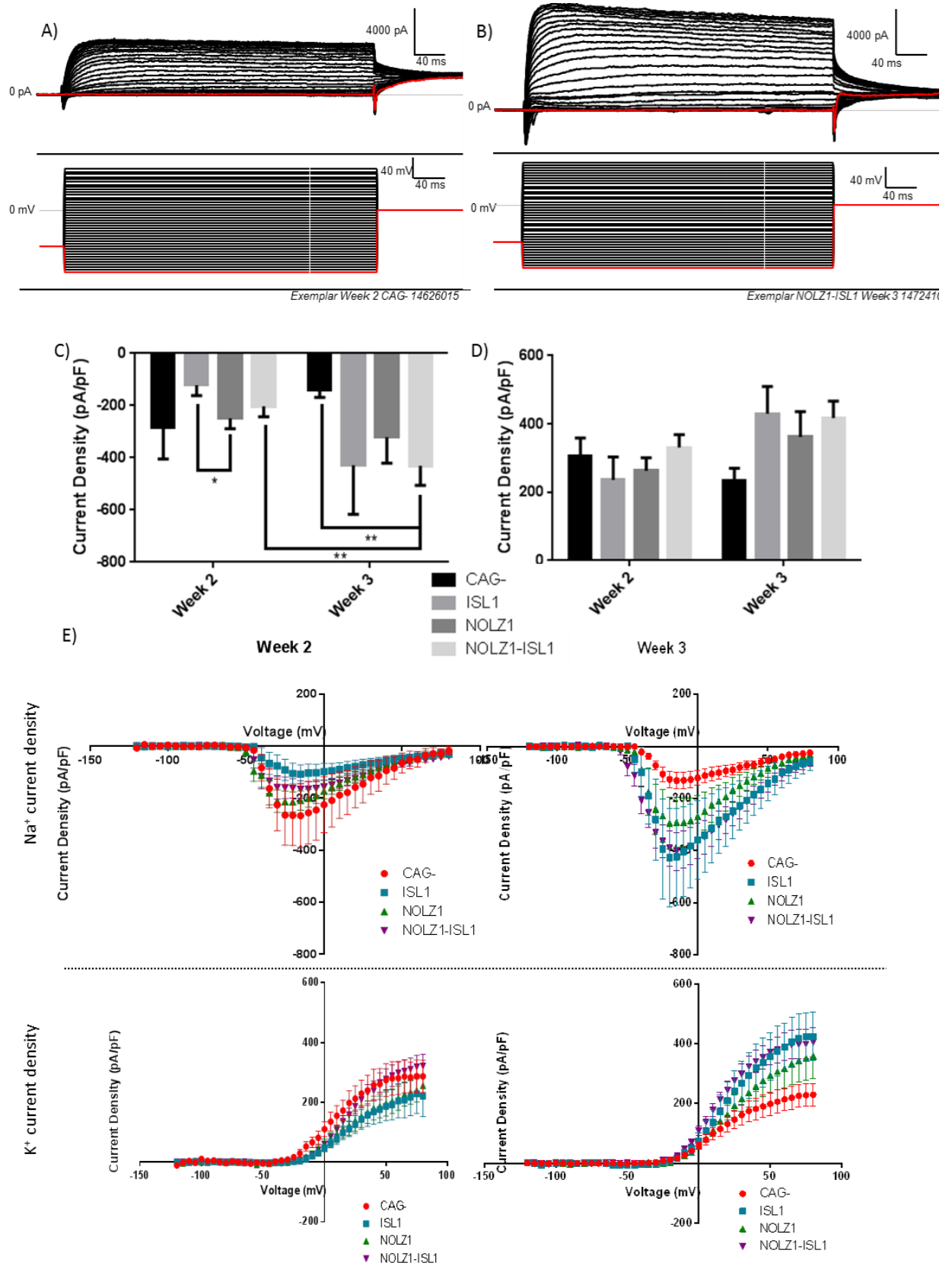


Figure 5.10: The sodium and potassium currents of neurons 2 and 3 weeks post transfection. Cells were analysed in voltage clamp protocol in order to elicit Na⁺ and K⁺ currents. The currents were subsequently normalised to the cell capacitance. A) An

exemplar trace from a neuron 2 weeks post transfection in voltage clamp, top panel shows current generated, bottom panel the stimulus. B) An exemplar trace from a neuron 3 weeks post transfection in voltage clamp, top panel shows current generated C) Bar graph showing the maximal Na^+ current from each of the transfections, at 2 and 3 weeks post transfection. There was a significant increase at week 2 between NOLZ1 & ISL1 $p=0.02$ Dunn's multiple comparison Kruskal-Wallis test=9.284 $p=0.03$. At week 3 there was a significant increase between CAG- and NOLZ1-ISL1 Kruskal-Wallis test=10.31, $p=0.02$ Dunn's multiple comparison $p<0.01$. Between week 2 and week 3, there was a significant increase in Na^+ current in NOLZ1-ISL1 transfected cells Mann-Whitney $U=53$, $p<0.005$. D) Bar graph showing the maximal K^+ current from each of the transfections. No significant difference at either of the time points, week 2 Kruskal-Wallis test=6.54 $p=0.09$, week Kruskal-Wallis test=6.71 $p=0.08$. E) Scatter plots showing the mean current density of Na^+ (top panel) and K^+ (bottom panel) at 2 (left) and 3 (right) weeks post transfection. Error bars on all graphs represent SEM.

5.3.5 Voltage gated Na^+ channel activation and inactivation

To measure the voltage-dependant activation and inactivation of the voltage-gated Na^+ channels, a protocol was performed to activate the Na^+ channels (as per 5.3.4) and inactivate them by stepping from the variable voltage sweep (-120 mV and up) to 0 mV.

The voltage at which the hypothetical peak Na^+ window current occurs is where the activation and inactivation relationships of the Na^+ channels meet. This was determined because it allows a comparison of both the activation and inactivation voltages of the Na^+ current, with different subtypes of voltage-gated Na^+ channels showing different voltage ranges for both (Rush et al., 2005). The larger the sodium window is, the more likely a cell is to be able to fire spontaneous action potentials as there is a wider range of voltages in which the cells Na^+ channels are not inactivated and so Na^+ ions can move across the membrane from outside of the cell to inside, depolarising the membrane potential, which if depolarised enough by the flow of Na^+ into the cell, causes an action potential to be generated. In order to plot the Na^+ current activation and inactivation, the non-leak subtracted currents were corrected for the driving force of Na^+ ions across the membrane, which is +66.68 mV, determined from the Nernst equation of Na^+ ions, then normalised to the maximal current per cell.

Nernst equation:

$$E_{Na^+} = 2.303 \cdot \frac{RT}{ZF} \cdot \log \frac{[Na^+]_o}{[Na^+]_i}$$

Where R=gas constant (1.98 cal deg⁻¹ mole⁻¹), T=temperature in Kelvin (273.15 + temperature in centigrade), Z=valence of ion, F=Faraday constant (23,060 cal volt⁻¹ equiv⁻¹), [Na⁺]_o=Na⁺ concentration outside the cell (135 mM), [Na⁺]_i= Na⁺ concentration inside the cell (127 mM).

The Na⁺ window current of the cells at 2 weeks post transfection (Figure 5.11) was larger in cells which have been transfected with ISL1, NOLZ1 or NOLZ1-ISL1 in comparison to CAG- transfected cells; this was also evident at 3 weeks post transfection. The voltage at which the peak of the Na⁺ window current was observed was determined by the crossing point of the fitted sigmoidal Boltzmann curves. This was more hyperpolarised in CAG- transfected cells (-42.7 mV) at week 2 than in the NOLZ1 (-41.1 mV), ISL1 (-38.4 mV) or NOLZ1-ISL1 (-39.8 mV) transfected cells. At 3 weeks, this was depolarised for all the cells (CAG-: -41.3 mV, ISL1: -35.5 mV, and NOLZ1: -39.0 mV), with the exception of NOLZ1-ISL1 transfected cells (-40.7 mV).

When the Na⁺ channel activation and inactivation data are separated by whether the cell was spontaneously firing, attempting to fire or not firing action potentials at all, then there also tends to be an increase in the size of the Na⁺ window in the cells which are spontaneously active (week 2: Figure 5.12 and week 3: 5.13). Also cells which are spontaneously active at resting V_m, tend to have a resting V_m which lies within the Na⁺ window.

5. Morphological and electrophysiological characterisation of transfected neurons

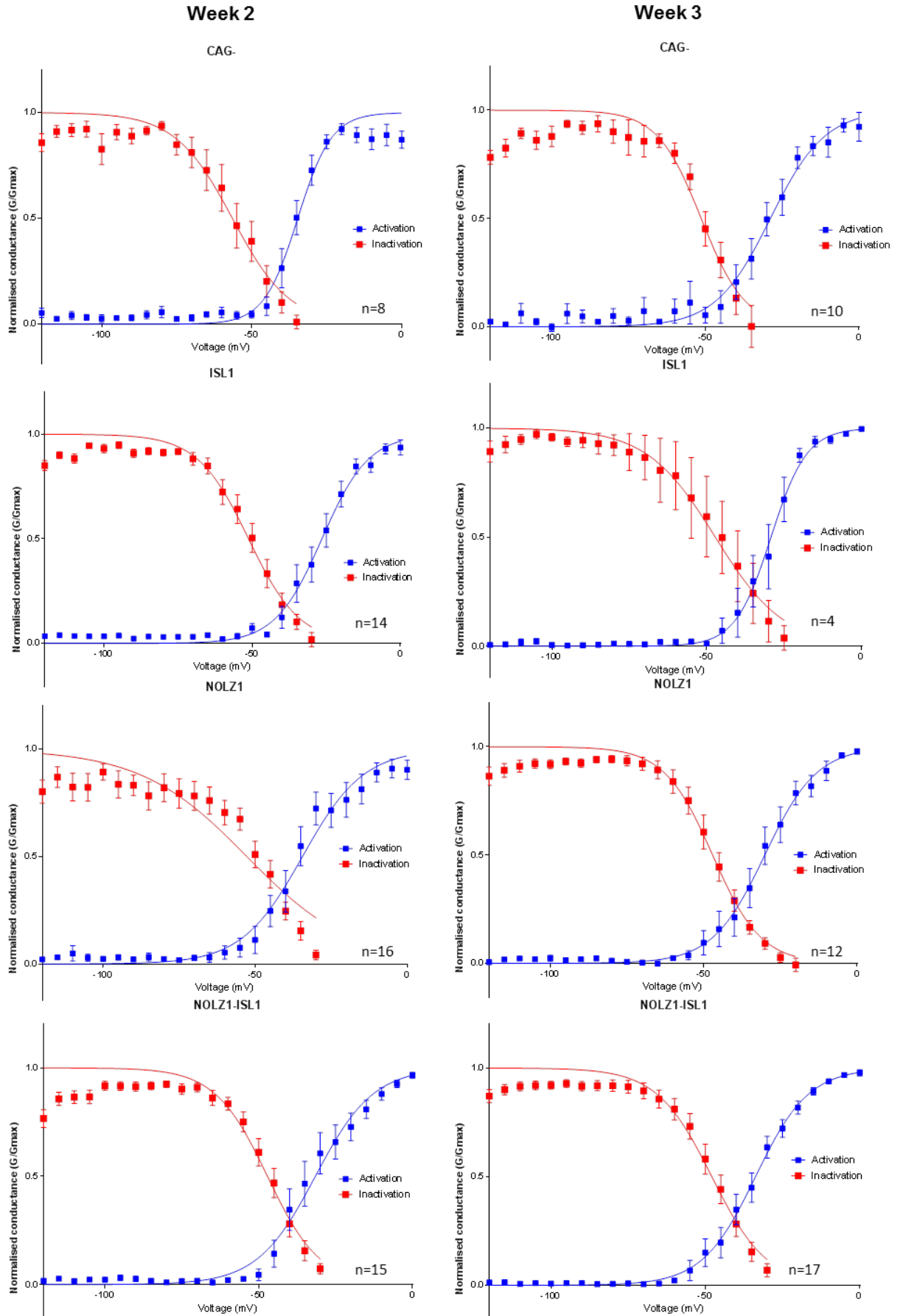


Figure 5.11 (above): The sodium window of neurons 2 and 3 weeks post transfection. Scatter plots showing the Na⁺ activation window indicated with arrows under the activation and inactivation curves. First column are data from 2 weeks after transfection and the second column 3 weeks post transfection. Activation and inactivation data were fitted with Sigmoidal Boltzmann equations, to determine the peak of the Na⁺ window. Error bars represent SEM. Number of cells analysed stated under each graph.

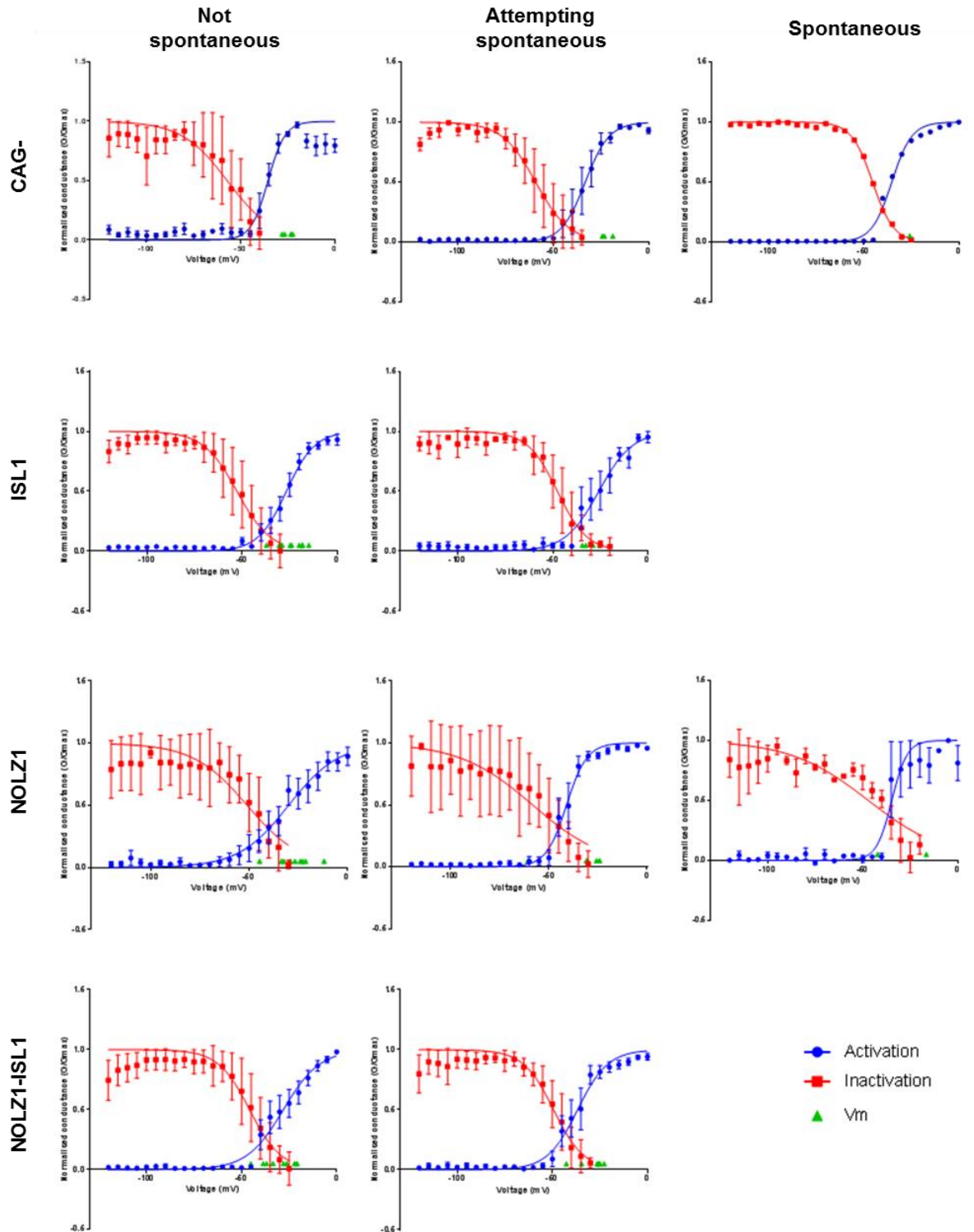


Figure 5.12: The sodium current window of neurons 2 weeks post transfection plotted with V_m. Break down of scatter plots showing the Na⁺ activation window of cells which were not spontaneous (1st column), attempting spontaneous activity (2nd column) and

spontaneously active cells (3rd column). The resting membrane potentials of the cells are also plotted. Top row CAG-, 2nd row, ISL1, 3rd row NOLZ1, 4th row NOLZ1-ISL1. Error bars represent SEM.

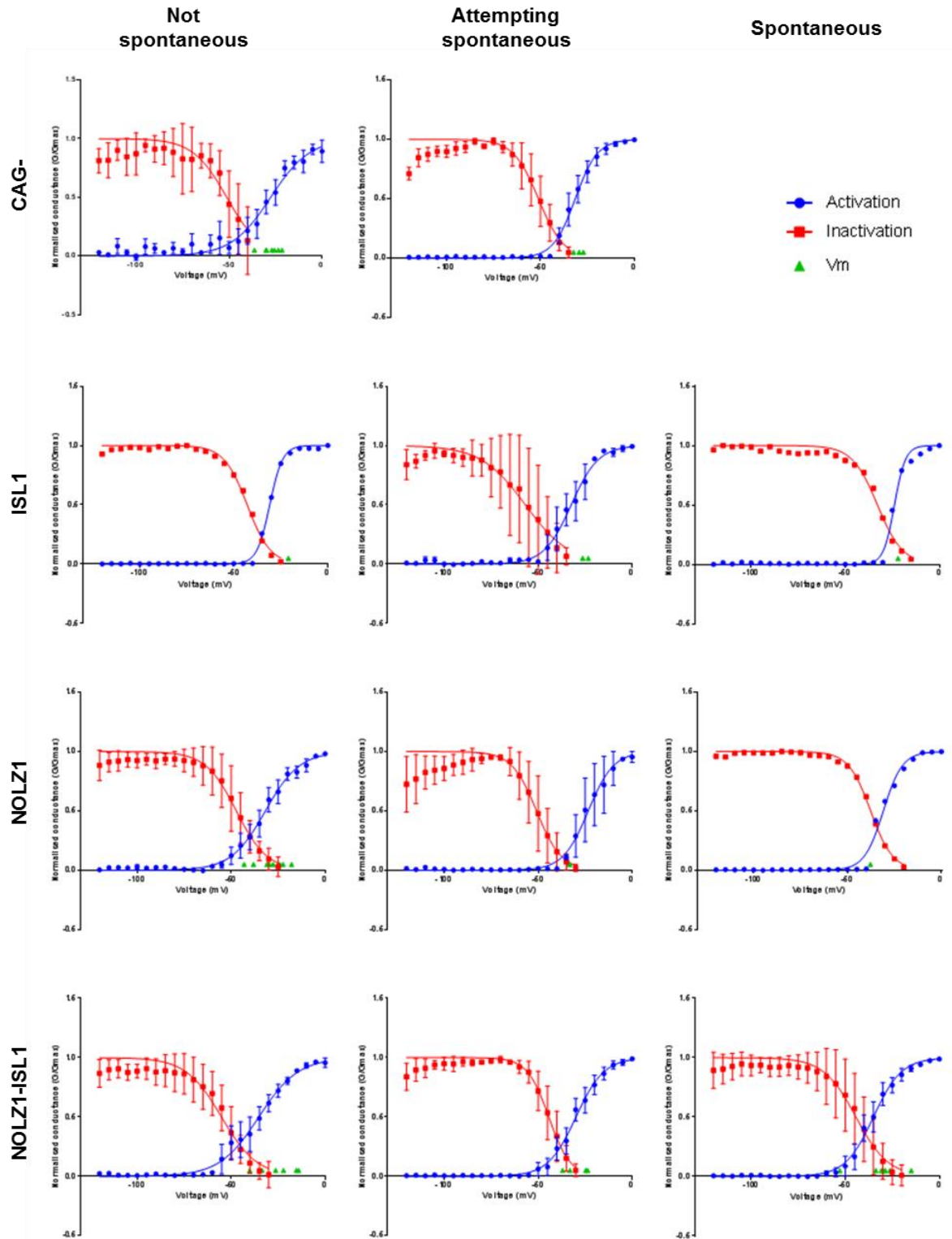


Figure 5.13: The sodium current window of neurons 3 weeks post transfection plotted with V_m . Break down of scatter plots showing the Na⁺ activation window of cells which were not spontaneous (1st column), attempting spontaneous activity (2nd column) and spontaneously active cells (3rd column). The resting membrane potentials of the cells are

also plotted. Top row CAG-, 2nd row, ISL1, 3rd row NOLZ1, 4th row NOLZ1-ISL1. Error bars represent SEM.

5.4 GABA currents and NMDA currents with enhancement by dopamine D1 agonist

In order to determine if the neurons were able to respond to GABA and NMDA, a characteristic of MSNs, cells at 3 weeks post transfection were recorded in whole cell patch clamp utilising bath and pipette solutions from Flores-Hernández et al., (2002). This bath solution contained no Mg^{2+} so not to inactivate the NMDA receptors; a holding voltage of -40 mV was used to inactivate the Na^+ and Ca^{2+} conductances. The bath and pipette solutions allowed the distinction between NMDA- and GABA-evoked currents and between NMDA and GABA miniature synaptic currents, with NMDA evoking an inward current and GABA evoking an outward current. This was because NMDA channels allow the flow of cations and GABA receptors are Cl^- channels.

Dopamine D1 agonist enhancement of NMDA currents were investigated, as this has been found to be a characteristic of MSNs and one physiological role of DARPP32 in MSNs (Flores-Hernández et al., 2002).

5.4.1 GABA miniature post synaptic currents

In order to determine whether cells were forming synapses, the cells were recorded to see if they generated any $GABA_A$ miniature synaptic currents indicative of spontaneous release of GABA at the presynaptic terminal, as exemplified in Figure 5.14A.

The proportion of cells which demonstrated GABA miniature synaptic currents was 7% for the CAG- controls (Figure 5.14B) but rose to 26.3% for ISL1 and 27.8% for NOLZ1; interestingly, both together, suppressed GABA currents, only 5.88% of cells demonstrated GABA miniature synaptic currents. The number of miniature synaptic

currents recorded per cell (Figure 5.14C) showed that on average NOLZ1 transfected cells had the highest frequency of miniature synaptic currents (26.4 ± 13.1 per minute, $n=5$) compared to ISL1 (4.4 ± 0.68 $n=5$), NOLZ-ISL1 (25, $n=1$) and CAG- transfected cells (18, $n=1$). NOLZ1 transfected cells also had the largest amplitude of GABA miniature synaptic currents (10.9 pA ± 1.31 $n=5$) in comparison to ISL1 (8.87 pA ± 0.95 $n=5$), CAG- (8.50 pA $n=1$) and NOLZ1-ISL1 (8.83 pA, $n=1$, Figure 5.14D). The inter-event interval was longest in ISL1 transfected cells (11364.6 ms ± 2183.9 $n=5$, Figure 5.14E) in comparison to NOLZ1 (3641.9 ms ± 1316.3 $n=5$), NOLZ1-ISL1 (2357.1 ms, $n=1$) and CAG- transfected cells (3225.0 ms, $n=1$), this was to be expected as they had the fewest number of miniature synaptic currents per cell. No cells showed NMDA miniature synaptic currents.

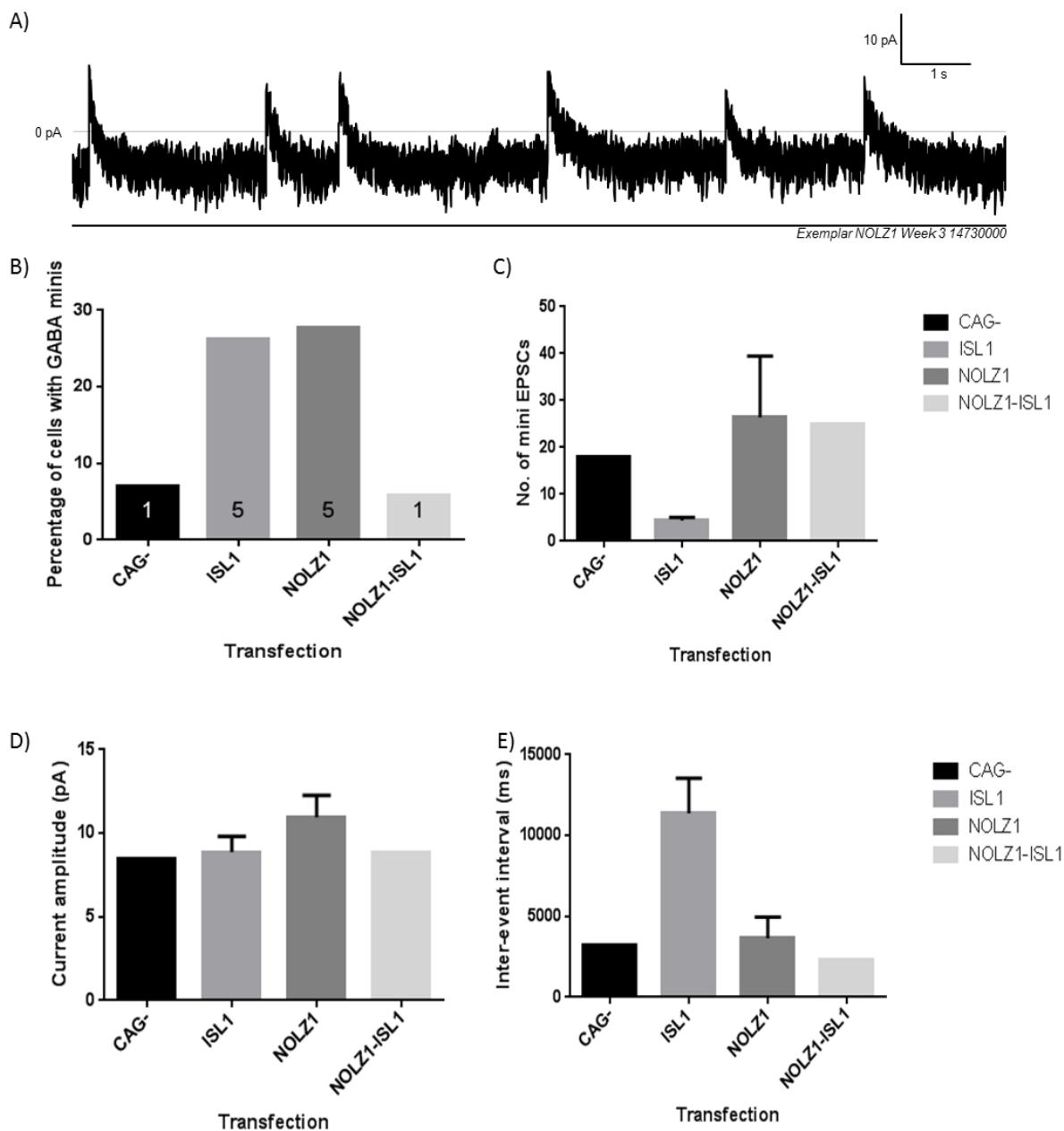


Figure 5.14: GABA miniature synaptic currents in neurons 3 weeks post transfection.

A) An exemplar trace of GABA induced miniature synaptic currents in a neuron B) Bar graph showing the percentage of cells which possess GABA miniature synaptic currents, number of cells with GABA miniature synaptic currents was indicated on each bar. C) Bar graph showing the mean no. of GABA miniature synaptic currents in the neurons. D) Bar graph showing the mean current amplitude of GABA miniature synaptic currents of the neurons. E) Bar graph showing the inter-event interval of GABA mini miniature synaptic currents in neurons.

5.4.2 GABA currents

In order to measure post-synaptic GABA currents, cells were held at -40 mV by current injection and underwent 3 applications of GABA (100 μ M) for 5 seconds,

with 90 seconds recovery between each repeat before the next application. The average of 3 repeats was taken for GABA application.

All of the cells responded to GABA (100 μ M). The current densities for the cells (figure 5.16B) showed that ISL1 transfected cells (46.46132 pA/pF \pm 9.99, n=11) marginally had the biggest current density in response to GABA, compared to NOLZ1 (37.2 pA/pF \pm 9.00, n=12), CAG- (41.7 pA/pF \pm 7.25, n=13) and NOLZ1-ISL1 transfected cells (41.4 pA/pF \pm 7.60, n=11).

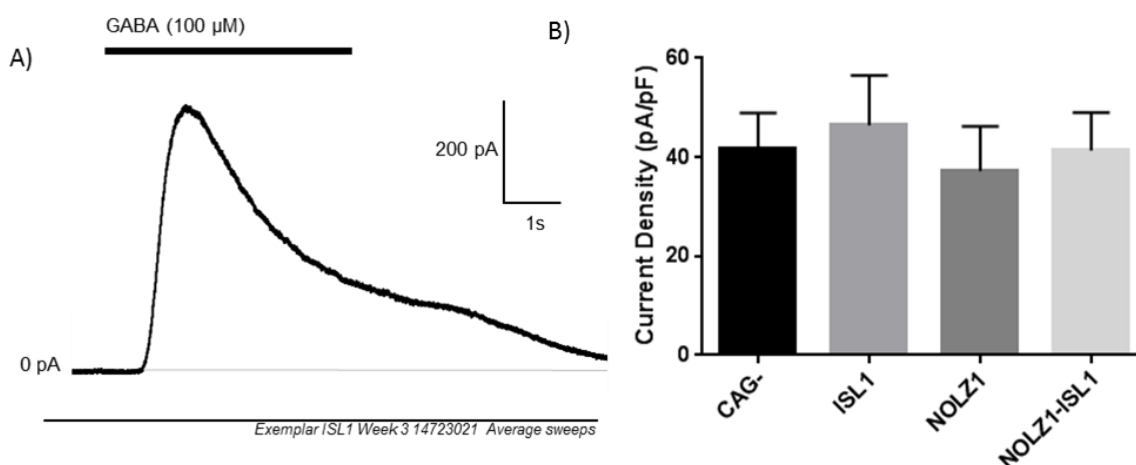


Figure 5.15: GABA currents in neurons 3 weeks post transfection. Neurons were analysed at 3 weeks post-transfection by whole cell patch clamp using GABA (100 μ M) application to elicit GABA currents. All cells which were tested responded to GABA. A) Exemplar average trace of GABA currents, averaging 3 GABA applications B) Bar graph showing the mean GABA current densities from averaged traces. All graph error bars = SEM.

5.4.3 NMDA currents with D1 enhancement

In order to determine whether the cells expressed NMDA receptors post-synaptically, and investigate whether the NMDA current could be potentiated by the dopamine D1 agonist, SKF 81297, cells were held at -40 mV and underwent between 3 and 9 repeats of NMDA (100 μ M) application for 5 seconds, with 90 seconds recovery each repeat before the next application. The average of 3 repeats were taken for each application period; NMDA application, NMDA with dopamine D1 agonist SKF 81297 (10 μ M) application and the final 3 sweeps of NMDA only wash.

Not all of the cells responded to NMDA (100 μ M). The percentage of cells that responded to NMDA was 35.7% for control, 61.5% for NOLZ1, 35.7% in NOLZ1-ISL1 transfected cells and 53.9% of ISL1 transfected cells. The average current densities for the cells for the 3 sweeps, which did respond (Figure 5.16B) show that NOLZ1 transfected cells (-2.69 pA/pF \pm 0.57, n=7) had the biggest current density in response to NMDA, which was increased from ISL1 (-1.67 pA/pF \pm 0.40, n=7) and significantly increased from the currents in CAG- (-1.51 pA/pF \pm 0.55, n=5) and NOLZ1-ISL1 transfected cells (-1.29 pA/pF \pm 0.36, n=5, two-way ANOVA $F=4.09$ $DF=3$, 60 $p=0.01$ Tukey's multiple comparisons CAG- vs. NOLZ1 $p<0.05$, NOLZ1-ISL1 vs NOLZ1 $p<0.05$). The proportion of cells which responded to NMDA and that were then enhanced by SKF 81297 application, a specific dopamine D1 agonist, (Figure 5.16C) shows that ISL1 (-1.74 pA/pF \pm 0.34, n=7) and NOLZ1-ISL1 transfected cells (-1.47 pA/pF \pm 0.44, n=5) showed enhancement of NMDA current with dopamine D1 agonist application in comparison to the CAG- (-1.40 pA/pF \pm 0.63, n=5) or NOLZ1 transfected cells (-2.58 pA/pF \pm 0.52, n=7). The cells which showed enhancement of NMDA currents by dopamine D1 application showed an average increase of current of 24% for ISL1 (range 1-77% n=4), 12.9% for NOLZ1 (range 1-15% n=3), 25.1% for NOLZ1-ISL1 (range 18.5-35.5% n=3) and for CAG- 10.5% (range 10-11% n=2). The response of the cells to NMDA in this manner showed that they may be of a medium spiny neuronal phenotype (Flores-Hernández et al., 2002). This is the first time that this has been reported for human stem cell derived neurons.

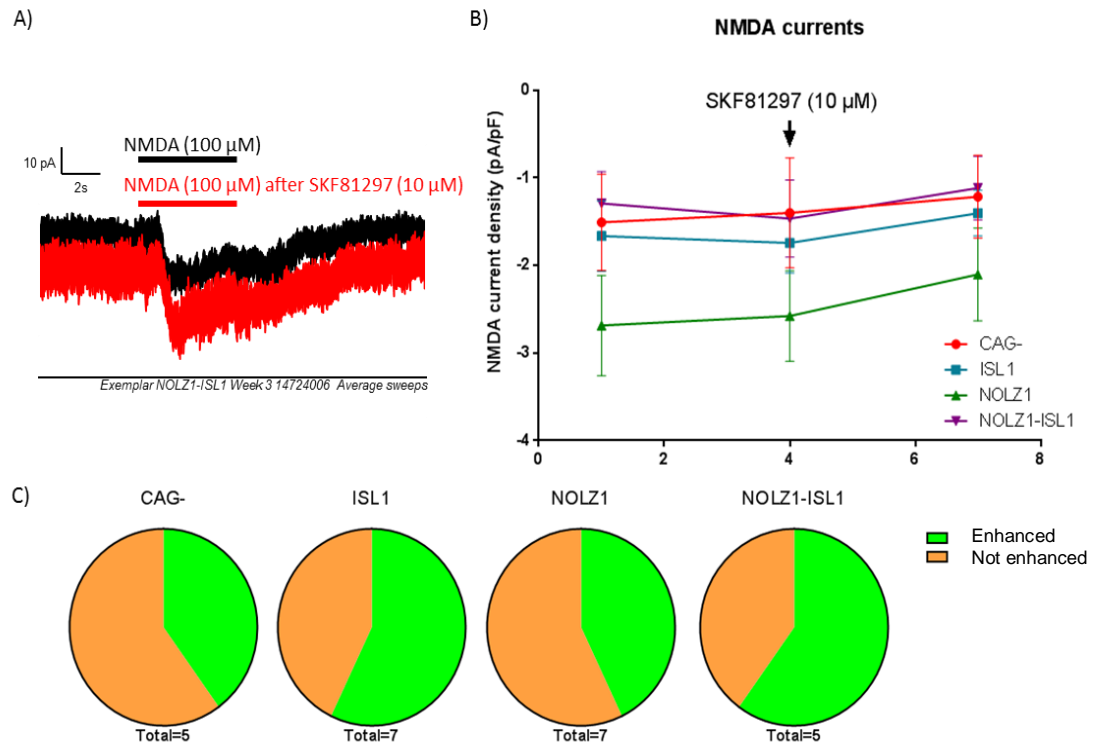


Figure 5.16: NMDA currents in neurons. Neurons were analysed at 3 weeks post-transfection by whole cell patch clamp using NMDA (100 μ M) application to elicit NMDA currents. Dopamine D1 agonist SKF 81297 (10 μ M) was co-applied with NMDA to try and elicit a potentiation of NMDA current. A) An exemplar trace of NMDA currents observed in a neuron with an increase in current when the dopamine D1 agonist was applied to cells B) Line graph showing the mean NMDA current from averaged traces with or without the addition of the D1 dopamine agonist. There was a significant difference between transfections two-way repeated measures ANOVA $F=4.09$ $DF=3, 60$ $p=0.01$ with Tukey's multiple comparisons NOLZ1 current densities are significantly different from CAG- and NOLZ1-ISL1 both $p<0.05$. C) Pie charts showing the proportion of cells which showed an enhanced/decreased NMDA current after application of the dopamine D1 agonist. Error bars = SEM.

5.5 Conclusions

At the end of the differentiation protocol (3 weeks):

Neurons were morphologically more complex with any of the transcription factor transfections, alone or in combination than with the control plasmid (Figure 5.3), the capacitance of the cells supports this finding at week 3 (Figure 5.4B). The cells transfected with NOLZ1-ISL1 displayed a more mature neuronal phenotype, with enhanced levels of spontaneous and induced activity, and increased Na^+ and K^+ current densities (Figures 5.5, 5.6, 5.7, 5.8, and 5.10). All the neurons responded to GABA (Figure 5.15), and an increased number of neurons which responded to

NMDA was seen in NOLZ1 and ISL1 transfected cells compared to control. The neurons did not show NMDA miniature synaptic currents, but did show GABA miniature synaptic currents; this suggests that there may be NMDA and GABA receptors extra-synaptically, but only GABA receptors synaptically in the transfected cultures (Figure 5.14). Finally, ISL1 and NOLZ1-ISL1 transfected cells demonstrated a functional phenotype that more closely matched that reported for rodent MSNs, as judged by NMDA current potentiation by dopamine D1 agonist (Figure 5.16).

5.5.1 Cells become less complex during *in vitro* culture

Comparison of complexity between cells at week 1 (Figure 5.1) and week 2 (Figure 5.2) during differentiation for each of the transfections, showed a decrease in complexity with time, in terms of Sholl analysis and number of branches recorded per cell. This may have been as a result of axonal pruning (reviewed by Vanderhaegen & Cheng 2010). This takes place during brain development, to compensate for the overproduction of neurons and synaptic connections between neurons (reviewed by Vanderhaegen & Cheng 2010). These are removed by programmed cell death and axosome degradation of aberrant dendrites, to produce a mature neuronal network (reviewed by Vanderhaegen & Cheng 2010). Different signalling molecules are involved in the pruning of different neuronal populations, the striatonigral pathway requires the correct signalling of PlexinD1 expression by striatonigral neurons and Sema3E expression in the globus pallidus to repel the striatonigral axons, in order to form the correct pathway through the internal capsule (Ehrman et al., 2013, Chauvet et al., 2007). The genetic deletion of *Plexnd1* (encoding PlexinD1) in the striatum, results in aberrant synapse formation in the thalamo-striatal neurons (Ding et al., 2011). This could be investigated by examining the expression of the polysialylated form of neural cell adhesion molecule (PSA-NCAM) *in vitro* to analyse if the cells are undergoing dendritic pruning. PSA-NCAM

was expressed during rat neuritogenesis, with progressive localisation to the synapse in the postnatal rat dorsolateral striatum and undetectable post synaptic pruning (Butler et al., 1998).

The cells are also not as complex as those observed in native MSNs, when cultured *in vitro* (Lerner et al., 2012, Gertler et al., 2008). This could be as a result of not receiving the correct external inputs. Mono-culture of E16 (Penrod et al., 2011), E19 (Segal et al., 2003) and postnatal mouse MSNs (Tian et al., 2010) produced stunted dendritic growth. Spine density and dendrite complexity was improved by co-culture with mouse E16-19 cortical neurons (Penrod et al., 2011, Tian et al., 2010) or P1 cortical neurons (Segal et al., 2003). However, there was still a decrease in complexity with mouse E16 striatal cultures from 14 to 21 DIV (Penrod et al., 2011). Another issue could be that the cells are differentiated in a 2D *in vitro* system, which does not replicate the *in vivo* environment. Protocols have been developed which try to replicate the *in vivo* conditions, by culturing the cells in scaffolds. Although there have been no reports of this with MSNs, cortical neurons have been cultured in 3D scaffolds, with improved complexity of morphology, with matrigel and increased collagen concentration in the scaffold proving beneficial to neurite outgrowth and turning (Srinivasan et al., 2014). Another culture system exploiting the use of laminin I in PuraMatrix™, also increased neurite outgrowth, compared with no laminin and monolayer culture (Ortinou et al., 2010).

5.5.2 NOLZ1/ISL1 combined transfections improved the neuronal phenotype at week 3

Morphologically, the most complex neurons at 3 weeks post-platedown were the NOLZ1-ISL1 transfected neurons (Figure 5.3). These neurons were the least complex when under selection, most likely due to the lower transfection efficiency, and consequently, the reduced cell density. The levels of spontaneous and induced

electrical activity, as well as the density of the Na⁺ and K⁺ currents, were also increased in the NOLZ1-ISL1 transfected cells.

Comparisons between the striatonigral and striatopallidal pathway neurons often show little difference in the basic electrophysiological properties in the cells with a V_m of approximately -80 mV, but the threshold voltage for action potentials is increased in D2⁺ receptor neurons from -45 mV to -50 mV (Cepeda et al., 2008). The threshold voltages observed in the cells transfected with any of the transcription factors and control had a threshold voltage of induced action potentials of ~ -30 mV (Figure 5.7B), which were not as hyperpolarised as those observed in the mouse (Cepeda et al., 2008). The action potential half-width of ~ -0.5-1 ms was observed in slices *in vivo* (Cepeda et al., 2008, Planert et al., 2013), which was smaller than that which was observed *in vitro* in this chapter (Figure 5.7H). Therefore it is likely that the cells need to be matured further *in vitro*, either by co-culture with the correct inputs from cortical co-culture, or maintained for longer *in vitro*, in order to observe the decrease in halfwidth, increase in threshold voltage and hyperpolarisation of the V_m . However, the amplitude of the action potentials generated by current injection was comparable to that seen *in vivo*. NOLZ1-ISL1 transfected cells had a mean spike height of 85.7 mV, which compared to the range observed for cells *in vivo* was comparable (78-100 mV) (Klapstein et al., 2001, Cepeda et al., 2008, Planert et al., 2013).

5.5.3 ISL1 and NOLZ1-ISL1 were the best at inducing a MSN-like phenotype

In support of the protein characterisation (Chapter 4), the morphological and physiological data provided an observation that upon ISL1 transfection, a phenotype most similar to striatonigral neurons was generated. Sholl analysis of cells transfected with ISL1 showed that they formed the more complex neurons at 1 and 2 weeks with G418 selection (Figure 5.1 and 5.2). At 3 weeks (Figure 5.3), when not under selection, NOLZ1-ISL1, followed by ISL1 transfected cells, were the most

complex. Evaluation of the neurons of the striatonigral pathway, in comparison to the cells of the striatopallidal pathway showed that morphologically, they were more complex by Sholl analysis at 10-135 μm from the cell soma and there was a greater cumulative neurite length and cell capacitance (Gertler et al., 2008). ISL1 transfected cells (Figure 5.6) showed decreased excitability in evoked action potentials at 3 weeks, but NOLZ1-ISL1 transfected cells more closely resembled NOLZ1-transfected cells in terms of excitability of induced action potentials. Physiologically, the neurons of the striatonigral pathway are less excitable, with a higher rheobase current and the neurons have a more hyperpolarised resting membrane potential (Gertler et al., 2008).

ISL1 and NOLZ1-ISL1 transfected cells also showed an increase in the proportion of cells which had NMDA current potentiation by the dopamine D1 agonist (Figure 5.16). This regulation by dopamine D1 receptors has been shown to be a characteristic of rodent MSNs (Flores-Hernández et al., 2002). The majority of research supports the idea that the striatonigral neurons are the MSN cell population which express dopamine D1 receptors (Gertler et al., 2008, Gerfen et al., 1990, Hersch et al., 1995, LeMoine & Bloch 1995), suggesting the forced expression of ISL1 might result in more efficient specification of striatonigral neurons. The differential expression of some proteins such as the dopamine D1 receptor, substance P and dopamine D2 receptors, enkephalin and Adora2a (Schiffman & Vanderhaegen 1993, LeMoine & Bloch 1995) could be exploited for validation that ISL1 transfection causes differentiation to cells of the D1⁺ striatonigral pathway.

The observation that the neurons in all transfections responded to GABA (Figure 5.15), showed they expressed GABA receptors. While not all cells responded to NMDA, 35.7% of NOLZ1-ISL1 transfected cells and 53.9% of ISL1 transfected cells responded to NMDA, showing that these cells have the glutamate receptors

required to receive glutamatergic input (Ferino et al., 1987, Jones et al., 1977, Royce 1982, Wilson 1987). The fact that no NMDA miniature synaptic currents were observed *in vitro*, showed that there are not likely to be synaptic glutamatergic currents generated by neurons in the differentiation protocol.

In summary, co-transfection of NOLZ1-ISL1 produced cells which were both morphologically and electrophysiologically more similar to mature MSNs than cells transfected with the control plasmid. Dopamine D1 enhancement of NMDA currents were observed in the majority of cells which were transfected with ISL1 or NOLZ1-ISL1 constructs, in comparison to control.

5.5.4 Limitations of the methods in this chapter

The use of electrophysiology allows a vast array of data to be obtained on a cell by cell basis. The ability to patch the GFP⁺ cells means that the cells analysed are only those which have been transfected. However, due to the time-consuming nature of data collection, there is a limit to the number of cells which can be analysed. Therefore data collected is from a small proportion of the population, although differences were still observed between the transfections. More cells could be analysed with the use of calcium imaging, using a fluorescent Ca²⁺-sensitive dye to monitor responses to different neurotransmitters, however more information could not be gathered on the neuronal phenotype.

***CHAPTER 6:
DISCUSSION & FUTURE
WORK***

6. Discussion & Future work

6.1 Summary of data in this thesis

This thesis is the first report of attempting to make MSNs *in vitro* from neural progenitors derived from pluripotent stem cells by transcription factor transfection. In Chapter 3, the formation of the plasmids to be used in Chapters 4 and 5 was detailed. The resulting 8 plasmids and control were utilised in the newly validated SCM1/2 protocol (Chapter 4) and as a result of an initial screen of plasmids, NOLZ1 was chosen for further investigation, along with ISL1 and the combination of the two transcription factors in plasmids. Further protein characterisation (Chapter 4) at 3 weeks post-transfection, highlighted ISL1 transfected cells as the most efficient at inducing FOXP1, CTIP2 and DARPP32/CTIP2 combined expression.

These plasmids were also utilised to analyse the form and function of the neurons which had been transfected (Chapter 5). The resulting morphology data showed ISL1 transfected cells to possess the more complex dendritic arborisation at 1 and 2 weeks post transfection when selected with G418, to enrich the transfected cell population. At 3 weeks NOLZ1-ISL1 and ISL1 transfected cells were the most complex. The complexity of the cells decreased from week 1 to week 2. The electrophysiological properties of the neurons were also analysed at weeks 2 and 3 post-transfection and showed transfection of NOLZ1-ISL1 to increase excitability, spontaneous activity and the size of the Na⁺ and K⁺ current densities. Electrophysiological properties which replicate those observed in MSNs, such as NMDA currents and potentiation of the current by a dopamine D1 agonist, were observed in ISL1 and NOLZ1-ISL1 transfected cells.

6.2 ISL1 transfections improve MSN phenotype

In comparison to the majority of other protocols, the percentage of DARPP32/CTIP2 co-localisation and FOXP1 expression was increased in the GFP⁺ cells after ISL1 transfection. In another protocol, FOXP1 expression was analysed during differentiation, where it was observed at 45 DIV post differentiation (Delli Carri et al., 2013 a&b), and FOXP1 was co-expressed with CTIP2 at 18 DIV in ~30% of cells (Danjo et al., 2011). The proportion of DARPP32/CTIP2 co-expression in the protocol described in this thesis was higher than has been previously reported by the HD iPSC consortium (2012) with results of 5% population of DARPP32⁺/CTIP2⁺ neurons. The proportion of cells that expressed DARPP32 after ISL1 transfection (~12% of the total population) was increased above the 10% observed in several protocols (Aubry et al., 2008, Delli Carri et al., 2013 a&b, Shin et al., 2012, El Akabawy et al., 2011), but less than others. Indeed, Ma et al., (2012) report having made a population of neurons in which 89% of the GABA⁺ population were DARPP32⁺, and Danjo et al., (2011), show ~50% of cells expressing DARPP32.

In comparison to MSNs generated from either iPS or ES cells previously (highlighted in Chapter 1), the functional properties of the neurons generated here by the co-transfection of NOLZ1-ISL1 are certainly comparable, if not superior, to those described by other protocols, and are generated in a comparatively short period. In the protocol using monolayer differentiation with N2:B27 medium, only 65% of the cells produced induced action potentials (Shin et al., 2012). In addition to this, the differentiation protocol which used dual SMAD inhibition for neuronal induction and subsequent use of N2:B27 media, produced a population of neurons 13% of which showed no firing and 57% showed repetitive firing at 87 days post induction (Delli Carri et al., 2013a). In comparison to this study, the NOLZ1-ISL1 transfected cells produced action potentials in 100% of the cells and 75% of cells

produced action potential trains. These results were also obtained after only 37 DIV post neural induction, which by comparison shows a dramatic improvement.

With regards to GABA responses, only 74% of neurons responded to GABA application (Delli Carri et al., 2013a), in comparison to 100% of neurons in this study, no matter which plasmid was transfected. Comparing Na⁺ and K⁺ currents between these protocols cannot be performed effectively, due to the way in which results have been reported. However, looking at the raw traces (Delli Carri et al., 2013a), it seemed that cells transfected with NOLZ1-ISL1 produce larger Na⁺ and K⁺ currents than do those of the Delli Carri protocol. Delli Carri et al., (2013a) also report that in a fraction of cells there was a significant attenuation of GABA current by dopamine D1 agonist (Delli Carri et al., 2013a). The protocol described herein, showed that ISL1 and NOLZ1-ISL1 transfected cells showed enhancement of the NMDA current by dopamine D1 agonist, a characteristic of rodent MSNs that has never been reported for pluripotent stem cell derived neurons.

A comparable capacitance and a decreased input resistance was seen at 3 weeks post transfection with NOLZ1-ISL1 transfection to a previously reported protocol using Shh and VPA for differentiation and recorded at 10 weeks post differentiation (Ma et al., 2012). The transfection of NOLZ1-ISL1 gave comparable results for physiological properties to the differentiation protocol from the HD iPSC consortium which showed spontaneously active cells at 2 weeks and also the cells responded to GABA application and produced Na⁺ and K⁺ currents during voltage clamp (HD iPSC consortium 2012).

Reports of differentiating HD patient-derived stem cells (ES or iPS) have been limited, and have not necessarily been aimed at generating MSNs. MAP2⁺ neurons were made within 3 weeks of neural induction of HD hES cells (Feyeux et al., 2012), and Tuj1⁺/MAP2⁺ neurons have also been generated (Lu & Palacino 2013). Others have had issues with control cells differentiating better than HD lines with a

decrease in MAP2⁺ neurons from 80% (H9 control) to 36-43% in the HD hESC lines (Chae et al., 2012). GABAergic neurons have been formed from HD72 iPSCs (Jeon et al., 2012), which also express DARPP32 in 27% of the neurons (Jeon et al., 2014).

The increase in effectiveness of differentiation towards MSN phenotype of neuroprogenitors transfected with ISL1 and NOLZ1 was not surprising as both play a major role in development of the striatum and MSNs.

NOLZ1 has been shown to be co-expressed with GFP in the *Drd1:EGFP* and *Drd2:EGFP* BAC transgenic mice implicating it in both the striatonigral and striatopallidal pathways (Ko et al., 2013). NOLZ1 overexpression led to the up-regulation of DARPP32 expression in both the initial screen of plasmids and the further characterisation, most likely due to its role in activation of RAR β , which in turn activates expression of DARPP32 (Liao & Liu 2005, Urbán et al., 2010).

ISL1 has been shown to have a more specific role in the development of the striatonigral pathway and inhibits the differentiation of cells into the striatopallidal pathway (Ehrman et al., 2013, Lu et al., 2014). ISL1 is expressed in the MAP2⁺ precursors in the rat, and these cells continue developing in the rat in order to form the DARPP32⁺ neurons (Wang & Liu 2001): ISL1 may therefore play a role switching on DARPP32 expression. ISL1 overexpression led to an increased expression of FOXP1. As ISL1 is expressed with FOXP1 not only in the striatum, but also in the spinal cord (Shu et al., 2001, Ericson et al., 1992, Tsuchida et al., 1994) it may therefore play a role in switching on FOXP1 expression in both locations.

NOLZ1 and ISL1 are co-expressed in the SVZ and MZ at E16.5, and later in development NOLZ1 is co-expressed with FOXP1 (Ko et al., 2013), further reinforcing the idea that ISL1 plays a role in switching on FOXP1 expression

6.3 Driving differentiation with forced expression of NOLZ1 and ISL1

In comparison with other transcription factor driven protocols, the protocol outlined in this thesis has been fairly successful, with MSN markers being expressed and functional characteristics similar to MSNs being observed. Other protocols (summarised in Chapter 1) often utilise viruses in order to gain a higher efficiency of differentiation. These protocols have also started with a variety of cell types, either fibroblasts (Vierbuchen et al., 2010, Pfisterer et al., 2011), astroglia (Berninger et al., 2007, Heinrich et al., 2010) or PSCs (Zhang et al., 2013). With the cells in this thesis already being partially specified into ventral forebrain like precursors possibly aided in differentiation, as the fact the method of transcription factor delivery was less efficient than these other protocols. The use of viruses would allow for improved transcription factor delivery in order to specify a higher proportion of the population of cells with the view to making a higher proportion of MSNs *in vitro*. These other protocols have managed to induce neurons which are functionally active (Berninger et al., 2007, Vierbuchen et al., 2010, Pfisterer et al., 2011), express markers of glutamatergic or GABAergic neurons (Heinrich et al., 2010), and have been shown to integrate into the mouse brain (Zhang et al., 2013). Therefore improving transcription factor delivery, would likely result in a higher percentage of MSNs.

6.4 Limitations of the thesis

The molecular, morphological and electrophysiological characteristics of the neurons presented herein are characteristic of but not specific to MSNs. FOXP1 is a transcription factor that is also expressed in the spinal cord motor column (Shu et al., 2001, Ericson et al., 1992, Tsuchida et al., 1994). In the adult mouse, it is also expressed (although not exclusively) in the substantia nigra, cerebral cortical layers

III-V, pontine nucleus, superior colliculus thalamus, olfactory tubercle and inferior olive (Ferland et al., 2003), but it is expressed in the developing striatum and the MSNs (Tamura et al., 2003, Takahashi et al., 2003, Tamura et al., 2004).

CTIP2 is another marker which has widespread expression in the brain, and is localised to cerebral cortical layers IV and VI, hippocampal neurons, olfactory cortex and the amygdala (Leid et al., 2004). CTIP2 is also expressed in the GABA interneurons of the accessory olfactory bulb (Enomoto et al., 2011).

Supplementary to calbindin as a marker of striatal matrix, it is also considered a marker of interneurons (Pickel & Heras 1996, Prensa et al., 1998). Therefore co-localisation with other markers (of MSNs) was required to determine that it was MSNs and not interneurons that were arising from differentiation.

Similarly, DARPP32, is not specific to the MSNs. The original report of DARPP32 expression showed it was enriched in the striatum, but was also expressed in astrocytes of the medial habenula, along with neurons of the deep perirhinal, cingulate and prefrontal cortex (Ouimet et al., 1994). Thus, although DARPP32 expression alone is not definitive of MSNs, the dopamine enhancement of NMDA currents is a physiological characteristic of MSNs, which is dependent upon DARPP32 expression (Flores-Hernández et al., 2002).

As a result of there currently being no definitive MSN marker, these factors need to be used together, in order to confirm identity, which is what has been attempted in this thesis.

6.4 Future work:

6.4.1 Improving the transcription factor delivery

In order to improve efficiency of conversion into MSNs, there is a need to improve transcription factor delivery either with viruses, or by performing drug screens to replace NOLZ1 and ISL1 transfection. This has been done for the induction of

pluripotent stem cells in a study by Hou et al., (2013), and for the differentiation of neural stem cells into neurons ISX9 which activates NeuroD1 expression (Schneider et al., 2008) and so it is feasible that this could be done in order to replace the need for transfection. Such a small molecule based approach might both increase the uniformity of differentiation and by virtue of being able to generate neurons by GMP, increase the potential use of the resultant cells in replacement therapies.

6.4.2 A Huntington's disease model

The main motivation behind the development of the differentiation protocol was to utilise the protocol in iPSCs derived from HD patient fibroblasts, in order to create an *in vitro* disease model. This seems very possible now, with an increased percentage of cells which have a phenotype similar to that seen in MSNs, but one major consideration needs to be addressed. It has already been shown that there is differential transcription factor expression in HD samples in comparison to control (Desplats et al., 2008, HD iPSC consortium 2012). In mouse ESCs expressing a mutated form of *Htt* with 150 CAG repeats, there was differential expression of ISL1 and NOLZ1 compared to control (Lorincz & Zawitowski 2009). NOLZ1 was upregulated with a greater than 2-fold change in the CAG150 cells, and ISL1 was decreased in the CAG150 cells in comparison to control after 7 days of differentiation (Lorincz & Zawitowski 2009). This will need to be addressed by using an inducible system of expression of the transcription factors in order to aid differentiation, which can be effectively switched off before it masks any disease phenotype.

CHAPTER 7:
CONCLUSIONS

7. Thesis conclusion

This thesis has shown that ventral forebrain-like neuroprogenitors can be differentiated into cells of an MSN phenotype by NOLZ1-ISL1 and ISL1 transfection. Technical limitations notwithstanding, this thesis presents data which give us cause for optimism. Forced expression of neuron-specific transcription factors may represent an exciting way by which to specify homogeneous populations of neurons from patient-derived iPS cells for high throughput drug screening, high content disease modelling and, potentially, cell-replacement therapies.

***CHAPTER 8:
BIBLIOGRAPHY***

8. References

- Abellan A. & Medina L. (2009) Subdivisions and Derivatives of the Chicken Subpallium Based on Expression of LIM and Other Regulatory Genes and Markers of Neuron Subpopulations During Development. *The Journal of Comparative Neurology* **515**:465–501
- Albin R.L., Reiner A., Anderson K.D. et al. (1992) Preferential loss of striato-external pallidal projection neurons in presymptomatic Huntington's disease *Annals of Neurology* **31**(4), 425–430
- Alvarez-Bolado G., Rosenfeld M.G., And Swanson L.W. (1995) Model of Forebrain Regionalization Based on Spatiotemporal Patterns of POU-III Homeobox Gene Expression, Birthdates, and Morphological Features *The Journal Of Comparative Neurology* **355** 237-295
- An MC, Zhang N, Scott G, et al., (2012) Genetic correction of Huntington's disease phenotypes in induced pluripotent stem cells. *Cell Stem Cell*;**11**(2):253-63. doi: 10.1016/j.stem.2012.04.026. Epub 2012 Jun 28.
- Anderson SA, Qiu M, Bulfone A, et al., (1997) Mutations of the homeobox genes Dlx-1 and Dlx-2 disrupt the striatal subventricular zone and differentiation of late born striatal neurons. *Neuron*. **19**(1):27-37.
- Arlotta P, Molyneaux BJ, Chen J et al (2005) Neuronal subtype-specific genes that control corticospinal motor neuron development in vivo *Neuron*. **45**(2):207-21.
- Arlotta, P., Molyneaux, B.J., Jabaudon, D., et al. (2008) *Ctip2* controls the Differentiation of Medium Spiny Neurons and the Establishment of the Cellular Architecture of the Striatum. *The Journal of Neuroscience* **28**; 622-632
- Ashley Z, Sutherland H, Lanmuller H, et al., (2005) Determination of the chronaxie and rheobase of denervated limb muscles in conscious rabbits. *Artif Organs*;**29**(3):212-5.
- Athanikar JN, Sanchez HB, Osborne TF. (1997). Promoter selective transcriptional synergy mediated by sterol regulatory element binding protein and Sp1: A critical role for the Btd domain of Sp1. *Mol Cell Biol* **17**:5193–5200
- Aubry L, Bugi A, Lefort N, et al., (2008) Striatal progenitors derived from human ES cells mature into DARPP32 neurons in vitro and in quinolinic acid-lesioned rats. *Proc Natl Acad Sci U S A*. **105**(43): 16707-12.
- Backman M, Machon O, Mygland L, et al., (2005) Effects of canonical Wnt signaling on dorso-ventral specification of the mouse telencephalon. *Dev Biol*. **279**(1):155-68.
- Baharvand H, Mehrjardi NZ, Hatami M, et al., (2007) Neural differentiation from human embryonic stem cells in a defined adherent culture condition. *Int J Dev Biol*;**51**(5):371-8.
- Bain G, Kitchens D, Yao M, et al., (1995) Embryonic stem cells express neuronal properties in vitro. *Dev Biol* **168**(2):342-57.
- Baliko L, Csala B, Czopf J. (2004) Suicide in Hungarian Huntington's disease patients. *Neuroepidemiology*;**23**(5):258-60.
- Beal, M. F., Kowall N.W., Ellison D.W., et al. (1986) Replication of the neurochemical characteristics of Huntington's disease by quinolinic acid. *Nature* **321**, 168–171
- Beal, M. F., Ferrante, R. J., Swartz, K. J. et al., (1991) Chronic quinolinic acid lesions in rats closely resemble Huntington's disease. *J. Neurosci*. **11**, 1649–1659
- Bean BP (2007) The action potential in mammalian central neurons *Nature Reviews Neuroscience* **8**, 451-465
- Beaudoin GM 3rd, Lee SH, Singh D, et al., (2012) Culturing pyramidal neurons from the early postnatal mouse hippocampus and cortex. *Nat Protoc*. **7**(9):1741-54. doi: 10.1038/nprot.2012.099. Epub 2012 Aug 30.
- Bennett BD & Bolam JP. (1993) Two populations of calbindin D28k-immunoreactive neurones in the striatum of the rat. *Brain Res*;**610**(2):305-10.
- Berninger, B., Costa, M.R., Koch, U., et al., (2007) Functional Properties of Neurons Derived from *In Vitro* Reprogrammed Postnatal Astroglia *J. Neurosci*., **27**(32):8654–8664

- Bilican B, Serio A, Barmada SJ, et al., (2012) Mutant induced pluripotent stem cell lines recapitulate aspects of TDP-43 proteinopathies and reveal cell-specific vulnerability. *Proc Natl Acad Sci U S A.* **109**(15):5803-8.
- Bolam JP, Wainer BH, Smith AD. (1984) Characterization of cholinergic neurons in the rat neostriatum. A combination of choline acetyltransferase immunocytochemistry, Golgi-impregnation and electron microscopy. *Neuroscience.*; **12**(3):711-8.
- Borello U, Cobos I, Long JE, et al., (2008) FGF15 promotes neurogenesis and opposes FGF8 function during neocortical development. *Neural Dev.* **3**:17.
- Borghese L, Dolezalova D, Opitz T, Haupt S, Leinhaas A et al. (2010) Inhibition of notch signaling in human embryonic stem cell-derived Accelerating iPSC Neuronal Differentiation neural stem cells delays G1/S phase transition and accelerates neuronal differentiation in vitro and in vivo. *Stem Cells* **28**: 955-964.
- Bouyer JJ, Park DH, Joh TH, et al., (1984) Chemical and structural analysis of the relation between cortical inputs and tyrosine hydroxylase-containing terminals in rat neostriatum. *Brain Res.*; **302**(2):267-75.
- Boylan J F and Gudas L J (1992) The level of CRABP-I expression influences the amounts and types of all-trans-retinoic acid metabolites in F9 teratocarcinoma stem cells. *J. Biol. Chem.* **267**: 21486-21491
- Bradbury JW & Vehrenkamp SL (2011) Principles of Animal Communication Second Edition Companion Website Sinauer Associates <http://sites.sinauer.com/animalcommunication2e/chapter08.07.html>
- Bradley CK, Scott HA, Chami O, et al., (2011) Derivation of Huntington's disease-affected human embryonic stem cell lines. *Stem Cells Dev.*; **20**(3):495-502. doi: 10.1089/scd.2010.0120. Epub 2010 Aug 31.
- Butler AK, Uryu K, Chesselet MF. (1998) A role for N-methyl-D-aspartate receptors in the regulation of synaptogenesis and expression of the polysialylated form of the neural cell adhesion molecule in the developing striatum. *Dev Neurosci.*; **20**(2-3):253-62.
- Camnasio S, Delli Carri A, Lombardo A, et al., (2012) The first reported generation of several induced pluripotent stem cell lines from homozygous and heterozygous Huntington's disease patients demonstrates mutation related enhanced lysosomal activity. *Neurobiol Dis.*; **46**(1):41-51. doi: 10.1016/j.nbd.2011.12.042.
- Campbell K. (2003) Dorsal-ventral patterning in the mammalian telencephalon. *Curr Opin Neurobiol.* **13**(1):50-6.
- Carpenter AE, Jones TR, Lamprecht MR, et al., (2006) CellProfiler: image analysis software for identifying and quantifying cell phenotypes. *Genome Biology* **7**:R100. PMID: 17076895
- Casarosa S, Fode C, Guillemot F. (1999) Mash1 regulates neurogenesis in the ventral telencephalon. *Development.* **126**(3):525-34.
- Castiglioni V, Onorati M, Rochon C, et al., (2012) Induced pluripotent stem cell lines from Huntington's disease mice undergo neuronal differentiation while showing alterations in the lysosomal pathway. *Neurobiol Dis.*; **46**(1):30-40. doi: 10.1016/j.nbd.2011.12.032. Epub 2011
- Castro DS, Martynoga B, Parras C, et al., (2011) A novel function of the proneural factor *Ascl1* in progenitor proliferation identified by genome-wide characterization of its targets. *Genes Dev.* **25**(9):930-45.
- Cepeda C, André VM, Yamazaki I, et al., (2008) Differential electrophysiological properties of dopamine D1 and D2 receptor-containing striatal medium-sized spiny neurons. *Eur J Neurosci.* **27**(3):671-82. doi: 10.1111/j.1460-9568.2008.06038.x.
- Chae JI, Kim DW, Lee N, et al., (2012) Quantitative proteomic analysis of induced pluripotent stem cells derived from a human Huntington's disease patient. *Biochem J.*; **446**(3):359-71. doi: 10.1042/BJ20111495.
- Chambers SM, Fasano CA, Papapetrou EP, et al., (2009) Highly efficient neural conversion of human ES and iPS cells by dual inhibition of SMAD signaling. *Nat Biotechnol.* **27**(3):275-80.

- Chan AW, Cheng PH, Neumann A, et al., (2010) Reprogramming Huntington monkey skin cells into pluripotent stem cells. *Cell Reprogram.*;12(5):509-17. doi: 10.1089/cell.2010.0019.
- Chang SL-Y, Chen S-Y, Huang H-H, et al. (2013) Ectopic Expression of Nolz-1 in Neural Progenitors Promotes Cell Cycle Exit/Premature Neuronal Differentiation Accompanying with Abnormal Apoptosis in the Developing Mouse Telencephalon. *PLoS ONE* 8(9): e74975. doi:10.1371/journal.pone.0074975
- Chang, C.-W., Tsai, C.-W., Wang, H.-F., (2004) Identification of a developmentally regulated striatum-enriched zinc-finger gene, Nolz-1, in the mammalian brain *PNAS* 101(8) 2613–2618
- Chauvet S, Cohen S, Yoshida Y, et al., (2007) Gating of Sema3E/PlexinD1 signaling by neuropilin-1 switches axonal repulsion to attraction during brain development. *Neuron.*;56(5):807-22.
- Chavez-Noriega LE, Stevens CF (1994). Increased transmitter release at excitatory synapses produced by direct activation of adenylate cyclase in rat hippocampal slices. *J Neurosci* 14:310–317.
- Chen C, Regehr WG (1997). The mechanism of cAMP mediated enhancement at a cerebellar synapse. *J Neurosci* 17:8687–8694.
- Cheng L, Chong M, Fan W, et al. (2007) Molecular cloning, characterization, and developmental expression of foxp1 in zebrafish. *Dev Genes Evol.* 217(10):699-707.
- Cheng PH, Li CL, Chang YF, et al., (2013) miR-196a ameliorates phenotypes of Huntington disease in cell, transgenic mouse, and induced pluripotent stem cell models. *Am J Hum Genet.*;93(2):306-12. doi: 10.1016/j.ajhg.2013.05.025. Epub 2013 Jun 27.
- Chevalier G, Vacher S, Deniau JM, et al., (1985) Disinhibition as a basic process in the expression of striatal functions. I. The striato-nigral influence on tecto-spinal/tecto-diencephalic neurons. *Brain Res*;334(2):215-26.
- Chiang C, Litingtung Y, Lee E, et al., (1996) Cyclopia and defective axial patterning in mice lacking Sonic hedgehog gene function. *Nature.* 383(6599):407-13.
- Chatzi C, Brade T, Duester G. (2011) Retinoic acid functions as a key GABAergic differentiation signal in the basal ganglia. *PLoS Biol.* 9(4):e1000609. doi: 10.1371/journal.pbio.1000609. Epub 2011 Apr 12.
- Choi J, Costa ML, Mermelstein CS, et al., (1990) MyoD converts primary dermal fibroblasts, chondroblasts, smooth muscle, and retinal pigmented epithelial cells into striated mononucleated myoblasts and multinucleated myotubes. *Proc Natl Acad Sci U S A.*;87(20):7988-92.
- Corbin JG, Gaiano N, Machold RP. et al., (2000) The Gsh2 homeodomain gene controls multiple aspects of telencephalic development. *Development.* 127(23):5007-20.
- Coyle, J. T. & Schwarcz, R. (1976) Lesion of striatal neurones with kainic acid provides a model for Huntington's chorea. *Nature* 263, 244–246
- Danesin C, Peres JN, Johansson M, et al., (2009) Integration of telencephalic Wnt and hedgehog signaling center activities by Foxg1. *Dev Cell.* 16(4):576-87.
- Danjo T, Eiraku M, Muguruma K, et al., (2011) Subregional specification of embryonic stem cell-derived ventral telencephalic tissues by timed and combinatory treatment with extrinsic signals. *J Neurosci.* 31(5):1919-33. doi: 10.1523/JNEUROSCI.5128-10.2011.
- Dasen, J.S., Tice, B.C., Brenner-Morton, S., and Jessell, T.M. (2005). A Hox regulatory network establishes motor neuron pool identity and target-muscle connectivity. *Cell* 123, 477–491.
- Davila J, Chanda S, Ang CE, et al., (2013) Acute reduction in oxygen tension enhances the induction of neurons from human fibroblasts. *J Neurosci Methods.*;216(2):104-9. doi: 10.1016/j.jneumeth.2013.03.020. Epub 2013 Apr 3.
- de Felipe P. (2004) Skipping the co-expression problem: The new 2A “CHYSEL” technology. *Genetic Vaccines and Therapy* 2: 13-18
- De la Monte, S.M., Vonsattel, J-P, Richardson, E.P. (1988) Morphometric Demonstration of Atrophic Changes in the Cerebral Cortex, White Matter, and Neostriatum in Huntington's Disease *Journal of Neuropathology & Experimental Neurology.* 47(5):516-525 [Abstract]

- Deacon TW, Pakzaban P, Isacson O. (1994) The lateral ganglionic eminence is the origin of cells committed to striatal phenotypes: neural transplantation and developmental evidence. *Brain Res.* **668**(1-2):211-9.
- Delli Carri A, Onorati M, Castiglioni V, et al., (2013b) Human pluripotent stem cell differentiation into authentic striatal projection neurons. *Stem Cell Rev.* **9**(4):461-74.
- Deniau JM, Chevalier G. (1985) Disinhibition as a basic process in the expression of striatal functions. II. The striato-nigral influence on thalamocortical cells of the ventromedial thalamic nucleus. *Brain Res.*; **334**(2):227-33.
- Desplats, P.A., Kass, K.E., Gilmartin, T., et al. (2006) Selective deficits in the expression of striatal-enriched mRNAs in Huntington's disease. *Journal of Neurochemistry*, **96**, 743–757
- Desplats, P.A., Lambert, J.R., Thomas, E.A. (2008) Functional roles for the striatal-enriched transcription factor, Bcl11b, in the control of striatal gene expression and transcriptional dysregulation in Huntington's disease *Neurobiology of Disease* **31**; 298–308
- Di Maio L, Squitieri F, Napolitano G, et al. (1993) Suicide risk in Huntington's disease. *J Med Genet* **30**: 293–95.
- DiFiglia M, Aronin N. (1982) Ultrastructural features of immunoreactive somatostatin neurons in the rat caudate nucleus. *J Neurosci.* **2**(9):1267-74.
- Ding JB, Oh WJ, Sabatini BL, et al., (2011) Semaphorin 3E-Plexin-D1 signaling controls pathway-specific synapse formation in the striatum. *Nat Neurosci.*; **15**(2):215-23. doi: 10.1038/nn.3003.
- Dong G, Ferguson JM, Duling AJ, et al., (2011) Modeling pathogenesis of Huntington's disease with inducible neuroprogenitor cells. *Cell Mol Neurobiol.* ; **31**(5):737-47. doi: 10.1007/s10571-011-9679-0. Epub 2011 Mar 31.
- Dunnett S.B., Rosser A.E. (2007) Cell transplantation for Huntington's disease Should we continue? *Brain Res Bull.* **72**(2-3):132-47.
- El-Akabawy G, Medina LM, Jeffries A, et al., (2011) Purmorphamine increases DARPP-32 differentiation in human striatal neural stem cells through the Hedgehog pathway. *Stem Cells Dev.* **20**(11):1873-87. doi: 10.1089/scd.2010.0282.
- Enomoto T, Ohmoto M, Iwata T, et al. (2011) Bcl11b/Ctip2 controls the differentiation of vomeronasal sensory neurons in mice. *J Neurosci.* **31**(28):10159-73.
- Ericson J, Muhr J, Placzek M, et al., (1995) Sonic hedgehog induces the differentiation of ventral forebrain neurons: a common signal for ventral patterning within the neural tube. *Cell.* **81**(5):747-56.
- Ericson J, Thor S, Edlund T et al., (1992) Early stages of motor neuron differentiation revealed by expression of homeobox gene *Islet-1*. *Science.* **256**(5063):1555-60.
- Evans AE, Kelly CM, Precious SV, et al., (2012) Molecular regulation of striatal development: a review. *Anat Res Int.*; **2012**:106529.
- Evans MJ & Kaufman MH. (1981) Establishment in culture of pluripotential cells from mouse embryos. *Nature.* **292**(5819):154-6.
- Faber PW, Alter JR, MacDonald ME, et al., (1999) Polyglutamine-mediated dysfunction and apoptotic death of a *Caenorhabditis elegans* sensory neuron. *Proc Natl Acad Sci U S A* **96**(1):179-84.
- Ferino F, Thierry AM, Saffroy M, et al., (1987) Interhemispheric and subcortical collaterals of medial prefrontal cortical neurons in the rat. *Brain Res.*; **417**(2):257-66.
- Ferland RJ, Cherry TJ, Preware PO. et al. (2003) Characterization of *Foxp2* and *Foxp1* mRNA and protein in the developing and mature brain. *J Comp Neurol.* **460**(2):266-79.
- Ferrante, R. J., Kowall, N. W., Cipolloni, P. B., et al., (1993) Excitotoxin lesions in primates as a model for Huntington's disease: histopathologic and neurochemical characterization. *Exp. Neurol.* **119**, 46–71.
- Feyeux M, Bourgois-Rocha F, Redfern A, et al., (2012) Early transcriptional changes linked to naturally occurring Huntington's disease mutations in neural derivatives of human embryonic stem cells. *Hum Mol Genet.*; **21**(17):3883-95. doi: 10.1093/hmg/dds216. Epub 2012 Jun 7.

- Flores-Hernández J1, Cepeda C, Hernández-Echeagaray E, et al., (2002) Dopamine enhancement of NMDA currents in dissociated medium-sized striatal neurons: role of D1 receptors and DARPP-32. *J Neurophysiol.*; **88**(6):3010-20.
- Fode C, Ma Q, Casarosa S, et al., (2000) A role for neural determination genes in specifying the dorsoventral identity of telencephalic neurons. *Genes Dev.* **14**(1):67-80.
- Folstein S. (1989) Huntington's disease: a disorder of families. *Maryland: The Johns Hopkins University Press.*
- Fonnum F, Gottesfeld Z, Grofova I. (1978) Distribution of glutamate decarboxylase, choline acetyl-transferase and aromatic amino acid decarboxylase in the basal ganglia of normal and operated rats. Evidence for striatopallidal, striatoentopeduncular and striatonigral GABAergic fibres. *Brain Res.*; **143**(1):125-38.
- Frantz G.D., Bohner, A. P. Akers, R. M. et al 1994,. Regulation of the POU Domain Gene SCIP during Cerebral Cortical Development *The Journal of Neuroscience*, **14**(Z): 472485
- Freund TF, Powell JF, Smith AD. (1984) Tyrosine hydroxylase-immunoreactive boutons in synaptic contact with identified striatonigral neurons, with particular reference to dendritic spines. *Neuroscience.*; **13**(4):1189-215.
- Fry DW, Harvey PJ, Keller PR *et al* (2004) Specific inhibition of cyclin-dependent kinase 4/6 by PD 0332991 and associated antitumor activity in human tumor xenografts. *Mol.Cancer Ther.* **3** 1427.
- Fuccillo M, Rallu M, McMahon AP, et al., (2004) Temporal requirement for hedgehog signaling in ventral telencephalic patterning. *Development*; **131**(20):5031-40.
- Furuta Y, Piston DW, Hogan BL. (1997) Bone morphogenetic proteins (BMPs) as regulators of dorsal forebrain development. *Development.* **124**(11):2203-12.
- Gabut M, Samavarchi-Tehrani P, Wang X, et al. (2011) An alternative splicing switch regulates embryonic stem cell pluripotency and reprogramming. *Cell.* **147**(1):132-46.
- Garcia-Dominguez, M., Poquet, C., Garel S., et al. (2003) Ebf gene function is required for coupling neuronal differentiation and cell cycle exit *Development* **130** (24) 6013-6025
- Garel, S., Marín, F., Ve Matté M., et al. (1997) Family of *Ebf/Olf-1*-Related Genes Potentially Involved in Neuronal Differentiation and Regional Specification in the Central Nervous System *Developmental Dynamics* **210**:191–205
- Gerfen C.R., Wilson C.J. (1996) The basal ganglia ,in: L.W. Swanson, A. Bjorklund, T. Hokfelt (Eds.), *Handbook of Chemical Neuroanatomy, Integrated Systems of the CNS, Part III, vol. 12*, Elsevier Science, Amsterdam
- Gerfen CR, Engber TM, Mahan LC, et al., (1990) D1 and D2 dopamine receptor-regulated gene expression of striatonigral and striatopallidal neurons. *Science.*; **250**(4986):1429-32.
- Gerfen CR. (1992) The neostriatal mosaic: multiple levels of compartmental organization in the basal ganglia. *Annu Rev Neurosci.*; **15**:285-320.
- Gerfen, C. R., Young, W. S. (1988). Distribution Of Striatonigral And Striatopallidal Peptidergic Neurons In Both Patch And Matrix Compartments: An In Situ Hybridization Histochemistry And Fluorescent Retrograde Tracing Study. *Brain Res.* **460**:161–167
- Gerfen, C. R., Baimbridge, K. G., Thibault, J. (1987b). The Neostriatal Mosaic. III. Biochemical And Developmental Dissociation Of Dual Nigrostriatal Dopaminergic Systems. *J. Neurosci.* **7**: 3935–3944
- Gerfen, C. R., Herkenham, M., Thibault, J. (1987a). The Neostriatal Mosaic. II. Patch– And Matrix-Directed Mesostriatal Dopaminergic And Non-Dopaminergic Systems. *J. Neurosci.* **7**: 3915–3934
- Gertler TS, Chan CS, Surmeier DJ. (2008) Dichotomous anatomical properties of adult striatal medium spiny neurons. *J Neurosci*; **28**(43):10814-24.
- Giménez-Amaya JM, Graybiel AM. (1990) Compartmental origins of the striatopallidal projection in the primate. *Neuroscience.*; **34**(1):111-26.
- Golden JA, Bracilovic A, McFadden KA, et al., (1999) Ectopic bone morphogenetic proteins 5 and 4 in the chicken forebrain lead to cyclopia and holoprosencephaly. *Proc Natl Acad Sci U S A.* **96**(5):2439-44.

- Graybiel AM, Ragsdale CW Jr. (1978) Histochemically distinct compartments in the striatum of human, monkeys, and cat demonstrated by acetylthiocholinesterase staining. *Proc Natl Acad Sci U S A.*; **75**(11):5723-6.
- Grove EA, Tole S, Limon J, et al., (1998) The hem of the embryonic cerebral cortex is defined by the expression of multiple Wnt genes and is compromised in Gli3-deficient mice. *Development.* **125**(12): 2315-25.
- Gründemann D, Schömig E. (1996) Protection of DNA during preparative agarose gel electrophoresis against damage induced by ultraviolet light. *Biotechniques.* **21**(5):898-903.
- Gunhaga L, Marklund M, Sjödal M, et al., (2003) Specification of dorsal telencephalic character by sequential Wnt and FGF signaling. *Nat Neurosci.* **6**(7):701-7.
- Gusella, J. F., Wexler, N. S., Conneally, P. M., et al. (1983). A polymorphic DNA marker genetically linked to Huntington's disease. *Nature* **306**, 234-238.
- Hagman, J., Belanger, C., Travis, A., et al. (1993) Cloning and functional characterization early B-cell factor, a regulator lymphocyte-specific gene expression *Genes Dev.* **7**: 760-773
- Hagman J, Gutch MJ, Lin H, Grosschedl R (1995). "EBF contains a novel zinc coordination motif and multiple dimerization and transcriptional activation domains". *EMBO J.* **14** (12): 2907–16.
- Hatta, K., Puschel, A. W. and Kimmel, C. B. (1994). Midline signalling in the primordium of the zebrafish anterior central nervous system. *Proc. Natl. Acad. Sci. USA* **91**, 2061-2065.
- Hattori T, McGeer EG, McGeer PL. (1979) Fine structural analysis of the cortico-striatal pathway. *J Comp Neurol.*; **185**(2):347-53.
- HD iPSC Consortium. (2012) Induced pluripotent stem cells from patients with Huntington's disease show CAG-repeat-expansion-associated phenotypes. *Cell Stem Cell.*; **11**(2):264-78. doi: 10.1016/j.stem.2012.04.027. Epub 2012 Jun 28.
- Hébert JM, McConnell SK. (2000) Targeting of cre to the Foxg1 (BF-1) locus mediates loxP recombination in the telencephalon and other developing head structures. *Dev Biol.* **222**(2):296-306.
- Heiman M., Schaefer A., Gong S., et al. (2008) A Translational Profiling Approach for the Molecular Characterization of CNS Cell Types *Cell* **135**, 738–748,
- Heinrich C, Blum R, Gascón S, et al. (2010) Directing Astroglia from the Cerebral Cortex into Subtype Specific Functional Neurons. *PLoS Biol* **8**(5): e1000373. doi:10.1371/journal.pbio.1000373
- Hersch SM, Ciliax BJ, Gutekunst CA, et al., (1995) Electron microscopic analysis of D1 and D2 dopamine receptor proteins in the dorsal striatum and their synaptic relationships with motor corticostriatal afferents. *J Neurosci.*; **15**(7 Pt 2):5222-37.
- Hobert, O., & Westphal, H. (2000) Functions of LIM-homeobox genes *Trends in Genetics* **16**(2);75–83
- Hou P, Li Y, Zhang X, et al., (2013) Pluripotent stem cells induced from mouse somatic cells by small-molecule compounds. *Science.* **341**(6146):651-4.
- Hsiao HY, Chiu FL, Chen CM, et al., (2014) Inhibition of soluble tumor necrosis factor is therapeutic in Huntington's disease. *Hum Mol Genet.*; **23**(16):4328-44. doi: 10.1093/hmg/ddu151. Epub 2014 Apr 3.
- Hsieh-Li HM, Witte DP, Szucsik JC, et al., (1995) Gsh-2, a murine homeobox gene expressed in the developing brain. *Mech Dev.* **50**(2-3):177-86.
- Hutchinson AN, Deng JV, Aryal DK, Wetsel WC, West AE (2012). Differential regulation of MeCP2 phosphorylation in the CNS by dopamine and serotonin. *Neuropsychopharmacology* **37**: 321–337.
- Ichida JK, Blanchard J, Lam K, et al.(2009) A small-molecule inhibitor of tgf-Beta signaling replaces sox2 in reprogramming by inducing nanog. *Cell Stem Cell*; **5**:491–503.
- Ilia, M. Sugiyama, Y. Price J. (2003b) Gender and age related expression of Oct-6 – a POU III domain transcription factor, in the adult mouse brain *Neuroscience Letters* **344**(2), , 138–140

- Imafuku I., Kamei M., Kanazawa I., et al. (1996) POU Transcription Factors Differentially Regulate the D1ADopamine Receptor Gene in Cultured Cells *Biochemical and Biophysical Research Communications* **222**(3), 736–741 [abstract only]
- Inoue F, Kurokawa D, Takahashi M., et al. (2012) Gbx2 Directly Restricts *Otx2* Expression to Forebrain and Midbrain, Competing with Class III POU Factors *Mol. Cell. Biol.* **32**(13) 2618-2627
- Ivkovic S, Ehrlich ME (1999) Expression of the striatal DARPP-32/ARPP-21 phenotype in GABAergic neurons requires neurotrophins in vivo and in vitro. *J Neurosci.* **19**(13):5409-19.
- Ivkovic S., Polonskaia O., Farin I., et al., (1997) Brain-Derived Neurotrophic Factor Regulates Maturation Of The Darpp-32 Phenotype In Striatal Medium Spiny Neurons: Studies In Vivo And In Vitro *Neuroscience* **79**(2), 509–516.
- Jackson GR, Salecker I, Dong X, et al., (1998) Polyglutamine-expanded human huntingtin transgenes induce degeneration of *Drosophila* photoreceptor neurons. *Neuron*; **21**(3):633-42.
- Jaegle M., Mandemakers W., Broos L., et al. (1996) The POU Factor Oct-6 And Schwann Cell Differentiation *Science* **273**. 507-510
- Jaegle M, & Meijer D. (1998) Role of Oct-6 in Schwann cell differentiation. *Microsc Res Tech*; **41**(5):372-8.
- Jeon I, Choi C, Lee N, et al., (2014) In Vivo Roles of a Patient-Derived Induced Pluripotent Stem Cell Line (HD72-iPSC) in the YAC128 Model of Huntington's Disease. *Int J Stem Cells.* ; **7**(1):43-7. doi: 10.15283/ijsc.2014.7.1.43.
- Jeon I, Lee N, Li JY, et al., (2012) Neuronal properties, in vivo effects, and pathology of a Huntington's disease patient-derived induced pluripotent stem cells. *Stem Cells.* **30**(9):2054-62. doi: 10.1002/stem.1135.
- Joannides, A.J., Fiore-H´Erich´E, C., Battersby, A.A., et al. (2007) A Scaleable And Defined System For Generating Neural Stem Cells From Human Embryonic Stem Cells *Stem Cells* **25**; 731-737
- Johnson MA, Weick JP, Pearce RA, et al., (2007) Functional neural development from human embryonic stem cells: accelerated synaptic activity via astrocyte coculture. *J Neurosci.* **27**(12):3069-77.
- Jones EG, Coulter JD, Burton H, et al., (1977) Cells of origin and terminal distribution of corticostriatal fibers arising in the sensory-motor cortex of monkeys. *J Comp Neurol.*; **173**(1):53-80.
- Jones-Villeneuve EM, McBurney MW, Rogers KA, et al., (1982) Retinoic acid induces embryonal carcinoma cells to differentiate into neurons and glial cells. *J Cell Biol.*; **94**(2):253-62.
- Juopperi TA, Kim WR, Chiang CH, et al., (2012) Astrocytes generated from patient induced pluripotent stem cells recapitulate features of Huntington's disease patient cells. *Mol Brain.*; **5**:17. doi: 10.1186/1756-6606-5-17.
- Kaji K, Norrby K, Paca A, et al., (2009): Virus-free induction of pluripotency and subsequent excision of reprogramming factors. *Nature*, **458**:771-775.
- Kaltenbach LS, Romero E, Becklin RR, et al., (2007) Huntingtin interacting proteins are genetic modifiers of neurodegeneration. *PLoS Genet.*; **3**(5):e82.
- Kane NM, Nowrouzi A, Mukherjee S, et al., (2010) Lentivirus-mediated reprogramming of somatic cells in the absence of transgenic transcription factors. *Mol Ther.* **18**(12):2139-45. doi: 10.1038/mt.2010.231. Epub 2010 Oct 26.
- Kawaguchi Y, Wilson CJ, Emson PC. (1990) Projection subtypes of rat neostriatal matrix cells revealed by intracellular injection of biocytin. *J Neurosci.*; **10**(10):3421-38.
- Kawasaki H, Mizuseki K, Nishikawa S, et al., (2000) Induction of midbrain dopaminergic neurons from ES cells by stromal cell-derived inducing activity. *Neuron.* **28**(1):31-40.
- Kaye JA, Finkbeiner S. (2013) Modeling Huntington's disease with induced pluripotent stem cells. *Mol Cell Neurosci.*; **56**:50-64. doi: 10.1016/j.mcn.2013.02.005. Epub 2013 Feb 28.

- Keilani, S., Chandwani, S., Dolios, G., et al., (2012) Egr-1 Induces DARPP-32 Expression in Striatal Medium Spiny Neurons via a Conserved Intragenic Element. *The Journal of Neuroscience*, **32**(20):6808-6818
- Kemp JM, Powell TP. (1971) The structure of the caudate nucleus of the cat: light and electron microscopy. *Philos Trans R Soc Lond B Biol Sci.*; **262**(845):383-401.
- Kim JH, Lee S-R, Li L-H, et al., (2011) High Cleavage Efficiency of a 2A Peptide Derived from Porcine Teschovirus-1 in Human Cell Lines, Zebrafish and Mice. *PLoS ONE* **6**(4): e18556.
- Kita H, Kitai ST. (1988) Glutamate decarboxylase immunoreactive neurons in rat neostriatum: their morphological types and populations. *Brain Res.*; **447**(2):346-52.
- Klapstein GJ, Fisher RS, Zanjani H, et al., (2001) Electrophysiological and morphological changes in striatal spiny neurons in R6/2 Huntington's disease transgenic mice. *J Neurophysiol.* **86**(6):2667-77.
- Ko H.-A., Chen S.-Y., Chen H.-Y., et al. (2013), Cell type-selective expression of the zinc finger-containing gene *Nolz-1/Zfp503* in the developing mouse striatum, *Neuroscience Letters* **548**, 44–49
- Kohtz JD, Baker DP, Corte G et al., (1998) Regionalization within the mammalian telencephalon is mediated by changes in responsiveness to Sonic Hedgehog. *Development.* **125**(24):5079-89.
- Konstantoulas CJ, Parmar M, Li M. (2010) FoxP1 promotes midbrain identity in embryonic stem cell-derived dopamine neurons by regulating Pitx3. *J Neurochem.* **113**(4):836-47.
- Laowtammathron C, Cheng ECh, Cheng PH, et al., (2010) Monkey hybrid stem cells develop cellular features of Huntington's disease. *BMC Cell Biol.*; **11**:12. doi: 10.1186/1471-2121-11-12.
- Le Moine C, Bloch B. (1995) D1 and D2 dopamine receptor gene expression in the rat striatum: sensitive cRNA probes demonstrate prominent segregation of D1 and D2 mRNAs in distinct neuronal populations of the dorsal and ventral striatum. *J Comp Neurol.*; **355**(3):418-26.
- Leid M, Ishmael JE, Avram D, et al. (2004) CTIP1 and CTIP2 are differentially expressed during mouse embryogenesis. *Gene Expr Patterns.* **4**(6):733-9.
- Lerner RP, Trejo Martinez Ldel C, Zhu C et al., (2012) Striatal atrophy and dendritic alterations in a knock-in mouse model of Huntington's disease. *Brain Res Bull.* **87**(6):571-8.
- Lester J, Fink S, Aronin N, et al., (1993) Colocalization of D1 and D2 dopamine receptor mRNAs in striatal neurons. *Brain Res.*; **621**(1):106-10.
- Li M, Pevny L, Lovell-Badge R et al., (1998) Generation of purified neural precursors from embryonic stem cells by lineage selection. *Curr Biol.*; **8**(17):971-4.
- Li S, Weidenfeld J, Morrisey EE. (2004) Transcriptional and DNA binding activity of the Foxp1/2/4 family is modulated by heterotypic and homotypic protein interactions. *Mol Cell Biol* **24**(2):809-22.
- Li W, Zhou H, Abujarour R et al., (2009a) Generation of human-induced pluripotent stem cells in the absence of exogenous Sox2. *Stem Cells.*; **27**(12):2992-3000. doi: 10.1002/stem.240.
- Li Y, Zhang Q, Yin X et al., (2011) Generation of iPSCs from mouse fibroblasts with a single gene, Oct4, and small molecules. *Cell Res.* **21**(1):196-204. doi: 10.1038/cr.2010.142. Epub 2010 Oct 19.
- Liao W-L, Liu FC. (2005) RARbeta isoform-specific regulation of DARPP-32 gene expression: an ectopic expression study in the developing rat telencephalon. *Eur J Neurosci.* **21**(12):3262-8.
- Liao, W.-L., Wang, H.-F., Tsai, H.-C., et al., (2005) Retinoid signaling competence and RARb-mediated gene regulation in the developing mammalian telencephalon. *Dev. Dyn.*, **232**, 887–900.
- Liu JK, Ghattas I, Liu S, et al., (1997) Dlx genes encode DNA-binding proteins that are expressed in an overlapping and sequential pattern during basal ganglia differentiation. *Dev Dyn.* **210**(4):498-512.

- Lobo M.K., Karsten S.L., Gray M., et al. (2006) FACS-array profiling of striatal projection neuron subtypes in juvenile and adult mouse brains. *Nat Neurosci* **9**:443–452.
- Lobo, M.K., Yeh, C., and Yang X.W., (2008) Pivotal Role of Early B-Cell Factor 1 in Development of Striatonigral Medium Spiny Neurons in the Matrix Compartment *Journal of Neuroscience Research* **86**:2134–2146
- Long JE, Swan C, Liang WS, et al.. (2009). Dlx1&2 and Mash1 transcription factors control striatal patterning and differentiation through parallel and overlapping pathways. *J Comp Neurol* **512**:556–572.
- Lorincz MT, Zawistowski VA. (2009) Expanded CAG repeats in the murine Huntington's disease gene increases neuronal differentiation of embryonic and neural stem cells. *Mol Cell Neurosci*; **40**(1):1-13. doi: 10.1016/j.mcn.2008.06.004. Epub 2008 Jun 19.
- Lu B, Palacino J. (2013) A novel human embryonic stem cell-derived Huntington's disease neuronal model exhibits mutant huntingtin (mHTT) aggregates and soluble mHTT-dependent neurodegeneration. *FASEB J.* **27**(5):1820-9. doi: 10.1096/fj.12-219220. Epub 2013 Jan 16.
- Lu KM, Evans SM, Hirano S, et al., (2014) Dual role for Islet-1 in promoting striatonigral and repressing striatopallidal genetic programs to specify striatonigral cell identity. *Proc Natl Acad Sci U S A.* **111**(1):E168-77.
- Luria, V., and Laufer, E. (2007). Lateral motor column axons execute a ternary trajectory choice between limb and body tissues. *Neural Develop.* **2**, 13.
- Ma L, Hu B, Liu Y, et al., (2012) Human embryonic stem cell-derived GABA neurons correct locomotion deficits in quinolinic acid-lesioned mice. *Cell Stem Cell*; **10**(4):455-64.
- Maherali N, Hochedlinger K. (2009) Tgfbeta signal inhibition cooperates in the induction of iPSCs and replaces Sox2 and cMyc. *Curr Biol* ; **19**:1718–1723
- Mangiarini L, Sathasivam K, Seller M, et al., (1996) Exon 1 of the HD gene with an expanded CAG repeat is sufficient to cause a progressive neurological phenotype in transgenic mice. *Cell.* **87**(3):493-506.
- Manuel M, Martynoga B, Yu T, et al., (2010) The transcription factor Foxg1 regulates the competence of telencephalic cells to adopt subpallial fates in mice. *Development.* **137**(3):487-97.
- Manuel MN, Martynoga B, Molinek MD, et al., (2011) The transcription factor Foxg1 regulates telencephalic progenitor proliferation cell autonomously, in part by controlling Pax6 expression levels. *Neural Dev.* **6**:9.
- Marklund M, Sjödal M, Beehler BC, et al., (2004) Retinoic acid signalling specifies intermediate character in the developing telencephalon. *Development.* **131**(17):4323-32.
- Martín-Ibáñez R, Crespo E, Urbán N, et al. (2010). Ikaros-1 couples cell cycle arrest of late striatal precursors with neurogenesis of enkephalinergic neurons. *J Comp Neurol* **518**:329–351.
- Martín-Ibáñez R, Crespo E, Esgleas M et al. (2012) Helios transcription factor expression depends on Gsx2 and Dlx1&2 function in developing striatal matrix neurons. *Stem Cells Dev.* **21**(12):2239-51.
- Martynoga B, Morrison H, Price DJ, et al., (2005) Foxg1 is required for specification of ventral telencephalon and region-specific regulation of dorsal telencephalic precursor proliferation and apoptosis. *Dev Biol.* **283**(1):113-27.
- McGeer, E. G. & McGeer, P. L. (1976). Duplication of biochemical changes of Huntington's chorea by intrastriatal injections of glutamic and kainic acids. *Nature* **263**, 517–519
- McGinty JF (2012) The Many Faces of MeCP2. *Neuropsychopharmacology* **37**, 313–314;
- Messmer K., Shen W., Remington M., et al., (2012) Induction of neural differentiation by the transcription factor NeuroD2 *Int. J. Devl Neuroscience* **30** 105–112
- Miranda TB, Cortez CC, Yoo CB, et al., (2009) DZNep is a global histone methylation inhibitor that reactivates developmental genes not silenced by DNA methylation. *Mol Cancer Ther.*; **8**(6):1579-88. doi: 10.1158/1535-7163.MCT-09-0013. Epub 2009 Jun 9.

- Mizuguchi, H., Xu, Z., Ishii-Watabe, A., et al., (2000) IRES-dependent second gene expression is significantly lower than cap-dependent first gene expression in a bicistronic vector. *Mol. Ther.* **1**, 376–382.
- Mongiati LA, Espósito MS, Lombardi G, Schinder AF (2009) Reliable Activation of Immature Neurons in the Adult Hippocampus. *PLoS ONE* **4**(4): e5320 doi:10.1371/journal.pone.0005320
- Monuki, E. S., Weinmaster, G., Kuhn, R., and Lemke, G. (1989) SCIP:A glial POU domain gene regulated by cyclic AMP. *Neuron*, **3**:783–793.
- Monuki E.S., Kuhn R., Weinmaster G., et al, (1990) Expression and Activity of the POU Transcription Factor SCIP *Science* **249** 1300-1303
- Murray AM, Ryoo HL, Gurevich E, et al., (1994) Localization of dopamine D3 receptors to mesolimbic and D2 receptors to mesostriatal regions of human forebrain. *Proc Natl Acad Sci U S A.*; **91**(23):11271-5.
- Nakamura M., Runko A.P., Sagerström C.G. (2004) A novel subfamily of zinc finger genes involved in embryonic development, *J. Cell. Biochem.* **93** 887–895.
- Niclis J, Trounson AO, Dottori M, et al., (2009) Human embryonic stem cell models of Huntington disease. *Reprod Biomed Online.* **19**(1):106-13.
- Niclis JC, Pinar A, Haynes JM, et al., (2013) Characterization of forebrain neurons derived from late-onset Huntington's disease human embryonic stem cell lines. *Front Cell Neurosci.* ; **7**:37. doi: 10.3389/fncel.2013.00037. eCollection 2013.
- Ohkubo Y, Chiang C, Rubenstein JL. (2002) Coordinate regulation and synergistic actions of BMP4, SHH and FGF8 in the rostral prosencephalon regulate morphogenesis of the telencephalic and optic vesicles. *Neuroscience.*; **111**(1):1-17.
- Okabe S, Forsberg-Nilsson K, Spiro AC, et al., (1996) Development of neuronal precursor cells and functional postmitotic neurons from embryonic stem cells in vitro. *Mech Dev.*; **59**(1):89-102.
- Okita K, Nakagawa M, Hyenjong H, et al., (2008): Generation of mouse induced pluripotent stem cells without viral vectors. *Science*, **322**:949-953.
- Okita, K., Ichisaka, T., and Yamanaka, S. (2007). Generation of germline competent induced pluripotent stem cells. *Nature* **448**, 313–317.
- Ortinou S, Schmich J, Block S, et al., (2010) Effect of 3D-scaffold formation on differentiation and survival in human neural progenitor cells. *Biomed Eng Online.* **9**:70. doi: 10.1186/1475-925X-9-70.
- Ouimet CC, Miller PE, Hemmings HC Jr, et al., (1984) DARPP-32, a dopamine- and adenosine 3':5'-monophosphate-regulated phosphoprotein enriched in dopamine-innervated brain regions. III. Immunocytochemical localization. *J Neurosci.* **4**(1):111-24.
- Oyanagi K., Takeda S., Takahashi H., et al. (1989) A quantitative investigation of the substantia nigra in Huntington's disease. *Ann Neurol* ; **26**:13-19
- Paek H, Gutin G, Hébert JM. (2009) FGF signaling is strictly required to maintain early telencephalic precursor cell survival. *Development.* **136**(14):2457-65.
- Pang ZP, Yang N, Vierbuchen T et al (2011) Induction of human neuronal cells by defined transcription factors. *Nature.* **476**(7359):220-3.
- Park IH, Arora N, Huo H, et al., (2008) Disease-specific induced pluripotent stem cells. *Cell.* **134**(5):877-86. doi: 10.1016/j.cell.2008.07.041. Epub 2008 Aug 7.
- Parker JA, Connolly JB, Wellington C, et al., (2001) Expanded polyglutamines in *Caenorhabditis elegans* cause axonal abnormalities and severe dysfunction of PLM mechanosensory neurons without cell death. *Proc Natl Acad Sci U S A.*; **98**(23):13318-23. Epub 2001 Oct 30.
- Pei Z, Wang B, Chen G, et al., (2011) Homeobox genes Gsx1 and Gsx2 differentially regulate telencephalic progenitor maturation. *Proc Natl Acad Sci U S A.* **108**(4):1675-80.
- Penrod RD, Kourrich S, Kearney E et al., (2011) An embryonic culture system for the investigation of striatal medium spiny neuron dendritic spine development and plasticity. *J Neurosci Methods*; **200**(1):1-13. doi: 10.1016/j.jneumeth.2011.05.029. Epub 2011 Jun 13.

- Perrier AL, Tabar V, Barberi T, et al., (2004) Derivation of midbrain dopamine neurons from human embryonic stem cells. *Proc Natl Acad Sci U S A.*; **101**(34):12543-8. Epub 2004 Aug 13.
- Pfaff S.L., Mendelsohn M, Stewart CL, et al. (1996), Requirement for LIM homeobox gene *Is11* in motor neuron generation reveals a motor neuron-dependent step in interneuron Differentiation *Cell*, **84** Pp. 309–320
- Pfisterer U, Kirkeby A, Torper O, et al., (2011) Direct conversion of human fibroblasts to dopaminergic neurons. *Proc Natl Acad Sci U S A.*; **108**(25):10343-8.
- Pickel VM, Heras A. (1996) Ultrastructural localization of calbindin-D28k and GABA in the matrix compartment of the rat caudate-putamen nuclei. *Neuroscience.*; **71**(1):167-78.
- Pirchio M, Turner JP, Williams SR et al., (1997) Postnatal development of membrane properties and delta oscillations in thalamocortical neurons of the cat dorsal lateral geniculate nucleus. *J Neurosci.* **17**(14):5428-44.
- Planert H, Berger TK, Silberberg G (2013) Membrane Properties of Striatal Direct and Indirect Pathway Neurons in Mouse and Rat Slices and Their Modulation by Dopamine. *PLoS ONE* **8**(3): e57054. doi: 10.1371/journal.pone.0057054
- Porteus MH, Bulfone A, Liu JK, et al., (1994) DLX-2, MASH-1, and MAP-2 expression and bromodeoxyuridine incorporation define molecularly distinct cell populations in the embryonic mouse forebrain. *J Neurosci.* **14**(11 Pt 1):6370-83.
- Pouladi MA, Morton AJ, Hayden MR. (2013) Choosing an animal model for the study of Huntington's disease. *Nat Rev Neurosci*; **14**(10):708-21. doi: 10.1038/nrn3570.
- Prensa L, Giménez-Amaya JM, Parent A. (1998) Morphological features of neurons containing calcium-binding proteins in the human striatum. *J Comp Neurol.*; **390**(4):552-63.
- Rallu M, Machold R, Gaiano N, et al., (2002) Dorsoventral patterning is established in the telencephalon of mutants lacking both Gli3 and Hedgehog signaling. *Development.* **129**(21):4963-74.
- Redies C., Takeichi M., (1996) Cadherins in the Developing Central Nervous System: An Adhesive Code for Segmental and Functional Subdivisions, *Developmental Biology*, **180**, 413-423
- Renner K, Sock E, Bermingham JR Jr, et al. 1996 Expression of the gene for the POU domain transcription factor Tst-1/Oct6 is regulated by an estrogen-dependent enhancer. *Nucleic Acids Res.* **24**(22):4552-7.
- Richfield E.K., Maguire-Zeiss K.A., Vonkeman H.E., et al. (1995) Preferential loss of preproenkephalin versus preprotachykinin neurons from the striatum of Huntington's disease patients *Annals of Neurology* **38**(6), 852–861
- Robbe D, Alonso G, Duchamp F, Bockaert J, Manzoni OJ (2001). Localization and mechanisms of action of cannabinoid receptors at the glutamatergic synapses of the mouse nucleus accumbens. *J Neurosci* **21**: 109–116.
- Romero E, Cha GH, Verstreken P, et al., (2008) Suppression of neurodegeneration and increased neurotransmission caused by expanded full-length huntingtin accumulating in the cytoplasm. *Neuron*; **57**(1):27-40. doi: 10.1016/j.neuron.2007.11.025.
- Ross, C.A. & Tabrizi, S.J. (2011) Huntington's disease: from molecular pathogenesis to clinical treatment. *The Lancet Neurology* **10**(1), 83–98
- Rouso DL, Gaber ZB, Wellik D et al. 2008 Coordinated actions of the forkhead protein Foxp1 and Hox proteins in the columnar organization of spinal motor neurons. *Neuron* **59**(2):226-40.
- Royce GJ. (1982) Lamina origin of cortical neurons which project upon the caudate nucleus: a horseradish peroxidase investigation in the cat. *J Comp Neurol.*; **205**(1):8-29.
- Runko A.P. & Sagerström C.G. (2004) Isolation of *nIz2* and Characterization of Essential Domains in Niz Family Proteins *Journal of Biological Chemistry* **279**, 11917-11925
- Rush AM, Dib-Hajj SD, Waxman SG. (2005) Electrophysiological properties of two axonal sodium channels, Nav1.2 and Nav1.6, expressed in mouse spinal sensory neurones. *J Physiol.*; **564**(Pt 3):803-15. Epub 2005 Mar 10.

- Rushton DJ, Mattis VB, Svendsen CN, et al., (2013) Stimulation of GABA-Induced Ca²⁺ Influx Enhances Maturation of Human Induced Pluripotent Stem Cell-Derived Neurons. *PLoS ONE* **8**(11): e81031.
- Ryan MD, King AM, Thomas GP. (1991) Cleavage of foot-and-mouth disease virus polyprotein is mediated by residues located within a 19 amino acid sequence. *J Gen Virol.* **72** (Pt 11):2727-32.
- Safren N, El Ayadi A, Chang L, et al., (2014) Ubiquitin-1 overexpression increases the lifespan and delays accumulation of Huntingtin aggregates in the R6/2 mouse model of Huntington's disease. *PLoS One.*; **9**(1):e87513. doi: 10.1371/journal.pone.0087513.
- Sambrook, J., Fritsch, E. F., and Maniatis, T. 1989. *Molecular Cloning: A Laboratory Manual*, 2nd ed. Cold Spring Laboratory, Cold Spring Harbor, NY
- Schiffmann SN, Vanderhaeghen JJ. (1993) Adenosine A2 receptors regulate the gene expression of striatopallidal and striatonigral neurons. *J Neurosci.*; **13**(3):1080-7.
- Schneider RA, Hu D, Rubenstein JL, et al., (2001) Local retinoid signaling coordinates forebrain and facial morphogenesis by maintaining FGF8 and SHH. *Development.* **128**(14):2755-67.
- Schneider JW, Gao Z, Li S, et al., (2008) Small-molecule activation of neuronal cell fate. *Nat Chem Biol.*; **4**(7):408-10. doi: 10.1038/nchembio.95. Epub 2008 Jun 15.
- Schöler HR (1991) Octamania: the POU factors in murine development. *Trends Genet.* **7**(10):323-9.
- Schwarcz R, Whetsell WO Jr, Mangano RM. (1983) Quinolinic acid: an endogenous metabolite that produces axon-sparing lesions in rat brain. *Science.*; **219**(4582):316-8.
- Schwarcz, R., Foster, A. C., French, E. D., et al., (1984) Excitotoxic models for neurodegenerative disorders. *Life Sci.* **35**, 19–32 .
- Segal M, Greenberger V, Korkotian E. (2003) Formation of dendritic spines in cultured striatal neurons depends on excitatory afferent activity. *Eur J Neurosci.* **17**(12):2573-85.
- Shanmugalingam S, Houart C, Picker A et al., (2000) *Ace/Fgf8* is required for forebrain commissure formation and patterning of the telencephalon. *Development.* **127**(12):2549-61.
- Shawlot, W. and Behringer, R. R. (1995). Requirement for *Lim1* in head organizer function. *Nature* **374**, 425-430.
- Shimamura K, Hartigan DJ, Martinez S et al., (1995) Longitudinal organization of the anterior neural plate and neural tube. *Development.* **121**(12):3923-33.
- Shimamura K, Rubenstein JL. (1997) Inductive interactions direct early regionalization of the mouse forebrain. *Development*; **124**(14):2709-18.
- Shin S, Mitalipova M, Noggle S, et al., (2006) Long-term proliferation of human embryonic stem cell-derived neuroepithelial cells using defined adherent culture conditions. *Stem Cells.*; **24**(1):125-38. Epub 2005 Aug 11.
- Shin E, Palmer MJ, Li M, et al., (2012) GABAergic neurons from mouse embryonic stem cells possess functional properties of striatal neurons in vitro, and develop into striatal neurons in vivo in a mouse model of Huntington's disease. *Stem Cell Rev.* **8**(2):513-31. doi: 10.1007/s12015-011-9290-2.
- Sholl DA. (1953) Dendritic organization in the neurons of the visual and motor cortices of the cat. *J Anat.*; **87**(4):387-406
- Shu W, Yang H, Zhang L, et al. (2001) Characterization of a new subfamily of winged-helix/forkhead (Fox) genes that are expressed in the lung and act as transcriptional repressors. *J Biol Chem.* **276**(29):27488-97
- Silva J, Barrandon O, Nichols J, et al. (2008) Promotion of Reprogramming to Ground State Pluripotency by Signal Inhibition. *PLoS Biol* **6**(10): e253. doi: 10.1371/journal.pbio.0060253
- Slow EJ, van Raamsdonk J, Rogers D, et al., (2003) Selective striatal neuronal loss in a YAC128 mouse model of Huntington disease. *Hum Mol Genet.* Jul 1; **12**(13):1555-67.

- Sock E., Enderich J., Rosenfeld M.G. et al. (1996) Identification of the Nuclear Localization Signal of the POU Domain Protein Tst-1/Oct6 *The Journal of Biological Chemistry*, **271**, 17512-17518.
- Soldner F, Hockemeyer D, Beard C, et al., (2009) Parkinson's disease patient-derived induced pluripotent stem cells free of viral reprogramming factors. *Cell*, **136**:964-977.
- Spargo E, Everall IP, Lantos PL. (1993) Neuronal loss in the hippocampus in Huntington's disease: a comparison with HIV infection. *J Neurol Neurosurg Psychiatry*; **56**: 487-91.
- Srinivasan P, Zervantonakis IK, Kothapalli CR. (2014) Synergistic effects of 3D ECM and chemogradients on neurite outgrowth and guidance: a simple modeling and microfluidic framework. *PLoS One*; **9**(6):e99640. doi: 10.1371/journal.pone.0099640. eCollection 2014.
- Steffan JS, Agrawal N, Pallos J, et al., (2004) SUMO modification of Huntingtin and Huntington's disease pathology. *Science*. **304**(5667):100-4.
- Steffan JS, Bodai L, Pallos J et al., (2001) Histone deacetylase inhibitors arrest polyglutamine-dependent neurodegeneration in *Drosophila*. *Nature*. **413**(6857):739-43.
- Stenman, Toresson, Campbell (2003) Identification of two distinct progenitor populations in the lateral ganglionic eminence: implications for striatal and olfactory bulb neurogenesis *J Neurosci* **23**;167-174
- Storm EE, Garel S, Borello U et al., (2006) Dose-dependent functions of Fgf8 in regulating telencephalic patterning centers. *Development*. **133**(9):1831-44.
- Strausberg RL, Feingold EA, Grouse LH et al. (2002) Generation and initial analysis of more than 15,000 full-length human and mouse cDNA sequences. *Proc Natl Acad Sci U S A*. **99**(26):16899-903.
- Sturm RA, & Herr W. (1988) The POU domain is a bipartite DNA-binding structure. *Nature*. **336**(6199):601-4.
- Suzuki N., Rohdewohid H., Neuman T., et al. (1990) Oct-6: a POU transcription factor expressed in embryonal stem cells and in the developing brain *The EMBO Journal* **9**:3723 - 3732,
- Szucsik JC, Witte DP, Li H, et al., (1997) Altered forebrain and hindbrain development in mice mutant for the Gsh-2 homeobox gene. *Dev Biol*. **191**(2):230-42.
- Szymczak AL, Workman CJ, Wang Y, et al., (2004) Correction of multi-gene deficiency in vivo using a single 'self-cleaving' 2A peptide-based retroviral vector. *Nat Biotechnol*. **22**(5):589-94.
- Takahashi K, Liu FC, Hirokawa K et al. (2003) Expression of Foxp2, a gene involved in speech and language, in the developing and adult striatum. *J Neurosci Res*. **73**(1):61-72.
- Takahashi K, Tanabe K, Ohnuki M, et al., (2007) Induction of pluripotent stem cells from adult human fibroblasts by defined factors. *Cell*. **131**(5):861-72.
- Takahashi K, Yamanaka S. (2006) Induction of pluripotent stem cells from mouse embryonic and adult fibroblast cultures by defined factors. *Cell*. **126**(4):663-76.
- Tamura, S., Morikawa, Y., Iwanishi, H., et al. (2003) Expression pattern of the winged-helix/forkhead transcription factor Foxp1 in the developing central nervous system *Gene Expression Patterns* **3** 193-197
- Tamura S, Morikawa Y, Iwanishi H, et al. (2004) Foxp1 gene expression in projection neurons of the mouse striatum. *Neuroscience*. ;**124**(2):261-7.
- Tang B., Becanovic K., Desplats P.A., et al. (2012) Forkhead box protein p1 is a transcriptional repressor of immune signaling in the CNS; implications for transcriptional dysregulation in Huntington disease *Hum Mol Genet*. **21**(14):3097-3111.
- Tao W, Lai E. (1992) Telencephalon-restricted expression of BF-1, a new member of the HNF-3/fork head gene family, in the developing rat brain. *Neuron*. **8**(5):957-66.
- Tapscott SJ, Davis RL, Thayer MJ, et al., (1988) MyoD1: a nuclear phosphoprotein requiring a Myc homology region to convert fibroblasts to myoblasts. *Science*. ;**242**(4877):405-11.
- The Huntington's Disease Collaborative Research Group* (1993) A Novel Gene Containing a Trinucleotide Repeat That Is Expanded and Unstable on Huntington's Disease Chromosomes *Cell*, **72**, 971-963.

- Theil T, Alvarez-Bolado G, Walter A, et al., (1999) Gli3 is required for Emx gene expression during dorsal telencephalon development. *Development*. **126**(16):3561-71.
- Thomson JA, Itskovitz-Eldor J, Shapiro SS, et al., (1998a) Embryonic stem cell lines derived from human blastocysts. *Science*. **282**(5391):1145-7.
- Thomson JA, Marshall VS. (1998b) Primate embryonic stem cells. *Curr Top Dev Biol.*; **38**:133-65.
- Tian X, Kai L, Hockberger PE, et al., (2010) MEF-2 regulates activity-dependent spine loss in striatopallidal medium spiny neurons. *Mol Cell Neurosci.*; **44**(1):94-108. doi: 10.1016/j.mcn.2010.01.012.
- Tobler A., Schreiber E. and Fontana A. (1993) The human Oct-6 POU transcription factor lacks the first 50 amino acids of its murine counterpart *Nucleic Acids Research*, , **21**(4) 1043
- Tole S, Ragsdale CW, Grove EA. (2000) Dorsoventral patterning of the telencephalon is disrupted in the mouse mutant extra-toes(J). *Dev Biol*. **217**(2):254-65.
- Toogood PL, Harvey PJ, Repine JT, et al (2005) Discovery of a potent and selective inhibitor of cyclin-dependent kinase 4/6. *J Med Chem*. **48**(7):2388-406.
- Toresson H, Mata de Urquiza A, Fagerström C, et al., (1999) Retinoids are produced by glia in the lateral ganglionic eminence and regulate striatal neuron differentiation. *Development*. **126**(6):1317-26.
- Toresson H, Parmar M, Campbell K. (2000b) Expression of Meis and Pbx genes and their protein products in the developing telencephalon: implications for regional differentiation. *Mech Dev*. **94**(1-2):183-7.
- Toresson H, Potter SS, Campbell K. (2000a) Genetic control of dorsal-ventral identity in the telencephalon: opposing roles for Pax6 and Gsh2. *Development*. **127**(20):4361-71.
- Toresson H. & Campbell K. (2001) A role for Gsh1 in the developing striatum and olfactory bulb of Gsh2 mutant mice *Development* **128**, 4769-4780.
- Tsuchida T, Ensini M, Morton SB et al., 1994 Topographic organization of embryonic motor neurons defined by expression of LIM homeobox genes. *Cell*. **79**(6):957-70.
- Urbán, N., Martín-Ibáñez, R., Herranz, C., et al. (2010) Nolz1 promotes striatal neurogenesis through the regulation of retinoic acid signaling *Neural Development* **5**; 21
- Valerius MT, Li H, Stock JL, et al., (1995) Gsh-1: a novel murine homeobox gene expressed in the central nervous system. *Dev Dyn*. **203**(3):337-51.
- Vanderhaeghen P, Cheng HJ. (2010) Guidance molecules in axon pruning and cell death. *Cold Spring Harb Perspect Biol.*; **2**(6):a001859. doi: 10.1101/cshperspect.a001859. Epub 2010 Apr 21.
- Vierbuchen T, Ostermeier A, Pang ZP, et al., (2010) Direct conversion of fibroblasts to functional neurons by defined factors. *Nature.*; **463**(7284):1035-41. doi: 10.1038/nature08797. Epub 2010 Jan 27.
- Vincent SR, Johansson O. (1983) Striatal neurons containing both somatostatin- and avian pancreatic polypeptide (APP)-like immunoreactivities and NADPH-diaphorase activity: a light and electron microscopic study. *J Comp Neurol.*; **217**(3):264-70.
- Waclaw RR, Wang B, Campbell K. (2004) The homeobox gene Gsh2 is required for retinoid production in the embryonic mouse telencephalon. *Development*. **131**(16):4013-20.
- Walker, F. (2007) Huntington's Disease *Lancet* **369**; 218–28
- Wang B, Lin D, Li C, et al. (2003) Multiple domains define the expression and regulatory properties of Foxp1 forkhead transcriptional repressors. *J Biol Chem* **278**(27):24259-68.
- Wang H.-F. & Liu F.-C. (2001) Developmental Restriction Of The Lim Homeodomain Transcription Factor Islet-1 Expression To Cholinergic Neurons In The Rat Striatum *Neuroscience* **103**(4), 999-1016
- Wichterle H, Turnbull DH, Nery S, et al., (2001) In utero fate mapping reveals distinct migratory pathways and fates of neurons born in the mammalian basal forebrain. *Development*. **128**(19):3759-71.

- Wilson CJ, Groves PM. (1980) Fine structure and synaptic connections of the common spiny neuron of the rat neostriatum: a study employing intracellular inject of horseradish peroxidase. *J Comp Neurol.* ;**194**(3):599-615.
- Wilson, C. J. (1987). Morphology and synaptic connections of crossed corticostriatal neurons in the rat. *J. Comp. Neurol.* **263**: 567-80
- Wolf M., Lommes P., Sock E., et al. (2009) Replacement of related POU transcription factors leads to severe defects in mouse forebrain development *Developmental Biology* **332** 418–428
- Woltjen K, Michael IP, Mohseni P, D. et al. (2009), piggyBac transposition reprograms fibroblasts to induced pluripotent stem cells. *Nature*, **458**:766-770.
- Xuan S, Baptista CA, Balas G, et al., (1995) Winged helix transcription factor BF-1 is essential for the development of the cerebral hemispheres. *Neuron*. **14**(6):1141-52.
- Yamamizu, K. Piao, Y. Sharov, A.A. et al., (2013) Identification of Transcription Factors for Lineage-Specific ESC Differentiation *Stem Cell Reports* **1** 545–559
- Yang N, Zuchero JB, Ahlenius H, et al., (2013) Generation of oligodendroglial cells by direct lineage conversion. *Nat Biotechnol.*;**31**(5):434-9. doi: 10.1038/nbt.2564. Epub 2013 Apr 14.
- Yang SH, Cheng PH, Banta H, et al., (2008) Towards a transgenic model of Huntington's disease in a non-human primate. *Nature*. **453**(7197):921-4. doi: 10.1038/nature06975. Epub 2008 May 18.
- Yang Y, Jiao J, Gao R, et al., (2013) Direct conversion of adipocyte progenitors into functional neurons. *Cell Reprogram.*;**15**(6):484-9. doi: 10.1089/cell.2013.0013. Epub 2013 Nov 4.
- Yasuhara N, Yamagishi R, Arai Y, et al. (2013) Importin alpha subtypes determine differential transcription factor localization in embryonic stem cells maintenance. *Dev Cell*. **26**(2):123-35.
- Ye W, Shimamura K, Rubenstein JL, Hynes MA, Rosenthal A. (1998) FGF and Shh signals control dopaminergic and serotonergic cell fate in the anterior neural plate. *Cell.*;**93**(5):755-66.
- Ying QL, Stavridis M, Griffiths D et al., (2003) Conversion of embryonic stem cells into neuroectodermal precursors in adherent monoculture. *Nat Biotechnol.*;**21**(2):183-6. Epub 2003 Jan 13.
- Yun K, Fischman S, Johnson J, et al., (2002) Modulation of the notch signaling by Mash1 and Dlx1/2 regulates sequential specification and differentiation of progenitor cell types in the subcortical telencephalon. *Development*. **129**(21):5029-40.
- Yun K, Potter S, Rubenstein JL. (2001) Gsh2 and Pax6 play complementary roles in dorsoventral patterning of the mammalian telencephalon. *Development*. **128**(2):193-205.
- Yu-Taeger L, Petrasch-Parwez E, Osmand AP, et al., (2012) A novel BACHD transgenic rat exhibits characteristic neuropathological features of Huntington disease. *J Neurosci*;**32**(44):15426-38. doi: 10.1523/JNEUROSCI.1148-12.2012.
- Zhang N, An MC, Montoro D, et al., (2010) Characterization of Human Huntington's Disease Cell Model from Induced Pluripotent Stem Cells. *PLoS Curr.*;**2**:RRN1193. doi: 10.1371/currents.RRN1193.
- Zhang, Y., Pak, C., Han, Y., et al., (2013) Rapid Single-Step Induction of Functional Neurons from Human Pluripotent Stem Cells. *Neuron*. **78**(5): 785–798.
- Zhou H, Wu S, Joo JY, et al., (2009) Generation of induced pluripotent stem cells using recombinant proteins. *Cell Stem Cell*, **4**:381-384.
- Zwart R., Broos L., Grosveld G., et al. (1996) The restricted expression pattern of the POU factor Ott-6 during early development of the mouse nervous system *Mechanisms of Development* **54**185-194

CHAPTER 9:
APPENDIX

9. Appendix

9.1 Sequencing alignments

Line breaks indicate where sequencing alignments have been run off separate primers in order to obtain accurate sequencing data for each gene.

9.1.1.1 Homo sapiens ISL LIM homeobox 1 (ISL1), mRNA

Sequence ID: [ref|NM_002202.2|](#)

```

Query 1 ATGGGAGACATGGGAGATCCACCaaaaaaaaaCGTCTGATTTCCTATGTGTTGGTTGC 60
      |
      |
Sbjct 549 ATGGGAGACATGGGAGATCCACCAAAAAAAAAACGTCTGATTTCCTATGTGTTGGTTGC 608
Query 61 GGCAATCAGATTCACGATCAGTATATCTGAGGGTTCTCCGATTTGGAATGGCATGCG 120
      |
      |
Sbjct 609 GGCAATCAGATTCACGATCAGTATATCTGAGGGTTCTCCGATTTGGAATGGCATGCG 668
Query 121 GCATGTTTGAATGTGCGGAGTGAATCAGTATTTGGACGAGAGCTGTACATGCTTTGTT 180
      |
      |
Sbjct 669 GCATGTTTGAATGTGCGGAGTGAATCAGTATTTGGACGAGAGCTGTACATGCTTTGTT 728
Query 181 AGGGATGGGAAAACCTACTGTAAAAGAGATTATATCAGGTTGTACGGGATCAAATGCGCC 240
      |
      |
Sbjct 729 AGGGATGGGAAAACCTACTGTAAAAGAGATTATATCAGGTTGTACGGGATCAAATGCGCC 788
Query 241 AAGTGCAGCATCGGCTTCAGCAAGAACGACTTCGTGATGCGTGCCCGCTCCAAGGTGTAT 300
      |
      |
Sbjct 789 AAGTGCAGCATCGGCTTCAGCAAGAACGACTTCGTGATGCGTGCCCGCTCCAAGGTGTAT 848
Query 301 CACATCGAGTGTTCGCTGTGTGGCTGCAGCCGCCAGCTCATCCCTGGGGACGAATTT 360
      |
      |
Sbjct 849 CACATCGAGTGTTCGCTGTGTGGCTGCAGCCGCCAGCTCATCCCTGGGGACGAATTT 908
Query 361 GCGCTTCGGGAGGACGGTCTCTTCTGCCGAGCAGACCACGATGTGGTGGAGAGGGCCAGT 420
      |
      |
Sbjct 909 GCGCTTCGGGAGGACGGTCTCTTCTGCCGAGCAGACCACGATGTGGTGGAGAGGGCCAGT 968
Query 421 CTAGGCGCTGGCGACCCGCTCAGTCCCTGCATCCAGCGCGGCCACTGCAAATGGCAGCG 480
      |
      |
Sbjct 969 CTAGGCGCTGGCGACCCGCTCAGTCCCTGCATCCAGCGCGGCCACTGCAAATGGCAGCG 1028
Query 481 GAGCCCATCTCCGCCAGGCAGCCGGCCCTGCGGCCCCACGTCCACAAGCAGCCGAGAAG 540
      |
      |
Sbjct 1029 GAGCCCATCTCCGCCAGGCAGCCGGCCCTGCGGCCCCACGTCCACAAGCAGCCGAGAAG 1088
Query 541 ACCACCCGCTGCGGACTGTGCTGAACGAGAAGCAGCTGCACACCTTGCGGACCTGTAC 600
      |
      |
Sbjct 1089 ACCACCCGCTGCGGACTGTGCTGAACGAGAAGCAGCTGCACACCTTGCGGACCTGTAC 1148
Query 601 GCCGCAAACCCGCGCCAGATGCGCTCATGAAGGAGCAACTGGTAGAGATGACGGGCTC 660
      |
      |

```

```

Sbjct  1149  GCCGCAAACCCGCGGCCAGATGCGCTCATGAAGGAGCAACTGGTAGAGATGACGGGCCTC 1208
Query  661  AGTCCCCGTGTGATCCGGGTCTGGTTTCAAACAAGCGGTGCAAGGACAAGAAGCGAAGC 720
      |
      |
Sbjct  1209  AGTCCCCGTGTGATCCGGGTCTGGTTTCAAACAAGCGGTGCAAGGACAAGAAGCGAAGC 1268
Query  721  ATCATGATGAAGCAACTCCAGCAGCAGCAGCCCAATGACAAAATAATATCCAGGGGATG 780
      |
      |
Sbjct  1269  ATCATGATGAAGCAACTCCAGCAGCAGCAGCCCAATGACAAAATAATATCCAGGGGATG 1328
Query  781  ACAGGAACTCCCATGGTGGCTGCCAGTCCAGAGAGACACGACGGTGGCTTACAGGCTAAC 840
      |
      |
Sbjct  1329  ACAGGAACTCCCATGGTGGCTGCCAGTCCAGAGAGACACGACGGTGGCTTACAGGCTAAC 1388
Query  841  CCAGTGAAGTACAAAGTTACCAGCCACCTTGAAAGTACTGAGCGACTTCGCCTTGCGAG 900
      |
      |
Sbjct  1389  CCAGTGAAGTACAAAGTTACCAGCCACCTTGAAAGTACTGAGCGACTTCGCCTTGCGAG 1448
Query  901  AGTGACATAGATCAGCCTGCTTTTCAGCAACTGGTCAATTTTTCAGAAGGAGACCGGGC 960
      |
      |
Sbjct  1449  AGTGACATAGATCAGCCTGCTTTTCAGCAACTGGTCAATTTTTCAGAAGGAGACCGGGC 1508
Query  961  TCTAATCCACTGGCAGTGAAGTAGCATCAATGTCTCTCAACTTCCAGATACACCTAAC 1020
      |
      |
Sbjct  1509  TCTAATCCACTGGCAGTGAAGTAGCATCAATGTCTCTCAACTTCCAGATACACCTAAC 1568
Query  1021  AGCATGGTAGCCAGTCTATTGAGGC 1046
      |
      |
Sbjct  1569  AGCATGGTAGCCAGTCTATTGAGGC 1594

```

9.1.1.2 Re-cloned Homo sapiens ISL LIM homeobox 1 (ISL1), mRNA

Sequence ID: [ref|NM_002202.2|](#) Length: 2729 Number of Matches: 1

```

Query  50  ATGGGAGACATGGGAGATCCACCaaaaaaaaaCGTCTGATTTCCCTATGTGTTGGTTGC 109
      |
      |
Sbjct  549  ATGGGAGACATGGGAGATCCACCAAAAAAAAAAACGTCTGATTTCCCTATGTGTTGGTTGC 608
Query  110  GGCAATCAGATTCACGATCAGTATATTTCTGAGGGTTTCTCCGATTTGGAATGGCATGCG 169
      |
      |
Sbjct  609  GGCAATCAGATTCACGATCAGTATATTTCTGAGGGTTTCTCCGATTTGGAATGGCATGCG 668
Query  170  GCATGTTTGAATGTGCGGAGTGTAATCAGTATTTGGACGAGAGCTGTACATGCTTTGTT 229
      |
      |
Sbjct  669  GCATGTTTGAATGTGCGGAGTGTAATCAGTATTTGGACGAGAGCTGTACATGCTTTGTT 728
Query  230  AGGGATGGGAAAACCTACTGTAAAAGAGATTATATCAGGTTGTACGGGATCAAATGCGCC 289
      |
      |
Sbjct  729  AGGGATGGGAAAACCTACTGTAAAAGAGATTATATCAGGTTGTACGGGATCAAATGCGCC 788
Query  290  AAGTGCAGCATCGGCTTCAGCAAGAACGACTTCGTGATGCGTGCCCGCTCCAAGGTGTAT 349
      |
      |
Sbjct  789  AAGTGCAGCATCGGCTTCAGCAAGAACGACTTCGTGATGCGTGCCCGCTCCAAGGTGTAT 848
Query  350  CACATCGAGTGTTCGCTGTGTGGCTGCAGCCGCCAGCTCATCCCTGGGGACGAATTT 409
      |
      |
Sbjct  849  CACATCGAGTGTTCGCTGTGTGGCTGCAGCCGCCAGCTCATCCCTGGGGACGAATTT 908
Query  410  GCGCTTCGGGAGGACGGTCTCTTCTGCCGAGCAGACCAGATGTGGTGGAGAGGGCCAGT 469

```

```

|||||
Sbjct 909 GCGCTTCGGGAGGACGGTCTCTTCTGCCGAGCAGACCACGATGTGGTGGAGAGGGCCAGT 968
Query 470 CTAGGCGCTGGCGACCCGCTCAGTCCCCTGCATCCAGCGCGGCCACTGCAAATGGCAGCG 529
|||||
Sbjct 969 CTAGGCGCTGGCGACCCGCTCAGTCCCCTGCATCCAGCGCGGCCACTGCAAATGGCAGCG 1028
Query 530 GAGCCCATCTCCGCCAGGCAGCCGGCCCTGCGGCCCCACGTCCACAAGCAGCCGGAGAAG 589
|||||
Sbjct 1029 GAGCCCATCTCCGCCAGGCAGCCAGCCCTGCGGCCCCACGTCCACAAGCAGCCGGAGAAG 1088
Query 590 ACCACCCGCGTGGGACTGTGCTGAACGAGAAGCAGCTGCACACCTTGGCGACCTGTCTAC 649
|||||
Sbjct 1089 ACCACCCGCGTGGGACTGTGCTGAACGAGAAGCAGCTGCACACCTTGGCGACCTGTCTAC 1148
Query 650 GCCGCAAACCCGCGGCCAGATGCGCTCATGAAGGAGCAACTGGTAGAGATGACGGGCCTC 709
|||||
Sbjct 1149 GCCGCAAACCCGCGGCCAGATGCGCTCATGAAGGAGCAACTGGTAGAGATGACGGGCCTC 1208
Query 1 TCGGGCCCCACGTCCACAAGCAGCCGGAGAAGACCACCCGCGTGGGACTGTGCTGAACG 60
|||||
Sbjct 1057 TCGGGCCCCACGTCCACAAGCAGCCGGAGAAGACCACCCGCGTGGGACTGTGCTGAACG 1116
Query 61 AGAAGCAGCTGCACACCTTGGCGACCTGCTACGCCGCAAACCCGCGGCCAGATGCGCTCA 120
|||||
Sbjct 1117 AGAAGCAGCTGCACACCTTGGCGACCTGCTACGCCGCAAACCCGCGGCCAGATGCGCTCA 1176
Query 121 TGAAGGAGCAACTGGTAGAGATGACGGGCCTCAGTCCCCGTGTGATCCGGGTCTGGTTTC 180
|||||
Sbjct 1177 TGAAGGAGCAACTGGTAGAGATGACGGGCCTCAGTCCCCGTGTGATCCGGGTCTGGTTTC 1236
Query 181 AAAACAAGCGGTGCAAGGACAAGAAGCGAAGCATCATGATGAAGCAACTCCAGCAGCAGC 240
|||||
Sbjct 1237 AAAACAAGCGGTGCAAGGACAAGAAGCGAAGCATCATGATGAAGCAACTCCAGCAGCAGC 1296
Query 241 AGCCCAATGACAAAATAATATCCAGGGGATGACAGGAACTCCCATGGTGGCTGCCAGTC 300
|||||
Sbjct 1297 AGCCCAATGACAAAATAATATCCAGGGGATGACAGGAACTCCCATGGTGGCTGCCAGTC 1356
Query 301 CAGAGAGACACGACGGTGGCTTACAGGCTAACCAGTGGAAGTACAAAGTTACCAGCCAC 360
|||||
Sbjct 1357 CAGAGAGACACGACGGTGGCTTACAGGCTAACCAGTGGAAGTACAAAGTTACCAGCCAC 1416
Query 361 CTTGGAAAGTACTGAGCGACTTCGCCTTGCAGAGTGACATAGATCAGCCTGCTTTTCAGC 420
|||||
Sbjct 1417 CTTGGAAAGTACTGAGCGACTTCGCCTTGCAGAGTGACATAGATCAGCCTGCTTTTCAGC 1476
Query 421 AACTGGTCAATTTTTCAGAAGGAGGACCGGGCTCTAATTCCTACTGGCAGTGAAGTAGCAT 480
|||||
Sbjct 1477 AACTGGTCAATTTTTCAGAAGGAGGACCGGGCTCTAATTCCTACTGGCAGTGAAGTAGCAT 1536
Query 481 CAATGTCCTCTCAACTTCCAGATACACCTAACAGCATGGTAGCCAGTCCTATTGAGGCA 539
|||||
Sbjct 1537 CAATGTCCTCTCAACTTCCAGATACACCTAACAGCATGGTAGCCAGTCCTATTGAGGCA 1595

```

9.1.2 Homo sapiens zinc finger protein 503 (ZNF503), mRNA

Sequence ID: [ref|NM_032772.4|](#) Length: 3198 Number of Matches: 1


```
|||||
Sbjct 1164 CACGGGGCTGGCACACGGCCGGATTAGCTGCGGCGGGGATTAATGTGGATGTGAACCA 1223
Query 541 GCATCCGGATGGGGGGCCGGGAGGCAAGGCTCTGGGCTCGGACTGCGGCGGTTCATCGGG 600
|||||
Sbjct 1224 GCATCCGGATGGGGGGCCGGGAGGCAAGGCTCTGGGCTCGGACTGCGGCGGTTCATCGGG 1283
Query 601 CTCCAGCTCCGGCTCCGGCCCCAGCGCGCCACCTCCTCCTCAGTGTGGGCTCTGGGCT 660
|||||
Sbjct 1284 CTCCAGCTCCGGCTCCGGCCCCAGCGCGCCACCTCCTCCTCAGTGTGGGCTCTGGGCT 1343
Query 661 GGTGGTCCCCTGTACCCCTACAAGCCGGGCCAGACAGTGTCCCTCTGCCTCCCGCGGG 720
|||||
Sbjct 1344 GGTGGTCCCCTGTACCCCTACAAGCCGGGCCAGACAGTGTCCCTCTGCCTCCCGCGGG 1403
Query 721 TATGACCTACCCAGGCAGCCTGGCCGGGGCCTACGCCGGCTACCCGCCCCAGTTCCCTGCC 780
|||||
Sbjct 1404 TATGACCTACCCAGGCAGCCTGGCCGGGGCCTACGCCGGCTACCCGCCCCAGTTCCCTGCC 1463
Query 1 AGCCTGGCCGGGGCCTACGCCGGCTACCCGCCCCAGTTCCCTGCCACACGGCGTGGCACTT 60
|||||
Sbjct 1420 AGCCTGGCCGGGGCCTACGCCGGCTACCCGCCCCAGTTCCCTGCCACACGGCGTGGCACTT 1479
Query 61 GACCCACCAAGCCGGGCAGCCTGGTGGGGGCGCAGCTGGCGGCGGCCGCGCCGGGTCT 120
|||||
Sbjct 1480 GACCCACCAAGCCGGGCAGCCTGGTGGGGGCGCAGCTGGCGGCGGCCGCGCCGGGTCT 1539
Query 121 CTGGGCTGCAGTAAGCCGGCCGGCTCCAGTCCTTTGGCCGGAGCGTCTCCGCCGTCCGTG 180
|||||
Sbjct 1540 CTGGGCTGCAGTAAGCCGGCCGGCTCCAGTCCTTTGGCCGGAGCGTCTCCGCCGTCCGTG 1599
Query 181 ATGACAGCCAGTTTGTGCCGGGACCCTTACTGCCTCAGCTACCACTGCGCTAGCCACCTG 240
|||||
Sbjct 1600 ATGACAGCCAGTTTGTGCCGGGACCCTTACTGCCTCAGCTACCACTGCGCTAGCCACCTG 1659
Query 241 GCAGGGGCGGCGGCCGCCAGCGCTTCTTGCGCACATGATCCGGCTGCTGCGGCTGCGGCG 300
|||||
Sbjct 1660 GCAGGGGCGGCGGCCGCCAGCGCTTCTTGCGCACATGATCCGGCTGCTGCGGCTGCGGCG 1719
Query 301 CTGAAGTCCGATAACCCGCTGGTGTACCCACGCACCCGCTGCACGGTGTGCACTCCTCG 360
|||||
Sbjct 1720 CTGAAGTCCGATAACCCGCTGGTGTACCCACGCACCCGCTGCACGGTGTGCACTCCTCG 1779
Query 361 CTAACGGCCGCGCGGCTGCTGGCGCCACACCGCCCTCCCTGGCCGGCCACCCCTCTAC 420
|||||
Sbjct 1780 CTAACGGCCGCGCGGCTGCTGGCGCCACACCGCCCTCCCTGGCCGGCCACCCCTCTAC 1839
Query 421 CCCTACGGCTTTATGCTCCCTAACGACCCACTCCCCACATCTGCAACTGGGTGTCGGCC 480
|||||
Sbjct 1840 CCCTACGGCTTTATGCTCCCTAACGACCCACTCCCCACATCTGCAACTGGGTGTCGGCC 1899
Query 481 AACGGGCCGTGCGACAAGCGCTTCGCCACGTCCGAAGAGCTGCTGAGCCACTTGGCGGACC 540
|||||
Sbjct 1900 AACGGGCCGTGCGACAAGCGCTTCGCCACGTCCGAAGAGCTGCTGAGCCACTTGGCGGACC 1959
Query 541 CATAAGGCATTTCCCGGGACAGACAACTGCTGTGGGCTACCCAGCTCGTCTCTCTG 600
|||||
Sbjct 1960 CATAAGGCATTTCCCGGGACAGACAACTGCTGTGGGCTACCCAGCTCGTCTCTCTG 2019
Query 601 GCCAGCGCTGCCGCGGCCCATGGCTTGCCACATGCACATCCCCACCTCGGGCGCACCG 660
```

```

|||||
Sbjct 2020 GCCAGCGCTGCCGCGCCGCCATGGCTTGCCACATGCACATCCCCACCTCGGGCGCACCG 2079
Query 661 GGCAGCCCTGGGACGCTGGCGCTGCGCAGCCCCACCACGCGCTGGGACTCAGCAGCCGC 720
|||||
Sbjct 2080 GGCAGCCCTGGGACGCTGGCGCTGCGCAGCCCCACCACGCGCTGGGACTCAGCAGCCGC 2139
Query 721 TACCACCCCTACTCCAAGAGCCCGCTTCCCACGCTGGCGCCCCCGTGCCGGTGCCCGCC 780
|||||
Sbjct 2140 TACCACCCCTACTCCAAGAGCCCGCTTCCCACGCTGGCGCCCCCGTGCCGGTGCCCGCC 2199
Query 781 GCCACCGGACCGTACTACTCCCCTACGCCCTCTACGGACAGAGACTGACCACCGCCTCG 840
|||||
Sbjct 2200 GCCACCGGACCGTACTACTCCCCTACGCCCTCTACGGACAGAGACTGACCACCGCCTCG 2259
Query 841 GCGCTGGGGTATCAG 855
|||||

```

Sbjct 2260 GCGCTGGGGTATCAG 2274

Query **L G C S K P A G S S P L A G A S P P S V**

Subject **L G C S K P A G S S P L A G A S P P S V**

MSTAPLSALRSSKHSGGGGGGGGGGADPAWTSALSGNSSGPGPGSSPAGSTKPFVHAVPPSDPLRQANR
LPIKVLKMLTARTGHI LHPEYLQPLPSTPVSPIELDAKKSPLALLAQTC SQIGKPDSPSSKLSSVASNGG
GAGGAGGGAAGDKDTKSGPLKLSDIGVEDKSSFKPYSKPGSDKKEPGGGGGGGGGGGGGGGVSSEKSGFR
VPSATCQPFTRTGSPSSASACSPGMLSSAGGAPEGKDDKDDTDVGGGGKGTGGASAEGGPTGLAHGRI
SCGGGINVDVNQHPDGGPGKALGSDCGSSGSSSGSPAPTSSSVLGSGLVAPVSPYKPGQTVFPLPPA
GMTYPGSLAGAYAGYPPQFLPHGVALDPTKPGSLVGAQLAAAAAGS **LGCSKPAAGSSPLAGASPPSV**MTASL
CRDPYCLSYHCASHLAGAAAASASCAHDPAAAAAALKSGYPLVYPTHPLHGVSLSITAAAAGATPPSLAG
HPLYPYGFMLPNDPLPHICNWSANGPCDKRFATSEELLSHLRTHTAFFPGTDKLLSGYPSSSLASAAAAA
MACHMHIPTSGAPGSPGTLALRSPHHALGLSSRYHPYKSKSPLPTPGAPVPVPAATGPYYSPYALYGQLTT
ASALGYQ

9.1.3 Homo sapiens zinc finger protein 503, mRNA (cDNA clone IMAGE:2967616), complete cds

```

Query 52 CTGATACCCCAGCGCCGAGGCGGTGGTCAGTCTCTGTCCGTAGAGGGCGTAGGGGGAGTA 111
|||||
Sbjct 1185 CTGATACCCCAGCGCCGAGGCGGTGGTCAGTCTCTGTCCGTAGAGGGCGTAGGGGGAGTA 1126
Query 112 GTACGGTCCGGTGGCGGGCGGCACCGGCACGGGGGCCAGGCGTGGGAAGCGGGCTCTT 171
|||||
Sbjct 1125 GTACGGTCCGGTGGCGGGCGGCACCGGCACGGGGGCCAGGCGTGGGAAGCGGGCTCTT 1066
Query 172 GGAGTAGGGGTGGTAGCGGCTGCTGAGTCCCAGCGCGTGGTGGGGGCTGCGCAGCGCCAG 231
|||||
Sbjct 1065 GGAGTAGGGGTGGTAGCGGCTGCTGAGTCCCAGCGCGTGGTGGGGGCTGCGCAGCGCCAG 1006
Query 232 CGTCCCAGGGCTGCCCGGTGCGCCCGAGGTGGGGATGTGCATGTGGCAAGCCATGGCGGC 291
|||||
Sbjct 1005 CGTCCCAGGGCTGCCCGGTGCGCCCGAGGTGGGGATGTGCATGTGGCAAGCCATGGCGGC 946
Query 292 CGCGGCAGCGCTGGCCAGAGACGACGAGCTGGGGTAGCCCGACAGCAGTTTGTCTGTCCC 351

```

```

|||||
Sbjct  945  CGCGGCAGCGCTGGCCAGAGACGACGAGCTGGGGTAGCCCGACAGCAGTTTGTCTGTCCC 886
Query  352  GGGAAATGCCGTATGGGTCCGCAAGTGGCTCAGCAGCTCTTCGGACGTGGCGAAGCGCTT 411
|||||
Sbjct  885  GGGAAATGCCGTATGGGTCCGCAAGTGGCTCAGCAGCTCTTCGGACGTGGCGAAGCGCTT 826
Query  412  GTCGCACGGCCCGTTGGCCGACACCCAGTTGCAGATGTGGGGGAGTGGGTCGTTAGGGAG 471
|||||
Sbjct  825  GTCGCACGGCCCGTTGGCCGACACCCAGTTGCAGATGTGGGGGAGTGGGTCGTTAGGGAG 766
Query  472  CATAAAGCCGTAGGGGTAGAGGGGTGGCCGGCCAGGGAGGGCGAGGGGTTCGGCTTCCC 531
|||||
Sbjct  765  CATAAAGCCGTAGGGGTAGAGGGGTGGCCGGCCAGGGAGGGCGAGGGGTTCGGCTTCCC 706
Query  532  GATCTGCGAACATGTTTGCGCCAACAGCGCCAGCGGCTCTTCTTGGCATCGAGCTCGAT 591
|||||
Sbjct  705  GATCTGCGAACATGTTTGCGCCAACAGCGCCAGCGGCTCTTCTTGGCATCGAGCTCGAT 646
Query  592  GGGGCTGACCGGCGTGAAGGCAGGGGCTGCAGGTAAGTGGGTCGAAAATGTGGCCAGT 651
|||||
Sbjct  645  GGGGCTGACCGGCGTGAAGGCAGGGGCTGCAGGTAAGTGGGTCGAAAATGTGGCCAGT 586
Query  652  TCGTGCCGTCAGCATCTTACGACCTTGATTGGCAGGCGGTTGGCCTGGCGCAGGGGTC 711
|||||
Sbjct  585  TCGTGCCGTCAGCATCTTACGACCTTGATTGGCAGGCGGTTGGCCTGGCGCAGGGGTC 526
Query  712  AGAGGGGGGCACGGCGTGCACAAAAGGCTTGGTGTGCCGGCCGGGACGAGCCTGGGCC 771
|||||
Sbjct  525  AGAGGGGGGCACGGCGTGCACAAAAGGCTTGGTGTGCCGGCCGGGACGAGCCTGGGCC 466
Query  772  GGGGCCGGAGCTATTTCCAGAGAGCGCGCTGGTCCAGGCAGGGTCTGCAccgcgcgctcc 831
|||||
Sbjct  465  GGGGCCGGAGCTATTTCCAGAGAGCGCGCTGGTCCAGGCAGGGTCTGCACCGCCGCCTCC 406
Query  832  gcctccgcgcgcccgcgcgcgctGTGCTTACTGCTTCTTAGGGCAGAAAGCGAGGGCGC 891
|||||
Sbjct  405  GCCTCCGCCCGCCGCCCGCCGCTGTGCTTACTGCTTCTTAGGGCAGAAAGCGAGGGCGC 346
Query  892  TGTGTCAT  900
|||||
Sbjct  345  TGTGTCAT  337

```

9.1.4 Homo sapiens early B-cell factor 1 (EBF1), mRNA

Sequence ID: [ref|NM_024007.3|](#) Length: 5288 Number of Matches: 1

```

Query  35  CATGTTTGGGATT CAGGAAAGCATCCAACGGAGTGAAGCAGCATGAAGGAAGAGCCGCT 94
|||||
Sbjct  302  CATGTTTGGGATT CAGGAAAGCATCCAACGGAGTGAAGCAGCATGAAGGAAGAGCCGCT 361
Query  95  GGGCAGCGGCATGAACGCGGTGCGGACGTGGATGCAGGGCGCCGGGTGCTGGACGCCAA 154
|||||
Sbjct  362  GGGCAGCGGCATGAACGCGGTGCGGACGTGGATGCAGGGCGCCGGGTGCTGGACGCCAA 421
Query  155  CACGGCGGCGCAGAGCGGGTGGGTCTGCCCGGGCTCACTTTGAGAAGCAGCCGCTTC 214
|||||
Sbjct  422  CACGGCGGCGCAGAGCGGGTGGGTCTGCCCGGGCTCACTTTGAGAAGCAGCCGCTTC 481
Query  215  CAATCTGCGGAAATCCAACCTCTTCCACTTCGTCTGGCCCTCTACGACAGACAGGGCCA 274

```

```

|||||
Sbjct 482 CAATCTGCGGAAATCCAACCTTCTTCCACTTCGTCTCGTCCCTGGCCCTCTACGACAGACAGGGCCA 541
Query 275 GCCCGTGGAGATCGAGAGGACAGCGTTTGTGGGGTTCGTGGAGAAGGAAAAAGAAGCCAA 334
|||||
Sbjct 542 GCCCGTGGAGATCGAGAGGACAGCGTTTGTGGGGTTCGTGGAGAAGGAAAAAGAAGCCAA 601
Query 335 CAGCGAAAAGACCAATAACCGAATTCACTACCGGCTTCAGCTTCTCTACAGCAATGGGAT 394
|||||
Sbjct 602 CAGCGAAAAGACCAATAACCGAATTCACTACCGGCTTCAGCTTCTCTACAGCAATGGGAT 661
Query 395 AAGGACGGAGCAGGATTTCTACGTGCGCCTCATTGACTCCATGACAAAACAAGCCATAGT 454
|||||
Sbjct 662 AAGGACGGAGCAGGATTTCTACGTGCGCCTCATTGACTCCATGACAAAACAAGCCATAGT 721
Query 455 GTATGAAGGCCAAGACAAGAACCAGAAATGTGCCGAGTCTTGCTCACACATGAGATCAT 514
|||||
Sbjct 722 GTATGAAGGCCAAGACAAGAACCAGAAATGTGCCGAGTCTTGCTCACACATGAGATCAT 781
Query 515 GTGCAGCCGCTGTTGTGACAAGAAAAGCTGTGGCAACCGAAATGAGACTCCCTCAGATCC 574
|||||
Sbjct 782 GTGCAGCCGCTGTTGTGACAAGAAAAGCTGTGGCAACCGAAATGAGACTCCCTCAGATCC 841
Query 575 AGTGATAATTGACAGGTTCTTCTTGAATTTTCTCAAATGTAACCAAAATGCCTAAA 634
|||||
Sbjct 842 AGTGATAATTGACAGGTTCTTCTTGAATTTTCTCAAATGTAACCAAAATGCCTAAA 901
Query 635 GAATGCGGGAAACCCACGTGACATGCGGAGATTCAGGTCGTGGTGTCTACGACAGTCAA 694
|||||
Sbjct 902 GAATGCGGGAAACCCACGTGACATGCGGAGATTCAGGTCGTGGTGTCTACGACAGTCAA 961
Query 695 TGTGGATGGCCATGTCTTGGCAGTCTCTGATAACATGTTTGTCCATAATAATCCAAGCA 754
|||||
Sbjct 962 TGTGGATGGCCATGTCTTGGCAGTCTCTGATAACATGTTTGTCCATAATAATCCAAGCA 1021
Query 755 TGGGCGGAGGGCTCGGAGGCTTGACCCTCGGAAGGTACGCCCTCTTATCTGGAACATGC 814
|||||
Sbjct 1022 TGGGCGGAGGGCTCGGAGGCTTGACCCTCGGAAGGTACGCCCTCTTATCTGGAACATGC 1081
Query 815 TACTCCCTGTATCAAAGCCATCAGCCGAGTGAAGGATGGACGACGGGAGGTGCGACTGT 874
|||||
Sbjct 1082 TACTCCCTGTATCAAAGCCATCAGCCGAGTGAAGGATGGACGACGGGAGGTGCGACTGT 1141
Query 875 GATCATCATAGGGGACAATTTCTTTGATGGGTACAGGTCATATTCCGTACCATGCTGGT 934
|||||
Sbjct 1142 GATCATCATAGGGGACAATTTCTTTGATGGGTACAGGTCATATTCCGTACCATGCTGGT 1201
Query 935 CTGGAGTGAGTTGATCACTCCTCATGCCATCCGTGTGCAG 974
|||||
Sbjct 1202 CTGGAGTGAGTTGATCACTCCTCATGCCATCCGTGTGCAG 1241
-----
Query 241 TCACTCCTCATGCCATCCGTGTGCAGACCCCTCCTCGGCACATCCCTGGTGTGTGGAAG 300
|||||
Sbjct 1216 TCACTCCTCATGCCATCCGTGTGCAGACCCCTCCTCGGCACATCCCTGGTGTGTGGAAG 1275
Query 301 TCACACTGTCCTACAAATCTAAGCAGTTCTGCAAAGGAACACCAGGAGATTCAATTTATA 360
|||||
Sbjct 1276 TCACACTGTCCTACAAATCTAAGCAGTTCTGCAAAGGAACACCAGGAGATTCAATTTATA 1335

```

```

Query 361 CAGCGCTCAACGAACCCACCATCGATTATGGTTTCCAGAGGTTACAGAAGGTCATTCTC 420
          |||
Sbjct 1336 CAGCGCTCAACGAACCCACCATCGATTATGGTTTCCAGAGGTTACAGAAGGTCATTCTC 1395
Query 421 GGCACCCTGGTGACCCTGAGCGTTTGCCAAAGGAAGTAATACTCAAAGGGGTGCGGATC 480
          |||
Sbjct 1396 GGCACCCTGGTGACCCTGAGCGTTTGCCAAAGGAAGTAATACTCAAAGGGGTGCGGATC 1455
Query 481 TGGTAGAAGCACTGTATGGGATGCCACACAACAACCAGGAAATCATCTGAAGAGAGCGG 540
          |||
Sbjct 1456 TGGTAGAAGCACTGTATGGGATGCCACACAACAACCAGGAAATCATCTGAAGAGAGCGG 1515
Query 541 CCGACATTGCCGAGGCCCTGTACAGTGTCCCGCAACCACAACCAACTCCCGGCCCTTG 600
          |||
Sbjct 1516 CCGACATTGCCGAGGCCCTGTACAGTGTCCCGCAACCACAACCAACTCCCGGCCCTTG 1575
Query 601 CTAACACCTCGGTCCACGCAGGGATGATGGGCGTGAATTCGTTTCACTGGACAACCTGGCCG 660
          |||
Sbjct 1576 CTAACACCTCGGTCCACGCAGGGATGATGGGCGTGAATTCGTTTCACTGGACAACCTGGCCG 1635
Query 661 TGAATGTCTCCGAGGCATCACAAGCCACCAATCAGGGTTTCACCCGCAACTCAAGCAGCG 720
          |||
Sbjct 1636 TGAATGTCTCCGAGGCATCACAAGCCACCAATCAGGGTTTCACCCGCAACTCAAGCAGCG 1695
Query 721 TATCACCACACGGGTACGTGCCGAGCACCCTCCCGCAGCAGACCAACTATAACTCCGTCA 780
          |||
Sbjct 1696 TATCACCACACGGGTACGTGCCGAGCACCCTCCCGCAGCAGACCAACTATAACTCCGTCA 1755
Query 781 CCACGAGCATGAACGGATACGGCTCTGCCGCAATGTCCAATTTGGGGGGCTCCCCACCT 840
          |||
Sbjct 1756 CCACGAGCATGAACGGATACGGCTCTGCCGCAATGTCCAATTTGGGGGGCTCCCCACCT 1815
Query 841 TCCTCAACGGCTCAGCTGCCAACTCCCCCTATGCCATAGTGCCATCCAGCCCCACCATGG 900
          |||
Sbjct 1816 TCCTCAACGGCTCAGCTGCCAACTCCCCCTATGCCATAGTGCCATCCAGCCCCACCATGG 1875
Query 901 CCTCTCCACAAGCCTCCCCTCCAATGCAGCAGCTCCTCGGGCATCTTCTCTTCTCAC 960
          |||
Sbjct 1876 CCTCTCCACAAGCCTCCCCTCCAATGCAGCAGCTCCTCGGGCATCTTCTCTTCTCAC 1935
Query 961 CAGCCAACATGGTCTCAGCCGTGAAACAGAAGAGTGCTTTTCGCACCAGTCGTGAGCCCC 1020
          |||
Sbjct 1936 CAGCCAACATGGTCTCAGCCGTGAAACAGAAGAGTGCTTTTCGCACCAGTCGTGAGCCCC 1995
          _____
Query 421 GAAACAGAAGAGTGCTTTTCGCACCAGTCGTGAGCCCCAGACCTCCCCACCTCCCACCTG 480
          |||
Sbjct 1958 GAAACAGAAGAGTGCTTTTCGCACCAGTCGTGAGCCCCAGACCTCCCCACCTCCCACCTG 2017
Query 481 CACCAGCACCAACGGGAACAGCCTGCAAGCGATATCTGGCATGATTGTTCTCCTATG 538
          |||
Sbjct 2018 CACCAGCACCAACGGGAACAGCCTGCAAGCGATATCTGGCATGATTGTTCTCCTATG 2075

```

9.1.5 Homo sapiens POU class 3 homeobox 1 (POU3F1), mRNA

```

Query 23 TTACCGTAGAGCGTGCCAGCGCCAGCCCCACGTCGGCCTGCGTAAAGCCCAGCTTGATG 82
          |||
Sbjct 892 TTACCGTAGAGCGTGCCAGCGCCAGCCCCACGTCGGCCTGCGTAAAGCCCAGCTTGATG 833

```



```

Sbjct  885  TACGGTAACGTGTTCTCGCAGACCACCATCTGCCGCTTCGAGGCCCTGCAGCTGAGCTTC  944

Query  85  AAGAACATGTGCAAGCTCAAGCCGCTGCTCAACAAGTGGCTGGAGGAGACCGACTCGTCC  144
      |
Sbjct  945  AAGAACATGTGCAAGCTCAAGCCGCTGCTCAACAAGTGGCTGGAGGAGACCGACTCGTCC  1004
Query  145  AGCGGCAGCCCCACCAACCTGGACAAGATCGCGGCGCAGGGCCGCAAGCGCAAGAAGCGC  204
      |
Sbjct  1005  AGCGGCAGCCCCACCAACCTGGACAAGATCGCGGCGCAGGGCCGCAAGCGCAAGAAGCGC  1064
Query  205  ACGTCCATCGAGGTGGGGTCAAAGCGCGCTCGAGAGCCACTTTCTCAAGTGCCCAAG  264
      |
Sbjct  1065  ACGTCCATCGAGGTGGGGTCAAAGCGCGCTCGAGAGCCACTTTCTCAAGTGCCCAAG  1124
Query  265  CCCTCGGCGCACGAGATCACCGGCTTGGCAGACAGCCTGCAGCTGGAGAAGGAGGTGGTG  324
      |
Sbjct  1125  CCCTCGGCGCACGAGATCACCGGCTTGGCAGACAGCCTGCAGCTGGAGAAGGAGGTGGTG  1184
Query  325  CGCGTCTGGTTCTGCAACCGGCGGCAGAAGGAGAAGCGCATGACCCCTGCGGCCGGCGCG  384
      |
Sbjct  1185  CGCGTCTGGTTCTGCAACCGGCGGCAGAAGGAGAAGCGCATGACCCCTGCGGCCGGCGCG  1244
Query  385  GGCCACCCGCCATGGACGATGTATACGCGCCTGGGGAGCTAGGGCCTGGCGGGGGCGGC  444
      |
Sbjct  1245  GGCCACCCGCCATGGACGATGTATACGCGCCTGGGGAGCTAGGGCCTGGCGGGGGCGGC  1304
Query  445  GCATcgccaccctccgcgccccaccgcccccgccggcggtgcaccaccaccaccac  504
      |
Sbjct  1305  GCATCGCCACCCTCCGCGCCCCACCGCCCCCGCGGCGGCGCTGCACCACCACCACCAC  1364
Query  505  cacacacTGCCCGGCTCAGTGCAG  528
      |
Sbjct  1365  CACACACTGCCCGGCTCAGTGCAG  1388

```

9.1.6 Homo sapiens forkhead box P1 (FOXP1), transcript variant 1, mRNA

Sequence ID: [ref|NM_032682.5|](#) Length: 7102 Number of Matches: 1

```

Query  1  TTCAGCCATCCAGAATGGGTGCGGCGGCAGCAACCACTTACTAGAGTGCGGCGGTCTTCG  60
      |
Sbjct  565  TTCAGCCATCCAGAATGGGTGCGGCGGCAGCAACCACTTACTAGAGTGCGGCGGTCTTCG  624
Query  61  GGAGGGGCGGTCCAACGGAGAGACGCCGCGCTGGACATCGGGGCAGCTGACCTCGCCCA  120
      |
Sbjct  625  GGAGGGGCGGTCCAACGGAGAGACGCCGCGCTGGACATCGGGGCAGCTGACCTCGCCCA  684
Query  121  CGCCcagcagcagcagcaacaggcacttcaggtggcaagacagctccttcttcagcagca  180
      |
Sbjct  685  CGCCCAGCAGCAGCAGCAACAGGCACTTCAAGTGGCAAGACAGCTCCTTCTTCAGCAGCA  744
Query  181  acagcagcagcaaGTTAGTGGATTAAAATCTCCCAAGAGGAATGACAAACAACCAGCTCT  240
      |
Sbjct  745  ACAGCAGCAGCAAGTTAGTGGATTAAAATCTCCCAAGAGGAATGACAAACAACCAGCTCT  804
Query  241  TCAGGTTCCCGTGTCAAGTGGCTATGATGACACCTCAAGTTATCACTCCCAGCAAATGCA  300
      |

```

```
Sbjct 805 TCAGGTTCCCGTGTCAAGTGGCTATGATGACACCTCAAGTTATCACTCCCCAGCAAATGCA 864
Query 301 GCAGATCCTCCAGCAACAAGTGTGAGCCCTCAGCAGCTCCAGGTTCTCTCCAGCAGCA 360
|
|
|
Sbjct 865 GCAGATCCTCCAGCAACAAGTGTGAGCCCTCAGCAGCTCCAGGTTCTCTCCAGCAGCA 924
Query 361 GCAGGCCCTCATGCTTCAACAGCAGCAGCTTCAAGAGTTTTATAAAAAACAACAGGAACA 420
|
|
|
Sbjct 925 GCAGGCCCTCATGCTTCAACAGCAGCAGCTTCAAGAGTTTTATAAAAAACAACAGGAACA 984
Query 421 GTTGCAGCTTCAACTTTTACAACAACAACATGCTGGAAAACAGCCTAAAGAGCAACAGCA 480
|
|
|
Sbjct 985 GTTGCAGCTTCAACTTTTACAACAACAACATGCTGGAAAACAGCCTAAAGAGCAACAGCA 1044
Query 481 GGTGGCTACCcagcagttggcttttcagcagcagcttttacagatgcagcagttacagca 540
|
|
|
Sbjct 1045 GGTGGCTACCCAGCAGTTGGCTTTTTCAGCAGCAGCTTTTACAGATGCAGCAGTTACAGCA 1104
Query 541 gcagcaCCTCCTGTCTTTGCAGCGCCAAGGCCTTCTGACAATTCAGCCCGGCAGCCTGC 600
|
|
|
Sbjct 1105 GCAGCACCTCCTGTCTTTGCAGCGCCAAGGCCTTCTGACAATTCAGCCCGGCAGCCTGC 1164
Query 601 CCTTCCCCTTCAACCTCTTGCTCAAGGCATGATTCCAACAGAAGTGCAGCAGCTCTGGAA 660
|
|
|
Sbjct 1165 CCTTCCCCTTCAACCTCTTGCTCAAGGCATGATTCCAACAGAAGTGCAGCAGCTCTGGAA 1224
Query 661 AGAAGTGACAAGTGTCTATACTGCAGAAGAAACCACAGGCAACAATCACAGCAGTTTGA 720
|
|
|
Sbjct 1225 AGAAGTGACAAGTGTCTATACTGCAGAAGAAACCACAGGCAACAATCACAGCAGTTTGA 1284
Query 721 TCTGACCACGACATGTGTCTCCTCCTCTGCACCTTCCAAGACCTCCTTAATAATGAACCC 780
|
|
|
Sbjct 1285 TCTGACCACGACATGTGTCTCCTCCTCTGCACCTTCCAAGACCTCCTTAATAATGAACCC 1344
Query 781 ACATGCCTCTACCAATGGACAGCTCTCAGTCCACACTCCCAAAGGAAAGTTTGTCCCA 840
|
|
|
Sbjct 1345 ACATGCCTCTACCAATGGACAGCTCTCAGTCCACACTCCCAAAGGAAAGTTTGTCCCA 1404
Query 841 TGAGGAGCACCCCATAGCCATCCTCTCTATGGACATGGTGTATGCAAGTGGCCAGGCTG 900
|
|
|
Sbjct 1405 TGAGGAGCACCCCATAGCCATCCTCTCTATGGACATGGTGTATGCAAGTGGCCAGGCTG 1464
Query 901 TGAAGCAGTGTGCGAAGATTTCCAATCATTTCTAAAACATCTCAACAGTGAGCATGCGCT 960
|
|
|
Sbjct 1465 TGAAGCAGTGTGCGAAGATTTCCAATCATTTCTAAAACATCTCAACAGTGAGCATGCGCT 1524
Query 961 GGACGATAGAAGTACAGCCCAATGTAGAGTACAAATGCAGGTTGTACAGCAGTTAGAGCT 1020
|
|
|
Sbjct 1525 GGACGATAGAAGTACAGCCCAATGTAGAGTACAAATGCAGGTTGTACAGCAGTTAGAGCT 1584
Query 1 AATCTGGACTGTGGTTGGCTGTTGTCTACTAAGGACAGGGGCCCTTCAGCTTCTCTGGAT 60
|
|
|
Sbjct 2507 AATCTGGACTGTGGTTGGCTGTTGTCTACTAAGGACAGGGGCCCTTCAGCTTCTCTGGAT 2448
Query 61 CGAGGGGCTCTTCTTTGACGTGTACAGGATGCACGGCTTGCATAGGAGATCTGCCTGGAC 120
|
|
|
Sbjct 2447 CGAGGGGCTCTTCTTTGACGTGTACAGGATGCACGGCTTGCATAGGAGATCTGCCTGGAC 2388
Query 121 TGCTGTCACTCTCGTTGCTGTTGGTATGCTCCATTGCCCGTTCAGCTTCTCCCGTATTG 180
|
|
|
```

```

Sbjct 2387 TGCTGTCACTCTCGTTGCTGTTGGTATGCTCCATTGCCCGTTCAGCTCTCCCGTATTG 2328
Query 181 CGCTGGCTAAGTTGCCAGAGTGGGATTTCCCATGGAAGCGGTAGTGTATAGAGGTATAC 240
|
|
|
Sbjct 2327 CGCTGGCTAAGTTGCCAGAGTGGGATTTCCCATGGAAGCGGTAGTGTATAGAGGTATAC 2268
Query 241 TATTCTCAGCCATTGAAGCCTGTAAAGCTGCATTGAGAGGTGTGCAGTAGGCGTGGCTGC 300
|
|
|
Sbjct 2267 TATTCTCAGCCATTGAAGCCTGTAAAGCTGCATTGAGAGGTGTGCAGTAGGCGTGGCTGC 2208
Query 301 TCTGCATGTTTTTAATAAGGGAAGGGTTACCACTGATCTTTTGTGGCCTTCGTTTTTGA 360
|
|
|
Sbjct 2207 TCTGCATGTTTTTAATAAGGGAAGGGTTACCACTGATCTTTTGTGGCCTTCGTTTTTGA 2148
Query 361 ATTCTACTTCATCCACTGTCCATACTGCCCTTTAACGTTTTCTACTCGCACAAAACACT 420
|
|
|
Sbjct 2147 ATTCTACTTCATCCACTGTCCATACTGCCCTTTAACGTTTTCTACTCGCACAAAACACT 2088
Query 421 TGTGAAGACTAAGATTATGACGCACTGCATTCTTCCACGTGGCCGCGTTGCGTCGGAAGT 480
|
|
|
Sbjct 2087 TGTGAAGACTAAGATTATGACGCACTGCATTCTTCCACGTGGCCGCGTTGCGTCGGAAGT 2028
Query 481 AAGCAAACATTCGTGTGAACCAGTTATAGATCTCATTTAGTGTAGCTGCTTTTCTGGAG 540
|
|
|
Sbjct 2027 AAGCAAACATTCGTGTGAACCAGTTATAGATCTCATTTAGTGTAGCTGCTTTTCTGGAG 1968
Query 541 ATTCGAGAATGGCCTGCCTAATTAAGATGCATATGTAAATGGTGGTCTAACTTCTGCGT 600
|
|
|
Sbjct 1967 ATTCGAGAATGGCCTGCCTAATTAAGATGCATATGTAAATGGTGGTCTAACTTCTGCGT 1908
Query 601 TCTTATAAAATTTCTTGGTTCTGCGCAATATCTGCTGACGAAATGGGCACGTTGTATTTGT 660
|
|
|
Sbjct 1907 TCTTATAAAATTTCTTGGTTCTGCGCAATATCTGCTGACGAAATGGGCACGTTGTATTTGT 1848
Query 661 CTGAGTACCGCTGCGGATGGGTCCCACCGTGTGCATGCTGGTGGTGTGATGACAGAGG 720
|
|
|
Sbjct 1847 CTGAGTACCGCTGCGGATGGGTCCCACCGTGTGCATGCTGGTGGTGTGATGACAGAGG 1788
Query 721 GGCCTTGGGTGACGGGAGTCAGGGGGCGGTTGGGGTCGTTGGAGTATGAGGTAAGCTCT 780
|
|
|
Sbjct 1787 GGCCTTGGGTGACGGGAGTCAGGGGGCGGTTGGGGTCGTTGGAGTATGAGGTAAGCTCT 1728
Query 781 GTGGAGAAGCCTCCGATGCGGACTTGAGAGAGTGACACTTGATACCAGATTCAAGGGCT 840
|
|
|
Sbjct 1727 GTGGAGAAGCCTCCGATGCGGACTTGAGAGAGTGACACTTGATACCAGATTCAAGGGCT 1668
Query 841 GAGGGGCGGCTTTGGGTTCTGTAGACTTCACATGCAGGTGGGTCATCATGGCTTGCAGGC 900
|
|
|
Sbjct 1667 GAGGGGCGGCTTTGGGTTCTGTAGACTTCACATGCAGGTGGGTCATCATGGCTTGCAGGC 1608
Query 901 GTTCTTTGTCTTTTGAAGCTGTAGCTCTAACTGCTGTACAACCTGCATTTGTACTCTAC 960
|
|
|
Sbjct 1607 GTTCTTTGTCTTTTGAAGCTGTAGCTCTAACTGCTGTACAACCTGCATTTGTACTCTAC 1548
Query 961 ATTGGGCTGTACTTCTATCGTCCAGCGCATGCTCACTGTTGAGATGTTTTAGAAAATGATT 1020
|
|
|
Sbjct 1547 ATTGGGCTGTACTTCTATCGTCCAGCGCATGCTCACTGTTGAGATGTTTTAGAAAATGATT 1488
Query 1021 GGAAATCTTCGCACACTGCTTACAGCC 1048
|
|
|

```

```
Sbjct 1487 GGAAATCTTCGCACACTGCTTCACAGCC 1460
Query 1 GCACCTCCTGTCTTTGCGAGCGCCAAGGCCTTCTGACAATTCAGCCCGGGCAGCCTGCCCT 60
|
|
Sbjct 1108 GCACCTCCTGTCTTTGCGAGCGCCAAGGCCTTCTGACAATTCAGCCCGGGCAGCCTGCCCT 1167
Query 61 TCCCCTTCAACCTCTTGCTCAAGGCATGATTC AACAGA AACTGCAGCAGCTCTGGAAAGA 120
|
|
Sbjct 1168 TCCCCTTCAACCTCTTGCTCAAGGCATGATTC AACAGA AACTGCAGCAGCTCTGGAAAGA 1227
Query 121 AGTGACAAGTGCTCATACTGCAGAAGAAACCACAGGCAACAATCACAGCAGTTTGGATCT 180
|
|
Sbjct 1228 AGTGACAAGTGCTCATACTGCAGAAGAAACCACAGGCAACAATCACAGCAGTTTGGATCT 1287
Query 181 GACCACGACATGTGTCTCCTCCTCTGCACCTTCCAAGACCTCCTTAATAATGAACCCACA 240
|
|
Sbjct 1288 GACCACGACATGTGTCTCCTCCTCTGCACCTTCCAAGACCTCCTTAATAATGAACCCACA 1347
Query 241 TGCCTCTACCAATGGACAGCTCTCAGTCCACACTCCCAAAGGGAAAGTTTGTCCCATGA 300
|
|
Sbjct 1348 TGCCTCTACCAATGGACAGCTCTCAGTCCACACTCCCAAAGGGAAAGTTTGTCCCATGA 1407
Query 301 GGAGCACCCCATAGCCATCCTCTCTATGGACATGGTGTATGCAAGTGGCCAGGCTGTGA 360
|
|
Sbjct 1408 GGAGCACCCCATAGCCATCCTCTCTATGGACATGGTGTATGCAAGTGGCCAGGCTGTGA 1467
Query 361 AGCAGTGTGCGAAGATTTCCAATCATTTCTAAAACATCTCAACAGT GAGCATGCGCTGGA 420
|
|
Sbjct 1468 AGCAGTGTGCGAAGATTTCCAATCATTTCTAAAACATCTCAACAGT GAGCATGCGCTGGA 1527
Query 421 CGATAGAAGTACAGCCCAATGTAGAGTACAAATGCAGGTTGTACAGCAGTTAGAGCTACA 480
|
|
Sbjct 1528 CGATAGAAGTACAGCCCAATGTAGAGTACAAATGCAGGTTGTACAGCAGTTAGAGCTACA 1587
Query 481 GCTTGCAAAGACAAAGAACGCTGCAAGCCATGATGACCCACCTGCATGTGAAGTCTAC 540
|
|
Sbjct 1588 GCTTGCAAAGACAAAGAACGCTGCAAGCCATGATGACCCACCTGCATGTGAAGTCTAC 1647
Query 541 AGAACCCAAAGCCGCCCTCAGCCCTTGAATCTGGTATCAAGTGTCACTCTCTCCAAGTC 600
|
|
Sbjct 1648 AGAACCCAAAGCCGCCCTCAGCCCTTGAATCTGGTATCAAGTGTCACTCTCTCCAAGTC 1707
Query 601 CGCATCGGAGGCTTCTCCACAGAGCTTACCTCATACTCCAACGACCCCAACGCCCCCCT 660
|
|
Sbjct 1708 CGCATCGGAGGCTTCTCCACAGAGCTTACCTCATACTCCAACGACCCCAACGCCCCCCT 1767
Query 661 GACTCCCGTACCCCAAGGCCCTCTGTCATCACAACCACCAGCATGCACACGGTGGGACC 720
|
|
Sbjct 1768 GACTCCCGTACCCCAAGGCCCTCTGTCATCACAACCACCAGCATGCACACGGTGGGACC 1827
Query 721 CATCCGAGGGGTA CT CAGACAAATACAACGTGCCCATTTTCGTCAGCAGATATTGCGCA 780
|
|
Sbjct 1828 CATCCGAGGGGTA CT CAGACAAATACAACGTGCCCATTTTCGTCAGCAGATATTGCGCA 1887
Query 781 GAACCAAGAATTTTATAAGAACGCAGAAGTTAGACCACCATTTACATATGCATCTTTAAT 840
|
|
Sbjct 1888 GAACCAAGAATTTTATAAGAACGCAGAAGTTAGACCACCATTTACATATGCATCTTTAAT 1947
Query 841 TAGGCAGGCCATTCTCGAATCTCCAGAAAAGCAGCTAACACTAAATGAGATCTATAACTG 900
|
|
```


Sbjct	2051	TGGAAGAATGCAGTGCCTCATAATCTTAGTCTTCACAAGTGTTTTGTGCGAGTAGAAAAC	2110
Query	480	GTTAAAGGGGCAGTATGGACAGTGGATGAAGTAGAATTCCAAAAACGAAGGCCACAAAAG	539
Sbjct	2111	GTTAAAGGGGCAGTATGGACAGTGGATGAAGTAGAATTCCAAAAACGAAGGCCACAAAAG	2170
Query	540	ATCAGTGGTAACCCCTCCCTTATTA AAAACATGCAGAGCAGCCACGCCTACTGCACACCT	599
Sbjct	2171	ATCAGTGGTAACCCCTCCCTTATTA AAAACATGCAGAGCAGCCACGCCTACTGCACACCT	2230
Query	600	CTCAATGCAGCTTTACAGGCTTCAATGGCTGAGAATAGTATACCTCTATACTACTACCGCT	659
Sbjct	2231	CTCAATGCAGCTTTACAGGCTTCAATGGCTGAGAATAGTATACCTCTATACTACTACCGCT	2290
Query	660	TCCATGGGAAATCCCCTCTGGGCAACTTAGCCAGCGCAATACGGGAAGAGCTGAACGGG	719
Sbjct	2291	TCCATGGGAAATCCCCTCTGGGCAACTTAGCCAGCGCAATACGGGAAGAGCTGAACGGG	2350
Query	720	GCAATGGAGCATAACCAACAGCAACGAGAGTGACAGCAGTCCAGGCAGATCTCCTATGCAA	779
Sbjct	2351	GCAATGGAGCATAACCAACAGCAACGAGAGTGACAGCAGTCCAGGCAGATCTCCTATGCAA	2410
Query	780	GCCGTGCATCCTGTACACGTCAAAGAAGAGCCCCTCGATCCAGAGGAAGCTGAAGGGCCC	839
Sbjct	2411	GCCGTGCATCCTGTACACGTCAAAGAAGAGCCCCTCGATCCAGAGGAAGCTGAAGGGCCC	2470
Query	840	CTGTCCTTAGTGACAACAGCCAACCACAGTCCAGATTTTGACCATGACAGAGATTACGAA	899
Sbjct	2471	CTGTCCTTAGTGACAACAGCCAACCACAGTCCAGATTTTGACCATGACAGAGATTACGAA	2530
Query	900	GATGAACCAGTAAACGAGGACATGGAG 926	
Sbjct	2531	GATGAACCAGTAAACGAGGACATGGAG 2557	
Query	60	TTGTATTTGTCTGAGTACCGCTGCGGATGGGTCCCACCGTGTGCATGCTGGTGGTTGTG	119
Sbjct	1857	TTGTATTTGTCTGAGTACCGCTGCGGATGGGTCCCACCGTGTGCATGCTGGTGGTTGTG	1798
Query	120	ATGACAGAGGGCCTTGGGTGACGGGAGTCAGGGGGCGGTTGGGGTCGTTGGAGTATGA	179
Sbjct	1797	ATGACAGAGGGCCTTGGGTGACGGGAGTCAGGGGGCGGTTGGGGTCGTTGGAGTATGA	1738
Query	180	GGTAAGCTCTGTGGAGAAGCCTCCGATGCGGACTTGGAGAGAGTGACACTTGATAACCAGA	239
Sbjct	1737	GGTAAGCTCTGTGGAGAAGCCTCCGATGCGGACTTGGAGAGAGTGACACTTGATAACCAGA	1678
Query	240	TTCAAGGGCTGAGGGGCGCTTTGGGTTCTGTAGACTTCACATGCAGGTGGGTCATCATG	299
Sbjct	1677	TTCAAGGGCTGAGGGGCGCTTTGGGTTCTGTAGACTTCACATGCAGGTGGGTCATCATG	1618
Query	300	GCTTGCAGGCGTCTTTGTCTTTTGCAAGCTGTAGCTCTAACTGCTGTACAACCTGCATT	359
Sbjct	1617	GCTTGCAGGCGTCTTTGTCTTTTGCAAGCTGTAGCTCTAACTGCTGTACAACCTGCATT	1558
Query	360	TGTACTCTACATTGGGCTGTACTTCTATCGTCCAGCGCATGCTCACTGTTGAGATGTTTT	419
Sbjct	1557	TGTACTCTACATTGGGCTGTACTTCTATCGTCCAGCGCATGCTCACTGTTGAGATGTTTT	1498
Query	420	AGAAATGATTGAAATCTTCGCACACTGCTTCACAGCCTGGCCACTGCATACACCATGT	479

```

Sbjct  1497  AGAAATGATTGGAAATCTTCGCACACTGCTTCACAGCCTGGCCACTTGCATACACCATGT  1438
Query  480  CCATAGAGAGGATGGCTATGGGGGTGCTCCTCATGGGACAAACTTTCCCTTTTGGGAGTG  539
      |||
Sbjct  1437  CCATAGAGAGGATGGCTATGGGGGTGCTCCTCATGGGACAAACTTTCCCTTTTGGGAGTG  1378
Query  540  TGGACTGAGAGCTGTCCATTGGTAGAGGCATGTGGGTTCAATTATTAAGGAGGTCTTGGAA  599
      |||
Sbjct  1377  TGGACTGAGAGCTGTCCATTGGTAGAGGCATGTGGGTTCAATTATTAAGGAGGTCTTGGAA  1318
Query  600  GGTGCAGAGGAGGAGACACATGTCGTGGTCAGATCCAAACTGCTGTGATTGTTGCCTGTG  659
      |||
Sbjct  1317  GGTGCAGAGGAGGAGACACATGTCGTGGTCAGATCCAAACTGCTGTGATTGTTGCCTGTG  1258
Query  660  GTTCTTCTGCAGTATGAGCACTTGTCACTTCTTTCCAGAGCTGCTGCAGTTCTGTTGGA  719
      |||
Sbjct  1257  GTTCTTCTGCAGTATGAGCACTTGTCACTTCTTTCCAGAGCTGCTGCAGTTCTGTTGGA  1198
Query  720  ATCATGCCTTGAGCAAGAGGTTGAAGGGGAAGGGCAGGCTGCCCGGCTGAATTGTCAGA  779
      |||
Sbjct  1197  ATCATGCCTTGAGCAAGAGGTTGAAGGGGAAGGGCAGGCTGCCCGGCTGAATTGTCAGA  1138
Query  780  AGGCCTTGGCGCTGCAAAGACAGGAGGtgctgctgctgtaactgctgcatctgtaaaagc  839
      |||
Sbjct  1137  AGGCCTTGGCGCTGCAAAGACAGGAGGTGCTGCTGTGTAAGTCTGCTGCATCTGTAAGAGC  1078

```

9.2 Recipes

4% Paraformaldehyde

2 g Paraformaldehyde
5 ml 10x PBS pH 7.4

30 ml H₂O
pH to 7.4
To 50 ml H₂O

Stripping buffer 5x

40 g SDS
125 ml 1 M Tris pH 6.7
To 400 ml H₂O

Ponceau S

0.1% (w/v) Ponceau S
5% (v/v) Acetic acid
To 500 ml ddH₂O

TBS 10x

24.2 g Tris Base
87.6 g NaCl
To 900ml with H₂O
pH 7.5 then to 1L with H₂O

Alkaline phosphatase

lysis Solution I

Tris
EDTA
Glucose
H₂O

Alkaline phosphatase

lysis Solution II

50 µl 4 M NaOH
50 µl 20% SDS
900 µl H₂O

**Alkaline phosphatase
lysis Solution III**

5 M Potassium acetate

Acetic acid

H₂O

9.3 Materials

Product	Company	Cat. Number
0.05% Trypsin-EDTA	Life Technologies	25300-054
0.2 µm syringe filter	Sartorius Stedim	16534
0.2 ml PCR tubes	Alta Biosciences	LW2330AS
1.5 ml microcentrifuge tubes	Fisher Scientific	T331-10B
100 mm Sterilin plates	VWR	391-2016
100bp ladder	NEW ENGLAND BIOLABS	N3231L
1-200 µl filter tip	VWR	7320541
13 mm coverslips	VWR	631-0149
15 ml centrifuge tube	VWR	734-1813
1kb ladder	NEW ENGLAND BIOLABS	N3232L
24 well plate	Fisher Scientific	TKT-190-0104
2A antibody	Millipore	ABS31
2-Mercaptoethanol	Sigma-Aldrich	M3148
2-propanol	Sigma-Aldrich	I9516
30% Acrylamide	Biorad	161-0158
50ml Centrifuge tubes	VWR	7341827
50x TAE	MP Bio	11TAE50X01
6 well plates	Fisher Scientific	TKT190050T
96 well plate	Fisher Scientific	TKT-180-070U
99% Glycerol	Sigma-Aldrich	G5516
Acetic acid glacial	Fisher Scientific	A/0360/PB17
Advanced DMEM/F12	Life Technologies	12634010
Agarose	Melford	MB1200
Albumin from chick egg white	Sigma-Aldrich	A5378
Alexa Fluor 350 goat α mouse IgG (H&L)	Life Technologies	A11045
Alexa Fluor 350 goat α rat IgG (H&L)	Life Technologies	A21093
Alexa Fluor 488 Donkey α goat IgG (H&L)	Life Technologies	A11055
Alexa Fluor 488 goat α chicken IgY (H&L)	Abcam	ab150169
Alexa Fluor 488 goat α mouse IgG (H&L)	Life Technologies	A11001
Alexa Fluor 488 goat α rabbit IgG (H&L)	Life Technologies	A11008
Alexa Fluor 488 goat α rat IgG (H&L)	Life Technologies	A11006
Alexa Fluor 594 goat α mouse	Life Technologies	A11005

IgG (H&L)		
Alexa Fluor 594 goat α rabbit IgG (H&L)	Life Technologies	A11012
Alexa Fluor[®] Goat α rabbit IgG 594	Life Technologies	A11012
Ammonium acetate	Fisher Scientific	A/3440/50
Ammonium persulfate	Fisons	A/6160/53
Ampicillin sodium salt	Sigma-Aldrich	A9518
Ascorbic Acid	Sigma-Aldrich	A4544
BaCl₂		
BamHI-HF	NEW ENGLAND BIOLABS	R3136S
BDNF	Miltenyi	130-096-286
BglII	NEW ENGLAND BIOLABS	R0144S
Blotting paper	Sigma-Aldrich	Z74759-100
Bond breaker TCEP Solution neutral pH	Thermo Scientific	77720
Boric acid	Sigma-Aldrich	B6768
Bovine serum albumin	Sigma-Aldrich	A7906
CaCl₂	Sigma-Aldrich	499609
Calbindin	Swant	CB38a
Cell scraper	VWR	734-1527
CHIR 99021	CHDI	CHDI-00401952-0000
Complete mini EDTA-free protease inhibitor cocktail tablets	Roche	11873580001
Cryostor CS10	Stem cell technologies	7930
CsCl		
CTIP2 antibody	Abcam	ab18456
DAPT	CHDI	CHDI-00396736-0000
DARPP32 antibody	Abcam	ab40801
DCX antibody	Santa Cruz	sc8066
DEPC treated DNase free H₂O	Life Technologies	46-2224
Dimethyl formamide	Sigma-Aldrich	D8654
Dispase 1mg/ml	Stem cell technologies	7923
Distilled water	Life Technologies	15230-188
DMEM:F12	Life Technologies	21331-020
DMSO	Sigma-Aldrich	D2650
Donkey α rabbit IgG HRP	GE	NA934V
Ebf1 antibody	Abcam	Ab126135
EcoRI-HF	NEW ENGLAND BIOLABS	R3101S
EDTA	Sigma-Aldrich	E5134
EGTA		
Endo-free Maxi prep kit	Qiagen	12362
Ethanol	Sigma-Aldrich	E7023
Fetal Bovine Serum	Life Technologies	10437-028
Fluoromount-G[®]	Southern Biotech	0100-01

Forskolin	CHDI	CHDI-00000087-0000
FOXP1 (Mouse) antibody	Abcam	ab32010
FoxP1 (Rabbit) antibody	Abcam	Ab16645
GABA	Tocris	0344
GeneClean [®] Kit	MP Bio	111001200
Geneticin [®] 50 mg/ml solution	Life Technologies	10131-035
GFAP antibody	Sigma-Aldrich	G3893
GFP antibody	Abcam	ab13970
Glucose	BDH	101174Y
Glutamax [™]	Life Technologies	35050-061
Glycine	Sigma-Aldrich	G8790
Goat serum	Life Technologies	16210-064
Guanosine	Sigma-Aldrich	G6264
HBSS	Life Technologies	14170-120
HEPES	VWR	
HiSpeed Plasmid Midi prep kit	Qiagen	12643
Hoechst 33342	Thermo Scientific	62249
IPTG	Melford Biosciences	MB1008
Islet1 antibody	Abcam	Ab109517
IWR1	CHDI	CHDI-00476979-0000
Kanamycin sulphate	Life Technologies	11815-032
KCl		
Knockout DMEM	Life Technologies	10829-018
LB Agar	Life Technologies	22700-025
LB Broth Base	Life Technologies	12780-052
LDN 193189	Sigma-Aldrich	SML0559
LDN 193189	CHDI	CHDI-00396388-0000
Leupeptin		
L-Glutamine	Life Technologies	25030-024
Lipofectamine LTX	Life Technologies	15338030
Lipofectamine RNAiMAX	Life Technologies	13778030
Lumi-film chemiluminescent detection film	Roche	11666916001
MACS Neurobrew 21	Miltenyi	130-093-566
MACS Neurobrew 21 without vitamin A	Miltenyi	130-097-263
MAP2 (Mouse) antibody	Sigma-Aldrich	M1406
MAP2 (Rabbit) antibody	Abcam	ab32454
Marvel powdered skimmed milk	-	-
Matrigel hESC qualified	VWR	734-1440
Menzel Gläser Superfrost plus slides	VWR	631-9483
Methanol	Sigma-Aldrich	32213
MgCl ₂		
MicroAmp 96 well plate	Life Technologies	4314320
Mouse neural stem cell	Lonza	VPG-1004

nucleofector solution		
mTESR1 complete medium	Stem cell technologies	5879
Na.ATP		
Na.GTP		
NaCl		
NcoI-HF	NEW ENGLAND BIOLABS	R3193S
Neurobasal A	Life Technologies	10888-022
NheI-HF	NEW ENGLAND BIOLABS	R3131S
Nitric acid	Sigma-Aldrich	438073
Nitrocellulose membrane	Amersham	RPN203D
NMDA		
Normal goat serum	DAKO	X0907
NotI-HF	NEW ENGLAND BIOLABS	R3189S
Novex[®] Protein ladder	Life Technologies	LC5800
Nucleofector solution Cell line V	Lonza	VCA-1003
Nunc 60mm dishes	VWR	734-2040
Oct6 antibody	Abcam	Ab31766
One Shot[®] TOP10 Chemically competent E. coli	Life Technologies	C404003
OptiMEM reduced serum medium	Life Technologies	31985-062
Paraformaldehyde	Sigma-Aldrich	158127
PBS pH 7.4	Life Technologies	10010-056
PD0332991	CHDI	CHDI-00482855-0001
Penicillin-streptomycin 5000 U/ml	Life Technologies	15070-063
Petri dish with lid borosilicate glass	Fisher	11313704
pGEM[®] T easy vector	Promega	A1360
Phenol:Chloroform:Isoamyl alcohol 25:24:1	Sigma-Aldrich	P3803
Pierce BCA assay	Thermo Scientific	23225
Platinum[®] Taq Polymerase	Life Technologies	11304-011
Poly-D-Lysine hydrobromide	Sigma-Aldrich	P6407
Potassium acetate	Sigma-Aldrich	P1190
PSD-95	Abcam	ab18258
Random primers	Life Technologies	48190-011
Rat IgG2a kappa monoclonal isotype control	Abcam	ab18450
Ribonuclease A from bovine pancreas	Sigma-Aldrich	R4642
RIPA lysis buffer	Sigma-Aldrich	R0278
RNA Clean and Concentrator-5	Cambridge Biosciences	R1015
RNA Clean and	Cam Bio	R1015

Concentrator-5 (50)		
RNaseOUT™ Recombinant Ribonuclease Inhibitor	Life Technologies	10777019
RNeasy mini kit	QIAGEN	74104
S100β	Sigma-Aldrich	S2532
Safeview Nucleic Acid Stain	NBS Bio	NBS-SV1
Sall-HF	NEW ENGLAND BIOLABS	R3138S
Sample buffer Laemmli 2x	Sigma-Aldrich	S3401
SB431542	CHDI	CHDI-00447536-0000
Set of dATP, dCTP, dGTP, dTTP	Promega	U1240
Sheep α mouse IgG HRP	GE	NA931V
Smal	NEW ENGLAND BIOLABS	R0141S
SOC medium	Life Technologies	15544-034
Sodium Azide	Sigma-Aldrich	S8032
Sodium Dodecyl Sulphate	Sigma-Aldrich	L3771
Sodium hydroxide	Sigma-Aldrich	S5881
Sodium tetraborate	Sigma-Aldrich	221732
Stempro Accutase	Life Technologies	A1110501
Streptolysin-O	Sigma-Aldrich	S0149-25ku
Subcloning efficiency DH5α	Life Technologies	18265-017
Superscript II®	Life Technologies	18064-014
SuperSignal West Dura chemiluminescent substrate	Thermo Scientific	34075
SuperSignal West Pico chemiluminescent substrate	Thermo Scientific	34077
SYBR green	Thermo Scientific	F100L
Synaptophysin	Abcam	ab8049
SYTO16 green fluorescent nucleic acid stain	Life Technologies	S7578
T25 flask	BD Falcon	353108
T4 DNA ligase	NEW ENGLAND BIOLABS	M0202S
TEMED	Sigma-Aldrich	T9281
Thermo Scientific sensitive alkaline phosphatase	Promega	M9910
Total RNA - Human Fetal Normal Tissue: Brain: Frontal Lobe	Ambio	R1244051-50
Tris	Roche	10708976001
Tris HCl	Sigma-Aldrich	T5941
Triton X-100	Sigma-Aldrich	T8787
Trypan blue	Sigma-Aldrich	T8154
Tween 20	Sigma-Aldrich	P1379

Vectashield	Vector laboratories	H-1400
Xbal	NEW ENGLAND BIOLABS	R0145S
Xgal	Melford Biosciences	MB1001
Y27632 dihydrochloride	Abcam	AB120129
β-actin antibody	Sigma-Aldrich	A2228